Mathematical modeling of concentrated suspensions: Multiscale analysis and numerical solutions

vorgelegt von
M.Sc.
Tobias Ahnert
geb. in Berlin

Von der Fakultät II - Mathematik und Naturwissenschaften
der Technischen Universität Berlin
zur Erlangung des akademischen Grades

Doktor der Naturwissenschaften
- Dr. rer. nat. -

genehmigte Dissertation

Promotionsausschuss:

Vorsitzender:	Prof. Dr. Martin Skutella
Gutachter:	Prof. Dr. Rupert Klein
Gutachter:	Prof. Dr. Andreas Münch
Gutachterin:	Prof. Dr. Barbara Wagner

Tag der wissenschaftlichen Aussprache: 20. November 2015

Berlin 2015

D 83

Abstract

The present thesis studies multiphase models for complex fluids - in particular for concentrated suspensions. The subject is introduced by the derivation of a new thin-film model for the simulation of a drying front on a substrate. The proposed model has two main weaknesses: The mechanism of particle transport is not derived from the rheology of the fluid, but is hypothesized. And the model is not able to capture the behavior of the fluid in dry as well as in fluid regions, which are both present in a drying front.

This motivates the proposal of a new Eulerian-Eulerian multiphase model, that models the mass and momentum conservation of the liquid and solids separately. It is applied to plane Poiseuille flow, which allows the derivation of an exact analytic solution and shows a novel viscoplastic behavior of the multiphase model. Then, we derive a particle transport mechanism for viscoplastic fluids through the usage of asymptotic techniques. The stability of the multiphase model is analyzed using the method of normal modes, which allows us to find a previously unknown necessary criterion for well-posedness of the model. Additionally, we identify transient growing modes.

Then, the study of stability is redone using a new derivation of the multiphase model based on energetic principles. This allows for the systematic derivation of consistent free-boundary conditions and a generalization of the necessary criterion for well-posedness of the model to general flows.

Since the multiphase model is reducible to viscoplastic thin-film models, an alternative derivation for a known model is given that is based on a variational inequality framework. The existence of solutions for a particular model is proven using monotonicity methods.

Finally, the multiphase model is systematically analyzed for contained simpler models. In particular, a thin-film model with additional transport mechanism for the particles is derived from multiphase models. This shows how constitutive laws for the rheology of the multiphase model influence the transport mechanisms in thin-film models. Additionally, an assumption is given under which the multiphase model allows the derivation of a viscoplastic thin-film model.

In conclusion the following new scientific findings are part of the present thesis:

- A new multiphase model with viscoplastic properties is proposed

- The derivation of a new drift-flux equation for viscoplastic media is given
- Analysis of instabilities of the multiphase model and identification of a new necessary condition for well-posedness
- Proposal of energetic derivations of multiphase models, that allows for the identification of consistent free-boundary conditions
- Alternative derivation of a viscoplastic thin-film model through formulation as a variational inequality and proof of existence of solution for a regularized model is given
- Systematic reduction of the multiphase model to thin-film models and presentation of newly found connections between constitutive laws in multiphase and thin-film models

Zusammenfassung

Die vorliegende Arbeit beschäftigt sich mit Multiphasenmodellen für komplexe Flüssigkeiten, insbesondere mit Modellen für konzentrierte Suspensionen. Die Motivation ist gegeben durch die Herleitung eines neuen Dünnfilmmodells für eine Trocknungsfront auf einem Substrat. Das neue Modell hat den Nachteil, dass der genaue Transportmechanismus von Partikeln in der Suspension gemutmaßt wird und sich nicht aus der Rheologie der untersuchten Flüssigkeit herleiten lässt. Des Weiteren sind bei Trocknungsproblemen immer flüssige und trockene Gebiete vorhanden, so dass ein viskoplastisches Modell zu bevorzugen ist, dass beide Zustände simulieren kann.

Zur Lösung dieser Probleme wird ein neuartiges Euler-Euler-Multiphasenmodell vorgeschlagen, das die Massen- und Impulserhaltung der Flüssigkeit und der Partikel getrennt voneinander betrachtet. Dieses Modell beschreibt ein viskoplastisches Verhalten, was anhand der Herleitung einer exakten Lösung für die flache Poiseuille-Strömung gezeigt wird. Wir leiten anschließend mittels asymptotischer Methoden eine Gleichung für den Transport von Partikel in einer viskoplastischen Rheologie her. Danach wird die Stabilität des Multiphasenmodells in gescherten Strömungen untersucht. Wir finden eine vorher unbekannte notwendige Stabilitätsbedingung für Multiphasenmodelle und identifizieren Moden mit transientem Wachstum bei den betrachteten Strömungen.

Die Stabilität wird anschließend noch einmal für allgemeine Strömungen untersucht, indem das Modell aus energetischen Prinzipien neu hergeleitet wird. Dies erlaubt zusätzlich die Herleitung einer mit der Massenerhaltung konsistenten freien Randbedingung.

Da es eine direkte Verbindung zwischen einem viskoplastischen Dünnfilmmodell und unserem Multiphasenmodell gibt, geben wir eine alternative Herleitung des Dünnfilmmodells mittels Dünnfilmnäherung einer variationellen Ungleichung an. Es schließt sich ein Existenzbeweis für eine regularisierte Lösung des Dünnfilmmodells mit Monotoniemethoden an.

Zum Schluss wird das Multiphasemodell auf enthaltene Grenzmodelle mittels asymptotischen Methoden untersucht. Dabei wird unter anderem ein Modell für flache Suspensionen aus dem Multiphasenmodell hergeleitet, dass den Transportmechanismus direkt an die Rheologie der untersuchten Flüssigkeit koppelt und eine neuartige Verbindung zwischen Multiphasenmodellierung und Dünnfilmmodellierung erlaubt. Außerdem wird eine Bedingung angegeben, die es erlaubt, viskoplastische Dünnfilmmodelle aus dem Multiphasenmodell herzuleiten.

Zusammenfassend sind insbesondere die folgenden neuen wissenschaftlichen Erkenntnisse Teil dieser Arbeit:

- Modellierung eines Multiphasenmodells mit viskoplastischer Rheologie
- Herleitung eines Transportmechanismus für Partikel in einem viskoplastischen Medium
- Stabilitätsuntersuchung des neuen Multiphasenmodells und Identifizierung einer vorher unbekannten notwendigen Stabilitätsbedingung
- Neuartige energetische Herleitung von Multiphasenmodellen und Bestimmung von konsistenten freien Randbedingungen
- Alternative Herleitung eines bekannten viskoplastischen Dünnfilmmodells mittels variationeller Ungleichung und Untersuchung auf Existenz von Lösungen eines regularisierten Modells
- Systematische Herleitung von einfacheren Modellen aus dem Multiphasenmodell, insbesondere von Dünnfilmmodellen mit angeschlossenen Transportmechanismus von Partikeln, was eine neuartige Verbindung zwischen Dünnfilmmodellen und Multiphasenmodellen aufzeigt

Danksagung

Die hier vorliegende Dissertation ist das Produkt von drei Jahren Forschung, fünf Jahren Studium und dreizehn Jahren Schulzeit. Ohne die Unterstützung meiner Eltern Claudia und Gerald, meiner Schwester Franziska, meiner Lebensgefährtin Caren und meiner Freunde wären diese Jahre nicht so unbeschwert und erfolgreich gewesen.

Außerdem möchte ich mich bei meinen Betreuern Barbara und Andreas für das interessante Thema und die stets humorvollen Fachdiskussionen bedanken.

Ebenfalls vielen Dank an die ehemaligen und momentanen Mitarbeiter der Fachgruppe "Mathematische Methoden in der Photovoltaik" an der Technischen Universität Berlin - Dirk, Esteban, Maciek, Marion, Sebastian und Sibylle - für die stets freundliche, kommunikative und produktive Arbeitsatmosphäre.

Weiterer Dank geht an das "Kompetenzzentrum Dünnschicht- und Nanotechnologie für Photovoltaik Berlin" und die Technische Universität Berlin für die Finanzierung meiner Forschung.

Contents

Abstract i

Zusammenfassung iii

Danksagung v

Contents vi

1 Introduction 1
- 1.1 Simple fluids and suspensions . . . 4
- 1.2 Modeling particle transport . . . 9
- 1.3 Thin-film models . . . 14
- 1.4 Model for a horizontal drying front of a suspension . . . 17
- 1.5 Overview . . . 22

2 Multiphase model 25
- 2.1 Classes of multiphase models . . . 26
- 2.2 Derivation of an Eulerian-Eulerian model . . . 30
- 2.3 Constitutive laws . . . 38
- 2.4 Non-dimensionalization . . . 41

3 Simple laminar flows 45
- 3.1 Plane Couette flow . . . 45
- 3.2 Plane Poiseuille flow . . . 46
- 3.3 Drift-flux model for plane Poiseuille flow . . . 58
- 3.4 Boundary layer analysis for the drift-flux model . . . 63

4 Stability 65
- 4.1 Introduction . . . 65
- 4.2 Bingham-Orr-Sommerfeld system . . . 67
- 4.3 Governing equations for two-phase flow . . . 74

4.4 Plane Couette flow . . . 79
4.5 Plane Poiseuille flow . . . 88

5 Energy formulation **97**
5.1 Overview of dissipative formulations . . . 97
5.2 The normal velocity condition . . . 101
5.3 Deriving a multiphase model using a gradient flow structure . . . 102
5.4 Derivation of p_c term in energy formulation . . . 107

6 Viscoplastic thin-film equation **113**
6.1 Governing equations . . . 114
6.2 Derivation of thin-film inequality . . . 116
6.3 Solution of thin-film inequality . . . 119
6.4 Introduction into the theory of monotone operators . . . 123
6.5 Existence proof for regularized second order equation . . . 133

7 (Further) Reduced models **139**
7.1 Limit models . . . 140
7.2 Reduction to thin-film models . . . 151

8 Discussion and outlook **161**

Bibliography **165**

A Numerical Methods for Complex Fluid Simulation **175**
A.1 Finite difference method . . . 175
A.2 Numerical scheme for thin-film and drift-flux models . . . 184
A.3 Numerical scheme for the stability problem . . . 184
A.4 Riccati method for the Orr-Sommerfeld-Bingham problem . . . 185

B Vita **191**

Chapter 1

Introduction

The fundamental question leading to this thesis came to light in the University of Potsdam at April the 11th, 2012. A discussion between colleagues from the experimental physics department and our group came to the insight that during the production of organic solar cells a special phenomenon can be observed: A so-called "drying front" moves across the polymeric substrate while being heated as part of the production process, but the experimentalists did not understand the origin of this front and its consequences for the structuring of the solar cells. The modeling of this "toy problem" was given as a first assignment to us. The polymeric substrate can be modeled as a suspension and we soon realized that concentrated suspensions are not well understood. This thesis is meant to broaden the knowledge about macroscopic models for this class of suspensions and multiphase flows in general.

Organic photovoltaics

Since the motivation for this thesis is a better understanding of the structuring steps of organic photovoltaics (OPV), we first sketch the working principle and production steps of an organic solar cell, then we proceed with the idea of thermal annealing and the occurrence of a horizontal drying front and its possible implication for the final morphology of the cell. We will see that the concept of concentrated suspensions is important for this industrial application. This section is just intended as a motivational introduction into the subject and by no means a complete review of the material. For surveys of OPV see e.g. [54, 90] and the references cited therein.

Traditionally, solar cells consist of two semiconductor metalloid materials - a negatively charged n-type and a positively charged p-type material. At the boundary between these materials an electronic potential forms. If light is emitted on the solar cell, an electron and a positively charged hole forms and diffuses through the material. If they encounter the potential, only one of the two is able to pass. Thus, this process separates charges, which can then be collected at opposite sides of the device [94]. Nowadays, most solar cells consist of crystalline or amorphous silicon (c/a-Si), copper indium gallium selenide (CIGS) or Cadmium telluride (CdTe), but materials evolve fast

and new semiconductors are coming into the market, cf. [106]. However, all these materials have the disadvantage, that their production is highly energy demanding and after their lifetime the materials become special waste.

A possible alternative to semiconductor materials are organic solar cells, which do not possess these particular disadvantages, but currently lack efficiency and suffer under a limited lifetime [90]. Organic materials with conjugated atom bonds can be excited using UV light into emitting a closely bonded positive and negative charge - so-called excitons [54]. Nevertheless, these excitons can recombine very fast, losing their ability to produce a free charge, unless they encounter an interface of an electron rich (donor) and an electron poor (acceptor) material, where the bond breaks up and creates a free negative charged electron and positive charged hole. Hence, OPV are usually a blend of at least two materials. A common mixture is *poly(3-hexylthiophene-2,5-diyl):[6,6]-phenyl-C61-butyric acid methyl ester* (P3HT:PCBM), where PCBM is the donor and P3HT is the acceptor material [90]. On the one side the mixture must be thoroughly mixed since the average diffusion length before recombination of an exciton is just between 5 to 10 nm. On the other side, free electrons have a higher possibility of recombining with positive charges when the intermixing of both layers is too strong, as they have a higher chance of encountering a positive charge near an interface on their way to the surface of the OPV, where the electric circuit is attached. This race between length scales requires a tightly controlled structuring process.

Unfortunately, the production of an organic solar cell is by no means as simple as just mixing the two polymers. It is a procedure consisting of several steps. Figure 1.1 shows the most important

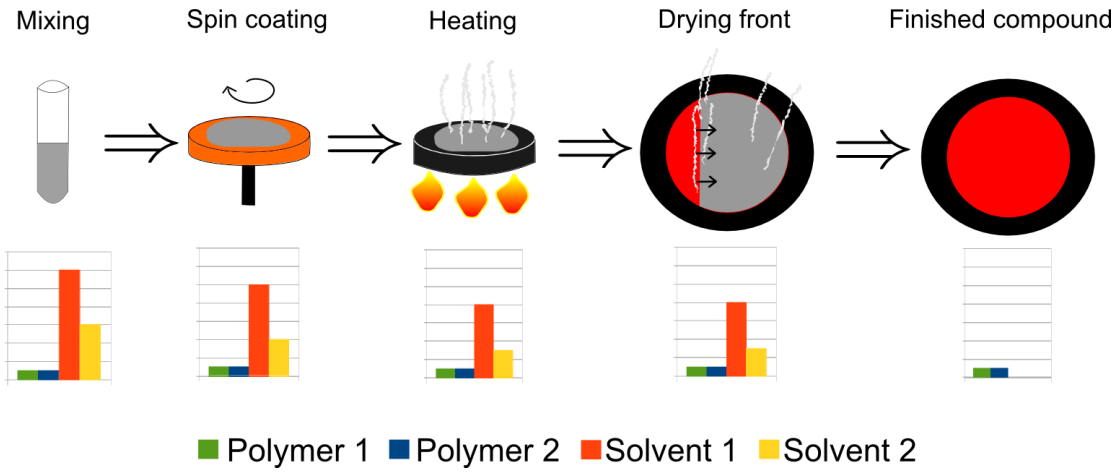

Figure 1.1: The first step in the production is to mix the donor and acceptor materials together with one or more solvents and possibly surfactants in order to get a liquid solution. Next, this solution is put into a spin-coating device in order to produce a flat film. Depending on the used solvents the solution is still wet after spin coating, so it is thermally annealed by putting it on a heater, which evaporates most of the remaining solvents and crystallizes a portion of the molecules. The final step is the back and front contacting as well as sealing of the dried, thin solar cell. The bar charts at the bottom of the figure represent the amount of polymer and solvents contained in the corresponding production step.

production steps for the structuring of the substrate.

The process of *thermal annealing* refers to an application of heat to an unfinished OPV as part of the production. Experiments showed the thermal annealing step changes the morphology of the OPV depending on the time, temperatures and amount as well as the kind of solvents used [8, 71, 108]. In case one uses solvents with high evaporation temperatures, the annealing evaporates the solvents creating a horizontal drying front, which could potentially reorder the molecules. If the annealing continues after evaporation stops, the material starts to form larger uniform domains due to spinodal decomposition, which can result in crystallization [35, 90].

As the liquid solutions used in the production consist of polymers and solvents, they are part of the larger class of complex fluids and in particular concentrated suspensions. Therefore, we study the behavior of this class of fluids for simple flow cases in order to create new insights into this highly complicated production process.

The process of drying

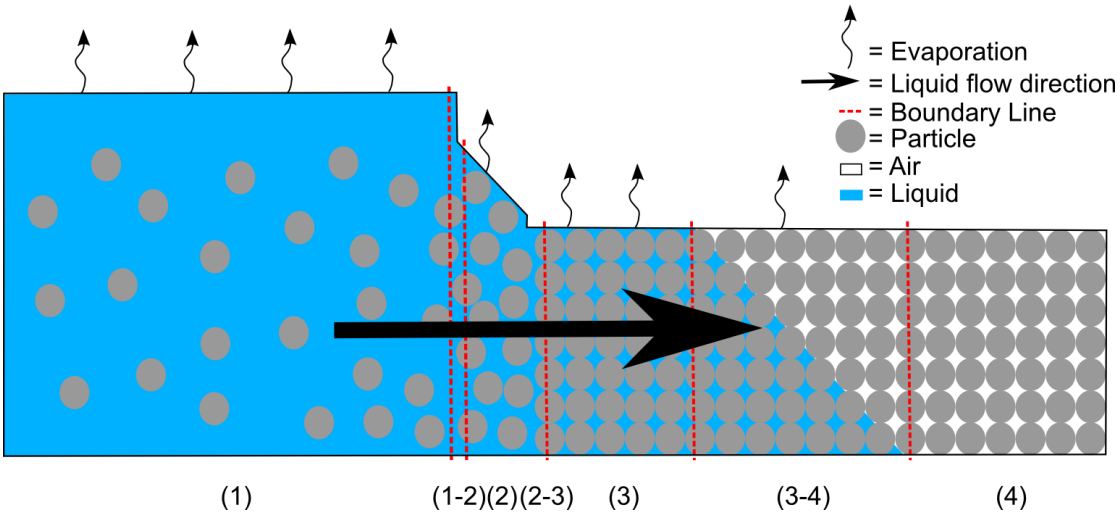

Figure 1.2: Shown is a horizontal drying front due to evaporation of liquid and its regions. Region (1) contains a dilute suspension with properties similar to a simple fluid. Over time evaporation concentrates the particles until jamming takes place as seen in region (2). Further evaporation creates a randomly ordered structure of particles in region (3). The evaporation over (3) sucks water from the liquid regions due to capillary forces and creates a superficial liquid flow into the densely packed regions. If capillary forces balance the pressure gradient by the superficial liquid flow, evaporation decreases the level of liquid between the particles as in region (3-4) until most of the liquid is evaporated and only a solid remains, see region (4). Depending on the material and thickness of the final film, cracks of the solid can appear in region (4).

We just described the significance of the process of drying for organic photovoltaics. Under the process of drying we understand the evaporation of fluid from a suspension, such that only a solid remains. Drying is not a simple transformation from a fluid to a solid, but undergoes

several regions in the process [28, 78, 110]. Figure 1.2 shows there are pure liquid, pure solid and intermediate regions with a complex dynamic between each other.

Li et al. [78] studied a horizontal drying front in more detail. They identified the main regions as described in Figure 1.2. These regions are an apparent fluid region, a jammed region, a densely packed region containing fluids and a dry solid. They found that the number of particles at a point in space is conserved throughout the drying process, which is in contrast to the coffee-stain-effect of a droplet by Deegan et al. [28], where particles are suck into a small region at the edge of the drop. In contrast to the coffee-stain-effect, they further concluded that the particles are not moving with the directed flow of liquid. As they have used mono-dispersed colloids of one kind in their experiments, they could not study a possible vertical structuring. Another known effect is that of a stick-slip motion of the drying front as described by Goehring et al. [48]. They found that the drying process shows three distinct fronts. A leading and a trailing solidification front as well as a cracking front [48]. The stick-slip motion describes an advancement of the leading front, while the trailing front sticks to its position, followed by a sudden movement of the trailing front until it sticks again [48].

The appearance of solid, liquid and intermediate regions in experiments motivated us to study viscoplastic models, which are able to represent solid and liquid behavior, in order to describe the process of drying. However, we first define standard models for suspensions, which do not possess viscoplastic stresses as it allows us to show shortcomings of the traditional models.

1.1 Simple fluids and suspensions

Fluids are omnipresent in our world. Living cells are not possible without water and humans are in need of a constant air supply in order to synthesize adenosine triphosphate - the cell's main energy resource. Our daily electric energy consumption would not be possible without fluids like oil, methane or hydrogen.

Although fluids are omnipresent, it is rather hard to define them exactly. A common definition of a *simple fluid* is twofold: Firstly, it must be a continuum; and secondly, it cannot withstand tangential forces [10, 114]. Nevertheless, some materials are also classified as fluids, although they do not fully comply with this definition of a simple fluid, but rather behave sometimes like solids and sometimes like simple fluids. An example for this behavior are *viscoplastic fluids*, that contain a solid/fluid transition. This transition happens at the *yield stress*, which marks the stress at which the fluid first starts to deform continuously [6]. We define as *fluid* the set of all simple fluids together with viscoplastic fluids.

What is a complex fluid and a suspension?

This and the following chapters contain formulas, which adhere to a uniform notation. Symbols and notations are introduced at the location of their first appearance and reused in the later parts of this thesis. A scalar quantity is denoted by a lower case letter, a vector quantity by a bold lower case letter and a tensorial quantity by a bold uppercase letter or a bold greek letter, e.g.

$$
\begin{aligned}
a &\in \mathbb{R}, & b &: \mathbb{R}^n \to \mathbb{R},\\
\boldsymbol{c} &\in \mathbb{R}^n, & \boldsymbol{d} &: \mathbb{R}^n \to \mathbb{R}^m,\\
\boldsymbol{E} &\in \mathbb{R}^{n\times m}, & \boldsymbol{\varphi} &: \mathbb{R} \to \mathbb{R}^{n\times m}.
\end{aligned}
$$

We denote the unit tensor by $\boldsymbol{I}$ and define the norm for symmetric tensors as

$$|\boldsymbol{A}| = \sqrt{\frac{1}{2}\boldsymbol{A} : \boldsymbol{A}}.$$

We use the shorthand notation $\partial_a f = \frac{\partial f}{\partial a}$ for the partial derivative by a and define the nabla-operator ∇ applied to functions $f : \mathbb{R}^n \to \mathbb{R}$ or $\boldsymbol{g} : \mathbb{R}^n \to \mathbb{R}^n$, respectively, as

$$\nabla f = \operatorname{grad}(f), \qquad \nabla \cdot \boldsymbol{g} = \operatorname{div}(\boldsymbol{g}),$$

where $\operatorname{grad}(\cdot)$ and $\operatorname{div}(\cdot)$ denote the usual gradient and divergence operators. In two-dimensional Cartesian coordinates, i.e. $n = 2$, the nabla-operator can be represented as the vector

$$\nabla = \begin{pmatrix} \partial_x \\ \partial_y \end{pmatrix}$$

and the usual vector operations hold.

In order to understand a complex fluid, we first have to define the terms stress, pressure and shear rate. *Stress* describes the amount of force acting on a surface of a volume element of fluid [10]. Its origin is in the short range interacting forces between fluid particles. Generally, the stress $\boldsymbol{\sigma}$ is split up into a volume changing part, the so-called *pressure* $\boldsymbol{\pi}$, which has non-zero trace and a deforming part, the so-called *deviatoric stress tensor* $\boldsymbol{\tau}$ [10]

$$\boldsymbol{\sigma} = \boldsymbol{\tau} + \boldsymbol{\pi}. \tag{1.1.1}$$

For most fluids the pressure is uniform in every direction, also called isotropic, so that

$$\boldsymbol{\pi} = p\boldsymbol{I}. \tag{1.1.2}$$

However, some fluids - like suspensions - might have a preferred direction, which is called anisotropic and has a pressure of the form

$$\boldsymbol{\pi} = p \begin{pmatrix} 1 & 0 & 0 \\ 0 & \lambda_2 & 0 \\ 0 & 0 & \lambda_3 \end{pmatrix},$$

where $\lambda_2, \lambda_3 > 0$, see e.g. [88]. We do not model anisotropic effects in this thesis, but we sometimes refer to models that include such effects. The *shear rate* describes the spatial change of the fluid velocity. For simple fluids we define it as

$$\dot{\gamma} = \nabla \boldsymbol{u} + (\nabla \boldsymbol{u})^T - \frac{2}{3}(\nabla \cdot \boldsymbol{u})\boldsymbol{I}. \tag{1.1.3}$$

This is equal to the so-called strain rate in case of incompressible fluids, for a definition see (1.1.8) and [10]. A fluid with a proportional relationship between the deviatoric stress and the shear rate, i.e.

$$\boldsymbol{\tau} = \mu\dot{\gamma}, \tag{1.1.4}$$

is called a *Newtonian fluid*, where the positive constant of proportion μ is called *dynamic viscosity* and has physical dimension of $\mathrm{kg\,m^{-1}\,s^{-1}}$. Alternatively, some applications use a proportionality factor that is divided by the density of the fluid, which is called *kinematic viscosity* and has dimensions $\mathrm{m^2\,s^{-1}}$. If the dimension of the proportionality factor are not central to the given arguments, we refer to either of them as *viscosity*.

A *complex fluid* is a fluid that is not a Newtonian fluid. Thus, a complex fluid has a non-proportional relationship between their deviatoric stress and shear rate, and is sometimes also referred to as non-Newtonian fluid or non-linear fluid [72].

Newtonian fluids are most often mono-molecular with small molecular weight. Water is a good[1] example of a Newtonian fluid. On the other side, fluids consisting of long polymers or different substances are often complex fluids. A simple example of a stress-relation in a complex fluid is

$$\boldsymbol{\tau} = \mu \dot{\boldsymbol{\gamma}}^{\alpha},$$

with positive $\alpha \neq 1$. For $\alpha \in]0, 1[$ and $\alpha > 1$ they are respectively classified as shear-thinning and shear-thickening fluids. Other classes of complex fluids are so-called viscoelastic fluids, whose stress-shear-rate dependence contains a time dependence. In this work we study complex fluids of viscoplastic type with a yield-stress $\tau_0 > 0$. The simplest stress-shear-rate relation of a viscoplastic fluid is

$$\begin{aligned} \boldsymbol{\tau} &= \mu \dot{\boldsymbol{\gamma}} && \text{for } |\boldsymbol{\tau}| > \tau_0 \\ \dot{\boldsymbol{\gamma}} &= 0 && \text{for } |\boldsymbol{\tau}| \leq \tau_0, \end{aligned}$$

which is also referred to as Bingham fluid. Figure 1.3 visualizes the different classes of fluids by the shape of their shear stress as function depending on shear rate.

A special class of complex fluids are *dispersions*. Dispersions are generally of two or more components that do mix, but not chemically react. Depending on the state of matter of the components they are classified as *emulsions* (liquid-liquid), *aerosol* (gas-liquid), *suspensions* (particles-liquid) or *granulate* (particles-gas). Suspensions are further classified depending on the size of the dispersed particles. Dispersions consisting of large particles (greater 1 µm), that settle in time under gravity are just named suspensions. A mixture with small particles (between 1 nm and 1 µm) are called *colloids* as they are neutral buoyance, hence do not settle in experimental time. Even smaller particles (smaller 1 nm) are called *Brownian suspensions*, as Brownian motion becomes dominant.

Packing and jamming

In this thesis we are mainly interested in non-Brownian suspensions. As they are a mix of at least two phases - one liquid and one solid phase - their rheology depends on the number of solids relative to the amount of liquid in the mix. Therefore, we need a quantity that measures this ratio.

Imaging a suspension consisting of n identical particles suspended in a liquid with a total volume V. The amount of particles in the suspensions has an upper limit not only due to the volume of

[1] Water might also exhibit a non-linear behavior, but is considered to be Newtonian for most reasonable uses.

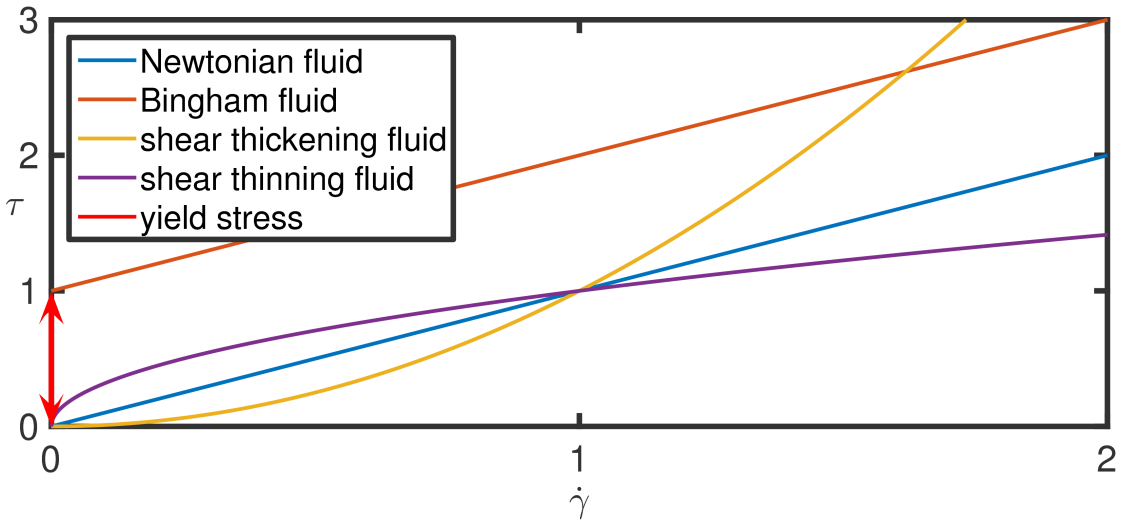

Figure 1.3: Shown is the relation of shear stress as a function of shear rate. A simple linear curve going through the origin describes a Newtonian fluid. Bingham fluids show also a linear shear stress - shear rate curve, but do not start at the graph's origin. The distance between the origin and the start of the Bingham curve is the yield stress. Many non-Newtonian fluids show nonlinear curves, which are either steepening or flatten with increasing shear rate and correspond to shear thickening or shear thinning fluids, respectively.

a single particle, V_p, relative to the total volume, i.e.

$$nV_p \leq V, \tag{1.1.5}$$

but also due to geometric constraints of the shape and ordering of particles. In order to describe the volume concentration of particles it is handy to define the so-called *volume fraction*, ϕ, as

$$\phi = \frac{nV_p}{V}. \tag{1.1.6}$$

We have $\phi \in [0, \phi_{\text{crit}}]$ with a *maximum packing* value of $\phi_{\text{crit}} = 1$ due to condition (1.1.5). For certain geometric shapes the maximum packing value is smaller. For example spherical particles allow values of $\phi_{\text{crit}} \approx 0.63$ in case of *random packing* and $\phi_{\text{crit}} \approx 0.74$ in case of *close packing* of the particles [113].

Jamming describes a state of a suspension, at which the viscosity divergence due to particle concentration reaching maximum packing and particles start to touch each other [80]. However, a fluid is still able to flow past them and particles can still be packed even denser due to particle deformation or repacking into different order. Jamming can occur for volume fractions as low as $\phi \approx 0.3$ up until closed packing. The relevance of jamming is, that suspensions start to show properties of solids rather than liquids once they reach this state.

Single-phase models for fluids

In fluid mechanics, it is common to define the *material derivative* $\frac{D}{Dt}$ as

$$\frac{D\xi}{Dt} = \frac{\partial \xi}{\partial t} + \boldsymbol{u} \cdot \nabla \xi,$$

where ξ is some arbitrary quantity depending on time and space. Its physical interpretation is a quantity changing in time and in the same moment being transported with the velocity $\boldsymbol{u}$ in Eulerian frame [10].

A fluid's mass, momentum and entropy conservation is described by the *Navier-Stokes equations*

$$\frac{1}{\rho}\frac{D\rho}{Dt} = \nabla \cdot \boldsymbol{u}, \tag{1.1.7a}$$

$$\rho \frac{D\boldsymbol{u}}{Dt} = \nabla \cdot \boldsymbol{\sigma} + \rho \boldsymbol{f},$$

$$T\frac{DS}{Dt} = \Phi + \frac{1}{\rho}\nabla \cdot (k \nabla T), \tag{1.1.7b}$$

where ρ is the density, $\boldsymbol{u}$ the velocity,$\boldsymbol{\tau}$ the stress, $\boldsymbol{f}$ external forces, S the entropy, k the thermal conductivity, T the temperature and Φ the rate of dissipation of mechanical energy [10]. For most practical considerations of slow moving fluids one assumes

$$\frac{D\rho}{Dt} = 0, \tag{1.1.8}$$

which holds approximately true for most fluids in the case of slow motion, with small temperature variations and small pressures.[2] Then, the mass conservation (1.1.7a) becomes the *incompressibility condition* $\nabla \cdot \boldsymbol{u} = 0$. It owes its name to the fact that after integration over any compact volume Ω with a piecewise smooth boundary and using the divergence theorem, it yields

$$\oint_{\partial\Omega} \boldsymbol{u} \cdot \boldsymbol{n} \, \mathrm{d}\boldsymbol{s} = 0, \tag{1.1.9}$$

where $\boldsymbol{n}$ denotes the unit normal pointing outwards of the surface. Equation (1.1.9) in turn implies that the volume of fluid flowing in and out of Ω has to cancel each other out. An even stronger assumption, we use throughout this thesis, is to consider the density to be constant, which directly implies (1.1.8). Further, using equation (1.1.8) the entropy conservation (1.1.7b) decouples from the other two equations. Thus, we receive the so-called *incompressible Navier-Stokes equations* [10]

$$\nabla \cdot \boldsymbol{u} = 0, \tag{1.1.10a}$$

$$\rho \frac{D\boldsymbol{u}}{Dt} = \nabla \cdot \boldsymbol{\sigma} + \rho \boldsymbol{f}. \tag{1.1.10b}$$

[2] The terms "slow" and "small" are to be understood in dependence of the fluid under consideration. For most practical applications water fulfills this incompressibility property although velocities and pressures can become huge, whereas gases hardly ever fulfill this relation in real world applications.

An incompressible Newtonian fluid with a Cauchy stress $\boldsymbol{\sigma}$ of the form (1.1.1), (1.1.2), (1.1.4) yields

$$\nabla \cdot \boldsymbol{u} = 0, \tag{1.1.11a}$$

$$\rho \left(\frac{\partial \boldsymbol{u}}{\partial t} + \boldsymbol{u} \cdot \nabla \boldsymbol{u} \right) = \mu \Delta \boldsymbol{u} - \nabla p + \rho \boldsymbol{f}, \tag{1.1.11b}$$

which is the most often encountered form of these equations.

The formulation of a PDE model is incomplete without stating appropriate boundary conditions. Common choices for the incompressible Navier-Stokes equations (1.1.10b) are the so-called *no-slip condition*

$$\boldsymbol{u} = \boldsymbol{0}$$

at solid boundaries and the *stress condition*

$$\boldsymbol{\sigma} \cdot \boldsymbol{n} = \sigma_0 \kappa \boldsymbol{n} + \nabla_S \sigma_0$$

at free-boundaries [10], where σ_0 is the surface tension, κ the surface curvature and ∇_S the surface gradient defined as

$$\nabla_S f := (\boldsymbol{I} - \boldsymbol{n} \otimes \boldsymbol{n}) \nabla f.$$

If the free-boundary is allowed to move, an additional boundary condition is needed, cf. Section 1.2.

1.2 Modeling particle transport

The process of drying is a phenomenon dominated by the transport of particles and liquid. As seen from the experiments presented before, particles are transported through convection and conserved in the process. For a mix of $n \in \mathbb{N}$ components the total density is defined as weighted average of the individual component's densities ρ_k, i.e.

$$\rho = \sum_{k=1}^{n} \phi_k \rho_k,$$

where ϕ_k is the k-th component volume fraction. The dynamic of the total density is described by (1.1.7a) and the k-th component fulfills the mass conservation [32]

$$\partial_t (\phi_k \rho_k) + \nabla \cdot (\boldsymbol{u}_k \phi_k \rho_k) = S_k, \tag{1.2.1}$$

where S_k is a possible sink or source term, e.g. due to chemical reactions between the components. Now suppose we have just two components, liquid (f) and particles (s), that do not react and have constant densities ρ_f and ρ_s, then equations (1.2.1) can be rewritten as

$$\partial_t \phi_f + \nabla \cdot (\boldsymbol{u}_f \phi_f) = 0, \tag{1.2.2a}$$

$$\partial_t \phi_s + \nabla \cdot (\boldsymbol{u}_s \phi_s) = 0. \tag{1.2.2b}$$

Since the volume fractions fulfill $\phi_s + \phi_f = 1$ it is sufficient to just consider (1.2.2b) and we define

$$\phi \equiv \phi_s.$$

This shifts the problem of describing the particle transport into finding a suitable expression for the particle velocity $\boldsymbol{u}_s$. The conceptual problem with the modeling of $\boldsymbol{u}_s$ is to find expressions that are consistent with the constitutive laws used in the total momentum equation (1.1.10b) for the stress and force terms. There is an immense number of expressions in use for $\boldsymbol{u}_s$, for surveys see e.g. [61, 82]. Most expressions are derived by conservation principles, where diffusive and convective relations are left open in the form of free parameters, which are taken from experiments and are specific to certain flow situations. We continue by stating some common expressions for $\boldsymbol{u}_s$.

Drift flux model

Direct modeling of the particle velocity is rather cumbersome and it is typical to make a so-called drift-flux ansatz, i.e. splitting the particle velocity $\boldsymbol{u}_s$ into the volumetric velocity

$$\boldsymbol{v} = \sum_{k=1}^{n} \phi_k \boldsymbol{u}_k$$

and a drift term [60, 82], i.e.

$$\boldsymbol{u}_s = \boldsymbol{v} + \boldsymbol{u}_d.$$

Then, an expression for the drift velocity $\boldsymbol{u}_d$ is formulated. As the volumetric velocity $\boldsymbol{v}$ is divergence free, see sum of (1.2.2), the transport equation (1.2.2b) becomes

$$\partial_t \phi + \boldsymbol{v} \nabla \phi = -\nabla \cdot (\boldsymbol{u}_d \phi),$$

which shows the particles are undergoing convective transport with $\boldsymbol{v}$ but drift by $\boldsymbol{u}_d$ - owing to the name of the model, cf. [82]. It is not necessary to define a drift velocity for the liquid, i.e.

$$\boldsymbol{u}_f = \boldsymbol{v} + \boldsymbol{u}_{fd},$$

since we can always use the relation

$$\phi \boldsymbol{u}_d + (1 - \phi) \boldsymbol{u}_{fd} = 0.$$

For the case of neutral buoyance particles of a concentrated suspension Leighton et al. [76] proposed a model for the drift velocity, which has been later applied to Couette and Poiseuille flows by Phillips et al. [103]. They propose

$$\boldsymbol{u}_d = a^2 K_c \nabla \cdot \left(\phi \nabla (|\dot{\boldsymbol{\gamma}}| \phi) \right) + a^2 K_\nu \nabla \cdot \left(|\dot{\boldsymbol{\gamma}}| \phi^2 \frac{1}{\mu} \nabla \mu \right), \tag{1.2.3}$$

where K_c and K_ν are constants and a is the particle radius. The exact numbers for K_c and K_ν are still unknown, but it is assumed commonly that $\frac{K_c}{K_\nu} = 0.66$ [95]. Expression (1.2.3) has been first derived by experimental method and scaling arguments by Leighton and Acrivos [76], but is later claimed to be contained in multiphase formulations, see [95].

Other flux models

Alternative approaches for the computation of the particle velocity do exist, see e.g. [82]. A popular alternative is the algebraic-slip model, often abbreviated as ASM [61, 102] and the diffusive model [82]. The basic idea of the diffusive model is to compute the momentum and mass conservation equations for the mass-weighted mixture velocity of n phases, i.e.

$$\boldsymbol{u}_m = \frac{\sum_{k=1}^{n} \rho_k \phi_k \boldsymbol{u}_k}{\sum_{k=1}^{n} \rho_k \phi_k}$$

and derive a term for the diffusive velocity $\boldsymbol{u}_D$, i.e.

$$\boldsymbol{u}_s = \boldsymbol{u}_m + \boldsymbol{u}_D.$$

This yields an equation of the form

$$\partial_t \phi + \nabla \cdot (\phi \boldsymbol{u}_m) = -\nabla \cdot (\phi \boldsymbol{u}_D).$$

As $\boldsymbol{u}_D$ can itself depend on $\nabla\phi$, this might be called a diffusion equation. In order to get an expression for $\boldsymbol{u}_D$ it is rewritten into a term containing the slip-velocity $\boldsymbol{u}_S$, that is defined as the difference between fluid and particle velocity [61]

$$\boldsymbol{u}_s = \boldsymbol{u}_f + \boldsymbol{u}_S.$$

Then, the slip velocity is computed using force balances yielding algebraic relations, see for example [102]. This approach is referred to as algebraic-slip model. The ASM can be used for flow problems, where the particles are relatively fast reaching a stationary velocity compared to the time scale characterizing the general flow [82], i.e. the forces acting on the particles must be in equilibrium [102]. However, this method is not currently suited for high concentrations of particles or for non-Newtonian fluids near turbulence [82]. For equal and constant densities, we have $\boldsymbol{u}_m = \boldsymbol{v}$ and the diffusive and drift-flux model coincide.

Darcy's law

As mentioned before, some solid materials allow fluid to pass through them under an applied pressure gradient. This class of solids is often referred to as porous media [10]. In the case of porous media the expression for the particle velocity is often trivially $\boldsymbol{u}_s = 0$. However, the liquid's momentum conservation has to be solved in a complicated domain, now. Avoiding this difficulty, a common relation between the applied pressure and the flow through the porous media under gravity is expressed by Darcy's law as [10, 52]

$$\bar{\boldsymbol{u}} = -\frac{k}{\mu}(\nabla p + \rho_f g \nabla y), \tag{1.2.4}$$

where

$$\bar{\boldsymbol{u}} = \phi_f \boldsymbol{u}_f \tag{1.2.5}$$

is the seepage velocity and k is the permeability depending on size and shape of the particles often given by the Kozeny-Carman relation [52] as

$$k = K \frac{{\phi_f}^3}{{\phi_s}^2}, \tag{1.2.6}$$

where K is a constant. This relation has been derived by experiment and averaging methods, cf. [131]. Well-known modifications of Darcy's law are due to Forchheimer [40] for the inertial regime and due to Brinkman [18] for better accounting of viscosity effects.

Stress relations for particle transport

Experimental results dictate that the viscosity of a suspension should depend on the amount of particles it contains. Thus, the stress strain relation (1.1.4) is not adequate for complex fluids. For most parts, this thesis deals with suspensions. Therefore, we list the two most common forms of the stress-strain relations for suspensions.

A common stress-strain relation for dilute suspensions of $\phi < 0.02$ [10] has been proposed by Einstein (cf. [37] and its correction [38]) as

$$\boldsymbol{\tau} = \mu \left(1 + \frac{5}{2}\phi\right) \dot{\boldsymbol{\gamma}}.$$

Higher order corrections are also known [113]. For the opposite case of highly concentrated suspensions a common choice is due to Krieger and Dougherty [72, 113]

$$\boldsymbol{\tau} = \mu \left(1 - \frac{\phi}{\phi_{\text{crit}}}\right)^{-\mu_i \cdot \phi_{\text{crit}}} \dot{\boldsymbol{\gamma}}, \tag{1.2.7}$$

where ϕ_{crit} is the maximum packing coefficient and μ_i is the intrinsic viscosity. In the case of spheres it is set as $\mu_i = 5/2$, and we retrieve Einstein's limit for dilute suspensions as a first order Taylor approximation of (1.2.7).

These two choices by Einstein and Krieger-Dougherty are not exhaustive, see [72, 113] for further proposals, which might also include normal stress differences, elasticity, shear-thinning and shear-thickening effects.

Mass conservation at a free boundary

Whenever there is a moving free-boundary in our model, there is need for a boundary condition guaranteeing mass-conservation. Therefore, we define the evaporative mass flux of a quantity ξ over the interface as [96, 97]

$$J_\xi = \left(\rho\xi(\boldsymbol{u}_\xi - \boldsymbol{u}_i) + \boldsymbol{\omega}_\xi\right) \cdot \boldsymbol{n}, \tag{1.2.8}$$

where $\boldsymbol{u}_\xi$ is the velocity of phase ξ, $\boldsymbol{\omega}_\xi$ are non-advective fluxes and $\boldsymbol{u}_i$ the interface velocity, respectively. This equation is commonly referred to as kinematic boundary condition.

For two-dimensional thin-film models (cf. Section 1.3), using the free boundary $h(t, x)$, the normal interface velocity can be written as

$$\boldsymbol{u}_i \cdot \boldsymbol{n} = \frac{\partial_t h}{\sqrt{1 + (\partial_x h)^2}}.$$

Then, the total mass conservation can be expressed using equation (1.2.8) and setting $\boldsymbol{\omega} = 0$ and $\xi = 1$ (as well as dropping the subscripts for total quantities) as

$$\frac{J}{\rho} = (u, v) \cdot \frac{(-\partial_x h, 1)}{\sqrt{1 + (\partial_x h)^2}} - \frac{\partial_t h}{\sqrt{1 + (\partial_x h)^2}} \qquad \text{at } y = h(t, x).$$

In case of asymptotic methods or linearizations, we use the Landau order symbols O and o, which are defined as [36]

$$f = O(g) \text{ for } \varepsilon \to 0+ \quad :\Leftrightarrow \quad \exists\, k, C > 0 : |f(\varepsilon)| \leq k|g(\varepsilon)| \text{ for } 0 < \varepsilon < C$$

and

$$f = o(g) \quad :\Leftrightarrow \quad \lim_{\varepsilon \to 0} \frac{f(\varepsilon)}{g(\varepsilon)} = 0.$$

In order to denote comparable orders in asymptotic expressions, we define

$$f \sim g \quad :\Leftrightarrow \quad f = O(g) \text{ and } g = O(f).$$

Note that for thin-film models, we have

$$\sqrt{1 + (\partial_x h)^2} = 1 + O(\varepsilon),$$

with $\varepsilon > 0$ very small, so typically the thin-film kinematic boundary condition is approximated by the equation

$$\partial_t h + u \partial_x h - v = -\frac{J}{\rho} \qquad \text{at } y = h(t, x).$$

In case of no-slip boundary conditions at $y = 0$, usage of the incompressibility condition (1.1.10a) gives

$$\partial_t h(t, x) + \partial_x \int_0^{h(t,x)} u(t, x, y)\, \mathrm{d}y = -\frac{J(t, x)}{\rho}. \tag{1.2.9}$$

Considering $\xi = \phi$, we can express the mass conservation of individual phases. Using equation (1.2.8) and choosing the phase velocity equal to the total velocity $\boldsymbol{u}_\xi = \boldsymbol{u}$; the non-advective fluxes as diffusive flux $\boldsymbol{\omega}_\phi = -\rho D \nabla \phi$ and neglecting evaporation $J_\phi = 0$, we get

$$0 = \Big(\phi(\boldsymbol{u} - \boldsymbol{u}_i) - D\nabla\phi\Big) \cdot \boldsymbol{n}$$

and for thin-film models

$$\phi \partial_t h = -\partial_x h(u\phi - D\partial_x \phi) + v\phi - D\partial_y \phi \qquad \text{at } y = h(t, x), \tag{1.2.10}$$

where $D > 0$ is some diffusion coefficient and $D\partial_x \phi$ is often of higher order in ε, so that this term is neglected, see e.g. [111].

1.3 Thin-film models

In order to understand a fluid in an arbitrary geometry we have to consider the full set of Navier-Stokes equations (1.1.10). Unfortunately, there is no analytic solution to the Navier-Stokes equations known and a numerical computation - if possible - is harder to analyze. However, we can reduce the full set of equations to simpler formulations for special geometries. One particular case is the *thin-film approximation*[3], which is applicable to fluids with asymmetric shape, where the size in one direction is much smaller than in the others directions. A typical example is the sessile drop, whose height Y is much smaller than its length X, see Figure 1.4. The literature for thin-film approximations is extensive, see e.g. [4, 24, 97] and the references therein.

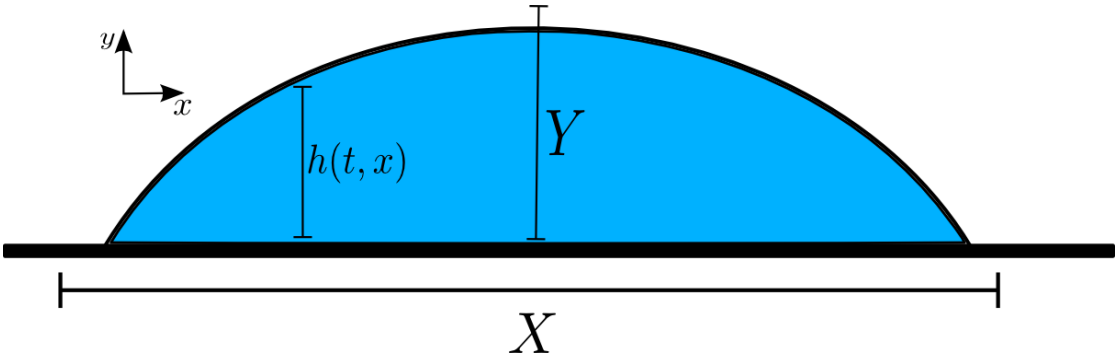

Figure 1.4: Geometry of a sessile drop allowing for a thin-film approximation, since the typical height scale Y is much smaller than the typical length scale X, so that the ratio X/Y is an asymptotically small number. The final equations of a thin-film model are formulated in terms of the free-boundary $h(t, x)$.

Derivation

The thin-film approximation is derived by first nondimensionalizing the Navier-Stokes equation and then using an asymptotic expansion ansatz in terms of a small parameter ε. We continue by showing the derivation for the two-dimensional Cartesian case. For a Newtonian incompressible fluid the two-dimensional Navier-Stokes equations in Cartesian coordinates are, cf. (1.1.11),

$$\begin{aligned} \partial_x u + \partial_y v &= 0, \\ \rho(\partial_t u + u\partial_x u + v\partial_y u) &= -\partial_x p + \mu(\partial_{xx} u + \partial_{yy} u) + \rho f_1, \\ \rho(\partial_t v + u\partial_x v + v\partial_y v) &= -\partial_y p + \mu(\partial_{xx} v + \partial_{yy} v) + \rho f_2, \end{aligned}$$

where we assume f_1, f_2 to be constants. Boundary conditions are the no-slip conditions at the substrate

$$u = v = 0 \quad \text{at } y = 0, \tag{1.3.1a}$$

[3] Other common names are lubrication approximation and long-wave approximation.

and stress-conditions at the free-boundary $h(t,x)$, i.e.

$$\boldsymbol{n}\cdot(-p\boldsymbol{I}+\boldsymbol{\tau})\cdot\boldsymbol{n}=\pi_0 \quad \text{at } y=h(x,t), \tag{1.3.1b}$$
$$\boldsymbol{t}\cdot(-p\boldsymbol{I}+\boldsymbol{\tau})\cdot\boldsymbol{n}=t_0 \quad \text{at } y=h(x,t), \tag{1.3.1c}$$

where π_0 and t_0 are the applied normal and shear stresses, respectively. Since we allow the free-boundary to move, we also demand the kinematic boundary condition (1.2.9) to hold at $y=h(x,t)$. We make the nondimensionalization ansatz

$$x=X\hat{x}, \qquad y=Y\hat{y}, \qquad t=T\hat{t}, \qquad \varepsilon=\frac{Y}{X},$$
$$u=U\hat{u}, \qquad v=V\hat{v}, \qquad p=P\hat{p}, \qquad h=Y\hat{h}.$$

Dropping the hats and rearranging, the continuum equation yields

$$\varepsilon\frac{U}{V}\partial_x u+\partial_y v=0. \tag{1.3.2}$$

The incompressibility condition (1.3.2) suggests a choice of

$$V=\varepsilon U$$

for the velocity scales. For the time and pressure scales we have multiple options to choose from depending on what the dominant driving force in our model is. For negligible inertial terms a common choice is [24, 97]

$$T=\frac{X}{U}, \qquad P=\frac{UX\mu}{Y^2}.$$

Applying these scales to the momentum equations and rearranging, it gives

$$\varepsilon\mathrm{Re}(\partial_t u+u\partial_x u+v\partial_y u)=-\partial_x p+\varepsilon^2\partial_{xx}u+\partial_{yy}u+F_1,$$
$$\varepsilon^3\mathrm{Re}(\partial_t v+u\partial_x v+v\partial_y v)=-\partial_y p+\varepsilon^4\partial_{xx}v+\varepsilon^2\partial_{yy}v+F_2,$$

where we have introduced the non-dimensional forces

$$F_1=\frac{\rho Y^2}{\mu U}f_1, \qquad F_2=\varepsilon\frac{\rho Y^2}{\mu U}f_2,$$

and the Reynolds number

$$\mathrm{Re}=\frac{\rho UY}{\mu},$$

which represents the ratio of inertial and viscous forces. Making an expansion ansatz of the form

$$u=u_0+u_1\varepsilon+u_2\varepsilon^2+O(\varepsilon^3)$$
$$v=v_0+v_1\varepsilon+v_2\varepsilon^2+O(\varepsilon^3)$$
$$p=p_0+p_1\varepsilon+p_2\varepsilon^2+O(\varepsilon^3)$$

and looking for leading order terms in ε yields

$$0 = -\partial_x p + \partial_{yy} u + F_1, \tag{1.3.3}$$
$$0 = -\partial_y p + F_2, \tag{1.3.4}$$

where we have retained the force terms as they might contain leading order contributions depending on the considered forces. Doing the same procedure for (1.3.1), the leading order boundary conditions are

$$\begin{aligned} u = v = 0 \quad & \text{at } y = 0, \\ -p = \Pi_0 \quad & \text{at } y = h, \\ \partial_y u = T_0 \quad & \text{at } y = h, \end{aligned}$$

with the scalings $t_0 = \varepsilon P T_0$ and $\pi_0 = P\Pi_0$. Integration of (1.3.4) yields

$$p(t, x, y) = F_2 y + p_1(t, x), \tag{1.3.5}$$

and using this equation in (1.3.3) gives

$$0 = -\partial_x p_1 + \partial_{yy} u + F_1.$$

Integrating from y to h and using the tangential stress condition yields

$$0 = (-\partial_x p_1 + F_1)(h - y) + T_0 - \partial_y u,$$

and integration from 0 to y using the no-slip conditions

$$u = \Big(-\partial_x p_1 + F_1 \Big)\Big(hy - \frac{y^2}{2} \Big) + T_0 y. \tag{1.3.6}$$

Substitution of (1.3.6) in the kinematic equation (1.2.9) and usage of (1.3.5) as well as the normal stress condition (1.3.1b) yields

$$\partial_t h + \partial_x \left(\big[\partial_x(\Pi_0 + F_2 h) + F_1\big] \frac{h^3}{3} + T_0 \frac{h^2}{2} \right) = -J, \tag{1.3.7}$$

where $J = \varepsilon U \rho \hat{J}$ is the scaling for the evaporation. In order to have a complete model the correct number of boundary conditions must be specified for h, which depend on the concrete flow situation.

Remarks

Since we assumed $\varepsilon = Y/X$ to be small, equation (1.3.7) is only valid for small angles, because $\partial_x h$ must stay of order one. This might create problems for solutions, where a shock-like profile emerges. Alternative derivations have been proposed in order to circumvent this problem, see e.g. [119].

The small parameter ε is usually chosen as quotient of two length scales [97]. Alternative approaches are based on choosing a non-dimensional number encoding a driving force as the small parameter, which again is scaling as a quotient of two length scales, e.g. the Capillary number [3].

A standard choice for surface tension driven fluids is, cf. [97],

$$J = F_1 = F_2 = T_0 = 0 \quad \text{and} \quad \Pi_0 = \partial_{xx} h,$$

which gives the equation

$$\partial_t h + \partial_x \Big(\partial_{xxx} h \frac{h^3}{3} \Big) = 0.$$

This equation gives a nonintegrable singularity at a contact line [55, 97]. There are at least two solutions to this problem. The first is to change the no-slip boundary conditions into allowing tangential slip [97]. Yet, for the case of non-zero evaporation, $J > 0$, this is still insufficient, see e.g. [81], thus another solution is to use a *disjoining pressure* that creates a precursor film, see [4, 81, 97]. The motivation for such a disjoining pressure are intermolecular forces between a substrate and the fluid that prefer a small layer of fluid on top of the surface. A common form for the disjoining pressure is

$$\Pi_0 = \frac{\Psi}{h^3},$$

with $\Psi > 0$ the Hamaker constant, see e.g. [4].

It is possible to generalize our derivation to x-dependent viscosities of the form $\bar{\mu} = \mu\, \eta(x)$. Then, the final equation becomes

$$\partial_t h + \partial_x \left(\frac{1}{\eta} \big(\big[\partial_x (\Pi_0 + F_2 h) + F_1 \big] \frac{h^3}{3} + T_0 \frac{h^2}{2} \big) \right) = -J.$$

This shows the movement of a thin fluid becomes slower for increasing viscosity and stops in case the viscosity goes towards infinity. Note, for concentrated suspensions without variation of concentration in the y-direction the Krieger-Dougherty relation (1.2.7) implies that for $\phi \to \phi_{\text{crit}}$ the movement of a fluid stops.

1.4 Model for a horizontal drying front of a suspension

So far we have derived the general form of a thin-film model in Section 1.3. In order to simulate a horizontal drying front on a heated plate, we combine models for a horizontal drying front by Routh and Russel [111] with the model of for a drying drop of a suspension on a heated surface by Ajaev [3]. We show that the model is indeed capable to predict the form of a horizontal drying front, however, it is not capable to reconstruct the experimental results of Li et al. [78] or Goering et al. [48]. In particular, the model does not correctly predict velocities and timings of the drying front, nor is it capable to predict morphologic changes or stick-slip motion.

Using the framework of Section 1.3, we are left with choosing specific forces and stresses for the horizontal drying front on a heated surface. Following Ajaev [3], we choose to scale the horizontal velocity with surface tension constant σ_0 and a Capillarity number C as

$$U = \frac{\sigma_0}{\mu} C, \qquad C = \frac{Y^3}{X^3},$$

and gravitational forces as

$$f_1 = 0 \qquad \Rightarrow \qquad F_1 = 0, \tag{1.4.1}$$
$$f_2 = -g \qquad \Rightarrow \qquad F_2 = -B, \tag{1.4.2}$$

where $B = \rho g X^2/\sigma_0$ is the nondimensional Bond number.

For the derivation of the tangential stress and evaporative flux we just state the necessary equations and the final terms. We are using the one-sided model of evaporation [4, 92]. The surface tension is described by Eötvös rule

$$\sigma = \sigma_0 - \gamma(T^* - T_S^*)$$

and the temperature T^* by the convective heat equation

$$\partial_t T^* + \boldsymbol{u} \cdot \nabla T^* = D_T \Delta T^*,$$

where γ is a constant, D_T a heat diffusion coefficient and T_S^* the saturation temperature. The used scales are the modified Marangoni number and non-dimensional temperature

$$M = \gamma T_S^*/\sigma_0, \qquad\qquad T = \frac{T^* - T_S^*}{T_S^* \frac{Y^2}{X^2}}.$$

If we choose the diffusion constant as $D_T = U\,Y$, then we get the leading order nondimensional equations

$$\frac{\sigma}{\sigma_0} = 1 - \varepsilon^2 M T,$$
$$\partial_{yy} T = 0, \tag{1.4.3}$$

where we kept the leading nonconstant orders in σ for use in the shear stress. The boundary conditions for the temperature are [3]

$$T = C_0 \qquad \text{for } y = 0,$$
$$J = -\partial_y T \qquad \text{for } y = h, \tag{1.4.4}$$

where condition (1.4.4) comes from the one-sided model of evaporation and assumes the velocity scale

$$U = \frac{D_T T_S^* \varepsilon}{\rho \mathcal{L}},$$

with $\mathcal{L}$ a constant describing the latent heat of evaporation. The normal stress contains contributions of the surface tension and a disjoining pressure. It is

$$\pi_0 = \kappa\sigma + \frac{\varepsilon A}{h^3} \qquad \Rightarrow \qquad \Pi_0 = \partial_{xx} h + \frac{\psi}{h^3}, \tag{1.4.5}$$

where we used the Hamaker constant $\psi = A/(\sigma_0 X^2 C)$ and the surface curvature definition [97]

$$\kappa = -\nabla \cdot \boldsymbol{n} = \frac{\partial_{xx} h}{\left(1 + (\partial_x h)^2\right)^{3/2}}.$$

Defining the tangential stress and integrating the temperature equation (1.4.3) yields

$$t_0 = \nabla_s \sigma \qquad \Rightarrow \qquad T_0 = M\partial_x(Jh). \tag{1.4.6}$$

The evaporation is defined by a nondimensional non-equilibrium condition of Ajaev and Homsy [3, 5] as

$$KJ = -\delta\Pi_0 + T \qquad \text{at } y = h,$$

so the evaporative flux becomes

$$J = \frac{C_0 - \delta(\partial_{xx}h + \psi h^{-3})}{K + h}. \tag{1.4.7}$$

The nondimensional parameter K describes kinetic effects at the interface and δ models effects of pressure change on the interface temperature, see [3]. Using (1.4.1), (1.4.2), (1.4.5), (1.4.6) and (1.4.7) in (1.3.7) the final equation reads

$$\begin{aligned} &\partial_t h + \partial_x\left(\frac{h^3}{3}\partial_x(\partial_{xx}h + \psi h^{-3} - h\,B)\right) \\ &\qquad + M\partial_x\left[\frac{h^2}{2}\partial_x\left(\frac{[C_0 - \delta(\partial_{xx}h + \psi h^{-3})]h}{K + h}\right)\right] = \frac{\delta(\partial_{xx}h + \psi h^{-3}) - C_0}{K + h} \end{aligned} \tag{1.4.8}$$

What is left is finding equations for the particle dynamic and provide reasonable boundary conditions. The discussion in Section 1.2 showed most of the necessary equations. Suppose particles are transported by convection and diffusion, then the bulk particle conservation can be described as

$$\partial_t \phi + \boldsymbol{u} \cdot \nabla\phi = \nabla \cdot (D\nabla\phi),$$

where $D > 0$ is some diffusion constant. Introducing thin-film scales and again dropping the hats, it becomes

$$\partial_t \phi + u\partial_x\phi + v\partial_y\phi = \frac{\varepsilon D}{UY}\partial_{xx}\phi + \frac{D}{\varepsilon UY}\partial_{yy}\phi.$$

This shows that depending on the size of D, we have up to three different scalings in our problem - one for the convection terms, one for the horizontal and one for the vertical diffusion terms. We proceed as in Routh and Russel [111] by assuming $D \sim UY\varepsilon^\beta$ with β between zero and one. This scaling implies vertical diffusion is acting instantly, hence the volume fraction is independent on y to leading order. Further, the horizontal diffusion is negligible. Integration from 0 to h, using incompressibility and the particle conservation at the boundary (1.2.10) yields

$$\partial_t c + \partial_x(\bar{u}c) = 0,$$

with $c = h\phi$ being the volume of particles and the vertical averaged velocity defined as

$$\bar{u} = \frac{1}{h}\int_0^h u\,\mathrm{d}y = -M\partial_x(Jh)\frac{h}{2} + \partial_x(\partial_{xx}h + \psi h^{-3} - hB)\frac{h^2}{3}.$$

The initial profiles are described by

$$h(0,x) = \begin{cases} h_\varepsilon + 0.5\,x^2 & \text{for } x \in [0,2] \\ h_\varepsilon + 1 & \text{for } x > 2, \end{cases}$$
$$c(0,x) = \begin{cases} \phi_{\text{crit}} h_\varepsilon + 0.2\,x^2 & \text{for } x \in [0,2] \\ \phi_{\text{crit}} h_\varepsilon + 0.4 & \text{for } x > 2, \end{cases}$$

where $h_\varepsilon = \left(\frac{\delta\psi}{T_0}\right)^3$ is the thickness of the precursor film. For $x \to \infty$ the film is altered only by evaporation. Therefore, the flat region stays flat and we are able to state the boundary conditions

$$\partial_x c = \partial_x h = \partial_{xxx} h = 0 \qquad \text{for } x \to \infty.$$

On the side of the drying front, i.e. $x = x_f$, we expect the film height to be constant, that is

$$\partial_t h = 0 \qquad \text{for } x = x_f.$$

As we are using a central scheme, we also have to give a boundary condition for c at $x = x_f$ for numerical reasons, though it should not be needed from a mathematical point of view, since it is a hyperbolic equation with an outflow at $x = x_f$, see [126] for a discussion of numeric boundary conditions for hyperbolic equations. We demand

$$c = h\phi_{\text{crit}} \qquad \text{for } x = x_f.$$

The film height equation (1.4.8) is of fourth order and we have a free-boundary problem in x_f, so we expect to have two more boundary conditions. The boundary conditions can be derived using a particle balance at the drying front as described in [111], which we repeat here for completeness sake. The profile at the boundary is being thought of as a shock in the velocity and volume fraction. Suppose the drying front is at position x_f and particles are packed at the negative side and still flowing at the positive side, i.e.

$$\begin{aligned} u_p^- &= 0, & u_p^+ &= \bar{u}, \\ h(1-\phi_{\text{crit}})u_f^- &= \int_{x_f(0)}^{x_f(t)} J(x)\,\mathrm{d}x, & u_f^+ &= \bar{u}, \\ \phi^- &= \phi_{\text{crit}}, & \phi^+ &= \phi. \end{aligned}$$

The drying front of the particles is expected to be a regular compressive shock and, therefore, should fulfill the Rankine-Hugoniot condition (see e.g. [74])

$$\partial_t x_f = \frac{[\![\phi u_p]\!]}{[\![\phi]\!]} = -\frac{\phi^+ u_p^+}{\phi_{\text{crit}} - \phi^+}, \tag{1.4.9}$$

where

$$[\![\boldsymbol{a}]\!] = \boldsymbol{a}^+\boldsymbol{n} - \boldsymbol{a}^-\boldsymbol{n} \qquad \text{with} \qquad \boldsymbol{a}^\pm = \lim_{\varepsilon \to 0+} \boldsymbol{a}(\boldsymbol{x} \pm \varepsilon \boldsymbol{n})$$

denotes the jump across an interface. Equation (1.4.9) is a condition for the movement of the free boundary. Doing the same for the fluid gives

$$\partial_t x_f = \frac{[\![(1-\phi)u_f]\!]}{[\![1-\phi]\!]} = \frac{(1-\phi_{\text{crit}})u_f^- - (1-\phi^+)u_f^+}{(1-\phi_{\text{crit}}) - (1-\phi^+)},$$

and equating with (1.4.9) yields that fluid flux at the fluid side must balance the evaporation on the solid side, i.e.

$$h\bar{u} = \int_{x_f(0)}^{x_f(t)} J(x)\,\mathrm{d}x. \tag{1.4.10}$$

Since $\bar{u}$ is just a function of h, this is another boundary condition for h at $x = x_f$ and represents together with (1.4.9) the two missing conditions.

Results

We have simulated a horizontal drying front using the model proposed in Section 1.3 using a finite difference scheme of second order with variable time step and ghost-point method. See Section A.2 for more details on the finite difference method. Figure 1.5 shows an exemplary result. At the beginning evaporation reduces the amount of liquid in the film, which in turn increases the volume fraction of the particles. If the volume fraction of the particles reaches maximum packing at a position $x_f(0)$ a drying front emerges and moves through the domain. The velocity $\partial_t x_f$ of the drying front is diverging, since the bulk evaporation continues to decrease the volume fraction everywhere the denominator in (1.4.9) goes towards zero. This is the reason the final profile is flat everywhere, since this effect is always dominating the dynamics for later times. At the position of the drying front x_f a shock in the volume fraction and height profile is visible. The shock in the height profile might violate the thin-film assumption $\partial_x h = O(1)$, as has been discussed in Section 1.3 above.

Here, we derived a general equation for thin-film models, followed by a model capable of simulating a horizontal drying front. The question is how much new information can be derived from the model about the problem. Unfortunately, the answer is not much as the most interesting phenomena have to be explicitly put into the model, rather than coming out of it.

The first weakness of the model is that we use the single-phase Navier-Stokes equation as starting point for our derivation. The transport of the particles is described by (1.2.2) and for the model of the particle velocity the most simple ansatz is used, that is the same-velocity ansatz $\boldsymbol{u}_d = 0$, which is a rough simplification at least in the case of highly concentrated suspensions. Further, we explicitly model the behavior of the drying front using conditions (1.4.9) and (1.4.10), which is based on simple mass balances, but does not take into account rheologic properties of the liquid or particles.

The model simulates the evolution of the film height during a drying front process and we are in theory able to retrieve stresses and velocities arising in the process. Nevertheless, these velocities and stresses are highly depending on the exact velocity of the drying front, which we explicitly build into the model. In general it is possible to use a more complex model at this point, see for example [111] for finite capillary pressure model, but the major weakness stays that every behavior of the drying front must be explicitly modeled, rather than being derived from the

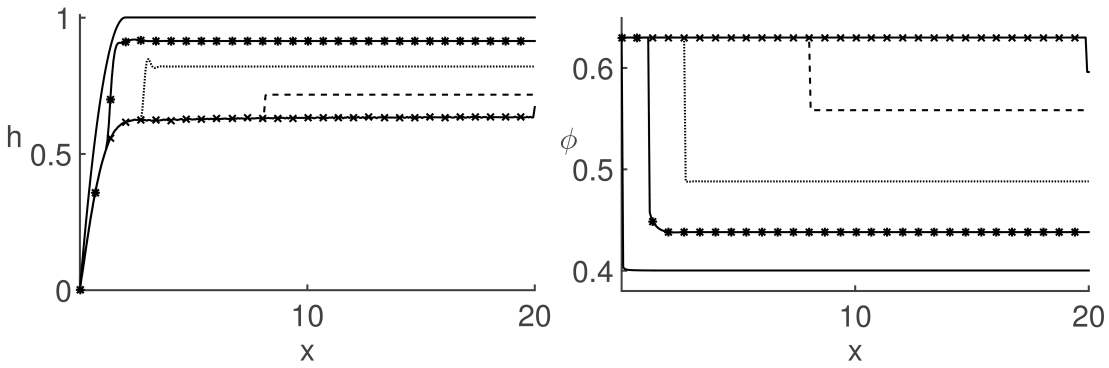

Figure 1.5: Height (left) and volume fraction (right) profiles for the horizontal drying front simulated using the thin-film model of Section 1.3 with parameters $\phi_{\text{crit}} = 0.63$, $B = 1$, $M = 1$, $K = 0.2$, $T_0 = 0$, $\delta = 10^{-3}$ and $\psi = 10^{-6}$. Shown are the times $t \in \{0, 0.1, 0.2, 0.3, 0.3406\}$ with straight, starred, dotted, dashed and crossed line, respectively. The drying front is seen as an advancing shock in the volume fraction with velocity $\partial_t x_f$. The final film profile is everywhere flat, but at the contact line at $x = 0$.

fluid and particle rheology. It is straightforward to extend the model to more than one particle phase, yet the model just gives volume fractions morphologies along the horizontal axis. Skinning, spinodal decomposition and similar effects demand a vertical change of the morphology.

A way around would be to state the thin-film model two-dimensionally, similar to what Craster and Matar [24] did. Then, one would need to derive a drift-flux for the particles, which again needs to be postulated rather than derived from first-principle. And although such a model has big advantages already, it is still unable to model stresses in the solid area of the domain as the fluid and particle velocities are not entirely independent. Yet, independent velocities of particles and fluid is a necessity for particles to get stuck and at the same time fluid to pass through them due to osmotic pressure as seen in experiments [48, 78].

The mentioned limitations of the given model motivate us to look for a more general class of models, that might be able to fix some or all of the weaknesses mentioned. One possible generalization is to separately model the behavior of the particles and liquid, in the hope that this yields some more insight into the behavior of concentrated suspensions. This approach has been pursued in the following chapters.

1.5 Overview

Chapter 1 motivates the need for progress in the theory of concentrated suspensions. We present organic solar cells as an industrial application for these fluids and then proceed with a short introduction into the basic equations of fluid mechanics for complex fluids. We propose some transport terms for particles, before finally showing a simple model for the simulation of a horizontal drying front. However, this model does not fully describe the behavior of concentrated suspensions, which leads us to consider multiphase models in this thesis.

Chapter 2 gives a general overview of multiphase models, their inherent well-posedness problem, and systematically derives a new two-phase model through ensemble averaging along the lines of Drew et al. [33] while incorporating recent non-Brownian constitutive laws by Boyer et al. [15] for the shear and normal viscosities for concentrated suspensions. The new model describes the flow of concentrated suspensions and can be applied to a number of different flow cases.

Chapter 3 shows particular applications to the plane Couette and plane Poiseuille flow. Plane Couette flow yields a solution similar to the Newtonian single-phase problem, but the multiphase Poiseuille flow exhibits a solution similar to single-phase Bingham flows. The study of plane Poiseuille flow using the two-phase model shows also the existence of unyielded or jammed regions. The width of such a region depends on the value of the applied pressure for given volume fraction of the solid phase. We also demonstrate the dependence of the profile for the volume fraction ϕ_s on the so-called "viscous number", which can induce a qualitative change in the approach towards maximum volume fraction. The momentum coupling between phases is typically very large because of small particle sizes, and for these values $w_1 = u_f - u_s$, i.e. the difference between the solid and liquid phase velocity, develops a boundary layer at the channel walls and at the interface between unyielded and yielded regions.

Then, we derive a new drift-flux model using matched asymptotic expansions in Section 3.3, that allows for the emergence of jammed regions. Our asymptotic analysis shows that in order for the drift-flux model to correctly capture shear-induced particle migration the boundary layer structure of the solution has to be resolved and matched to the "outer" problem of the drift-flux model. Our numerical solutions of the drift-flux model reveal how the jammed region emerges first at the center and then expands until the stationary state is reached. Further, the analysis suggests that the boundary layer acts as a source for the particle migration towards the unyielded region.

The stability properties of multiphase models for concentrated suspensions for plane Couette and plane Poiseuille flow are studied in Chapter 4. Our linear stability analysis shows two instabilities exhibited by the proposed model in case of plane Couette flow: a collision pressure driven ill-posedness and a convection induced instability. The convection driven instability is analyzed using a Kelvin-mode ansatz. The resulting time dependent ordinary differential equations showed a transient instability. We note that this might prohibit an experiment from showing the Couette or Poiseuille flow base state, because of the onset of turbulence or the occurrence of shocks for highly concentrated suspensions. In case of the Poiseuille flow, we also retrieve the multiphase instabilities and compare the multiphase model to the stability of the Bingham flow.

An analytic ansatz shows the ill-posedness stems from a competition between the solid phase viscosity and the collision pressure and poses a necessary stability condition on the size of the solid phase viscosity compared to the collision pressure. This has been reaffirmed by comparison between numerical and analytical results. It turns out the criterion depends on the base state, which shows the sufficient criterion, which is derived in Chapter 5, can be lowered for particular flows.

Chaper 5 uses a gradient-flow structure for the derivation of a purely dissipative Eulerian-Eulerian multiphase model. We first summarize the different approaches known from the literature for a gradient-flow system and show the connection between variational derivations, minimizations and variational inequality ansatzes. Next, we derive the condition of equal normal phasic velocities on a free-boundary, which should guarantee mass conservation. A derivation of the multiphase

model follows yielding the well-known momentum and mass conservation equations as well as a free-boundary stress condition. We then show how to include a collision pressure term similar to the one proposed in Chapter 2. Finally, this collision pressure yields a new stability condition similar to the one derived in Chapter 4 for the ratio between viscosity and collision pressure. Nevertheless, the energetic condition is more general, since it does not depend on the specific flow under consideration and implies an upper bound for the ratio that is necessary for the well-posedness of the system.

The similarities between our multiphase model and Bingham models lead us to reconsider a single-phase Bingham model in a thin-film approximation due to Balmforth et al. [9] in Chapter 6. We show an alternative derivation of the thin-film viscoplastic model using a variational inequality formulation. Its advantage is that it does not depend on implicit assumptions on the total stress and does not need the specification of boundary conditions at the yield-surface. We proceed with an introduction in monotonicity methods for the existence and uniqueness of operator equations. Furthermore, we show existence for a regularized version of the resulting viscoplastic thin-film equation.

In Chapter 7 we show a formal asymptotic approach to reduce the Eulerian-Eulerian model to simpler models. Specifically, we derive models for dilute or concentrated suspensions and with strong or weak coupling between phases. This allows comparing well-known single-phase models to the multiphase model, since the constitutive laws in the single-phase class models demand specific constitutive laws in the multiphase class and vice versa. Examples are Darcy's law with its dependence on the momentum coupling term definition, the Stokes settling velocity that also connects to the momentum coupling term and the drift-flux models, that depend on the collision pressure, the body forces as well as to the momentum coupling term.

We then proceed to show a formal approach on how to derive thin-film models from the multiphase model. This approach yields the same leading order momentum and mass conservation equations that are well-known from the thin-film community, but additionally gives a transport equation that needs to be hypothesized in the thin-film literature, but can be derived using our approach. The additional transport equation contains body force terms, the collision pressure and the momentum coupling term, which led us to review those terms and compare the resulting equation to a well-known model from the literature. Then, the connection between the Bingham models of Chapter 6 and our multiphase model is formally shown by assuming a constant collision pressure throughout the fluid domain, which yields a Bingham stress term that can also be reduced to a thin-film model as proposed by Balmforth et al. [9].

Finally, Chapter 8 discusses possible future work and open questions for the modeling of concentrated suspensions.

Chapter 2

Multiphase model

The previous chapter shows simulations based on single-phase Navier-Stokes equations for complex fluids. Section 1.5 shows a derivation of a thin-film model for a drying front. However, we are only able to derive an equation for the free-boundary profile, but miss a derivation of the convection-diffusion equation of the particles based on the rheology of the fluid. Hence, we are forced to postulate the existence of the convection-diffusion equation and have to guess the correct transport mechanism by physical intuition. Further, the boundary conditions next to the solid are also derived using a simple mass conservation argument, that does not take the rheology of the fluid into account.

A different approach is to assume the Navier-Stokes equations apply to each phase separately. This is the ansatz for so-called *multiphase models*. The difficulty in this approach is to keep track of the locations and interfaces of the phases and find suitable constitutive laws for each phase that are momentum, mass and energy preserving.

There are many ways to derive a multiphase model. As more general models are usually harder to analyze or require more complex numerical implementation, one should consider the simplest one for the considered problem. Typical questions in order to select an appropriate multiphase model are:

- Are we interested in the shape of interfaces between the phases?
- Is it important to track the energy and momentum for each phase or only for the total flow?
- What quantities do we measure in experiments?
- Are the phases immiscible, partially miscible or fully miscible?

Consider two examples - a rising gas bubble in a liquid and finely dispersed particles in a liquid. For the flow case of the rising gas bubble, it is most interesting to track the gas-liquid interface, but since the liquid and gas is well separated, it is enough to consider total momentum and energy

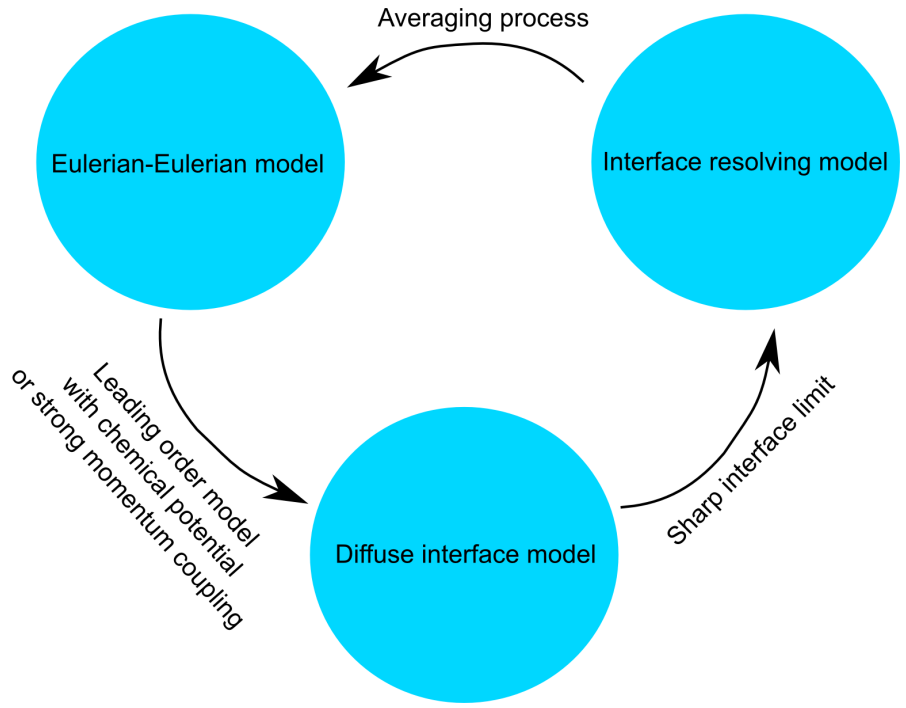

Figure 2.1: Shown are the three main classes of multiphase models. The arrows symbolize the technique by which a multiphase model class can be transformed from one into another. Note, the transformations demand certain scaling assumptions to hold, so generally it is not possible to make more than two transformations without implicitly assuming unphysical large scales, which prevents us to go around that circle multiple times.

balances and immiscible phases. On the other side, the interface of the dispersed particles are not easy to resolve, but it is often interesting to track mass, momentum and energy of the two phases - liquid and solids - separately, since e.g. only the liquids are able to evaporate if enough energy is available on a free surface.

The rest of this chapter gives an overview of typical classes of multiphase models. As we are interested in fully miscible flows, we derive the appropriate model via an average process. This average process yields new terms that must be modeled by constitutive laws given in the literature or by experiment. Our particular choice is based on the work of Boyer et al. [15] for the simulation of concentrated suspensions.

2.1 Classes of multiphase models

The term multiphase model is ambiguous as it refers to at least three different classes of models: the interface resolving models, the Eulerian-Eulerian models and the diffuse interface models. By means of asymptotic methods a particular class of multiphase methods can be transformed into one of the two other classes. In fact it is quite common to derive an Eulerian-Eulerian

model starting from an interface resolving model via an average process, cf. [32], or derive a diffuse interface model as a leading order approximation of an Eulerian-Eulerian model, cf. [16]. Figure 2.1 depicts the relations between the three model classes and their respective derivation techniques. Knowledge of all three classes is needed to understand the derivation of the proposed Eulerian-Eulerian model in this thesis. Therefore, a short overview of incompressible models for all three classes is given in this section.

Interface resolving models

The class of interface resolving models describes immiscible fluids and their interaction on interfaces between them. An often used alternate name is sharp interface models in order to distinguish them from diffusive interface models. For an exhaustive introduction into this class and their numerical solution see the review by Wörner [133] or the book by Tryggvason et al. [130]. Their most characteristic property is the fact that there can only be one phase at a certain position and time, which creates the need to track the interfaces between phases.

Consider a fixed domain $\Omega \subset \mathbb{R}^n$ and suppose we have two phases $j \in \{1, 2\}$ located in their respective domains $\Omega_j(t)$ with $\Omega_1(t) \cup \Omega_2(t) = \Omega$. Let us call Γ_{12} the interface between phase 1 and phase 2 with normal pointing from phase 1 to 2, and then the phase properties are stated like in an incompressible single-phase formulation (1.1.10) inside $\Omega_j(t)$ as

$$\begin{aligned} \rho \frac{D\boldsymbol{u}}{Dt} - \boldsymbol{\tau} + \nabla p &= \rho \boldsymbol{f}, \\ \nabla \cdot \boldsymbol{u} &= 0, \end{aligned}$$

where

$$\boldsymbol{\tau} = \begin{cases} \boldsymbol{\tau}_1 & \text{in } \Omega_1(t) \\ \boldsymbol{\tau}_2 & \text{in } \Omega_2(t), \end{cases} \qquad \boldsymbol{f} = \begin{cases} \boldsymbol{f}_1 & \text{in } \Omega_1(t) \\ \boldsymbol{f}_2 & \text{in } \Omega_2(t), \end{cases}$$

represent forces and stresses of the respective phases. On the interface between the two domains boundary conditions must be given for the momentum and the mass conservation, i.e. [31]

$$[\![\rho \boldsymbol{u} \otimes (\boldsymbol{u} - \boldsymbol{u}_i) - \boldsymbol{\tau}]\!] = \sigma_0 \kappa \boldsymbol{n} + \nabla_S \sigma_0, \qquad [\![\rho(\boldsymbol{u} - \boldsymbol{u}_i)]\!] = m_i,$$

where σ_0 is the surface tension, κ the surface curvature, ∇_S the surface derivative, m_i describes changes in the phases [31, 130]. The problem is to advance the domains in time. This is normally done by defining an appropriate interface velocity $\boldsymbol{u}_i$ that conserves mass and momentum.

It is worth adding, that most thin-film models are of the interface resolving type, where the second phase (mostly air) is taken only passively into account, but the interface is tracked via the evolution of the free-boundary h, cf. Chapter 1. This is also called the one-sided approach for thin-film models [4, 92]. The dependence of thin-film models on the second phase is more pronounced, when the properties of the second phase are solved for, too - like in the so-called 1.5 and two-sided models [92].

Microscopic models possess the advantage, that the properties of the bulk can be easily measured from experiment or are already known for many materials. The forces acting on the interface between two pure phases are also better understood as surface tension and chemical reactions are

often known for specific materials. In this sense the interface resolving models are more physical sound compared to other multiphase models.

On the downside, mixtures might have complicated interface structures that are too costly to track and might also change their topology, e.g. droplet coalescence or breakup. Related problems occur in fully miscible fluids that do not allow for a precise definition of an interface, thus rendering this approach inappropriate for these fluids.

Eulerian-Eulerian models

The Eulerian-Eulerian models - also known as two-fluid flow [77, 133, 134], two-phase flow [65, 120] or dispersed multicomponent flow [32] - are used when an explicit interface tracking is not possible or too time-consuming. For a more detailed survey see for example the reviews [31, 120] or the books [32, 60, 70, 132]. These models allow for every phase to have its own velocity and track the fraction of each phase j at each position via an indicator function ϕ_j.

Suppose we have two phases $j \in \{1, 2\}$, then the momentum and mass conservation of an incompressible multiphase flow is described by

$$\phi_1 + \phi_2 = 1, \tag{2.1.1a}$$

$$\rho_j \partial_t(\phi_j \boldsymbol{u}_j) + \rho_j \nabla \cdot (\phi_j \boldsymbol{u}_j \otimes \boldsymbol{u}_j) - \nabla \cdot (\phi_j \boldsymbol{\tau}_j) + \nabla(\phi_j p_j) = \phi_j \rho_j \boldsymbol{f}_j + \boldsymbol{d}_j, \tag{2.1.1b}$$

$$\partial_t \phi_j + \nabla \cdot (\phi_j \boldsymbol{u}_j) = m_j, \tag{2.1.1c}$$

where $\boldsymbol{d}_1 = D(\phi_j)(\boldsymbol{u}_2 - \boldsymbol{u}_1) = -\boldsymbol{d}_2$ models momentum coupling or drag effects and m_j models chemical reactions between phases. The stresses $\boldsymbol{\tau}_j$ might contain viscous and turbulent terms and the forces $\boldsymbol{f}_j$ might contain lift forces, drag forces, bulk forces and interface forces. Finding the correct terms for these models is still a matter of debate. For some proposals see [32, 46, 60, 70, 95]. Since system (2.1.1) contains the six unknowns ϕ_1, ϕ_2, $\boldsymbol{u}_1$, $\boldsymbol{u}_2$, p_1 and p_2, but poses just five equations, one needs an additional sixth equation in order to eliminate at least one of the pressures p_j, which is discussed in more detail in Section 2.2. These models are incompressible in the sense that their volumetric velocity $\boldsymbol{v} = \sum_j \phi_j \boldsymbol{u}_j$ together with the sum of the indicator transport equations (2.1.1c) yield $\nabla \cdot \boldsymbol{v} = 0$.

The main advantage of Eulerian-Eulerian models is they allow the simulation of highly miscible fluids. Interfaces are handled implicitly by force terms arising due to gradients of ϕ_j. The downside of this model is they are computational highly demanding due to the high number of unknowns. Another problem is that their mathematical analysis is still in a very early stage. The analytic main problem is that they contain two sets of Navier-Stokes equations, which are nonlinearly coupled and, additionally, they contain a potentially sever instability - called the loss-of-hyperbolicity problem, cf. [77] and Section 2.2.

It is not uncommon to substitute one of the single-phase momentum equations with the total momentum equation, see e.g. [95]. A rigorous derivation for the Eulerian-Eulerian models can be done based on an averaging process of interface resolving models for details see Section 2.2 and [32] or based on an averaging process of microscopic models, see e.g. [95].

Diffuse interface models

In the case of diffuse interface models the requirement of interface resolving models that every location should only contain one phase is weakened and instead the stress and forces of the different

phases are blended by an indicator field ϕ. This field is often associated with a concentration or volume fraction of the phases and normally one defines $\phi = 0$ or $\phi = 1$ whenever we have a pure phase 1 or 2, respectively. Additionally, $\phi = 0.5$ defines the interface between two phases [133]. For a detailed survey of this class see for example [7, 133].

The equations for the incompressible diffuse interface models typical take the form

$$\begin{aligned} \rho \frac{D\boldsymbol{u}}{Dt} - \nabla \cdot \boldsymbol{\tau} + \nabla p &= \rho \boldsymbol{f}, \\ \nabla \cdot \boldsymbol{u} &= 0, \\ \frac{D\phi}{Dt} - \nabla \cdot (D(\boldsymbol{u}, p, \phi, \nabla\phi, \Delta\phi, \ldots)) &= 0, \end{aligned} \tag{2.1.2}$$

where D contains drift-flux effects of the phases and might contain very high derivatives in ϕ. For example popular choices for (2.1.2) are drift flux models of second order as described in Section 1.2 or a modified Cahn-Hilliard equation, which is of fourth order [7, 125]. The stress and force terms are chosen as mean of the individual phasic properties and additional stresses and forces, $\boldsymbol{\tau}_K$ and $\boldsymbol{f}_K$, that might arise due to derivatives in ϕ, which represent interfaces between phases and are often named Korteweg terms [7], e.g.

$$\begin{aligned} \boldsymbol{\tau} &= (1-\phi)\boldsymbol{\tau}_1 + \phi\boldsymbol{\tau}_2 + \boldsymbol{\tau}_K(\nabla\phi, \Delta\phi, \ldots), \\ \boldsymbol{f} &= (1-\phi)\boldsymbol{f}_1 + \phi\boldsymbol{f}_2 + \boldsymbol{f}_K(\nabla\phi, \Delta\phi, \ldots). \end{aligned}$$

The stress sometimes also uses the harmonic instead of the arithmetic mean, see e.g. [133].

There are different use cases of a diffuse interface model. On the one hand they are used as a regularization for interface resolving models to efficiently track the interfaces, cf. [133]. In this case only a small portion of the domain has values of $\phi \in]0, 1[$. On the other hand, diffuse interface models are used for problems, where no apparent interface might exist like in a mixing device, channel flow of suspensions or when two fluids are partly or fully miscible [95, 111]. Another common usage scenario are fluids with a natural decomposition force, e.g. due to a chemical potential between phases [7].

The problem with diffuse interface models is to find physical sound expressions for D, $\boldsymbol{\tau}_K$ and $\boldsymbol{f}_K$. Many proposals can be found in the literature and one of the earliest diffuse interface models is the H-model due to Hohenberg and Halperin [53]. Derivations of such a model can be done based on energetic arguments [125] or from an Eulerian-Eulerian model by considering leading order terms, cf. [16]. As seen in the introduction of this thesis the form of the transport equation for ϕ is sometimes simply conjectured without a formal derivation, see for example Section 1.2 for a discussion of flux terms in use.

Some models - an example being the H-model - contain a small parameter ε proportional to an average interface thickness. Asymptotic techniques allow one to look for an effective model in the limit $\varepsilon \to 0$, so that one retrieves an interface resolving model with effective interface boundary conditions in the sharp interface limit, see e.g. [7]. On the other side, an Eulerian-Eulerian model can be transformed into a diffusive flux model by looking for the leading order approximation in case of large drag-terms, cf. [16] and Chapter 7.

Remark

A warning concerning the classification of multiphase models in the scientific literature is necessary at this point. Sometimes it is impossible to tell whether a publication uses a diffusive flux, an Eulerian-Eulerian or an interface resolving model. For example consider the suspension balance model [95], which is first derived as an Eulerian-Eulerian model based on an average process of a interface resolving model. Then, in case of computations, it is reduced into a diffusive flux model by transforming one of the momentum equations into a drift-flux expression [21]. So speaking of a certain model does not necessarily tell, which class of multiphase models one is talking about - even in the context of a single publication!

2.2 Derivation of an Eulerian-Eulerian model

An Eulerian-Eulerian model is derived by starting from an abstract interface resolving model using an average process. We do not derive constitutive laws from the interface resolving model, but rather propose them separately. The following discussion is a more detailed version of a short presentation by the author [2].

In order to understand why we need an average process for the Eulerian-Eulerian model suppose we have a deterministic interface resolving model of a two-phase flow. Thus, the domain of existence for phase one is $\Omega_1(t)$ and for phase two is $\Omega_2(t)$. The velocity fields for the phases are only defined in Ω_1 and Ω_2, respectively. For highly dispersed phases this renders any computation extremely complicated, since one has to solve for the domains of existence of both phases. Therefore, it would be computationally advantageous to look for everywhere defined velocity fields instead. For flows with highly dispersed phases, a solution is to instead of looking at fields at an exact location, to consider a field consisting of the averaged values of the nearby positions. Since both phases are present near each point in time and space, such a field would be defined everywhere. This is the motivation for a time and volume average ansatz as proposed for example by Ishii [60] and Whitaker [132].

A different motivation is given for the ensemble average by Drew and Passman [32]. They interpret every flow as a nondeterministic interface resolving model due to experimental errors. Thus, looking at the same flow multiple times under similar experimental setups, the phases can have different spatial and temporal distributions due to random fluctuations. Thus, instead of having domains $\Omega_1(t)$ and $\Omega_2(t)$ we now have realizations of domains $\Omega_1(t;i)$ and $\Omega_2(t;i)$ with i describing the experimental setup. The set of all i constitute an ensemble. Thus, instead of looking for a spatial and temporal average, one can consider the expected value over all realizations of an ensemble. This is the ansatz used for the ensemble or statistical averages, cf. [31, 32].

Both ansatzes - the deterministic of temporal and volume averages and the nondeterministic of ensemble and statistical averages - yield similar models, but differ in their assumptions on the average operators. For example the volume average demands the characteristic length scale of the experimental domain to be much larger than the length scale of the average used, which in turn must be much larger than the usual scale of the microscopic phase domains, cf. [132]. Whereas for the ensemble average, the assumption is to have measurable ensembles such that the expected value is defined [32].

In the following derivation, we do not use a specific average operator, but assume it to fulfill certain axioms instead that we use to derive the final equations. The volume [70, 132], temporal

[60] and ensemble averages [32] proposed do fulfill these axioms. For the connection between those averages, see the book by Drew and Passman [32].

Averaging axioms

We follow the mathematical framework by Drew and Passman [31, 32] in this section. Let f and g be arbitrary measurable functions, c a constant and $\langle\cdot\rangle$ an average operator obeying the so-called Reynolds' rules

$$\begin{aligned}\langle f+g\rangle &= \langle f\rangle + \langle g\rangle,\\ \langle\langle f\rangle g\rangle &= \langle f\rangle\langle g\rangle,\\ \langle c\rangle &= c,\end{aligned}$$

the Leibniz' rule

$$\partial_t\langle f\rangle = \langle\partial_t f\rangle,$$

and the Gauß' rule

$$\partial_{x_i}\langle f\rangle = \langle\partial_{x_i} f\rangle. \tag{2.2.1}$$

The functions should be weakly differentiable up to the required order. Admissible operators are for example the volume average [132], [70], time averages [60], the ensemble average [32] or a mixture of these [33].

We further need a component indicator function

$$X_k(\boldsymbol{x},t) = \begin{cases}1 & \text{if } (\boldsymbol{x},t)\in K\\ 0 & \text{if } (\boldsymbol{x},t)\notin K,\end{cases}$$

with K the set of states of the k-th-phase. In our model we use the average operator in a weighted form. Generally, there are two weighted averages in use, the intrinsic or phasic average

$$\overline{g} \equiv \frac{\langle X_k g\rangle}{\langle X_k\rangle}$$

and the mass-weighted or Favré average (in its three common forms)

$$\widehat{g} \equiv \frac{\overline{\rho g}}{\overline{\rho}} = \frac{\langle X_k\rho g\rangle}{\langle X_k\rangle\frac{\langle X_k\rho\rangle}{\langle X_k\rangle}} = \frac{\langle X_k\rho g\rangle}{\langle X_k\rho\rangle}.$$

The weighted averages adhere to the Reynolds' rules, but not to the Leibniz' and Gauss' rule. If we have multiple indicator functions, then an index states the indicator function we used in the average, e.g. $\overline{g}_s$ indicates the usage of X_s in the average. We define a fluctuation field (cf. [32]) as

$$g' := g - \overline{g} \qquad\qquad g^\circ := g - \widehat{g}$$

and due to the Reynolds rules $\overline{g'} = \widehat{g^\circ} = 0$ holds. This splitting together with the Reynolds rules yields the identity

$$\overline{fg} = \overline{f}\,\overline{g} + \overline{f'g'}$$

and similar for the Favré average

$$\widehat{fg} = \widehat{f}\widehat{g} + \widehat{f^{\circ}g^{\circ}}. \tag{2.2.2}$$

At an interface position $\boldsymbol{x}^*$ the phasic velocity $\boldsymbol{u}_k$ is defined as

$$\boldsymbol{u}_k(\boldsymbol{x}^*, t) \equiv \lim_{\boldsymbol{x}\to\boldsymbol{x}^*;\boldsymbol{x}\in K} \boldsymbol{u}(x,t),$$

where K denotes the set of points occupied by phase k, and similarly for the other quantities.

Note the derivatives are defined in the sense of distributions in this work. This implies $\langle f\nabla X_k\rangle$ can yield additional surface integrals, whereas in classical theories the Leibniz' and Gauss' rule are written explicitly with surface integrals, cf. [32] and [132]. Denote by Ω the domain of interest and by $\mathcal{S}_k$ the interface of phase k in space with outwards pointing normal $\boldsymbol{n}_k$. Then, following Drew [31, 32], the so-called Dirac delta property

$$\int_\Omega f\nabla X_k\psi \mathrm{d}\boldsymbol{x} = -\int_{\mathcal{S}_k} \boldsymbol{n}_k f_k\psi \mathrm{d}\boldsymbol{S} \tag{2.2.3}$$

of a quantity $\boldsymbol{f}$ holds for every test function ψ that is sufficiently smooth and has compact support. Thus, the delta-property shows how interface effects enter the equations via the average process. One of the main problems of Eulerian-Eulerian models is to find suitable constitutive laws for these interfacial terms in form of bulk terms.

The characteristic function fulfills the so-called topological equation (cf. [32])

$$\partial_t X_k + \boldsymbol{u}_i\cdot\nabla X_k = 0 \tag{2.2.4}$$

with $\boldsymbol{u}_i$ the interface velocity.

Averaging process

We consider two inert phases and denote with $k\in\{s,f\}$ the solid phase by s and the liquid phase by f. Inside each phase the incompressible[1] balance equations for mass and momentum

$$\partial_t\rho + \nabla\cdot(\rho\boldsymbol{u}) = 0, \tag{2.2.5a}$$

$$\partial_t(\rho\boldsymbol{u}) + \nabla\cdot(\rho\boldsymbol{u}\otimes\boldsymbol{u}) - \nabla\cdot\boldsymbol{\sigma} - \rho\boldsymbol{f} = \boldsymbol{0} \tag{2.2.5b}$$

are satisfied together with the two jump conditions (see e.g. [60])

$$\sum_k \rho_k(\boldsymbol{u}_k - \boldsymbol{u}_i)\cdot\boldsymbol{n}_k = 0, \tag{2.2.6}$$

$$\sum_k \rho_k\boldsymbol{u}_k(\boldsymbol{u}_k - \boldsymbol{u}_i)\cdot\boldsymbol{n}_k - \boldsymbol{\sigma}_k\cdot\boldsymbol{n}_k = \sigma_{fs}\kappa\boldsymbol{n}_s, \tag{2.2.7}$$

at the interfaces of the phases with $\boldsymbol{n}_k$ denoting the unit normal pointing out of phase k, σ_{fs} a surface tension coefficient and κ the curvature of the interface that is positive towards $-\boldsymbol{n}_s$; $\boldsymbol{u}_i$ is

[1] For a discussion of the seemingly "compressible" mass conservation used here, see the remark at the end of the derivation.

the interface velocity. The quantities ρ, $\boldsymbol{u}$, $\boldsymbol{\sigma}$ and $\boldsymbol{f}$ denote density, velocity, stress tensor and body force density in each phase, respectively.

Multiplication of (2.2.5) with X_k, followed by usage of the average operator and its linearity together with Gauss' and Leibniz' rules yield

$$\begin{aligned}\partial_t\langle X_k\rho\rangle + \nabla\cdot\langle X_k\rho\boldsymbol{u}\rangle &= \langle\rho(\partial_t X_k + \boldsymbol{u}_i\nabla\cdot X_k)\rangle \\ &\quad + \langle\rho(\boldsymbol{u}-\boldsymbol{u}_i)\cdot\nabla X_k\rangle, \end{aligned} \tag{2.2.8}$$

$$\begin{aligned}\partial_t\langle X_k\rho\boldsymbol{u}\rangle + \nabla\cdot\langle X_k\rho\boldsymbol{u}\otimes\boldsymbol{u}\rangle - \nabla\cdot\langle X_k\boldsymbol{\sigma}\rangle &= \langle X_k\rho\boldsymbol{f}\rangle \\ +\langle(\partial_t X_k + \boldsymbol{u}_i\cdot\nabla X_k)\rho\boldsymbol{u}\rangle + \langle[(\boldsymbol{u}-\boldsymbol{u}_i)\cdot\nabla X_k]\rho\boldsymbol{u}\rangle &- \langle\nabla X_k\cdot\boldsymbol{\sigma}\rangle. \end{aligned} \tag{2.2.9}$$

Above we assume that the interface velocity $\boldsymbol{u}_i$ has been smoothly extended for all x. Since the indicator function satisfies the topological equation (2.2.4) the first and the second term in equations (2.2.8) and (2.2.9) drop out, respectively, and we can write the system as

$$\begin{aligned}\partial_t\langle X_k\rho\rangle + \nabla\cdot\langle X_k\rho\boldsymbol{u}\rangle &= \boldsymbol{\Gamma}_k, \\ \partial_t\langle X_k\rho\boldsymbol{u}\rangle + \nabla\cdot\langle X_k\rho\boldsymbol{u}\otimes\boldsymbol{u}\rangle - \nabla\cdot\langle X_k\boldsymbol{\sigma}\rangle &= \langle X_k\rho\boldsymbol{f}\rangle + \boldsymbol{M}_k,\end{aligned}$$

where

$$\boldsymbol{\Gamma}_k \equiv \langle\rho(\boldsymbol{u}-\boldsymbol{u}_i)\cdot\nabla X_k\rangle, \tag{2.2.10}$$

$$\boldsymbol{M}_k \equiv \langle\nabla X_k\cdot[\rho(\boldsymbol{u}-\boldsymbol{u}_i)\otimes\boldsymbol{u}-\boldsymbol{\sigma}]\rangle, \tag{2.2.11}$$

denotes the average interfacial mass source and the average interfacial momentum source for the k-th phase, respectively.

Using the Dirac delta property (2.2.3) and (2.2.10), (2.2.11) in the jump conditions for mass (2.2.6) and momentum (2.2.7), these conditions become

$$\begin{aligned}\sum_k \boldsymbol{\Gamma}_k &= 0, \\ \sum_k \boldsymbol{M}_k &= \langle\sigma_{fs}\kappa\nabla X_1\rangle.\end{aligned} \tag{2.2.12}$$

We further introduce the following averaged quantities

$$\phi_k \equiv \langle X_k\rangle,$$

for the volume fraction, and

$$\overline{\rho}_k \equiv \frac{\langle X_k\rho\rangle}{\phi_k}, \qquad \widehat{\boldsymbol{u}}_k \equiv \frac{\langle X_k\rho\boldsymbol{u}\rangle}{\phi_k\overline{\rho}_k},$$

$$\overline{\boldsymbol{\sigma}}_k \equiv -\frac{\langle X_k\boldsymbol{\sigma}\rangle}{\phi_k}, \qquad \boldsymbol{\sigma}_k^{Re} \equiv -\frac{\langle X_k\rho\boldsymbol{u}_k^\circ\otimes\boldsymbol{u}_k^\circ\rangle}{\phi_k},$$

$$\widehat{\boldsymbol{f}}_k \equiv \frac{\langle X_k\rho\boldsymbol{f}\rangle}{\phi_k\overline{\rho}_k}, \qquad \boldsymbol{S}_k^d \equiv -\langle\nabla X_k\cdot\boldsymbol{\sigma}\rangle,$$

$$\overline{\boldsymbol{u}}_{ki}\boldsymbol{\Gamma}_k \equiv \langle\nabla X_k\cdot\rho(\boldsymbol{u}-\boldsymbol{u}_i)\otimes\boldsymbol{u}\rangle,$$

for the average density, velocity, stress, Reynolds stress, body forces, interfacial stress, interfacial velocity of the kth phase, respectively.

Then, after we split the interfacial momentum source as

$$\boldsymbol{M}_k = \boldsymbol{S}_k^d + \overline{\boldsymbol{u}}_{ki}\boldsymbol{\Gamma}_k, \tag{2.2.13}$$

and the momentum flux into an average flux and a Reynolds stress

$$\langle X_k \rho \boldsymbol{u} \otimes \boldsymbol{u}\rangle = \phi_k \overline{\rho}_k \widehat{\boldsymbol{u}}_k \otimes \widehat{\boldsymbol{u}}_k - \phi_k \boldsymbol{\sigma}_k^{Re},$$

and use the product rule (2.2.2) for the velocity, we obtain the following system of phase averaged mass and momentum equations

$$\begin{aligned}\partial_t(\phi_k\overline{\rho}_k) + \nabla\cdot(\phi_k\overline{\rho}_k\widehat{\boldsymbol{u}}_k) &= \boldsymbol{\Gamma}_k,\\ \partial_t(\phi_k\overline{\rho}_k\widehat{\boldsymbol{u}}_k) + \nabla\cdot(\phi_k\overline{\rho}_k\widehat{\boldsymbol{u}}_k\otimes\widehat{\boldsymbol{u}}_k) - \nabla\cdot(\phi_k\overline{\boldsymbol{\sigma}}_k) &= \nabla\cdot(\phi_k\boldsymbol{\sigma}_k^{Re}) + \overline{\rho}_k\phi_k\widehat{\boldsymbol{f}}_k + \boldsymbol{S}_k^d + \overline{\boldsymbol{u}}_{ki}\boldsymbol{\Gamma}_k.\end{aligned}$$

As we are interested in the laminar flow regime we neglect the Reynolds stress $\boldsymbol{\sigma}_k^{Re}$ and further assume no phase change occurs at the interface between particles and liquid, $\boldsymbol{\Gamma}_k = 0$.

We introduce the stress tensor as the sum of pressure and deviatoric stress in the form

$$\boldsymbol{\sigma} = -p\boldsymbol{I} + \boldsymbol{\tau},$$

so that for the averaged quantities $\overline{\boldsymbol{\sigma}}_k$ and

$$\overline{p}_k \equiv \frac{\langle X_k p\rangle}{\phi_k}, \qquad\qquad \overline{\boldsymbol{\tau}}_k \equiv -\frac{\langle X_k\boldsymbol{\tau}\rangle}{\phi_k},$$

we have correspondingly

$$\overline{\boldsymbol{\sigma}}_k = -\overline{p}_k\boldsymbol{I} + \overline{\boldsymbol{\tau}}_k.$$

The interfacial pressure of phase k and the interfacial force density is defined as

$$\begin{aligned}\tilde{p}_{ik} &\equiv \frac{\langle\nabla X_k p_k\rangle}{\langle\nabla X_k\rangle} = \frac{\langle\nabla X_k p_k\rangle}{\nabla\phi_k},\\ \boldsymbol{M}_k^d &\equiv \boldsymbol{S}_k^d - \langle\nabla X_k p_k\rangle = \langle\nabla X_k\cdot((p_k-\tilde{p}_{ik})\boldsymbol{I} - \boldsymbol{\tau})\rangle,\end{aligned} \tag{2.2.14}$$

respectively, where the second equality in (2.2.14) follows from an application of Gauss' rule (2.2.1). We have (from (2.2.13))

$$\boldsymbol{M}_k = \boldsymbol{M}_k^d + \tilde{p}_{ik}\nabla\phi_k$$

so that we obtain for the mass and momentum balance equations

$$\begin{aligned}\partial_t(\phi_k\overline{\rho}_k) + \nabla\cdot(\phi_k\overline{\rho}_k\widehat{\boldsymbol{u}}_k) &= 0,\\ \partial_t(\phi_k\overline{\rho}_k\widehat{\boldsymbol{u}}_k) + \nabla\cdot(\phi_k\overline{\rho}_k\widehat{\boldsymbol{u}}_k\otimes\widehat{\boldsymbol{u}}_k)&\\ -\nabla\cdot(\phi_k\overline{\boldsymbol{\tau}}_k) + \nabla(\phi_k\overline{p}_k) &= \boldsymbol{M}_k^d + \tilde{p}_{ik}\nabla\phi_k,\end{aligned}$$

where we have also assumed that no external body forces are applied, i.e. $\widehat{\boldsymbol{f}} = 0$.

We neglect surface tension forces between the solid and the liquid phase [31]. Setting $\sigma_{fs} = 0$ the interfacial pressure difference becomes

$$\sum_k \tilde{p}_{ik} \nabla \phi_k = \langle \sigma \kappa \nabla X_s \rangle = 0, \tag{2.2.15}$$

and we obtain together with the interfacial momentum jump condition (2.2.12) the relation

$$M_s^d = -M_f^d.$$

Since we only have two phases, we know $\phi_s + \phi_f = 1$, which directly leads to $\nabla \phi_s = -\nabla \phi_f$. Thus, equation (2.2.15) yields

$$\tilde{p}_{is} = \tilde{p}_{if}.$$

For the case of identical liquid interfacial and bulk pressure

$$\tilde{p}_{if} = \overline{p}_f,$$

and constant densities $\overline{\rho}_k$ within each phase, the balance equations reduce to

$$\partial_t \phi_s + \nabla \cdot (\phi_s \widehat{\boldsymbol{u}}_s) = 0, \tag{2.2.16a}$$

$$\partial_t \phi_f + \nabla \cdot (\phi_f \widehat{\boldsymbol{u}}_f) = 0, \tag{2.2.16b}$$

$$\begin{aligned} \overline{\rho}_s \partial_t (\phi_s \widehat{\boldsymbol{u}}_s) + \nabla \cdot (\phi_s \overline{\rho}_s \widehat{\boldsymbol{u}}_s \otimes \widehat{\boldsymbol{u}}_s) & \qquad (2.2.16c) \\ -\nabla \cdot (\phi_s \overline{\boldsymbol{\tau}}_s) + \nabla (\phi_s \overline{p}_s) &= \boldsymbol{M}_s^d + \overline{p}_f \nabla \phi_s, \end{aligned}$$

$$\begin{aligned} \overline{\rho}_f \partial_t (\phi_f \widehat{\boldsymbol{u}}_f) + \nabla \cdot (\phi_f \overline{\rho}_f \widehat{\boldsymbol{u}}_f \otimes \widehat{\boldsymbol{u}}_f) & \qquad (2.2.16d) \\ -\nabla \cdot (\phi_f \overline{\boldsymbol{\tau}}_f) + \nabla (\phi_f \overline{p}_f) &= -\boldsymbol{M}_s^d + \overline{p}_f \nabla \phi_f, \end{aligned}$$

$$\phi_s + \phi_f = 1. \tag{2.2.16e}$$

Remark

Note, we currently use (2.2.5a), which is a form of mass conservation usually employed only for compressible fluids. Since (1.1.8) holds for incompressible fluids, (2.2.5a) is equivalent to

$$\nabla \cdot \boldsymbol{u} = 0. \tag{2.2.17}$$

We use the "compressible" form (2.2.5a), because some steps of the derivation seem more natural to the reader and variables like the interfacial mass source $\boldsymbol{\Gamma}_k$ can be defined in their usual form. The derivation also works for the usual incompressible condition (2.2.17) without problems. Yet, the usage of the topological equation (2.2.4) always introduces a time derivative in the phasic mass conservation equations (2.2.16a) and (2.2.16b). The well-known incompressibility condition is regained by considering the sum of equations (2.2.16a) and (2.2.16b), i.e.

$$\nabla \cdot (\phi_s \boldsymbol{u}_s + \phi_f \boldsymbol{u}_f) = 0,$$

and usage of the volume averaged velocity

$$\boldsymbol{v} = \phi_s \boldsymbol{u}_s + \phi_f \boldsymbol{u}_f,$$

which yields the common incompressibility condition

$$\nabla \cdot \boldsymbol{v} = 0.$$

Therefore, it is to be expected that an incompressible Eulerian-Eulerian model shows effects due to incompressibility, but can also show effects only known from compressible single-phase models.

Closure problem and ill-posedness

System (2.2.16) consists of five equations, but contains six unknowns, i.e. $\boldsymbol{u}_s, \boldsymbol{u}_f, \phi_f, \phi_s, p_f$ and p_s. This suggests that we miss one equation. The exact cause for the missing equation is being argued, but is connected to total energy preservation and models for the microscopic and interface quantities [41, 77, 120]. To illustrate this consider the kth phase' total energy E_k defined as [77]

$$E_k = e_k + \boldsymbol{u}_k^2/2 + K_k,$$

where e_k is the internal energy of phase k and K_k is a so-called pseudo-turbulent kinetic energy. The pseudo-turbulent kinetic energy is directly connected to microscopic quantities like interface velocities $\boldsymbol{u}_i$, interface pressures p_i and velocity fluctuations $\boldsymbol{u}^\circ$, which are commonly not contained in a multiphase model formulation. The sum of total energies

$$\phi_s \rho_s E_s + \phi_f \rho_f E_f$$

must fulfill a conservation equation, which creates a new condition involving the constitutive laws of the model. This energy condition eliminates the additional degree of freedom [77]. As explained in the Eulerian-Eulerian model derivation, in contrast to single-phase models, incompressible multiphase models do not decouple from the energy equation as the pressures are intrinsically coupled to the microscopic quantities. Different forms of the total energy have been proposed [60, 120], but it is commonly understood that it should contain microscopic quantities. Unfortunately, there are no constitutive laws universally accepted for the microscopic quantities. It would also add additional degrees of freedom to the already large system, thus a common approach is to define a new pressure p_c - herein forth called collision pressure - as the difference between solid and liquid pressure, i.e.

$$p_c = \phi_s(p_s - p_f), \tag{2.2.18}$$

and propose a constitutive law for this term, cf. [31]. The introduction of an additional condition for the pressures allows the elimination of one variable and the system becomes closed.

The simplest approach is to set $p_c = 0$, which corresponds to setting $p_s = p_f$. This ansatz is called "one-pressure" or "equal-pressure" model [77, 120], but an analysis of the one-dimensional system shows it to be allegedly ill-posed, see e.g. the discussion in [31, 41]. The reason is, that a study of the one-dimensional first-order system's characteristics shows they contain complex parts, meaning the system is not hyperbolic in time, which contradicts the causality principle. Linear stability analysis showed, that additional second order terms do not fix this "loss of hyperbolicity" problem, as first order terms always become dominant in the long-wave limit [105]. Thus, a simple introduction of a small viscous term does not solve this problem. However, linear stability analysis of finite difference methods showed that in case of coarse grids the instability is suppressed and it only reoccurs for grid sizes that resolve microscopic sizes [121]. Thus, numerical approximations can be used in combination with coarse mesh sizes without occurrence of an instability [121].

A different line of thinking is to argue that the discussion about the "loss-of-hyperbolicity" is misleading, since the derivation of the problem needs two basic assumptions: First, the system is locally behaving as its linearized version and, secondly, its solutions are sufficient smooth [134]. The arguments against linearization of a nonlinear problem are well-known, since a linear stability analysis of a non-linear problem might show a system to be unconditional stable although it is

not, cf. Couette flow [117], and it might show a problem is linearly unstable although its nonlinear equation might be stable, cf. the Kuramoto-Sivashinsky equation [134]. The second argument against smooth solutions needs some more elaboration. It is a well-known phenomenon that nonlinear conservation laws of the form

$$\partial_t u + \partial_x f(u) = 0$$

create shocks. For physical plausibility we assume the shock solutions to adhere to the Rankine-Hugoniot and Lax entropy conditions

$$s = \frac{f(u_u) - f(u_d)}{u_u - u_d}, \qquad f'(u_u) > s > f'(u_d),$$

where u_u and u_d are the upwind and downwind solution at the shock, respectively [74]. Then, the shocks decay the total variation $\int_\Omega u^2 \mathrm{d}x$ for convex f and for long times [73, 74] and after some time the energy is expected to dissipate, i.e.

$$\frac{\mathrm{d}}{\mathrm{d}t} \int_\Omega u^2 \mathrm{d}x < 0 \qquad \text{for } t \gg 1.$$

The behavior of nonlinear systems of conservation laws can be more complex and Keyfitz et al. identified so-called singular shocks [65, 67, 68] in a reduced model of the incompressible Eulerian-Eulerian model. These singular shocks do not diminish the total variation of the solution, but Keyfitz [66] still argues for these special type of shocks:

> Shocks cause decay of energy even in the absence of an explicit dissipative mechanism such as viscosity.

and

> ... the variation of the solution grows without bound, as in some hyperbolic systems. However, there would be no catastrophic Hadamard instability for t positive.

This mechanism cannot be captured by linear stability analysis and might be a way to still consider the equal-pressure model. Further, it has been shown for a different reduced model, that viscous solutions fulfill certain amplitude bounds and in the weak limit one might expect a highly oscillatory weak-solution [65, 134].

In case one likes to fix the loss-of-hyperbolicity problem the one-dimensional linear stability analysis shows a force of the form

$$F = c(\boldsymbol{u}_s - \boldsymbol{u}_f)^2 \nabla \phi_s \tag{2.2.19}$$

renders all characteristics real and fixes the ill-posedness, where c is a positive constant depending on the additional forces in the model [2, 41, 77]. Unfortunately, this term does generally not fulfill the energy condition discussed above, thus is considered unphysical [77]. Besides the addition of (2.2.19) other attempts have been proposed to fix the loss-of-hyperbolicity problem, namely two-pressure models, introduction of added-mass forces and Reynolds stress terms, see e.g. [41, 77]. None of the proposed solutions is universally accepted, and it is still considered an open problem.

In what follows, we propose a one-pressure model, where we state an explicit term for p_c, which is of second order, thus the system might contain the instability. If necessary we can add a force of the form (2.2.19), then in the case of the plane Couette and plane Poiseuille flow this term does not change our results, since it does not appear at the considered asymptotic orders.

2.3 Constitutive laws

To complete model (2.2.16), we need to specify the stress terms $\boldsymbol{\tau}_f$ and $\boldsymbol{\tau}_s$, the momentum coupling term $\boldsymbol{M}_s^d$ and the collision pressure p_c. For a list of common choices for liquid and particle stresses see Chapter 1.

Coupling term choices in the literature

The exact form of $\boldsymbol{M}_s^d$ is still a matter of debate and several proposals can be found in the literature. See for example [31, 58, 88] and Drew [31] for an exhaustive list of possible terms.

The momentum coupling term $\boldsymbol{M}_s^d$ models the momentum transfer from one phase to the other. Common causes of such a momentum transfer are viscous drag, wake, boundary-layer formation, lift effects and virtual mass effects [31]. It is usually given as product of the difference velocity $\boldsymbol{w} = \boldsymbol{u}_f - \boldsymbol{u}_s$ and a function of ϕ_s, possible including their derivatives in space and time. Table 2.1 shows some common forms found in the literature.

Model proposed by	Constitutive law for the momentum coupling
Ahnert et al. [2]	$\boldsymbol{M}_s^d = \frac{\mu_f {\phi_s}^2}{K_P \phi_f} \boldsymbol{w}$
Morris et al. and Nott et al. [88, 95]	$\boldsymbol{M}_s^d = \frac{4.5\mu_f}{a^2} \frac{\phi_s}{{\phi_f}^3} \boldsymbol{w}$
Inkson [31, 58]	$\boldsymbol{M}_s^d = \frac{6}{8a}\phi_f\phi_s\rho_c\lvert\boldsymbol{w}\rvert \left[\frac{24}{\mathrm{Re}}\left(1+\mathrm{Re}^{0.681}\right)\right]\boldsymbol{w}$, with $\mathrm{Re} = 2\rho_c\lvert\boldsymbol{w}\rvert\frac{a}{\mu_f}$
Drew [31]	$\boldsymbol{M}_s^d = A_1\boldsymbol{w} + A_2(\partial_t\boldsymbol{u}_f + \boldsymbol{u}_s\nabla\boldsymbol{u}_f - (\partial(\boldsymbol{u}_s) + \boldsymbol{u}_f\nabla\boldsymbol{u}_s)) + A_3\boldsymbol{w}\dot{\boldsymbol{\gamma}}_s + A_4\boldsymbol{w}\dot{\boldsymbol{\gamma}}_f + A_5\boldsymbol{w}\cdot\nabla\boldsymbol{w} + A_6\boldsymbol{w}\cdot\nabla\boldsymbol{w}^T$

Table 2.1: Shown are different choices for the momentum coupling term $\boldsymbol{M}_s^d$ from the literature. It is commonly agreed upon that it should be a scalar, containing a ϕ_s dependence and is multiplied by the difference velocity $\boldsymbol{w}$, but constants and the exact terms are still unknown.

Collision pressure choices in the literature

As previously defined in Section 2.2 we denote by p_c the collision pressure function, which might depend on the solid volume fraction ϕ_s and a velocity $\boldsymbol{u}$. The definitions of p_c vary vastly in the scientific community, which is a strong hint, that the final form of this term is still unknown. There are three main classes of p_c functions. The first class consists of collision pressures that depend on only on ϕ_s, see e.g. [16, 31, 118]. It is often introduced solely for well-posedness

or stems from chemical potentials. The second class has a ϕ_s and $\boldsymbol{u}$ dependence, where the velocity is commonly used in the form of the shear rate [88]. Examples are the suspension balance model [95] and the model by Inkson et al. [58]. Finally, the third class contains non-local terms in ϕ_s and $\boldsymbol{u}$ [88], which can occur in the form of either integral terms or supplemental elliptic partial differential equations. For models using this kind of relations see for example [88] and the two-pressure model, cf. [77].

Authors	Constitutive law for the collision pressure p_c
Sjögreen et al. [118]	$p_c(\phi_s) = {\phi_s}^2$
Morris and Boulay [88]	$\boldsymbol{P}_c(\phi_s, \boldsymbol{v}) = \mu_f \eta_n(\phi_s) \begin{pmatrix} 1 & 0 & 0 \\ 0 & \lambda_2 & 0 \\ 0 & 0 & \lambda_3 \end{pmatrix} \lvert\dot{\boldsymbol{\gamma}}\rvert,$ $\eta_n(\phi_s) = K_n \left(\frac{\phi_s}{\phi_{\text{crit}} - \phi_s}\right)^2$
Inkson et al. [58]	$\boldsymbol{P}_c(\phi_s, \boldsymbol{u}_s) = \mu_f \eta_n(\phi_s) \begin{pmatrix} 1 & 0 & 0 \\ 0 & \lambda_2 & 0 \\ 0 & 0 & \lambda_3 \end{pmatrix} \lvert\dot{\boldsymbol{\gamma}}_s\rvert,$ $\eta_n(\phi_s) = K_n \left(\frac{\phi_s}{\phi_{\text{crit}} - \phi_s}\right)^2$
Nott and Brady [95]	$p_c(\phi_s, \boldsymbol{v}) = \mu_f p(\phi_s) \lvert\dot{\boldsymbol{\gamma}}\rvert,$ $p(\phi_s) = {\phi_s}^{1/2} \left[\left(\frac{\phi_{\text{crit}}}{\phi_{\text{crit}} - \phi_s}\right)^2 - 1 \right]$
Nott and Brady [95]	$p_c(\phi_s, \boldsymbol{v}) = \mu_f p(\phi_s) T^{1/2},$ $p(\phi_s) = {\phi_s}^{1/2} \left[\left(\frac{\phi_{\text{crit}}}{\phi_{\text{crit}} - \phi_s}\right)^2 - 1 \right]$ T solves an elliptic PDE of ϕ_s and $\boldsymbol{v}$
Drew [31]	$p_c(\phi_s) = \begin{cases} 0 & \text{for } \phi_s < \phi_{\text{crit}} \\ \text{divergent} & \text{for } \phi_s \geq \phi_{\text{crit}} \end{cases}$
Ahnert et al. [2, 15] and similar to Lecampion et al. [75]	$p_c(\phi_s, \boldsymbol{u}_s) = \mu_f \eta_n(\phi_s) \lvert\dot{\boldsymbol{\gamma}}_s\rvert,$ $\eta_n(\phi_s) = K_n \left(\frac{\phi_s}{\phi_{\text{crit}} - \phi_s}\right)^2$

Table 2.2: Shown are some common constitutive laws for the collision pressure. The proposed forms differ in their dependence on the velocity, usage of scalar or tensorial form and local vs. non-local terms in use.

Among the proposed models there are different velocities in use. For derivations based on the suspension balance model the collision pressure depends on the volumetric velocity $\boldsymbol{v}$ [95], whereas models with separate momentum equations for the phases usually have a dependence on one of the phase velocities $\boldsymbol{u}_f$ or $\boldsymbol{u}_s$ see e.g. [2, 41]. If anisotropic rheologies are to be modeled, then p_c is

given as a tensor quantity $\boldsymbol{P}_c$ and instead of the gradient of the collision pressure the divergence of the tensor is used, see e.g. [88]. This is a direct generalization of the scalar collision pressure, since a term of the form $\boldsymbol{P}_c = p_c(\phi_s, \boldsymbol{u})\boldsymbol{I}$ can model any scalar behavior. Table 2.2 shows some common forms found in the literature.

Choices for our model

Initially, we specify the momentum coupling $\boldsymbol{M}_s^d$. We choose a formulation that reduces to Darcy's law (1.2.4) in the appropriate asymptotic regime, see Section 7.1, so that

$$\boldsymbol{M}_s^d = \frac{\mu_f {\phi_s}^2}{K_p \phi_f}(\boldsymbol{u}_f - \boldsymbol{u}_s),$$

where K_p is the so-called permeability coefficient [10].

The liquid is assumed to have a Newtonian rheology, so that

$$\boldsymbol{\tau}_f = \mu_f \left(\nabla \boldsymbol{u}_f + (\nabla \boldsymbol{u}_f)^T - \frac{2}{3} \nabla \cdot \boldsymbol{u}_f \boldsymbol{I} \right) + \mu^* \nabla \cdot \boldsymbol{u}_f \boldsymbol{I},$$

where the first part describes Newtonian rheology for compressible liquids (1.1.3) - (1.1.4) and the second part describes the bulk effects with $\mu^* > 0$ the bulk viscosity [10, 122]. We need to use the compressible definition here, because the liquid velocity is not divergence-free, cf. Section 2.2. The total bulk viscosity can become dominant for concentrated suspensions [122], but for convenience we choose $\mu^* = \frac{2}{3}\mu_f$ in the current chapter, such that the liquid stress simplifies to

$$\boldsymbol{\tau}_f = \mu_f \dot{\boldsymbol{\gamma}}_f,$$

with the liquid shear rate definition

$$\dot{\boldsymbol{\gamma}}_f = \nabla \boldsymbol{u}_f + (\nabla \boldsymbol{u}_f)^T.$$

Since our original motivation for the model comes from drying front modeling, we like to describe dilute up to concentrated suspensions by our solid stress definition. We already showed popular choices for the viscosity of suspensions in Section 1.2. Recently, Jop et al. [63] proposed constitutive laws for granular flows, which is based on the idea, that they behave similar to viscoplastic fluids. They use a non-dimensional number - the so-called inertial number I - in order to collapse experimental results of different media onto a single curve [63]. Inspired by this work, Boyer et al. [15] proposed constitutive laws for suspensions that are supposed to be valid for dilute up to concentrated flows using the non-dimensional viscous number I_v. Their model contains five parameters: The maximum packing coefficient ϕ_{crit}, the minimum and maximum friction coefficients μ_1 and μ_2, the viscosity μ_f and a non-dimensional parameter I_0 describing the slope of the friction. All of which have to be chosen depending on the rheology of the suspension, but can be estimated using shear-flow experiments [15]. In their work they measured the values

$$\phi_{\text{crit}} = 0.585, \qquad \mu_1 = 0.32, \qquad \mu_2 = 0.7, \qquad I_0 = 0.005, \qquad \mu_f = 3.1\,\text{Pa}\,\text{s},$$

for a Triton X-100/water/zinc chloride mixture [15]. Further, the constitutive laws have been asserted with numerical simulations by Trulsson [129]. Hence, we use the shear stress definition [15]

$$\boldsymbol{\tau}_s = \mu_f \eta_s \dot{\boldsymbol{\gamma}}_s,$$

with the solid shear rate definition

$$\dot{\boldsymbol{\gamma}}_s = \nabla \boldsymbol{u}_s + (\nabla \boldsymbol{u}_s)^T,$$

and the solid viscosity functions

$$\eta_s(\phi_s) = 1 + \frac{5}{2}\frac{\phi_{\text{crit}}}{\phi_{\text{crit}} - \phi_s} + \mu_c(\phi_s)\frac{\phi_s}{(\phi_{\text{crit}} - \phi_s)^2}, \tag{2.3.1}$$

$$\mu_c(\phi_s) = \mu_1 + \frac{\mu_2 - \mu_1}{1 + I_0{\phi_s}^2(\phi_{\text{crit}} - \phi_s)^{-2}}. \tag{2.3.2}$$

Note, Boyer et al. [15] measured the total stress of a suspension, but we have to specify the phasic solid stress. Therefore, we adapted their constitutive law in order to yield the same total stress, i.e.

$$\boldsymbol{\tau} = \phi_s \boldsymbol{\tau}_s + \phi_f \boldsymbol{\tau}_f,$$

for our suspension. In contrast, a usage of these constitutive laws for the total momentum in combination with the volumetric velocity would result in unphysical behavior: Imaging a liquid flow through a porous medium. This setup would require the total viscosity to diverge since $\phi_s \approx \phi_{\text{crit}}$, so the volumetric velocity vanishes. But since the liquid still flows through the medium, an opposite solid flow would be induced, which has not been observed in experiments.

The collision pressure term p_c has been originally proposed as a convenient tool to state a closure condition for the multiphase model. However, a physical interpretation of the term can be given in terms of collisions between rigid particles [31]. Boyer et al. measured a normal stress of the particles due to shear, which we use for our collision pressure definition. The condition for the collision pressure (2.2.18) is

$$p_c = \eta_n(\phi_s)|\dot{\boldsymbol{\gamma}}_s|,$$

with the normal viscosity function

$$\eta_n(\phi_s) = \left(\frac{\phi_s}{\phi_{\text{crit}} - \phi_s}\right)^2. \tag{2.3.3}$$

The previous choices for p_c and $\boldsymbol{\tau}_s$ are just valid for $\dot{\boldsymbol{\gamma}}_s > 0$, since in the case $\dot{\boldsymbol{\gamma}}_s = 0$ the particle stress losses its meaning, cf. [75]. Thus, we demand for $\dot{\boldsymbol{\gamma}}_s = 0$ the relations

$$\phi_s = \phi_{\text{crit}}$$

and

$$|\phi_s \boldsymbol{\tau}_s| < \mu_1 p_c.$$

2.4 Non-dimensionalization

We introduce characteristic scales via

$$x = Lx', \qquad y = Ly', \qquad z = Lz',$$
$$t = \frac{L}{U}t', \qquad \boldsymbol{u}_k = U\boldsymbol{u}_k', \qquad p_k = \frac{U\mu_f}{L}p_k',$$

for $k \in \{s, f\}$. After non-dimensionalization, we drop the primes and also the bars and hats indicating averaging, and obtain the system

$$\partial_t \phi_f + \nabla \cdot (\phi_f \boldsymbol{u}_f) = 0, \tag{2.4.1a}$$

$$\partial_t \phi_s + \nabla \cdot (\phi_s \boldsymbol{u}_s) = 0, \tag{2.4.1b}$$

$$\mathrm{Re}[\partial_t(\phi_f \boldsymbol{u}_f) + \nabla \cdot (\phi_f \boldsymbol{u}_f \otimes \boldsymbol{u}_f)] \tag{2.4.1c}$$

$$-\nabla \cdot (\phi_f \boldsymbol{\tau}_f) + \phi_f \nabla p_f = -\mathrm{Da}\, \frac{{\phi_s}^2}{\phi_f}(\boldsymbol{u}_f - \boldsymbol{u}_s),$$

$$\frac{\mathrm{Re}}{r}[\partial_t(\phi_s \boldsymbol{u}_s) + \nabla \cdot (\phi_s \boldsymbol{u}_s \otimes \boldsymbol{u}_s)] \tag{2.4.1d}$$

$$-\nabla \cdot (\phi_s \boldsymbol{\tau}_s) + \phi_s \nabla p_f + \nabla p_c = \mathrm{Da}\, \frac{{\phi_s}^2}{\phi_f}(\boldsymbol{u}_f - \boldsymbol{u}_s).$$

Three dimensionless numbers appear here, namely the Reynolds number $\mathrm{Re} = UL\rho_f/\mu_f$, the Darcy number $\mathrm{Da} = L^2/K_p$ and the density ratio $r = \rho_f/\rho_s$. We focus on the case, where liquid and solid phases are density matched, i.e. $r = 1$.

The non-dimensional versions of the constitutive equations for the rheology are now as follows: For the liquid phase, we have

$$\boldsymbol{\tau}_f = \dot{\boldsymbol{\gamma}}_f.$$

For the solid phase, either $|\dot{\boldsymbol{\gamma}}_s| > 0$, then

$$\boldsymbol{\tau}_s = \eta_s(\phi_s)\dot{\boldsymbol{\gamma}}_s, \tag{2.4.2a}$$

$$p_c = \eta_n(\phi_s)|\dot{\boldsymbol{\gamma}}_s|, \tag{2.4.2b}$$

with (2.3.1)-(2.3.3); or $\dot{\boldsymbol{\gamma}}_s = 0$, and then we require

$$\phi_s = \phi_{\mathrm{crit}}$$

and

$$|\phi_s \boldsymbol{\tau}_s| \leq \mu_1 p_c.$$

The continuity conditions across yield surfaces carry over from the dimensional equations and also the parameters, μ_1, μ_2 and I_0 and ϕ_{crit}, which were non-dimensional to begin with.

Remark

Let us note that in the near-critical, or jamming limit, when $\phi_s \to \phi_{\mathrm{crit}}$, and for fixed contact pressure $p_c = \phi_s(p_s - p_f)$, it follows from (2.4.2b), (2.3.3) that $\dot{\boldsymbol{\gamma}}_s$ tends to zero as $O((\phi_{\mathrm{crit}} - \phi_s)^2)$. Thus, the solid phase velocity $\boldsymbol{u}_s$ becomes uniform, so that in a conveniently chosen reference frame, it is at rest. Notice, however, that $|\phi_s \boldsymbol{\tau}_s| \to \mu_1 p_c$ remains $O(1)$ due to (2.4.2a), (2.3.1), (2.3.2). The equations for the liquid phase become

$$\nabla \cdot \boldsymbol{u}_f = 0,$$

$$\mathrm{Re}\,[\partial_t \boldsymbol{u}_f + \nabla \cdot (\boldsymbol{u}_f \otimes \boldsymbol{u}_f)] = -\nabla p_f + \nabla \cdot \dot{\boldsymbol{\gamma}}_f - \mathrm{Da}\, \frac{{\phi_s}^2}{{\phi_f}^2}(\boldsymbol{u}_f - \boldsymbol{u}_s).$$

If, in addition, Da $\to \infty$, the term $\nabla \cdot \dot{\boldsymbol{\gamma}}_f$ and the inertia terms drop out from the second equation and we recover as a limiting case Darcy's law for a porous medium. This line of through leads to the study of highly dilute or concentrated flow cases in Chapter 7. There we also look for a thin-film approximation of the proposed model and find connections to single-phase Bingham flow.

Chapter 3

Simple laminar flows

In contrast to the single-phase case exact solutions of multiphase models are rarer. Here, we apply the new multiphase model from Chapter 2 to simple laminar flows. In particular we derive simple solutions for the plane Couette and plane Poiseuille flow. The solution for the plain Poiseuille flow has a solid and a liquid region, which shows the model contains a viscoplastic behavior trough the appearance of a yield-stress. This has not been reported for Eulerian-Eulerian models before. The derived solution is studied using phase space methods and approximated using the method of matched asymptotic expansions. In the final part of this chapter, we consider the evolution towards the plane Poiseuille flow solution by also considering a time dependence. This allows us the derivation of a novel drift-flux model for viscoplastic fluids via the method of matched asymptotic expansions.

3.1 Plane Couette flow

We consider a flow situation between a stationary bottom plate and the top plate that is moved at a fixed velocity, which by choice of scales can be set to one. Thus,

$$\boldsymbol{u}_s = \mathbf{0}, \qquad \boldsymbol{u}_f = \mathbf{0}, \qquad \text{at } y = 0 \tag{3.1.1}$$

and

$$\boldsymbol{u}_s = \begin{pmatrix} 1 \\ 0 \end{pmatrix}, \qquad \boldsymbol{u}_f = \begin{pmatrix} 1 \\ 0 \end{pmatrix}, \qquad \text{at } y = 1.$$

We seek stationary solutions with constant $\phi_s > 0$ and pressure and velocity components $\boldsymbol{u}_k = (u_k, v_k)$ that only depend on y for both phases.

From equations (2.4.1a), (2.4.1b) and the boundary conditions, we obtain

$$v_s = 0, \qquad v_f = 0,$$

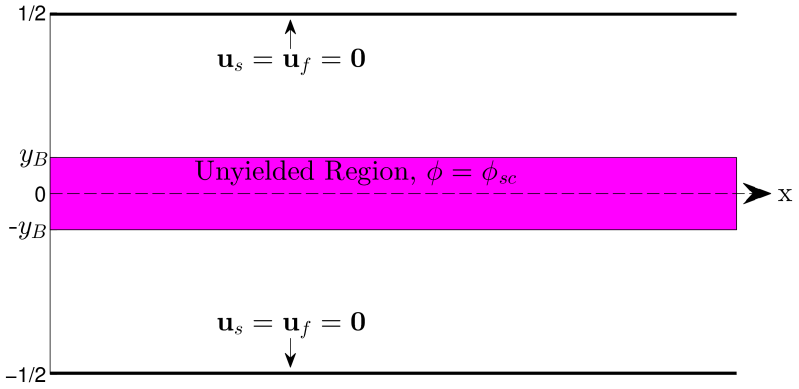

Figure 3.1: Sketch of the flow situation in a channel.

and therefore

$$\dot{\gamma}_s = \begin{pmatrix} 0 & \partial_y u_s \\ \partial_y u_s & 0 \end{pmatrix}, \qquad \dot{\gamma}_f = \begin{pmatrix} 0 & \partial_y u_f \\ \partial_y u_f & 0 \end{pmatrix}.$$

The second component of equations (2.4.1c) yield a constant fluid pressure, i.e. $p_f = \text{const}$. The same for the second component of (2.4.1d) yields a constant collision pressure, thus

$$p_c = \phi_s(p_s - p_f) = \eta_n(\phi_s)|\partial_y u_s| = \text{const}. \tag{3.1.2}$$

The total stress $\boldsymbol{\tau} \equiv \phi_s \boldsymbol{\tau}_s + \phi_f \boldsymbol{\tau}_f$ is constant as can be seen by summing equations (2.4.1c) and (2.4.1d). Using all this information for the first components of (2.4.1c) and (2.4.1d) gives

$$\begin{aligned} -\partial_y(\phi_f \partial_y u_f) &= -\mathrm{Da}\frac{{\phi_s}^2}{\phi_f}(u_f - u_s), \\ -\partial_y(\phi_s \eta_s(\phi_s)\partial_y u_s) &= \mathrm{Da}\frac{{\phi_s}^2}{\phi_f}(u_f - u_s). \end{aligned} \tag{3.1.3a}$$

Since we have assumed that ϕ_s is constant, and because of (3.1.2), we can conclude that the left hand side of (3.1.3a) is zero. Thus, together with the boundary conditions (3.1.1), we obtain that

$$u_s(y) = u_f(y) = y.$$

Note, this solution and derivation is similar to the single-phase case of the plane Couette flow, see e.g. [115].

3.2 Plane Poiseuille flow

It is instructive to investigate the properties of the model (2.4.1) for one of the classical flow situations, namely, plane Poiseuille or channel flow. We think it is the simplest flow geometry to

exhibit the emergence of a jammed region, because it is known from single-phase models that the total stress is a linear function of y and being zero at the center of the channel. Thus, any positive yield stress must become dominant near the center of the channel.

We suppose the dimensions of the channel are $0 < x < L$ and $-\frac{1}{2} < y < \frac{1}{2}$ and prescribe for the inlet conditions at $x = 0$

$$\phi_s = \phi_{s,in}, \quad \boldsymbol{u}_f = \begin{pmatrix} u_{f,in}\left(\frac{1}{4} - y^2\right) \\ 0 \end{pmatrix}, \quad \boldsymbol{u}_s = \begin{pmatrix} u_{s,in}\left(\frac{1}{4} - y^2\right) \\ 0 \end{pmatrix}$$

and for the outlet condition at $x = L$

$$\boldsymbol{n} \cdot (-p_s \boldsymbol{I} + \phi_s \eta_s (\nabla \boldsymbol{u}_s)^T) = 0, \quad \boldsymbol{n} \cdot (-p_f \boldsymbol{I} + \phi_f \eta_s (\nabla \boldsymbol{u}_s)^T) = 0.$$

In addition, the inertial effects are negligible since it is a parallel shear flow and we obtain for the bulk equations

$$\begin{aligned} \partial_t \phi_f + \nabla \cdot (\phi_f \boldsymbol{u}_f) &= 0, \\ \partial_t \phi_s + \nabla \cdot (\phi_s \boldsymbol{u}_s) &= 0, \\ -\nabla \cdot (\phi_f \boldsymbol{\tau}_f) + \phi_f \nabla p_f &= -\mathrm{Da} \frac{{\phi_s}^2}{\phi_f} (\boldsymbol{u}_f - \boldsymbol{u}_s), \\ -\nabla \cdot (\phi_s \boldsymbol{\tau}_s) + \phi_s \nabla p_f + \nabla p_c &= \mathrm{Da} \frac{{\phi_s}^2}{\phi_f} (\boldsymbol{u}_f - \boldsymbol{u}_s), \\ \phi_f + \phi_s &= 1, \end{aligned}$$

where

$$\begin{aligned} &\boldsymbol{\tau}_f = \dot{\boldsymbol{\gamma}}_f, \\ &|\phi_s \boldsymbol{\tau}_s| \le \mu_1 p_c, && \phi_s = \phi_{\mathrm{crit}}, && \text{if } |\dot{\boldsymbol{\gamma}}_s| = 0, \\ &\boldsymbol{\tau}_s = \eta_s(\phi_s) \dot{\boldsymbol{\gamma}}_s, && p_c = \eta_n(\phi_s) |\dot{\boldsymbol{\gamma}}_s|, && \text{if } |\dot{\boldsymbol{\gamma}}_s| \neq 0. \end{aligned} \tag{3.2.2a}$$

At the channel walls, we assume the no-slip conditions

$$\boldsymbol{u}_s = \boldsymbol{0}, \qquad \boldsymbol{u}_f = \boldsymbol{0}.$$

For the two-phase model at hand, it turns out to be advantageous to formulate the problem in terms of the flow variables

$$\boldsymbol{v} \equiv \phi_f \boldsymbol{u}_f + \phi_s \boldsymbol{u}_s, \qquad \boldsymbol{w} \equiv \boldsymbol{u}_f - \boldsymbol{u}_s.$$

In these variables, noting that $\boldsymbol{v} + \phi_s \boldsymbol{w} = \boldsymbol{u}_f$, $\boldsymbol{v} - \phi_f \boldsymbol{w} = \boldsymbol{u}_s$ and using $\phi_f = 1 - \phi_s$ the problem can be written as

$$\nabla \cdot \boldsymbol{v} = 0, \tag{3.2.3a}$$

$$\partial_t \phi_s + \nabla \cdot (\phi_s \boldsymbol{v} - \phi_s (1 - \phi_s) \boldsymbol{w}) = 0, \tag{3.2.3b}$$

$$-\nabla \cdot \left((1 - \phi_s) \dot{\boldsymbol{\gamma}}_f\right) + (1 - \phi_s) \nabla p_f = -\mathrm{Da} \frac{{\phi_s}^2}{1 - \phi_s} \boldsymbol{w}, \tag{3.2.3c}$$

$$-\nabla \cdot (\phi_s \eta_s \dot{\boldsymbol{\gamma}}_s) + \phi_s \nabla p_f + \nabla(\eta_n |\dot{\boldsymbol{\gamma}}_s|) = \mathrm{Da} \frac{{\phi_s}^2}{1 - \phi_s} \boldsymbol{w}, \tag{3.2.3d}$$

and with no-slip conditions at the walls $y = \pm\frac{1}{2}$

$$\boldsymbol{v} = \boldsymbol{0}, \qquad \boldsymbol{w} = \boldsymbol{0}. \tag{3.2.3e}$$

Phase space analysis of the stationary problem

For the system (3.2.3a)-(3.2.3e) we now derive conditions for the existence of stationary two-dimensional solutions, where all quantities, except for the pressure, depend only on y. In addition, to simplify notation, we set $\phi_s \equiv \phi$ from now on.

$$\begin{aligned} \phi &= \phi(y), & \boldsymbol{v} &= \boldsymbol{v}(y), & \boldsymbol{w} &= \boldsymbol{w}(y), \\ \boldsymbol{\tau}_f &= \boldsymbol{\tau}_f(y), & \boldsymbol{\tau}_s &= \boldsymbol{\tau}_s(y), & p_f &= p_f(x,y). \end{aligned}$$

The combination of no-slip boundary conditions (3.2.3e) with (3.2.3a), (3.2.3b) yields (if v_1, v_2 and w_1, w_2 denote the components of the vectors $\boldsymbol{v}$ and $\boldsymbol{w}$, respectively)

$$v_2 = 0, \qquad w_2 = 0,$$

and therefore

$$\dot{\boldsymbol{\gamma}}_s = \begin{pmatrix} 0 & \partial_y(v_1 - (1-\phi)w_1) \\ \partial_y(v_1 - (1-\phi)w_1) & 0 \end{pmatrix},$$

and

$$\dot{\boldsymbol{\gamma}}_f = \begin{pmatrix} 0 & \partial_y(v_1 + \phi w_1) \\ \partial_y(v_1 + \phi w_1) & 0 \end{pmatrix}.$$

The second component from (3.2.3c) requires p_f to be independent of y. For the total stress $\boldsymbol{\tau} \equiv \phi_f \boldsymbol{\tau}_f + \phi_s \boldsymbol{\tau}_s$ we get from (3.2.3c), (3.2.3d)

$$\begin{aligned} \partial_x p_f - \partial_y \tau_{12} &= 0, \\ \partial_y p_c = \partial_y(\eta_n |\dot{\boldsymbol{\gamma}}_s|) &= 0. \end{aligned} \tag{3.2.5}$$

This means that in equation (3.2.5), one term only depends on x and the other only on y, so both have to be constant, therefore the solution is

$$p_f(x) = p_1 x + p_0,$$

where p_0 is a constant of integration, which by a choice of origin, we can assume, without loss of generality, to be zero, and

$$\tau_{12}(y) = p_1 y. \tag{3.2.6a}$$

This shows that the total stress for the plane Poiseuille case in the multiphase model is a linear function just like in the single-phase case, cf. [115]. From now on, we only look at the case of solutions with velocities and volume fractions that are symmetric with respect to $y = 0$ and that have at most one unyielded region for $-y_B \leq y \leq y_B$, i.e. with at most one y_B, where $0 \leq y_B \leq 1/2$. Due to the symmetry assumption, the constant contribution to τ_{12} has been set to zero in (3.2.6a) and it is sufficient to consider only non-negative y. The same reasoning as above further shows

$$p_c = \text{const.} \qquad \text{if } |\dot{\boldsymbol{\gamma}}_s| > 0.$$

Thus, the contact pressure, p_c, is a constant here, which is free and thus acts as an additional parameter.

Overall we get the system: For $y \in [y_B; 1/2]$, ϕ, τ_{s12}, τ_{f12}, v_1 and w_1 satisfy

$$\partial_y((1-\phi)\tau_{f12}) = (1-\phi)p_1 + \mathrm{Da}\,\frac{\phi^2}{1-\phi}w_1, \tag{3.2.7a}$$

$$\phi_s \tau_{s12} = p_1 y - (1-\phi)\tau_{f12}, \tag{3.2.7b}$$

$$\partial_y w = \tau_{f12} - \frac{\tau_{s12}}{\eta_s(\phi)}, \tag{3.2.7c}$$

$$p_c = \eta_n(\phi)|\partial_y(v_1 - (1-\phi)w_1)|. \tag{3.2.7d}$$

In the unyielded region $y \in [0; y_B[$, equations (3.2.7a)-(3.2.7b) stay the same, but the two remaining ones are replaced by

$$\partial_y(v_1 - (1-\phi)w_1) \equiv \partial_y u_s = 0 \qquad \text{and} \qquad \phi = \phi_{\text{crit}}. \tag{3.2.7e}$$

The boundary conditions are the no-slip

$$v_1 = 0, \quad w_1 = 0, \qquad \text{at } y = 1/2, \tag{3.2.7f}$$

and symmetry conditions

$$\partial_y v_1 = 0, \quad \partial_y w_1 = 0, \qquad \text{at } y = 0. \tag{3.2.7g}$$

In case the unyielded region fills out the whole channel, i.e. $y_B = 1/2$, the no-slip boundary conditions together with (3.2.7e) gives $u_s = 0$. Then (3.2.7a) becomes the Brinkman equation, cf. [18] and Section 1.2. For the yield surface at $y = y_B$ we demand the continuity conditions

$$\begin{aligned} [\tau_{s12}]^+_- &= 0, & [\tau_{f12}]^+_- &= 0, & [v_1]^+_- &= 0, \\ [w_1]^+_- &= 0, & [\phi]^+_- &= 0, \end{aligned} \tag{3.2.7h}$$

where we denote $[g]^+_- = \lim_{y \searrow y_B} g - \lim_{y \nearrow y_B} g$. We remark that these conditions are not all independent, as, for example, the second condition in (3.2.7g) can be obtained from the first via (3.2.7e), and the continuity of one of the stresses in (3.2.7h) implies the other via (3.2.7b).

Notice that (3.2.7d) applies in the region $[y_B; 1/2]$ where $\dot{\boldsymbol{\gamma}}_s > 0$, so that, if $p_c = 0$, this implies $\phi = 0$, i.e. no solid phase, which seems ambiguous. We therefore assume $p_c > 0$. Then, we can remove p_c from the equations by rescaling

$$\begin{aligned} \tau_{s12} &= p_c\tilde{\tau}_{s12}, & \tau_{f12} &= p_c\tilde{\tau}_{s12}, & p_1 &= p_c\tilde{p}_1, \\ u_f &= p_c\tilde{u}_f, & u_s &= p_c\tilde{u}_s. \end{aligned}$$

The fact that p_c can be scaled out of the problem in this way implies that the width of the unyielded region i.e. y_B does not depend on p_c, as was reported in [59]. We note that in conventional Herschel-Bulkley models, which are also able to capture yield stress and shear-thinning, the unyielded region would change with p_c.

Phase space analysis

Using phase-space methods, we ask if for system (3.2.7) solutions exist and under which conditions, but first we reduce the system into a second order, non-autonomous system of ordinary differential equations for $w \equiv w_1$ and ϕ.

We first note that in the fluid region $y \in [y_B; 1/2]$ combining the definition of the solid stress (3.2.2a) and (3.2.7d) yields

$$\phi\tau_{s12} = \phi\eta_s\partial_y u_s = \frac{\phi\eta_s}{\eta_n}\text{sign}(\partial_y u_s) = -\frac{\phi\eta_s}{\eta_n}\text{sign}(y), \tag{3.2.8}$$

where we have made the assumption that $\text{sign}(\partial_y u_s) = \text{sign}(\boldsymbol{\tau}) = -\text{sign}(y)$ holds. This assumption is fundamental and based on the experimental observation, that channel velocity curves are roughly square profiles (cf. [50, 115]) and is further asserted by (3.2.6a), which states that the total stress is just a linear function. Since Da is large, we expect $\boldsymbol{u}_s \approx \boldsymbol{v}$ and this behavior should also be true for the solid velocity.

Then, using (3.2.7b) in (3.2.7a) and (3.2.8) yields

$$\partial_y N(\phi) = -\phi p_1 + \text{Da}\frac{\phi^2}{1-\phi}w, \tag{3.2.9a}$$

which is used as an equation for the solid volume fraction. We get an equation for w by combining (3.2.7b) and (3.2.7c) to give

$$\partial_y w = \frac{p_1 y + N(\phi)}{1-\phi} + \frac{1}{\eta_n(\phi)}. \tag{3.2.9b}$$

The function N, which is also referred to as friction coefficient [15, 75], is given by

$$N(\phi) \equiv \frac{\phi\eta_s(\phi)}{\eta_n(\phi)}.$$

In the unyielded region $y \in [0; y_B[$ we already know

$$\phi = \phi_{\text{crit}}$$

and since $\partial_y u_s = 0$, we have $\tau_{f12} = \partial_y u_f = \partial_y w$, which together with (3.2.7a) is

$$\partial_{yy} w = p_1 + \text{Da}\frac{\phi_{\text{crit}}^2}{(1-\phi_{\text{crit}})^2}w. \tag{3.2.9c}$$

Since $\partial_y u_s = 0$, we could choose $u_s = 0$ by considering an appropriate reference frame in the unyielded region. Then, equation (3.2.9c) is exactly Brinkman's equation for a porous medium, cf. [18] and Section 1.2.

At the channel wall and center, we have the boundary conditions

$$w = 0 \qquad \text{at } y = 1/2, \tag{3.2.9d}$$

$$\partial_y w = 0 \qquad \text{at } y = 0, \tag{3.2.9e}$$

and at the yield surface,

$$\phi = \phi_{\text{crit}}, \quad [w]^+_- = 0, \quad [w_y]^+_- = 0, \quad \text{at } y = y_B. \tag{3.2.9f}$$

The problem for w in the unyielded region, (3.2.9c) and (3.2.9e), can now be solved explicitly. For $\text{Da} > 0$, we have

$$w = \alpha_1 \cosh\left(\frac{\text{Da}^{1/2}\phi_{\text{crit}}}{1-\phi_{\text{crit}}} y\right) - \frac{(1-\phi_{\text{crit}})^2}{\text{Da}\,\phi_{\text{crit}}^2} p_1,$$

where α_1 is a constant of integration. We can use this in the last two conditions in (3.2.9f) to get

$$\partial_y w = \left(w + \frac{(1-\phi_{\text{crit}})^2}{\text{Da}\,\phi_{\text{crit}}^2} p_1\right) \frac{\text{Da}^{1/2}\phi_{\text{crit}}}{1-\phi_{\text{crit}}} \tanh\left(\frac{\text{Da}^{1/2}\phi_{\text{crit}}}{1-\phi_{\text{crit}}} y_B\right), \text{ at } y = y_B$$

and from this a new formulation of the free boundary condition

$$\phi = \phi_{\text{crit}}, \tag{3.2.10a}$$

$$w = W(y_B) \equiv \frac{p_1 y_B + \mu_1}{\text{Da}^{1/2}\phi_{\text{crit}} \tanh\left(\frac{\text{Da}^{1/2}\phi_{\text{crit}}}{1-\phi_{\text{crit}}} y_B\right)} - \frac{(1-\phi_{\text{crit}})^2}{\text{Da}\,\phi_{\text{crit}}^2} p_1, \quad \text{at } y = y_B. \tag{3.2.10b}$$

We have thus reduced the problem to a free boundary value problem for second order system of ODEs (3.2.9a), (3.2.9b) with a condition (3.2.9d) at the fixed boundary and two at the free boundary (3.2.10a), (3.2.10b).

For the solution of the boundary value problem (3.2.9), we proceed as follows. Rewriting (3.2.9a) for w, i.e.

$$w = \frac{(\partial_y N + \phi\, p_1)\,(1-\phi)}{\text{Da}\,\phi^2},$$

and using it in (3.2.9b) and the boundary conditions yields an equation solely in ϕ, i.e.

$$\partial_y\left(\frac{(\partial_y N + \phi\, p_1)\,(1-\phi)}{\text{Da}\,\phi^2}\right) = \frac{p_1 y + N}{1-\phi} + \frac{1}{\eta_n},$$

with boundary conditions

$$\begin{aligned} 0 &= \partial_y N + \phi_s\, p_1 && \text{at } y = \frac{1}{2}, \\ \phi &= \phi_{\text{crit}} && \text{at } y = y_B, \\ \frac{(\partial_y N + p_1)\,(1-\phi_{\text{crit}})}{\text{Da}\,\phi_{\text{crit}}^2} &= \frac{p_1 y_B + \mu_1}{\text{Da}^{\frac{1}{2}}\phi_{\text{crit}} \tanh\left(\frac{\text{Da}^{\frac{1}{2}}\phi_{\text{crit}}}{1-\phi_{\text{crit}}} y_B\right)} && \text{at } y = y_B. \end{aligned}$$

We transform the free-boundary problem (3.2.11) into fixed-domain problem via

$$y = \left(y_B - \frac{1}{2}\right)\zeta + \frac{1}{2},$$

where $\zeta \in [0,1]$, which introduces the free-boundary coordinate as an explicit parameter in the system, and then we add the trivial differential equation for the constant y_B to get the boundary value problem

$$\frac{1}{y_B - \frac{1}{2}} \partial_\zeta \left(\frac{\left(\frac{1}{y_B - \frac{1}{2}} \partial_\zeta N + \phi\, p_1 \right) (1-\phi)}{\mathrm{Da}\, \phi^2} \right) = \frac{p_1 \left((y_B - \frac{1}{2})\zeta + \frac{1}{2} \right) + N}{1-\phi} + \frac{1}{\eta_n},$$
$$\partial_\zeta y_B = 0,$$

with boundary conditions

$$\begin{aligned} 0 &= \partial_\zeta N + \left(y_B - \frac{1}{2} \right) \phi\, p_1 && \text{at } \zeta = 0, \\ \phi &= \phi_{\mathrm{crit}} && \text{at } \zeta = 1, \\ \partial_\zeta \phi &= -\frac{2(y_B - \frac{1}{2})}{5(1-\phi_{\mathrm{crit}})} \frac{\mathrm{Da}^{\frac{1}{2}} \phi_{\mathrm{crit}} (p_1 y_B + \mu_1)}{\tanh\left(\frac{\mathrm{Da}^{\frac{1}{2}} \phi_{\mathrm{crit}}}{1-\phi_{\mathrm{crit}}} y_B \right)} + \frac{2}{5} \left(y_B - \frac{1}{2} \right) p_1 && \text{at } \zeta = 1. \end{aligned}$$

We have thus reduced our original system into a nonlinear boundary value problem, which can be solved using standard methods like Matlab's *bvp5c* solver [85].

After solving for ϕ, we can determine the remaining variables by first using

$$\begin{aligned} p_c &= -\eta_n(\phi) \partial_y u_s, \\ u_f &= \frac{(\partial_y N + \phi p_1)(1-\phi)}{\mathrm{Da}\phi^2} + u_s, \end{aligned}$$

for the fluid region $y > y_B$ with no-slip boundary conditions and

$$\begin{aligned} \phi &= \phi_{\mathrm{crit}}, \\ \partial_y u_s &= 0, \\ \partial_y u_f &= \frac{p_1 y}{1-\phi_{\mathrm{crit}}}, \end{aligned}$$

in the plug-flow region with boundary conditions

$$[u_s]^+_- = [u_f]^+_- = 0 \quad \text{at } y = y_B.$$

Note, in contrast to the plane Couette flow, the base state for the multiphase Poiseuille flow is not similar to its corresponding single-phase solution, cf. [115]. Nevertheless, it has similarities with the solution of the Poiseuille flow of a single-phase Bingham fluid, cf. Section 4.2.

The minimum pressure condition

We now derive a condition for the minimum pressure gradient that guaranties the existence of nontrivial solutions of the stationary problem.

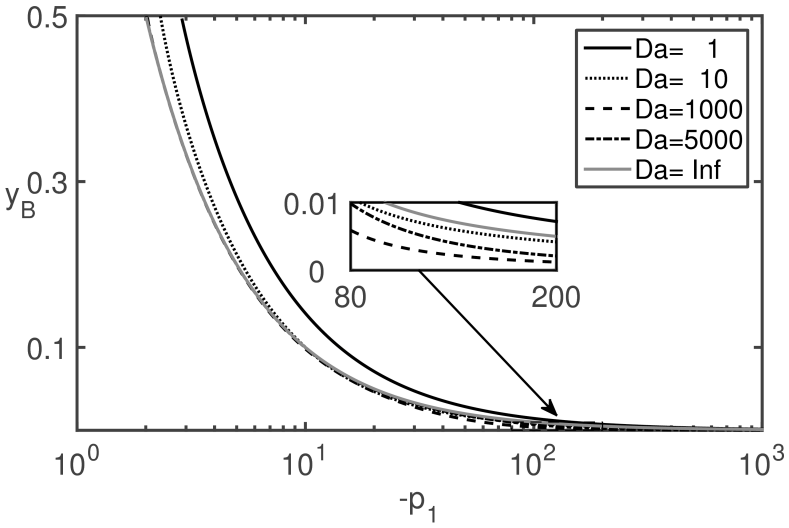

Figure 3.2: The dependence of the yield surface position y_B on the pressure gradient magnitude p_1, for parameters (3.2.14), $\mu_2 = 1$. The solid curve shows the results for Da $= 1$; the dotted one for Da $= 10$; the dashed curve for Da $= 1000$; the dotted-dashed curve for Da $= 5000$ and the gray curve for Da $= \infty$. For small $|p_1|$ we have a monotone dependence between Da and y_B - the bigger Da, the smaller y_B. For large $|p_1|$ (see inset) the behavior is more sophisticated, since we have a turning point $\mathrm{Da}_{\mathrm{turn}}$ depending on the parameters of the system. For Da $< \mathrm{Da}_{\mathrm{turn}}$ it shows the same behavior as for small $|p_1|$, but for Da $> \mathrm{Da}_{\mathrm{turn}}$ the value of y_B becomes larger for bigger Da.

Let y_{wall} be the position of the wall, i.e. in our case $y_{\mathrm{wall}} = 1/2$, then the minimum magnitude for the pressure gradient p_{min} can be explicitly computed from (3.2.10b) and $w(y_{\mathrm{wall}}) = 0$ as

$$p_{\mathrm{min}} = \frac{\phi_{\mathrm{crit}} \mathrm{Da}\, \mu_1}{y_{\mathrm{wall}} \mathrm{Da}\, \phi_{\mathrm{crit}} + \tanh\left(\dfrac{y_{\mathrm{wall}} \sqrt{\mathrm{Da}}\, \phi_{\mathrm{crit}}}{\phi_{\mathrm{crit}} - 1}\right) \sqrt{\mathrm{Da}}\, (1 - \phi_{\mathrm{crit}})^2}.$$

From this expression one can also see, that there must be always an unyielded region as $y_{\mathrm{wall}} \to 0$ implies $p_{\mathrm{min}} \to \infty$.

The dependence of the width of the unyielded zone on the pressure gradient is summarized in Figure 3.2. In all cases, there is a minimum magnitude for the pressure gradient, i.e. p_{min}, below which the unyielded region fills the entire channel. On the other hand, as p_1 decreases, the width of the unyielded region decreases as well. In fact, y_B tends to zero as $p_1 \to -\infty$, but always remains strictly positive for finite pressure gradients. For larger Da the unyielded region is getting smaller and in the limit Da $\to \infty$ it becomes the curve

$$y_B = -\frac{\mu_1}{p_1}. \tag{3.2.13}$$

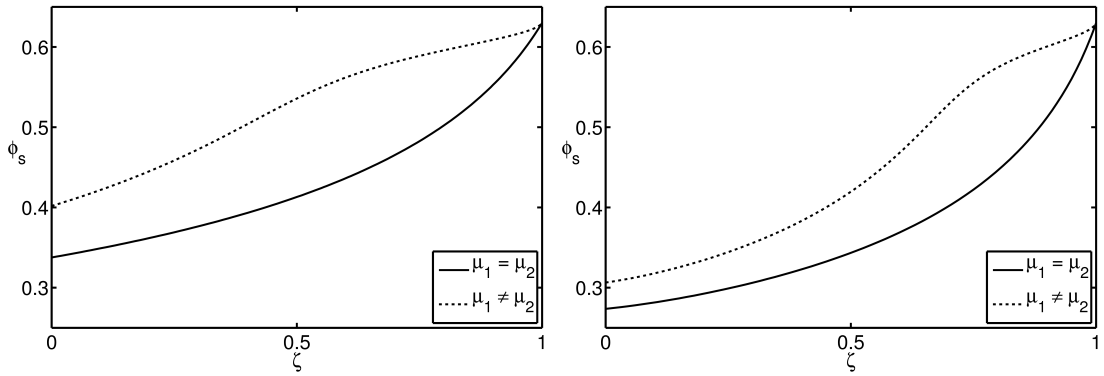

Figure 3.3: The trajectories for system (3.2.12), onto the ϕ_s-ζ-plane with $\mu_1 = \mu_2$ (continuous line) and $\mu_2 = 2$ (dotted line) as well as $\mathrm{Da} = 1$ (left) and $\mathrm{Da} = 1000$ (right).

Problem (3.2.9a), (3.2.9b) with boundary conditions (3.2.7f) and (3.2.10b) contains the parameters Da, ϕ_{crit}, p_1, μ_1, μ_2, I_0. The critical volume fraction ϕ_{crit} is typically chosen between 0.63 - 0.68 (volume fraction at maximum random packing). The channel pressure gradient value $p_1 \leq 0$ is a control parameter. Darcy's number Da is often given as the squared ratio of particle diameter, i.e. $\mathrm{Da} \approx (L/a)^2$, and can reach large values, see e.g. [88, 95]. The three parameters μ_1, μ_2 and I_0 are material parameters. In our study we fix

$$\phi_{\mathrm{crit}} = 0.63, \qquad \mu_1 = 1, \qquad I_0 = 0.005, \tag{3.2.14}$$

and vary p_1 and Da for $\mu_1 = \mu_2$. Notice that in this case, the term that depends on I_0 drops out. After that, we let $\mu_2 = 1.5$ and again vary p_1 and Da. Compare with the discussion of the parameters in Section 2.3 and note the different choices for μ_1 and μ_2, which has been done to circumvent an ill-posedness in the model as described in Chapter 4.

Case $\mu_1 = \mu_2$

Keeping in mind that we always keep the parameters in (3.2.14) fixed, we first consider $\mu_2 = \mu_1$ and let $\mathrm{Da} = 1$ and $p_1 = -5$, shown in Figure 3.3. If the magnitude of the pressure gradient is lowered below p_{min}, the yield surface position y_B is at the wall, implying there is no yielded region and the unyielded region extends through the entire cross section of the channel. If, on the other hand, Da is raised to a large value, e.g. $\mathrm{Da} = 1000$ with our first choice for the pressure gradient, the yield surface position becomes smaller, thus the unyielded region is thinner, as might have been expected for larger interphase stress due to drag. The effect in the $\phi_s - \zeta-$plane is a seemingly steeper ascent of the curve.

Case $\mu_1 \neq \mu_2$

Next, we consider $\mu_2 = 1.5 \neq \mu_1$ and $\mathrm{Da} = 1$, $p_1 = -5$. The profile of ϕ is very similar to the $\mu_1 = \mu_2$ case, but it additionally contains an inflection point just before the volume fraction reaches the critical value ϕ_{crit}. This is a consequence of the second term in μ_c dominating the first term, i.e. μ_1 for ϕ_s close to the maximum packing fraction, provided $\mu_2 > \mu_1$ and $I_0 > 0$.

Summarizing, unless the absolute pressure gradient becomes smaller than $p_{\min}$, the results suggest that there always exists a unique solution to the boundary value problem (3.2.9).

Full solutions

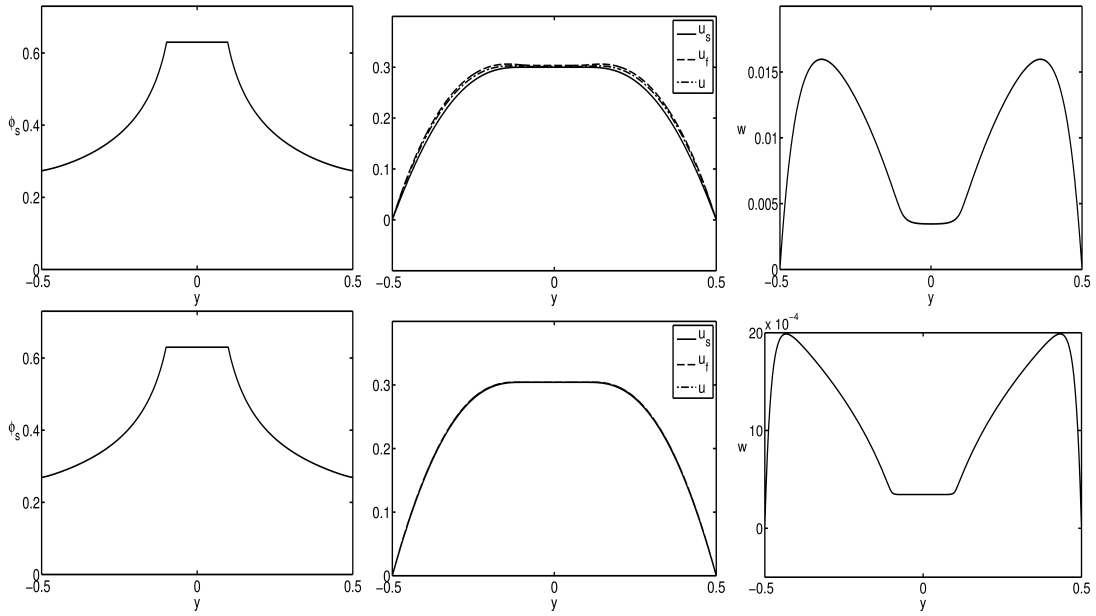

Figure 3.4: (left) The solid volume fraction ϕ_s, (middle) the velocities $\boldsymbol{u}_s, \boldsymbol{u}_f, \boldsymbol{u}$ and (right) the velocity difference w obtained by using the ODE problem (3.2.9). The parameters are given by (3.2.14), $\mu_2 = 1$, and $p_1 = -10$. Top figures show results for Da $= 1000$ and bottom figures for Da $= 10000$.

Figure 3.4 shows solutions for volume fraction, velocities and velocity difference across the whole channel. The solid volume fraction is usually increasing towards the channel center, where it has a non-vanishing region at maximum packing and falls back to its original value due to symmetry. The velocities are increasing towards the center, with a flattened profile around the unyielded region. We note that the fluid velocity has a dip around the center, thus reaches its maximum point not at the middle of the channel, but near the yield surface. The velocity difference w always has the form of an upside down w with a flattened region in the center.

We observe that for growing Da the solution of the stationary problem develops boundary layers, in particular the velocity w shows a pronounced sharp drop near the boundary $y = 1/2$. In the following section we make use of this property to derive an asymptotic solution of the stationary problem in the limit Da $= 1/\varepsilon \to \infty$. We expand on this analysis to derive a new drift-flux model from the time-dependent two-phase flow model for concentrated suspensions and use it to study the formation of unyielded or jammed regions in the flow.

Asymptotic analysis of the stationary state

For the typical physical situation Da can become quite large and as we observed in the previous paragraph, at the same time the value of w becomes very small. This suggest an asymptotic approximation of the problem using the ansatz

$$\mathrm{Da} = \frac{1}{\varepsilon}, \qquad w = \varepsilon \tilde{w}.$$

We drop from now on the tilde and obtain from (3.2.9a)-(3.2.9b)

$$w = p_1 \frac{1-\phi}{\phi} + \frac{1-\phi}{\phi^2} N'(\phi) \partial_y \phi. \tag{3.2.15a}$$

Substitution into equation for ϕ in (3.2.9b) yield the second order equation for ϕ

$$\varepsilon\, \partial_y \left(p_1 \frac{1-\phi}{\phi} + \frac{1-\phi}{\phi^2} N'(\phi) \partial_y \phi \right) = \frac{p_1 y + N(\phi)}{1-\phi} + \frac{(\phi_{\mathrm{crit}} - \phi)^2}{\phi^2}.$$

The boundary conditions at the yield interface $y = y_B$ are

$$\begin{aligned} \phi &= \phi_{\mathrm{crit}}, \\ \partial_y \phi &= -\varepsilon^{-1/2}\, \frac{2}{5}\, \frac{\phi_{\mathrm{crit}}}{1-\phi_{\mathrm{crit}}}\, \frac{p_1 y_B + \mu_1}{\tanh\left(\frac{\phi_{\mathrm{crit}}}{1-\phi_{\mathrm{crit}}} \varepsilon^{-1/2} y_B \right)} + \frac{2}{5} p_1, \end{aligned}$$

and at the channel wall $y = \frac{1}{2}$, we have $0 = p_1 \frac{1-\phi}{\phi} + \frac{1-\phi}{\phi^2} N'(\phi) \partial_y \phi$, since $w = 0$. Hence, we have the boundary condition

$$\partial_y \phi = -p_1 \frac{\phi}{N'(\phi)} \qquad \text{at } y = \frac{1}{2}.$$

Clearly, this is a singular perturbed problem with a boundary layer at $y = 1/2$ and $y = y_B$. In fact, if we assume that ϕ and y_B have asymptotic expansions

$$\phi(y) = \phi_0(y) + \varepsilon^{1/2} \phi_1(y) + O(\varepsilon), \qquad y_B = y_{B0} + \varepsilon\, y_{B1} + O(\varepsilon^2),$$

where we used to Landau O-notation. Then, to leading order, we have

$$0 = \frac{p_1 y + N(\phi_0)}{1-\phi_0} + \frac{(\phi_{\mathrm{crit}} - \phi_0)^2}{\phi_0^2}. \tag{3.2.16}$$

If we use this solution for ϕ in (3.2.15a), then the boundary conditions for w are not satisfied.

Boundary layer problem at $y = 1/2$

For the boundary layer variables $z = (\frac{1}{2} - y)\varepsilon^{-1/2}$ and $\Phi(z) = \phi(y)$ the governing equation is

$$\partial_z \left(-\varepsilon^{1/2}\, p_1 \frac{1-\Phi}{\Phi} + \frac{1-\Phi}{\Phi^2} N'(\Phi) \partial_z \Phi \right) = \frac{\frac{1}{2}\, p_1 + N(\Phi) - \varepsilon^{1/2}\, z}{1-\Phi} + \frac{(\phi_{\mathrm{crit}} - \Phi)^2}{\Phi^2},$$

with boundary condition at $z = 0$

$$(1-\Phi)\, N'(\Phi)\, \partial_z \Phi = \varepsilon^{1/2}\, p_1\, (1-\Phi)\Phi.$$

Assume the asymptotic expansion of the inner variables can be written as

$$\Phi(z) = \Phi_0(z) + \varepsilon^{1/2}\Phi_1(z) + O(\varepsilon),$$

so that the solution satisfies to leading order the problem

$$\partial_z \left(\frac{1-\Phi_0}{\Phi_0^2}\, N'(\Phi_0)\, \partial_z \Phi_0 \right) = \frac{\frac{1}{2}p_1 + N(\Phi_0)}{1-\Phi_0} + \frac{(\phi_{\rm crit} - \Phi_0)^2}{\Phi_0^2}$$
$$\partial_z \Phi_0 = 0 \qquad \text{at} \quad z = 0^+$$

since $(1-\Phi_0)\, N'(\Phi_0) \neq 0$. As $z \to \infty$ the solution approaches a constant, say $\Phi_0 \to \Phi_{0,\infty}$, which satisfies

$$\frac{\frac{1}{2}\, p_1 + N(\Phi_{0,\infty})}{1-\Phi_{0,\infty}} + \frac{(\phi_{\rm crit} - \Phi_{0,\infty})^2}{\Phi_{0,\infty}^2} = 0.$$

Hence, since for $y \to (1/2)^-$ in the leading order outer problem, then

$$0 = \frac{\frac{1}{2}\, p_1 + N\left(\phi_0(\frac{1}{2})\right)}{1-\phi_0(\frac{1}{2})} + \frac{\left(\phi_{\rm crit} - \phi_0(\frac{1}{2})\right)^2}{\phi_0^2(\frac{1}{2})}. \tag{3.2.19}$$

Therefore, matching yields $\Phi_{0,\infty} = \phi_0(1/2)$.

It is straightforward to solve the next order problem to obtain

$$\Phi_1(z) = \frac{A_2 N'(\phi_0\,(1/2)) - p_1 \phi_0\,(1/2)\, A_1}{A_1^{3/2} N'(\phi_0\,(1/2))} \exp\left(-\sqrt{A_1} z\right) + \frac{A_2}{A_1} z, \tag{3.2.20}$$

where

$$A_1 = \frac{\phi_0^2\,(1/2)}{(1-\phi_0\,(1/2))^2} + \frac{\phi_0^2\,(1/2)}{N'(\phi_0\,(1/2))} \frac{\frac{1}{2}p_1 + N(\phi_0\,(1/2))}{(1-\phi_0\,(1/2))^3}$$
$$- \frac{2}{N'(\phi_0\,(1/2))} \frac{\phi_{\rm crit}}{\phi_0\,(1/2)} \frac{\phi_{\rm crit} - \phi_0\,(1/2)}{1-\phi_0\,(1/2)},$$
$$A_2 = \frac{p_1}{N'(\phi_0\,(1/2))} \frac{\phi_0^2\,(1/2)}{(1-\phi_0\,(1/2))^2},$$

thus, using (3.2.19)

$$\frac{A_2}{A_1} = p_1 \left[N'(\phi_0\,(1/2)) + \frac{(\phi_{\rm crit} - \phi_0\,(1/2))\left(\phi_0^2\,(1/2) - 2\phi_{\rm crit} + \phi_{\rm crit}\phi_0\,(1/2)\right)}{\phi_0^3\,(1/2)} \right]^{-1}.$$

Taking the y-derivative of (3.2.16) we get

$$\partial_y \phi_0 = -p_1 \left[N'(\phi_0) + \frac{\phi_{\rm crit} - \phi_0}{\phi_0^3} \left(\phi_0^2 - 2\phi_{\rm crit} + \phi_0\phi_{\rm crit}\right) \right]^{-1}. \tag{3.2.22}$$

Therefore, the linear term in the expansion of the outer solution ϕ_0 and in the inner solution Φ_1, see (3.2.20), match as required.

Boundary layer problem at $y = y_B$

Similarly, we let the boundary layer variables be

$$\xi = \frac{y - y_B}{\varepsilon^{1/2}}, \qquad \varphi(\xi) = \phi(y).$$

To leading order the problem now reads

$$\partial_\xi \left(\frac{1-\varphi_0}{\varphi_0^2} N'(\varphi_0)\, \partial_\xi \varphi_0 \right) = \frac{p_1\, y_{B0} + N(\varphi_0)}{1-\varphi_0} + \frac{(\phi_{\text{crit}} - \varphi_0)^2}{\varphi_0^2},$$

with boundary condition at $\xi = 0^+$

$$\varphi_0(0) = \phi_{\text{crit}}$$

and

$$\partial_\xi \varphi_0(0) = -\frac{2}{5} \frac{\phi_{\text{crit}}}{1-\phi_{\text{crit}}} (p_1\, y_{B0} + \mu_1) = 0.$$

Note, if we assume that in the leading order outer equation, ϕ also satisfies $\phi = \phi_{\text{crit}}$ at $y = y_B$, then we must have that $p_1\, y_{B0} + \mu_1 = 0$, since $N(\phi_{\text{crit}}) = \mu_1$. Hence, the second boundary condition is also zero. This suggests $\varphi_0 = \phi_{\text{crit}}$. Matching this to the leading order outer problem

$$\frac{p_1\, y_{B0} + N(\phi_0(y_{B0}))}{1-\phi_0(y_B)} + \frac{(\phi_{\text{crit}} - \phi_0(y_B))^2}{\phi_0^2(y_B)} = 0.$$

Hence, $\phi_0(y_B) = \phi_{\text{crit}}$. Solving the next order problem

$$\partial_{\xi\xi} \varphi_1 = \left(\varphi_1 - \frac{2}{5} p_1\, \xi \right) \frac{\phi_{\text{crit}}^2}{(1-\phi_{\text{crit}})^2}$$

with boundary conditions

$$\varphi_1(0) = 0, \quad \partial_\xi \varphi_1(0) = \frac{2}{5}\, p_1$$

gives

$$\varphi_1(\xi) = \frac{2}{5} p_1 \xi.$$

This needs to be matched with the linear term in the Taylor expansion of the leading order outer solution ϕ_0, which can be obtained by taking the limit $\phi \to \phi_{\text{crit}}$ in (3.2.22). That limit gives $\partial_y \phi_0(y_B) = -p_1/N'(\phi_{\text{crit}}) = -p_1/(-5/2)$, that is, the coefficients are equal, hence the terms match.

Higher order approximations, that include the perturbation of the boundary only come in at $O(\varepsilon)$ and are therefore not considered here.

3.3 Drift-flux model for plane Poiseuille flow

It is known from the work of Nott and Brady [95] that the Eulerian-Eulerian model contains the drift-flux model in case of planar Poiseuille flow. Nevertheless, while drift-flux models have been proposed to study the evolution of two-phase flows of suspensions [76, 103] and are also used as transport equations for a suspended phase and combined with hydrodynamic equations [23, 93]

an asymptotically systematic derivation from the underlying two-phase model is still open. Here, we use matched asymptotic expansions along the lines of the analysis of the stationary problem, for the derivation of a new drift-flux model for the cross-section of the channel. Our analysis shows that the inclusion of the boundary layers leads to a drift-flux model that naturally accounts for the shear-induced flux of the suspended phase away from the boundaries. Moreover, the constitutive law for concentrated suspensions leads to the appearance of unyielded and yielded regions, which needs to be captured by the new drift-flux model.

Asymptotic model

To capture the evolution towards a Bingham-type flow it is instructive to investigate the problem for the cross-section. We assume therefore that all the variables depend only on y and t, except for the liquid pressure variable, which depends solely on x.

As in our previous section, the drift-flux regime is established for large Da and small velocity differences w, and in addition on a long time scale. Hence, we let

$$\mathrm{Da} = \frac{1}{\varepsilon}, \quad w_1 = \varepsilon w_1^*, \quad w_2 = \varepsilon w_2^*, \quad t = \frac{t^*}{\varepsilon}.$$

Then, the governing equations are, after we drop the "$*$"

$$\begin{aligned}
\partial_t \phi - \partial_y(\phi\,(1-\phi)\,w_2) &= 0,\\
-\partial_y\left[(1-\phi)\,\partial_y v_1 + \varepsilon(1-\phi)\,\partial_y(\phi w_1)\right] + (1-\phi)\partial_x p_f &= -\frac{\phi^2}{1-\phi} w_1,\\
-\partial_y\left[2\varepsilon(1-\phi)\,\partial_y(\phi w_2)\right] + (1-\phi)\partial_y p_f &= -\frac{\phi^2}{1-\phi} w_2,\\
-\partial_y\left[\phi\eta_s\partial_y v_1 - \varepsilon\phi\eta_s\partial_y((1-\phi)w_1)\right] + \phi\partial_x p_f &= \frac{\phi^2}{1-\phi} w_1,\\
\partial_y\left[2\varepsilon\phi\,\partial_y((1-\phi)w_2)\right] + \phi_s\partial_y p_f + \partial_y p_c &= \frac{\phi^2}{1-\phi} w_2,\\
p_c = \eta_n(\phi)\left[(\partial_y v_1 - \varepsilon\partial_y((1-\phi)w_1))^2 + 2\varepsilon[\partial_y((1-\phi)w_2)]^2\right]^{1/2},&
\end{aligned}$$

and no-slip conditions at $y = \pm 1/2$

$$v_1 = 0, \quad w_1 = 0, \quad w_2 = 0.$$

To leading order we obtain for the outer problem

$$\partial_t \phi - \partial_y(\phi(1-\phi)w_2) = 0,$$

$$-\partial_y[(1-\phi)\partial_y v_1] + (1-\phi)\partial_x p_f = -\frac{\phi^2}{1-\phi} w_1, \tag{3.3.2a}$$

$$(1-\phi)\partial_y p_f = -\frac{\phi^2}{1-\phi} w_2, \tag{3.3.2b}$$

$$-\partial_y[\phi\eta_s \partial_y v_1] + \phi\partial_x p_f + \partial_x p_c = \frac{\phi^2}{1-\phi} w_1, \tag{3.3.2c}$$

$$\phi\partial_y p_f + \partial_y p_c = \frac{\phi^2}{1-\phi} w_2, \tag{3.3.2d}$$

$$p_c = \eta_n \left|\partial_y v_1\right|,$$

and no-slip conditions at $y = \pm 1/2$

$$v_1 = 0, \quad w_1 = 0, \quad w_2 = 0.$$

We note that for ease of notation we have dropped the indices in the variables that denote the leading order solutions. Adding (3.3.2b) and (3.3.2d) yields $\partial_y(p_f + p_c) = 0$, hence $p_f + p_c = f(x)$. Adding (3.3.2a) and (3.3.2c) yields

$$-\partial_y\left(\left[\phi\eta_s + (1-\phi)\right]\partial_y v_1\right) + \partial_x(p_f + p_c) = 0.$$

Since the left hand side is only dependent on y as well as t and the right hand side only on x, they must be constants. Thus, defining $\partial_x(p_f + p_c) = p_1$, so that after integration

$$\left[\phi\eta_s + (1-\phi)\right]\partial_y v_1 = p_1 y + \alpha. \tag{3.3.3}$$

Adding $(1-\phi)\partial_y p_c$ on both sides of (3.3.2b) yields

$$\partial_y p_c = \frac{\phi^2}{(1-\phi)^2} w_2.$$

We have

$$w_2 = \frac{(1-\phi)^2}{\phi^2}\partial_y\left(\eta_n|\partial_y v_1|\right) = \frac{(1-\phi)^2}{\phi^2}\partial_y\left(\eta_n\dot{\gamma}\right).$$

In addition note that from (3.3.3) we obtain

$$\partial_y v_1 = \frac{p_1\, y}{\phi\eta_s + 1 - \phi},$$

where due to symmetry we have set $\alpha = 0$. Since $p_1 < 0$ the negative of this expression is always positive and we set

$$\dot{\gamma} = -\frac{p_1\, y}{\phi\eta_s + 1 - \phi},$$

so that

$$w_2 = -p_1\frac{(1-\phi)^2}{\phi^2}\partial_y\left[\frac{\eta_n y}{\phi\eta_s + 1 - \phi}\right].$$

Hence, we obtain for the drift-flux model

$$\partial_t \phi = -p_1 \partial_y \left[\frac{(1-\phi)^3}{\phi} \partial_y \left(\frac{y}{N(\phi) + \frac{1-\phi}{\eta_n(\phi)}} \right) \right]. \tag{3.3.4}$$

We note at this point that the drift-flux model we have just derived (3.3.4) is a nonlinear diffusion equation which admits constant solutions, say ϕ_0. Linearizing about these base states by making the ansatz $\phi(t,y) = \phi_0 + \delta\,\phi_1(t,y) + O(\delta^2)$ we obtain to $O(\delta)$

$$\partial_t \phi_1 = -p_1\, \partial_y \left[\frac{M'(\phi_0)}{K(\phi_0)} \phi_1 - M(\phi_0) \frac{K'(\phi_0)}{K^2(\phi_0)} \partial_y \left(y \phi_1 \right) \right],$$

where $M(\phi) = (1-\phi)^3/\phi$ and $K(\phi) = N(\phi) + (1-\phi)/\eta_n(\phi)$. Clearly, if $K'(\phi_0) < 0$ then any perturbation of the constant bases states is damped out and the flow remains constant. But we note that constant solutions do not satisfy the boundary conditions unless the constant is zero. Hence, we expect the nonlinear structure to come from the interplay between the drift-flux equation and the no-flux condition.

We now supplement this equation with boundary conditions. At the wall, $y = 1/2$, it seems plausible to use no-flux conditions, and indeed, matching to a boundary layer there gives $w_2 = 0$, see Section 3.4. We seek solutions that are symmetric with respect to the middle axis of the channel, thus we also impose $w_2 = 0$ at $y = 0$.

We expect that the flux of the solid phase leads to an increase of ϕ at the center of the channel. At some time, in fact, the solid volume fraction reaches ϕ_{crit} there and jamming occurs. After that, flow of both phases only occur for $y > y_B$, while for $y < y_B$, the solid phase is jammed, where y_B is a time dependent free boundary. In this region, the volume fractions are constant so that the mass conservation equations give $w_2 = w_2(t)$. Assuming symmetry at $y = 0$ it then fixes w_2 to be zero to all orders in ε for $0 < y < y_B$. At $y = y_B$, we therefore impose $\phi = \phi_{\text{crit}}$ and $w_2 = 0$, resulting in two boundary conditions as required at a free boundary.

Remark We remark that in the stationary case we let $\partial_t \phi = 0$ in (3.3.4), and integrate once. Using the condition that $w_2 = 0$ at the channel walls, the integration constant must be zero. Since $(1-\phi)^3/\phi$ is never zero, we can divide and integrate once more to obtain

$$\frac{y}{N(\phi) + \frac{1-\phi}{\eta_n(\phi)}} = c.$$

The free constant c is just the collision pressure p_c, which is a free-parameter in the stationary case. With $c = -1/p_1$ we obtain the stationary outer equation (3.2.16).

Numerical solution of the drift-flux model

In order to understand the time evolution of the solid volume fraction in a channel, we numerical solve (3.3.4) with no-flux boundary conditions

$$\partial_y \left(\frac{y}{N(\phi) + \frac{1-\phi}{\eta_n(\phi)}} \right) = 0 \qquad \text{at } y \in \left\{ y_B, \frac{1}{2} \right\}$$

using a central finite difference scheme of second order with a fully implicit Euler-Euler-2-step method. For more details on the scheme see Section A.2. The free-boundary condition

$$\phi = \phi_{\text{crit}} \quad \text{at } y = y_B$$

is used to update the position of the yield surface y_B.

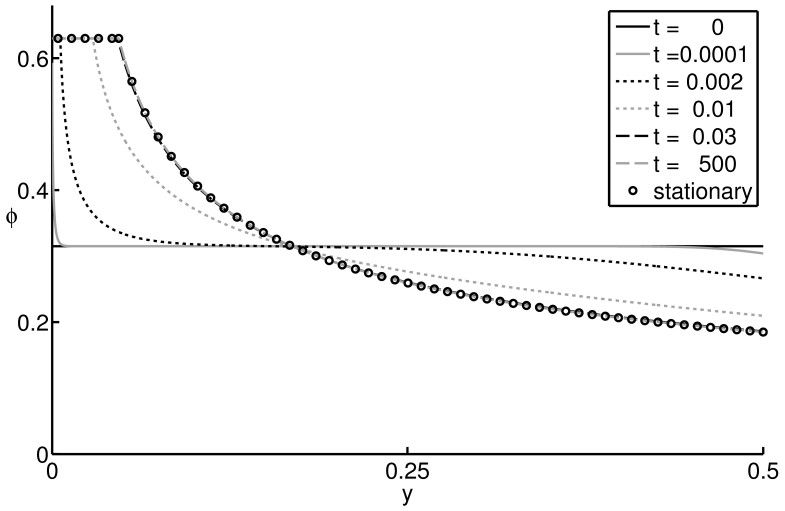

Figure 3.5: Time evolution of solid volume fraction using the outer drift-flux approximation (3.3.4).

The time evolution is shown in Figure 3.5 for the parameters from (3.2.14) with $\mu_1 = \mu_2$ and $p_1 = -10$, starting from an initial uniform profile of $\phi(0, y) = \frac{1}{2}\phi_{\text{crit}}$. The profile first changes near the channel center and wall. Next, the volume fraction increases near the center until maximum packing is reached, which spawns an unyielded region. Then, this unyielded region grows until the yield surface y_B reaches the value from (3.2.13), where the evolution stops as the stationary solution is reached.

The stationary profile obtained by the drift-flux model has the same parameters μ_1, μ_2, I_0, ϕ_{crit}, Da, but not p_1. Then, the pressure p_1 must be chosen, so that the volume of solids V_s in a cross section of the channel is matching, i.e.

$$V_s(t) = \int_{-1/2}^{1/2} \phi(t, y) \mathrm{d}y$$

must be the same for the stationary and the drift-flux solution. A simple way achieving this is to measure the yield surface position y_B and use equation (3.2.13) for the pressure of the stationary solution.

3.4 Boundary layer analysis for the drift-flux model

For the boundary layer analysis at the wall we introduce variable

$$z = \frac{\frac{1}{2} - y}{\varepsilon^{1/2}}, \qquad \Phi(t,z) = \phi_s(t,y) = \phi(t,y).$$

Then, we obtain

$$\begin{aligned}
\varepsilon^{1/2}\partial_t\Phi + \partial_z(\Phi\,(1-\Phi)\,w_2) &= 0\\
-\partial_z\left[(1-\Phi)\,\partial_z v_1 + \varepsilon(1-\Phi)\,\partial_z(\Phi w_1)\right] + \varepsilon(1-\Phi)\partial_x p_f &= -\varepsilon\frac{\Phi^2}{1-\Phi}w_1\\
\varepsilon^{1/2}\partial_z\left[2(1-\Phi)\,\partial_z(\Phi w_2)\right] + (1-\Phi)\partial_z p_f &= \varepsilon^{1/2}\frac{\Phi^2}{1-\Phi}w_2\\
-\partial_z\left[\Phi\eta_s\partial_z v_1 - \varepsilon\Phi\eta_s\partial_z((1-\Phi)w_1)\right] + \varepsilon\Phi\partial_x p_f &= \varepsilon\frac{\Phi^2}{1-\Phi}w_1\\
\varepsilon^{1/2}\partial_z\left[2\Phi\,\partial_z((1-\Phi)w_2)\right] - \Phi\partial_z p_f - \partial_z p_c &= \varepsilon^{1/2}\frac{\Phi^2}{1-\Phi}w_2
\end{aligned}$$

and

$$p_c = \eta_n\left[\frac{1}{\varepsilon}(\partial_z v_1 - \varepsilon\partial_z((1-\Phi)w_1))^2 + 2[\partial_z((1-\Phi)w_2)]^2\right]^{1/2}$$

and no-slip conditions at $z = 0$

$$v_1 = 0, \quad w_1 = 0, \quad w_2 = 0.$$

The leading order system is

$$\begin{aligned}
\partial_z(\Phi\,(1-\Phi)\,w_2) &= 0\\
-\partial_z\left[(1-\Phi)\,\partial_z v_1\right] &= 0\\
(1-\Phi)\partial_z p_f &= 0\\
-\partial_z\left[\Phi\eta_s\partial_z v_1\right] &= 0\\
-\partial_z p_c &= 0
\end{aligned}$$

and

$$p_c = \eta_n\left[(\partial_z v_1)^2\right]^{1/2}$$

and no-slip conditions at $z = 0$

$$v_1 = 0, \quad w_1 = 0, \quad w_2 = 0.$$

We see immediately that $w_2 = 0$, which provides, via matching, the boundary condition for the drift-flux model at $y = 1/2$ as claimed in the text.

Chapter 4

Stability

4.1 Introduction

A mathematical model is called well-posed in the sense of Hadamard if it suffices the following three conditions [32]:

1. The solution exists
2. The solution is unique
3. The solution depends continuously on the initial and boundary conditions

The existence and uniqueness of solutions even of the single-phase incompressible Navier-Stokes equations is still an open problem and part of the Millennium problems of the Clay Mathematical Institute. Nevertheless, it is possible to find solutions for special flows, e.g. parallel shear flows like the plane Couette and plane Poiseuille flow [115] and ask for the stability, i.e. condition three, of these particular solutions.

The stability of the Navier-Stokes equation can be studied by the well-known normal mode ansatz, which consists of linearization around a known base state and solution of the resulting linear system using a Fourier ansatz. This yields an initial boundary value problem, whose spectrum is directly related to the stability of the solution. For parallel shear flows, this ansatz yields the so-called Orr-Sommerfeld equation, see for example Drazin and Reid [30]. Using this equation, Orszag [98] showed that the plane Poiseuille flow of Newtonian fluids have a critical Reynolds number of $\mathrm{Re} \approx 5772.22$ beyond which point the flow becomes linearly unstable. Nevertheless, this analysis does not reveal all the unstable behavior seen in experiments as some nonlinear instabilities do seem to be initiated by linear transient growth of certain modes, which is possible since the eigenfunctions of the Orr-Sommerfeld boundary value problem are not orthogonal as discussed in Trefethen et al. [128]. Some of these modes have time to grow large enough to serve as finite amplitude perturbation and eventually lead to a nonlinear, possibly three-dimensional,

instability. While the literature on these fundamental hydrodynamic instabilities as well as their route to turbulence is quite extensive, much less is known if non-Newtonian fluids or multiphase liquids are considered [14, 44, 45].

Chapter 2 presents a two-phase model for concentrated suspensions and it has been shown in Section 3.2 that plane Poiseuille flow gives rise to unyielded regions and a Bingham-like rheology. This emerging flow structure is due to shear-induced migration, a phenomenon first discovered by Leighton and Acrivos [76]. Hence, of particular interest are the stability properties of Bingham fluids. One of the first to study the effect of the yield stress on the stability properties was Frigaard et al. [43]. Their analysis was based on the corresponding boundary value problem for the Orr-Sommerfeld equation for a Bingham fluid which has first been derived there. Further discussions by Frigaard et al. [42] and more recently by Metivier et al. [86] and Georgievskii [45] showed that the stability properties for plane Poiseuille flow depends critically on the choice of boundary conditions at the yield surface for the associated eigenvalue problem. Using symmetric boundary conditions for the velocity at the yield surface the well-known critical Reynolds number $\mathrm{Re} = 5772.22$ is approached as $\mathrm{B} \to 0$, while for non-symmetric boundary conditions all modes are stable also as $\mathrm{B} \to 0$ as noted by Métivier et al. [86]. This shows that the Orr-Sommerfeld-Bingham equation is not a canonical generalization of the standard Orr-Sommerfeld equation.

Guided by these investigations, we revisit the formulation of the boundary value problem for the Orr-Sommerfeld-Bingham equations, and then generalize the derivation to the eigenvalue problem for the two-phase flow of plane Couette and Poiseuille flow. In particular we show that for the two-phase Poiseuille flow model for concentrated suspensions the conditions at the yield surface of the corresponding eigenvalue problem are non-symmetric.

The stability analysis of the resulting boundary value problem carried out in this chapter thus constitutes a next step in complexity for the investigation of the dynamical behavior of two-phase flow models with yield-stress. The analysis will moreover serve to assess the necessary conditions to address the problem of well-posedness of the two-phase flow model.

The problem of well-posedness is in fact an inherent property of even the simplest multiphase model equations for suspension flow and many other applications, since its first derivations from an averaging method pioneered by Drew and Passmann [33] and Ishii [60]. The associated loss-of-hyperbolicity problem has already been discussed in Section 2.2. Nevertheless, such models have found widespread applications and using various forms of regularizations their study started the development of a number of numerical schemes described for example in Stewart and Wendroff [120].

In our investigations we will focus, after the formulation of the two-phase flow model and the derivation of the eigenvalue problem in Section 4.3, on the stability analysis of the plane Couette flow problem in Section 4.4. This problem is instructive since we can simplify the resulting eigenvalue problem considerably and derive criteria for an ill-posedness in the system that is related to the competition between the solid phase viscosity and the collision pressure. The study of these special cases is also used for the design of a reliable numerical scheme for the general eigenvalue problem.

In addition to the ill-posedness we also find a convection induced instability via a Kelvin-mode ansatz and show that in general, the growth of the unstable mode is transient. As the particle volume fraction approaches maximum packing the growth rates of the unstable modes increase, so that it can become strong enough to possibly trigger finite-amplitude, nonlinear instabilities.

For the two-dimensional Poiseuille flow, considered in Section 4.5, simplifications of the resulting eigenvalue problem, that allow analytical work are not possible. Here, our numerical parameter studies show the ill-posedness as well as the transient growth property occur again, however, for different parameter values. The main difference to the Couette flow is that for Poiseuille flow, there are volume fractions for which unyielded region emerge. The stability of the corresponding yielding surface is the final topic of our investigations.

For the derivation of the associated boundary value problem we found it helpful to first revisit the formulation of the eigenvalue problem for the Orr-Sommerfeld-Bingham equation.

4.2 Bingham-Orr-Sommerfeld system

One of the signatures of our two-phase flow model is that it contains a yield-stress similar to the classical (single-phase) Bingham fluid. Moreover, the stability properties for the Poiseuille flow of a Bingham fluid is a well-studied and intensely analyzed problem, see the review by Frigaard et al.[42] and the discussion in [43, 86, 100]. In addition, the derivation of the yield-surface boundary conditions of the two-phase model is guided by the derivation for the classical Bingham model.

It is therefore instructive to revisit the problem of plane Poiseuille flow for a Bingham fluid, in particular to specify and motivate the yield-surface conditions for the stability problem in the two-phase flow case.

Let us consider the governing equation for the Bingham flow, which are the Navier-Stokes equations with a yield-stress constitutive law [43], i.e.

$$\nabla \cdot \boldsymbol{u} = 0, \tag{4.2.1a}$$

$$\rho\left(\partial_t \boldsymbol{u} + (\boldsymbol{u}\cdot\nabla)\boldsymbol{u}\right) = \nabla\cdot\boldsymbol{\tau} - \nabla p, \tag{4.2.1b}$$

with

$$\boldsymbol{\tau} = \left(\mu_0 + \frac{\tau_0}{|\dot{\boldsymbol{\gamma}}|}\right)\dot{\boldsymbol{\gamma}} \qquad \text{for } |\boldsymbol{\tau}| \geq \tau_0, \tag{4.2.1c}$$

$$\dot{\boldsymbol{\gamma}} = \boldsymbol{0} \qquad \text{for } |\boldsymbol{\tau}| < \tau_0, \tag{4.2.1d}$$

where ρ, μ_0 and τ_0 denote the density, viscosity and yield-stress, respectively. The boundary conditions for Poiseuille flow are the no-slip boundary conditions

$$\boldsymbol{u} = \boldsymbol{0} \qquad \text{at } y \in \{-L, L\}. \tag{4.2.2}$$

In case there is a plug-flow, we additionally need conditions at the yield-surface. We demand the continuity of the velocity and the normal shear rate

$$[\![\boldsymbol{u}]\!] = [\![\dot{\boldsymbol{\gamma}}\cdot\boldsymbol{n}]\!] = \boldsymbol{0} \qquad \text{at } |\boldsymbol{\tau}| = \tau_0. \tag{4.2.3}$$

These equations can be non-dimensionalized by scaling the length by $2L$, the velocity by U_0, the time by $2L/U_0$ and stress by ρU_0^2, using the Reynolds number $\mathrm{Re} = \rho U_0 L/\mu_0$ and the Bingham number $\mathrm{B} = \tau_0 L/(\mu_0 U_0)$.

Remark

The yield-surface boundary conditions (4.2.3) are not identical with the paper by Frigaard et al. [43]. They use

$$\begin{aligned} [\![\boldsymbol{u}]\!] &= \mathbf{0} \\ [\![\dot{\boldsymbol{\gamma}}]\!] &= \mathbf{0} \\ \int_{\Omega_s} (\boldsymbol{\tau} - p\boldsymbol{I}) \cdot \boldsymbol{n} \, \mathrm{d}\boldsymbol{s} &= \int_{\Omega_s} \rho \frac{\mathrm{d}}{\mathrm{d}t} \boldsymbol{u} \, \mathrm{d}\boldsymbol{x} \end{aligned}$$

as yield-surface conditions, where the last condition describes the total linear momentum of the unyielded domain Ω_s. These conditions represent a superset of conditions (4.2.3) and are not all used in their derivation. It is unclear whether their system is overdetermined. A later work by Metivier et al. [86] just demands

$$[\![\boldsymbol{u}]\!] = \mathbf{0} \qquad \text{and} \qquad [\![\dot{\boldsymbol{\gamma}}]\!] = \mathbf{0}$$

at the yield-surface and derives the same equations, but it is still a superset of (4.2.3). We note that our conditions (4.2.3) are also independently proposed by Thual et al. [127] and in the book by Huilgol [56].

An analytic justification can also be given based on proofs for the existence of solutions of the equivalent variational inequality formulation. They show the stationary velocity solutions to be $\boldsymbol{u} \in (H^1(\Omega))^n$, which implies continuity in the one-dimensional case, see e.g. [34]. Equivalent dual formulations additionally show $\boldsymbol{\tau} \in H(\mathrm{div}; \Omega)$, which implies the normal continuity of the shear-rates, but not of the tangential components, see e.g. [20].

Base state

In order to derive the base state for the plane Poiseuille flow, we make the ansatz

$$\boldsymbol{u} = (U_B(y), V_B(y)), \qquad p = Px,$$

and split our domain into a plug-flow and a liquid region, i.e. $\Omega = \Omega_s \cup \Omega_f$.

The continuum equation (4.2.1a) immediately gives $V_B(y) = 0$ using the no-slip boundary conditions. This yields

$$\dot{\boldsymbol{\gamma}} = \begin{pmatrix} 0 & \partial_y U_B \\ \partial_y U_B & 0 \end{pmatrix} \text{ in } \Omega, \qquad \boldsymbol{\tau} = \frac{1}{\mathrm{Re}} \left(1 + \frac{\mathrm{B}}{|\partial_y U_B|} \right) \begin{pmatrix} 0 & \partial_y U_B \\ \partial_y U_B & 0 \end{pmatrix} \text{ in } \Omega_f,$$

and thus $|\boldsymbol{\tau}| = |\tau_{12}|$. The equation of motion (4.2.1b) yields $P = \partial_y \tau_{12}$ and after integration

$$\tau_{12} = Py + C_1, \tag{4.2.4}$$

which tells us the stress is a linear function of y in Ω_f. In order to derive the linear total stress we implicitly assumed the momentum equation to be valid everywhere without specifying a specific stress form in the unyielded region. This approach is justifiable by the equivalent variational inequality formulation, cf. [34].

The linear behavior of τ_{12} in Ω_f allows for exactly one plug-flow. This can be seen by considering a region with two plug-flows and a fluid region in between. There are two cases. Either the stress $\boldsymbol{\tau}_{12}$ in the fluid region goes from $-\tau_0$ to τ_0 and is by its definition no fluid region or it starts and finishes at the same value, which due to the linearity can only be true for $|\boldsymbol{\tau}| = \tau_0$ again connecting the two plug-flow regions with a solid region. On the other side, there must be at least one plug-flow region, as we know from Newtonian flows with no-slip boundary conditions, the stress crosses the zero at the channel center. Thus, as we have exactly one plug-flow region, we will call its upper and lower boundaries $h^-, h^+ \in (-1/2, 1/2)$, respectively.

Integration of equation (4.2.4) together with $|\dot{\boldsymbol{\gamma}}| = 0$ in Ω_s and boundary conditions (4.2.2) give the system

$$\begin{aligned} U_B(y) &= \mathrm{Re}\,\mathrm{P}\frac{y^2}{2} + C_2^{\pm} y + C_3^{\pm}, \\ U_B(\pm 1/2) &= 0, \\ \partial_y U_B(h^{\pm}) &= 0, \\ U_B(h^+) &= U(h^-), \end{aligned}$$

with

$$h^+ = -h^- = y_B = -\frac{\mathrm{B}}{\mathrm{Re}\,\mathrm{P}},$$

and solution

$$U_B(y) = \begin{cases} \frac{1}{2}\mathrm{Re}\,\mathrm{P}\left((|y| - y_B)^2 - (y_B - 1/2)^2\right) & \text{for } |y| \geq y_B \\ -\frac{1}{2}\mathrm{Re}\,\mathrm{P}(y_B - 1/2)^2 & \text{for } |y| < y_B. \end{cases}$$

Choosing

$$U_0 = -\frac{\mu_0}{\rho L}\frac{1}{2}\mathrm{P}(y_B - 1/2)^2$$

gives

$$U_B(y) = \begin{cases} 1 - \frac{(|y| - y_B)^2}{(1/2 - y_B)^2} & \text{for } y_b \leq |y| \leq 1/2 \\ 1 & \text{for } |y| < y_B \end{cases}$$

as our base state.

Figure 4.1 shows the base state for the single-phase Bingham model as computed from the relation above.

Linear stability problem

We linearize around the basic flow, i.e. $\boldsymbol{u} = \boldsymbol{U}_B + \delta\tilde{\boldsymbol{u}}$.

Let us define

$$\eta(\boldsymbol{U}) = \frac{1}{\mathrm{Re}}\left(1 + \frac{\mathrm{B}}{|\dot{\boldsymbol{\gamma}}|}\right),$$

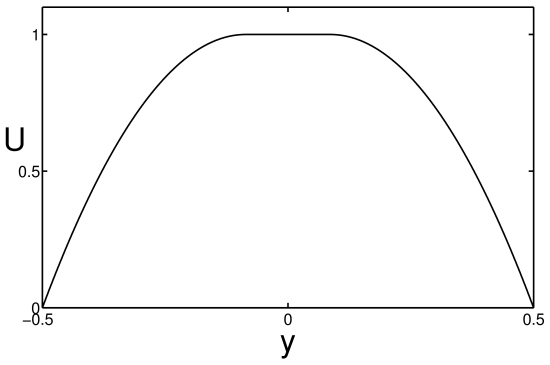

Figure 4.1: The base state for the single-phase Bingham model with parameters chosen as Re = 5772.22 and B = 1. It has a shape similar to the quadratic velocity profile of Newtonian Poiseuille flow, but is flat around the center, i.e. $y = 0$, due to the occurring plug-flow, there.

then

$$\begin{aligned}\eta(\boldsymbol{U}_B + \delta\tilde{\boldsymbol{u}}) &= \eta(\boldsymbol{U}_B) + \delta\dot{\gamma}_{ij}(\tilde{\boldsymbol{u}})\frac{\partial\eta}{\partial\dot{\gamma}_{ij}}(\boldsymbol{U}_B) + O(\delta^2)\\ &= \eta(\boldsymbol{U}_B) - \delta\frac{1}{2}\dot{\gamma}_{ij}(\tilde{\boldsymbol{u}})\dot{\gamma}_{ij}(\boldsymbol{U}_B)\frac{\mathrm{B}}{\mathrm{Re}\,|\dot{\boldsymbol{\gamma}}(\boldsymbol{U}_B)|^3} + O(\delta^2)\\ &= \eta(\boldsymbol{U}_B) + \delta\eta' + O(\delta^2).\end{aligned}$$

Further, we have

$$\begin{aligned}\tau_{ij} &= \eta(\boldsymbol{U}_B + \delta\tilde{\boldsymbol{u}})\dot{\gamma}_{ij}(\boldsymbol{U}_B + \delta\tilde{\boldsymbol{u}})\\ &= \eta(\boldsymbol{U}_B)\dot{\gamma}_{ij}(\boldsymbol{U}_B) + \delta(\eta'\dot{\gamma}_{ij}(\boldsymbol{U}_B) + \eta(\boldsymbol{U}_B)\dot{\gamma}_{ij}(\tilde{\boldsymbol{u}})) + O(\delta^2)\\ &= \tau_{ij}(\boldsymbol{U}_B) + \delta\tau'_{ij} + O(\delta^2),\end{aligned}$$

and

$$\tau(\boldsymbol{U}_B + \delta\tilde{\boldsymbol{u}}) = \tau(\boldsymbol{U}_B) + \delta\frac{1}{2}\frac{\tau'_{ij}(\tilde{\boldsymbol{u}})\tau_{ij}(\boldsymbol{U}_B)}{\sqrt{\tau(\boldsymbol{U}_B)}} + O(\delta^2).$$

Thus the yield criterion is also perturbed and we need to make the ansatz $H = \pm y_b \pm \delta h$ for the position of the yield-surface.

Linearizing the equations of motions via $\boldsymbol{u} = \boldsymbol{U}_B + \delta\tilde{\boldsymbol{u}}$, $p = Px + \delta\tilde{p}$ and subtracting the base state as well as using the continuum equation, yields

$$\begin{aligned}\nabla\cdot\tilde{\boldsymbol{u}} &= 0,\\ \partial_t\tilde{u} + U_B\partial_x\tilde{u} + \tilde{v}\partial_y U_B &= -\partial_x\tilde{p} + \frac{\Delta\tilde{u}}{\mathrm{Re}} + \frac{2\mathrm{B}\partial_{xx}\tilde{u}}{\mathrm{Re}\dot{\gamma}(\boldsymbol{U}_B)},\\ \partial_t\tilde{v} + U_B\partial_x\tilde{v} &= -\partial_y\tilde{p} + \frac{\Delta\tilde{v}}{\mathrm{Re}} + \frac{\mathrm{B}2\partial_{yy}\tilde{v}}{\mathrm{Re}\dot{\gamma}(\boldsymbol{U}_B)} + \frac{2\mathrm{B}\partial_y\tilde{v}}{\mathrm{Re}}\frac{\partial}{\partial y}\left(\frac{1}{\dot{\gamma}(\boldsymbol{U}_B)}\right).\end{aligned}$$

Inserting the ansatz

$$(\tilde{u}, \tilde{v}, \tilde{p}) = (\hat{u}(y), \hat{v}(y), \hat{p}(y))\mathrm{e}^{i\alpha(x-ct)}$$

into the linearized equations

$$\begin{aligned} i\alpha\hat{u} + \partial_y\hat{v} &= 0, \\ -i\alpha c\hat{u} + \boldsymbol{U}_B i\alpha\hat{u} + \hat{v}\partial_y\boldsymbol{U}_B &= -i\alpha\hat{p} - \frac{\alpha^2\hat{u}}{\mathrm{Re}} + \frac{\partial_{yy}\hat{u}}{\mathrm{Re}} - \frac{2\mathrm{B}\alpha^2\hat{u}}{\mathrm{Re}|\partial_y\boldsymbol{U}_B|}, \\ -i\alpha c\hat{v} + \boldsymbol{U}_B i\alpha\hat{v} &= -\partial_y\hat{p} - \frac{\alpha^2\hat{v}}{\mathrm{Re}} + \frac{\partial_{yy}\hat{v}}{\mathrm{Re}} + \frac{2\mathrm{B}\partial_{yy}\hat{v}}{\mathrm{Re}|\partial_y\boldsymbol{U}_B|} + \frac{2B\partial_y\hat{v}}{\mathrm{Re}}\frac{\partial}{\partial y}\left(\frac{1}{|\partial_y\boldsymbol{U}_B|}\right). \end{aligned}$$

Eliminating all $\hat{u}$ through $\hat{v}$ via the continuum equation results in

$$\begin{aligned} c\partial_y\hat{v} - U_B\partial_y\hat{v} + \hat{v}\partial_y U_B &= -i\alpha\hat{p} - \frac{\alpha i\partial_y\hat{v}}{\mathrm{Re}} + \frac{i\partial_{yyy}\hat{v}}{\alpha\mathrm{Re}} - \frac{2\mathrm{B}\alpha i\partial_y\hat{v}}{\mathrm{Re}|\partial_y U_B|}, \\ -i\alpha c\hat{v} + U_B i\alpha\hat{v} &= -\partial_y\hat{p} - \frac{\alpha^2\hat{v}}{\mathrm{Re}} + \frac{\partial_{yy}\hat{v}}{\mathrm{Re}} + \frac{2\mathrm{B}\partial_{yy}\hat{v}}{\mathrm{Re}|\partial_y U_B|} + \frac{2B\partial_y\hat{v}}{\mathrm{Re}}\frac{\partial}{\partial y}\left(\frac{1}{|\partial_y U_B|}\right). \end{aligned}$$

Finally, eliminating $\hat{p}$ via rewriting the first equation and inserting into the second gives the so-called Orr-Sommerfeld-Bingham equation

$$i\alpha\mathrm{Re}[(U_B - c)(\partial_{yy}\hat{v} - \alpha^2\hat{v}) - \hat{v}\partial_{yy}U_B] = \left(\frac{\partial^2}{\partial y^2} - \alpha^2\right)^2\hat{v} - 4\alpha^2\mathrm{B}\frac{\partial}{\partial y}\left(\frac{\partial_y\hat{v}}{|\partial_y U_B|}\right).$$

Remark

Note, we have eliminated the pressure and one of the velocity components by algebraic substitution of the linearized equations with normal mode ansatz. An equivalent approach is to define a so-called stream function ψ, such that

$$u = \partial_y\psi \qquad \text{and} \qquad v = -\partial_x\psi,$$

which is a valid ansatz for any divergence-free vector field. This approach is done by Frigaard et al. [43]. However, we used the direct approach since the stream-function ansatz is cumbersome in the multiphase model and demands the v/w-formulation (7.1.4). We have not further pursued this, but it might be done in a future work and could lead to new insights into the correct set of boundary conditions for the multiphase model.

Boundary conditions

The no-slip boundary condition at the wall yields

$$\hat{v}(\pm 1/2) = 0, \qquad \partial_y\hat{v}(\pm 1/2) = 0,$$

with usage of the continuum equation.

Linearization of the normal shear-rate condition at the yield-surface (4.2.3) gives

$$\begin{aligned} 0 = \dot{\gamma}_{i2}(\boldsymbol{U}_B + \delta\tilde{\boldsymbol{u}}, y_B + \delta h) &= \dot{\gamma}_{i2}(\boldsymbol{U}_B, \pm y_B) \pm \delta h \frac{\partial \dot{\gamma}_{i2}(\boldsymbol{U}_B, \pm y_b)}{\partial y} + \delta \dot{\gamma}_{i2}(\tilde{\boldsymbol{u}}, \pm y_B) + O(\delta^2) \\ &= \pm \delta h \frac{\partial \dot{\gamma}_{i2}(\boldsymbol{U}_B, \pm y_b)}{\partial y} + \delta \dot{\gamma}_{i2}(\tilde{\boldsymbol{u}}, \pm y_B) + O(\delta^2), \end{aligned}$$

and to leading order this yields

$$\dot{\gamma}_{i2}(\tilde{\boldsymbol{u}}, \pm y_B) = \mp h \frac{\partial \dot{\gamma}_{i2}(\boldsymbol{U}_B, \pm y_b)}{\partial y},$$

because $\dot{\gamma}_{i2}(\boldsymbol{U}_B, \pm y_b) = 0$.
Hence, we have

$$\begin{aligned} &\partial_x \tilde{u}(x, \pm y_B, t) = \partial_y \tilde{v}(x, \pm y_B, t) = 0, \\ &\partial_y \tilde{u}(x, \pm y_B, t) + \partial_x \tilde{v}(x, \pm y_B, t) = \mp h \frac{\partial \dot{\gamma}_{12}(\boldsymbol{U}_B, \pm y_b)}{\partial y} = \frac{\pm 2h}{(1/2 - y_B)^2}. \end{aligned}$$

This yields for the linearized system with normal mode ansatz

$$\hat{u} = \partial_y \hat{v} = 0, \qquad\qquad \partial_{yy}\hat{v} + \alpha^2 \hat{v} = \frac{\mp i\alpha 2h}{(1/2 - y_B)^2}.$$

In the plug-flow bulk region $(x, y) \in \Omega_s$, we have

$$\begin{aligned} 0 &= \dot{\boldsymbol{\gamma}}(x, y) \\ &= \nabla(\boldsymbol{U}_B(x, y) + \varepsilon\tilde{\boldsymbol{u}}(x, y)) + \nabla(\boldsymbol{U}_B(x, y) + \varepsilon\tilde{\boldsymbol{u}}(x, y))^T, \end{aligned}$$

and to order $O(\varepsilon)$

$$\begin{aligned} \partial_x \tilde{u}(x, y) &= 0, \\ \partial_y \tilde{v}(x, y) &= 0, \\ \partial_y \tilde{u}(x, y) + \partial_x \tilde{v}(x, y) &= 0. \end{aligned}$$

Using the normal mode ansatz, it becomes (due to $\hat{u} = 0$ for all x and y in Ω_s)

$$\begin{aligned} \hat{u}(x, y) &= 0, \\ \partial_y \hat{v}(x, y) &= 0, \\ \hat{v}(x, y) &= 0. \end{aligned}$$

Now using the continuity of $\boldsymbol{u}$ at the yield-surface, we get

$$\begin{aligned} [\![\boldsymbol{u}(x, y_B + \varepsilon\tilde{h})]\!] &= [\![\boldsymbol{u}(x, y_B) + \varepsilon\tilde{h}\partial_y \boldsymbol{U}_B(x, y_B) + \varepsilon\tilde{\boldsymbol{u}}(x, y_B)]\!] \\ &= \boldsymbol{U}_B(x, y_B)^+ - \boldsymbol{U}_B{}^-(x, y_B) + \varepsilon\tilde{h}(\partial_y \boldsymbol{U}_B{}^+(x, y_B) \\ &\quad - \partial_y \boldsymbol{U}_B{}^-(x, y_B)) + \varepsilon(\tilde{\boldsymbol{u}}^+(x, y_B) - \tilde{\boldsymbol{u}}^-(x, y_B)). \end{aligned}$$

Using $\boldsymbol{U}_B{}^+(y_B) = \boldsymbol{U}_B{}^-(y_B)$, we get

$$\varepsilon\tilde{h}(\partial_y \boldsymbol{U}_B{}^+(x, y_B) - \partial_y \boldsymbol{U}_B{}^-(x, y_B)) + \varepsilon(\tilde{\boldsymbol{u}}^+(x, y_B) - \tilde{\boldsymbol{u}}^-(x, y_B)) = 0.$$

We have $(\partial_y \boldsymbol{U}_B{}^+(x, y_B) - \partial_y \boldsymbol{U}_B{}^-(x, y_B)) = 0$, so

$$\tilde{\boldsymbol{u}}^+(x, y_B) = \tilde{\boldsymbol{u}}^-(x, y_B),$$

and since $\tilde{\boldsymbol{u}}^- = \hat{\boldsymbol{u}}^-(y)\mathrm{e}^{i\alpha(x-ct)} = 0$ due to $\hat{\boldsymbol{u}}^-(y) = 0$, we have

$$\tilde{\boldsymbol{u}}^+(x, y_B) = 0.$$

Overall we have the boundary conditions

$$\begin{aligned} \hat{v} = \partial_y \hat{v} &= 0 && \text{at } y = 1/2, \\ \hat{v} = \partial_y \hat{v} &= 0 && \text{at } y = y_B, \\ \partial_{yy}\hat{v} &= \frac{-i\alpha 2h}{(1/2 - y_B)^2} && \text{at } y = y_B. \end{aligned}$$

Results

In conclusion, one derives, as done by Frigaard et al. [43], the non-dimensionalized base state

$$\boldsymbol{U}_B = \begin{cases} 1 & \text{for } 0 \le |y| < y_B \\ 1 - \left(\frac{|y| - y_B}{1/2 - y_B}\right)^2 & \text{for } y_B \le |y| \le 1/2, \end{cases}$$

where $y_B = -B/(\mathrm{Re}P)$ and the Orr-Sommerfeld-Bingham equation

$$\begin{aligned} i\alpha\mathrm{Re}\left((\boldsymbol{U}_B - c)\left(\partial_{yy}\hat{v} - \alpha^2\hat{v}\right) - \hat{v}\partial_{yy}\boldsymbol{U}_B\right) = & \qquad (4.2.13a) \\ \partial_{yyyy}\hat{v} - 2\alpha^2\partial_{yy}\hat{v} + \alpha^4\hat{v} - 4\alpha^2 \mathrm{B}\partial_y\left(\frac{\partial_y\hat{v}}{|\partial_y \boldsymbol{U}_B|}\right), & \end{aligned}$$

with boundary conditions

$$\begin{aligned} \hat{v} = \partial_y \hat{v} &= 0 && \text{at } y = \pm 1/2, && (4.2.13b) \\ \hat{v} = \partial_y \hat{v} &= 0 && \text{at } y = \pm y_B, && (4.2.13c) \\ \partial_{yy}\hat{v} - \alpha^2\hat{v} &= \pm\frac{-2i\alpha h}{(1/2 - y_B)^2} && \text{at } y = \pm y_B. && (4.2.13d) \end{aligned}$$

The boundary value problem (4.2.13) has been implemented using a finite difference method with a central scheme, see Section A.3 for details on the scheme. As the problem contains a singularity at the yield-surface $y = y_B$, we also implemented a shooting method with Riccati transformation as proposed in [43], see Section A.4. Both methods gave accurate results, but the finite difference method creates a generalized eigenvalue problem, that can be solved with the help of standard solvers, giving the whole discrete spectrum at once. Whereas the shooting method avoids spurious eigenmodes, it is much harder to find all the relevant eigenmodes.

We note first that for the range of values of B, Re and α discussed in the literature, no unstable mode was found, in agreement with Métivier et al. [86]. However, inspired by the analysis of the Orr-Sommerfeld system [98], the symmetric boundary condition $\partial_y \hat{v}_s = \partial_{yyy} \hat{v}_s = 0$ has also been studied by Frigaard et al. [43]. Using these symmetric boundary conditions the well-known critical Reynolds number Re = 5772.22 is approached as B $\to$ 0, while for the boundary conditions (4.2.13c) all modes are stable also as B $\to$ 0, as noted by Métivier et al. [86] which shows that the Orr-Sommerfeld-Bingham equation is not a canonical generalization of the standard Orr-Sommerfeld equation.

Figure 4.2 shows the results for the classical Bingham model. As can be seen from the spectrum, no eigenvalue has a positive real part, thus the model is linearly stable.

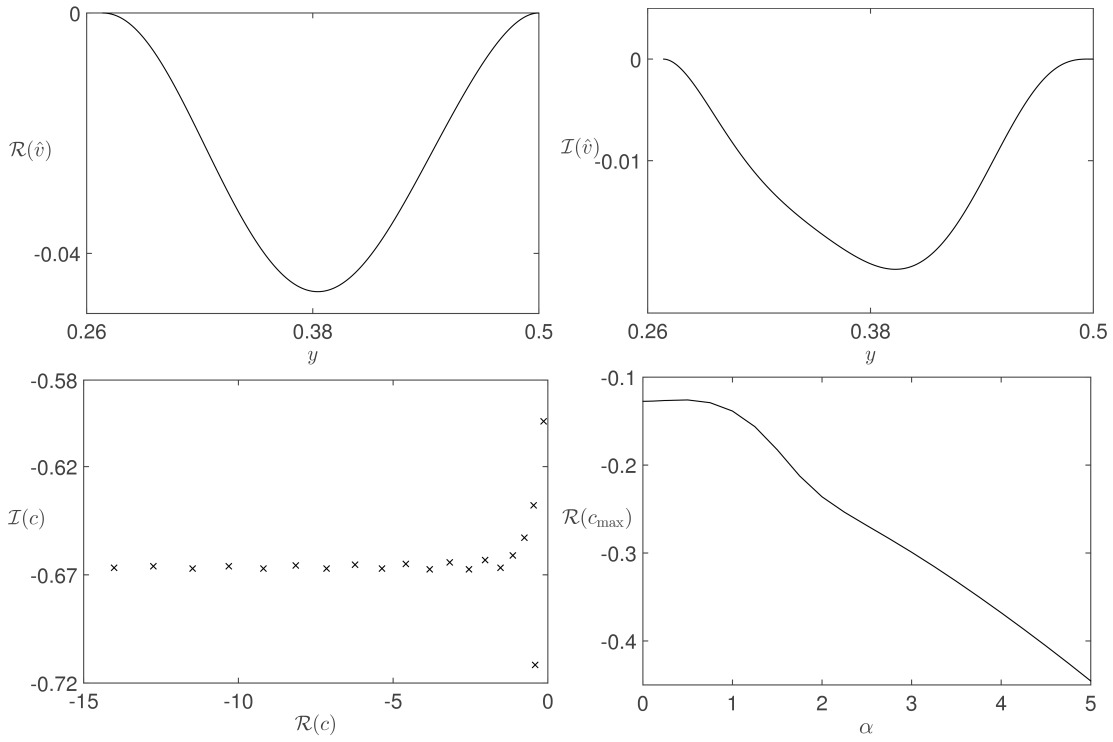

Figure 4.2: Shown is the real and imaginary part of the most unstable mode for B = 10, Re = 5772.22 and $\alpha = 1$ as well as the part of the spectrum with the most unstable modes. (top and bottom, left side) The dispersion relation of the most unstable mode (bottom, right side).

4.3 Governing equations for two-phase flow

Formulation of the model

We consider the two-phase flow model of a suspension consisting of solid particles fully dispersed in a liquid medium, that has been derived in Chapter 2.

In order to state the model, we define some quantities first. Let ϕ_j denote the volume fraction of phase j, $\boldsymbol{u}_j = (u_j, v_j)$ the velocity, p_j the pressure, $\boldsymbol{\tau}_j$ the shear-stress and $\dot{\boldsymbol{\gamma}}_j = \nabla \boldsymbol{u}_j + (\nabla \boldsymbol{u}_j)^T$ the shear rate, where $j \in \{s, f\}$ and the indices s and f denote the solid or liquid phase, respectively. The dimensional model contains the liquid viscosity μ_f, the densities ρ_j and the permeability K, for details see Chapter 2. Using the scales U_0 for velocity, L for length as well as $(U_0\mu_f)/L$ for the pressure and the stresses, the governing equations of the two-phase model are (cf. with (2.4.1))

$$\phi_s + \phi_f = 1, \tag{4.3.1a}$$

$$\partial_t \phi_f + \nabla \cdot (\phi_f \boldsymbol{u}_f) = 0, \tag{4.3.1b}$$

$$\partial_t \phi_s + \nabla \cdot (\phi_s \boldsymbol{u}_s) = 0, \tag{4.3.1c}$$

$$\mathrm{Re}[\partial_t(\phi_f \boldsymbol{u}_f) + \nabla \cdot (\phi_f \boldsymbol{u}_f \otimes \boldsymbol{u}_f)] - \nabla \cdot (\phi_f \boldsymbol{\tau}_f) + \phi_f \nabla p_f = -\mathrm{Da}\, \frac{{\phi_s}^2}{\phi_f}(\boldsymbol{u}_f - \boldsymbol{u}_s), \tag{4.3.1d}$$

$$\frac{\mathrm{Re}}{r}[\partial_t(\phi_s \boldsymbol{u}_s) + \nabla \cdot (\phi_s \boldsymbol{u}_s \otimes \boldsymbol{u}_s)] - \nabla \cdot (\phi_s \boldsymbol{\tau}_s) + \nabla p_c + \phi_s \nabla p_f = \mathrm{Da}\, \frac{{\phi_s}^2}{\phi_f}(\boldsymbol{u}_f - \boldsymbol{u}_s), \tag{4.3.1e}$$

where the Reynolds number, Darcy's number and the relative density are defined as

$$\mathrm{Re} = \frac{UL\rho_f}{\mu_f}, \qquad \mathrm{Da} = \frac{L^2}{K}, \qquad r = \frac{\rho_f}{\rho_s}.$$

The non-dimensionalized constitutive laws are a Newtonian stress for the liquid, i.e.

$$\boldsymbol{\tau}_f = \dot{\boldsymbol{\gamma}}_f. \tag{4.3.2a}$$

For the solid phase, either $|\dot{\boldsymbol{\gamma}}_s| > 0$, then we require

$$\boldsymbol{\tau}_s = \eta_s(\phi_s)\dot{\boldsymbol{\gamma}}_s, \tag{4.3.2b}$$

$$p_c = \eta_n(\phi_s)|\dot{\boldsymbol{\gamma}}_s|, \tag{4.3.2c}$$

with

$$\eta_s(\phi_s) = 1 + \frac{5}{2}\frac{\phi_{\mathrm{crit}}}{\phi_{\mathrm{crit}} - \phi_s} + \mu_c(\phi_s)\frac{\phi_s}{(\phi_{\mathrm{crit}} - \phi_s)^2}, \tag{4.3.2d}$$

$$\mu_c(\phi_s) = \mu_1 + \frac{\mu_2 - \mu_1}{1 + I_0 {\phi_s}^2(\phi_{\mathrm{crit}} - \phi_s)^{-2}}, \tag{4.3.2e}$$

$$\eta_n(\phi_s) = \left(\frac{\phi_s}{\phi_{\mathrm{crit}} - \phi_s}\right)^2, \tag{4.3.2f}$$

or $\dot{\boldsymbol{\gamma}}_s = \boldsymbol{0}$, and then we let

$$\phi_s = \phi_{\mathrm{crit}}$$

and leave $\boldsymbol{\tau}_s$ undefined, but impose the inequality

$$|\phi_s \boldsymbol{\tau}_s| \leq \mu_1 p_c. \tag{4.3.2g}$$

The parameters μ_1, μ_2, I_0 are experimentally determined material parameters of the friction law for dense suspensions and ϕ_{crit} is the maximum packing fraction, see [2, 15] and Chapter 2 for details.

Stability problem

For the cases of plane Couette flow and plane Poiseuille flow, stationary solutions of system (4.3.1) are derived in [2] and Chapter 3. The variables defining these base states depend on y only except for the pressure P_f for which $\partial_x P_f$ is a constant and the base states of the shear rate tensors, which are

$$\Gamma_j = \begin{pmatrix} 0 & \partial_y U_j \\ \partial_y U_j & 0 \end{pmatrix}, \qquad \boldsymbol{T}_f = \begin{pmatrix} 0 & \partial_y U_f \\ \partial_y U_f & 0 \end{pmatrix}, \qquad \boldsymbol{T}_s = \begin{pmatrix} 0 & \partial_y U_s \\ \partial_y U_s & 0 \end{pmatrix},$$

because $V_j = 0$ for parallel shear flow. We denote the base state variables by upper-case letters and the perturbation variables by lower-case letters with a tilde. Linearizing about the base states by using the ansatz

$$\begin{aligned} &\phi_j = \Phi_j + \delta\tilde{\phi}_j, && u_j = U_j + \delta\tilde{u}_j, && v_j = V_j + \delta\tilde{v}_j, && \text{(4.3.3a)}\\ &\dot{\boldsymbol{\gamma}}_j = \boldsymbol{\Gamma}_j + \delta\tilde{\boldsymbol{\gamma}}_j, && p_f = P_f + \delta\tilde{p}_f, && p_c = P_c + \delta\tilde{p}_c, && \text{(4.3.3b)}\\ &\boldsymbol{\tau}_j = \boldsymbol{T}_j + \delta\tilde{\boldsymbol{\tau}}_j, \end{aligned}$$

where $j \in \{f, s\}$ denote solid and liquid phase and δ denotes the small perturbation parameter, we obtain to order δ the linearized system

$$\tilde{\phi}_f + \tilde{\phi}_s = 0, \tag{4.3.4a}$$

$$\partial_t\tilde{\phi}_f + \partial_x(\Phi_f\tilde{u}_f + \tilde{\phi}_f U_f) + \partial_y(\Phi_f\tilde{v}_f + \tilde{\phi}_f V_f) = 0, \tag{4.3.4b}$$

$$\partial_t\tilde{\phi}_s + \partial_x(\Phi_s\tilde{u}_s + \tilde{\phi}_s U_s) + \partial_y(\Phi_s\tilde{v}_s + \tilde{\phi}_s V_s) = 0, \tag{4.3.4c}$$

$$\mathrm{Re}[\partial_t(\tilde{\phi}_f U_f + \Phi_f\tilde{u}_f) + \partial_x(2\Phi_f U_f\tilde{u}_f + \tilde{\phi}_f {U_f}^2) + \partial_y(\Phi_f U_f\tilde{v}_f)] - \partial_x(\Phi_f\tilde{\tau}_{f11}) \tag{4.3.4d}$$

$$\begin{aligned} -\partial_y(\Phi_f\tilde{\tau}_{f12} + \tilde{\phi}_f T_{f12}) + \Phi_f\partial_x\tilde{p}_f + \tilde{\phi}_f\partial_x P_f = -\mathrm{Da}\Bigg[&\frac{2\Phi_s\tilde{\phi}_s}{\Phi_f}(U_f - U_s) - \\ &\frac{{\Phi_s}^2}{{\Phi_f}^2}\tilde{\phi}_f(U_f - U_s) + \frac{{\Phi_s}^2}{\Phi_f}(\tilde{u}_f - \tilde{u}_s)\Bigg], \end{aligned}$$

$$\mathrm{Re}\,[\partial_t(\Phi_f\tilde{v}_f) + \partial_x(\Phi_f U_f\tilde{v}_f)] - \partial_x(\Phi_f\tilde{\tau}_{f12} + \tilde{\phi}_f T_{f12}) \tag{4.3.4e}$$

$$-\partial_y(\Phi_f\tilde{\tau}_{f22}) + \Phi_f\partial_y\tilde{p}_f = -\mathrm{Da}\left[\frac{{\Phi_s}^2}{\Phi_f}(\tilde{v}_f - \tilde{v}_s)\right],$$

$$\frac{\mathrm{Re}}{r}[\partial_t(\tilde{\phi}_s U_s + \Phi_s\tilde{u}_s) + \partial_x(2\Phi_s U_s\tilde{u}_s + \tilde{\phi}_s {U_s}^2) + \partial_y(\Phi_s U_s\tilde{v}_s)] - \partial_x(\Phi_s\tilde{\tau}_{s11}) \tag{4.3.4f}$$

$$\begin{aligned} -\partial_y(\Phi_s\tilde{\tau}_{s12} + \tilde{\phi}_s T_{s12}) + \partial_x\tilde{p}_c + \Phi_s\partial_x\tilde{p}_f + \tilde{\phi}_s\partial_x P_f = \mathrm{Da}\Bigg[&\frac{2\Phi_s\tilde{\phi}_s}{\Phi_f}(U_f - U_s) - \\ &\frac{{\Phi_s}^2}{{\Phi_f}^2}\tilde{\phi}_f(U_f - U_s) + \frac{{\Phi_s}^2}{\Phi_f}(\tilde{u}_f - \tilde{u}_s)\Bigg], \end{aligned}$$

$$\frac{\mathrm{Re}}{r}[\partial_t(\Phi_s\tilde{v}_s) + \partial_x(\Phi_s U_s\tilde{v}_s)] - \partial_x(\Phi_s\tilde{\tau}_{s12} + \tilde{\phi}_s T_{s12}) \tag{4.3.4g}$$

$$-\partial_y(\Phi_s\tilde{\tau}_{s22}) + \partial_y\tilde{p}_c + \Phi_s\partial_y\tilde{p}_f = \mathrm{Da}\left[\frac{{\Phi_s}^2}{\Phi_f}(\tilde{v}_f - \tilde{v}_s)\right],$$

which is amenable to normal mode analysis and thus we make the ansatz for the perturbation

$$\{\tilde{\phi}_j, \tilde{u}_j, \tilde{v}_j, \tilde{p}_f\} = \{\hat{\phi}_j(y), \hat{u}_j(y), \hat{v}_j(y), \hat{p}_f(y)\}\, e^{i\alpha x + ct}. \tag{4.3.5}$$

Note with this choice of ansatz functions an unstable mode fulfills that the real part $\mathcal{R}(c) > 0$. Plugging the ansatz into system (4.3.4) yields

$$-c\hat{\phi}_s + i\alpha(\Phi_f\hat{u}_f - \hat{\phi}_s U_f) + \partial_y(\Phi_f\hat{v}_f - \hat{\phi}_s V_f) = 0, \tag{4.3.6a}$$

$$c\hat{\phi}_s + i\alpha(\Phi_s\hat{u}_s + \hat{\phi}_s U_s) + \partial_y(\Phi_s\hat{v}_s + \hat{\phi}_s V_s) = 0, \tag{4.3.6b}$$

$$\mathrm{Re}[c(-\hat{\phi}_s U_f + \Phi_f\hat{u}_f) + i\alpha(2\Phi_f U_f\hat{u}_f - \hat{\phi}_s {U_f}^2) + \partial_y(\Phi_f U_f\hat{v}_f)] \tag{4.3.6c}$$

$$-i\alpha(\Phi_f\hat{\tau}_{f11}) - \partial_y(\Phi_f\hat{\tau}_{f12} - \hat{\phi}_s T_{f12}) + i\alpha\Phi_f\hat{p}_f - \hat{\phi}_s\partial_x P_f = -\mathrm{Da}\left[\frac{2\Phi_s\hat{\phi}_s}{\Phi_f}(U_f - U_s) + \frac{{\Phi_s}^2}{{\Phi_f}^2}\hat{\phi}_s(U_f - U_s) + \frac{{\Phi_s}^2}{\Phi_f}(\hat{u}_f - \hat{u}_s)\right],$$

$$\mathrm{Re}[c(\Phi_f\hat{v}_f) + i\alpha(\Phi_f U_f\hat{v}_f)] - i\alpha(\Phi_f\hat{\tau}_{f21} - \hat{\phi}_s T_{f21}) \tag{4.3.6d}$$

$$-\partial_y(\Phi_f\hat{\tau}_{f22}) + \Phi_f\partial_y\hat{p}_f = -\mathrm{Da}\left[\frac{{\Phi_s}^2}{\Phi_f}(\hat{v}_f - \hat{v}_s)\right],$$

$$\frac{\mathrm{Re}}{r}\left[c(\hat{\phi}_s U_s + \Phi_s\hat{u}_s) + i\alpha(2\Phi_s U_s\hat{u}_s + \hat{\phi}_s {U_s}^2) + \partial_y(\Phi_s U_s\hat{v}_s)\right] \tag{4.3.6e}$$

$$-i\alpha(\Phi_s\hat{\tau}_{s11}) - \partial_y(\Phi_s\hat{\tau}_{s12} + \hat{\phi}_s T_{s12}) + i\alpha\hat{p}_c + i\alpha\Phi_s\hat{p}_f + \hat{\phi}_s\partial_x P_f = \mathrm{Da}\left[\frac{2\Phi_s\hat{\phi}_s}{\Phi_f}(U_f - U_s) + \frac{{\Phi_s}^2}{{\Phi_f}^2}\hat{\phi}_s(U_f - U_s) + \frac{{\Phi_s}^2}{\Phi_f}(\hat{u}_f - \hat{u}_s)\right],$$

$$\frac{\mathrm{Re}}{r}\left[c(\Phi_s\hat{v}_s) + i\alpha(\Phi_s U_s\hat{v}_s)\right] - i\alpha(\Phi_s\hat{\tau}_{s21} + \hat{\phi}_s T_{s21}) \tag{4.3.6f}$$

$$-\partial_y(\Phi_s\hat{\tau}_{s22}) + \partial_y\hat{p}_c + \Phi_s\partial_y\hat{p}_f = \mathrm{Da}\left[\frac{{\Phi_s}^2}{\Phi_f}(\hat{v}_f - \hat{v}_s)\right],$$

with

$$\hat{\gamma}_j = \begin{pmatrix} 2i\alpha\hat{u}_j & \partial_y\hat{u}_j + i\alpha\hat{v}_j \\ \partial_y\hat{u}_j + i\alpha\hat{v}_j & 2\partial_y\hat{v}_j \end{pmatrix},$$
$$\hat{\tau}_f = \hat{\gamma}_f,$$
$$\hat{\tau}_s = \eta_s'(\Phi_s)\hat{\phi}_s\Gamma_s + \eta_s(\Phi_s)\hat{\gamma}_s,$$
$$\hat{p}_c = \eta_n'(\Phi_s)\hat{\phi}_s|\Gamma_s| + \eta_n(\Phi_s)\frac{\partial_y U_s}{|\partial_y U_s|}(\partial_y\hat{u}_s + i\alpha\hat{v}_s).$$

Discretization of system (4.3.6) yields a generalized eigenvalue problem of the form

$$c\boldsymbol{E}\boldsymbol{\psi} = \boldsymbol{A}\boldsymbol{\psi},$$

with $\boldsymbol{E}$,$\boldsymbol{A}$ matrices and ψ a vector of our variables. The matrix $\boldsymbol{E}$ is singular, thus we have infinite eigenvalues c as part of the solution, which create spurious eigenvalues depending on the

numerical scheme in use. The singularity of $\boldsymbol{E}$ stems from the incompressibility condition, which is eliminated by substitution of the liquid velocity

$$\hat{u}_f = \frac{-1}{i\alpha\Phi_f}\left(-i\alpha\hat{\phi}_s U_f + \partial_y(\Phi_f\hat{v}_f) + i\alpha(\Phi_s\hat{u}_s + \hat{\phi}_s U_s) + \partial_y(\Phi_s\hat{v}_s)\right), \tag{4.3.8}$$

and the pressure by

$$\begin{aligned}\hat{p}_f = \frac{-1}{i\alpha\Phi_f}\Bigg(&\mathrm{Re}\big[c(-\hat{\phi}_s U_f + \Phi_f\hat{u}_f) + i\alpha(2\Phi_f U_f\hat{u}_f - \hat{\phi}_s {U_f}^2) + \partial_y(\Phi_f U_f\hat{v}_f)\big] \\ &- i\alpha(\Phi_f\hat{\tau}_{f11}) - \partial_y(\Phi_f\hat{\tau}_{f12} - \hat{\phi}_s T_{f12}) - \hat{\phi}_s\partial_x P_f \\ &+ \mathrm{Da}\Big[\frac{2\Phi_s\hat{\phi}_s}{\Phi_f}(U_f - U_s) + \frac{{\Phi_s}^2}{{\Phi_f}^2}\hat{\phi}_s(U_f - U_s) + \frac{{\Phi_s}^2}{\Phi_f}(\hat{u}_f - \hat{u}_s)\Big]\Bigg).\end{aligned} \tag{4.3.9}$$

We note that similar approaches are known from the derivation of the Orr-Sommerfeld equation, where usually the stream function is introduced, which can then be used to eliminate the differential algebraic character from the single-phase equations, cf. [43, 83]. The remaining equations are

$$c\hat{\phi}_s + i\alpha(\Phi_s\hat{u}_s + \hat{\phi}_s U_s) + \partial_y(\Phi_s\hat{v}_s) = 0, \tag{4.3.10a}$$

$$\begin{aligned}&\mathrm{Re}[c(\Phi_f\hat{v}_f) + i\alpha(\Phi_f U_f\hat{v}_f)] - i\alpha(\Phi_f\hat{\tau}_{f21} - \hat{\phi}_s T_{f21}) \\ &\qquad -\partial_y(\Phi_f\hat{\tau}_{f22}) + \Phi_f\partial_y\hat{p}_f = -\mathrm{Da}\frac{{\Phi_s}^2}{\Phi_f}(\hat{v}_f - \hat{v}_s),\end{aligned}$$

$$\begin{aligned}&\frac{\mathrm{Re}}{r}\Big[c(\hat{\phi}_s U_s + \Phi_s\hat{u}_s) + i\alpha(2\Phi_s U_s\hat{u}_s + \hat{\phi}_s {U_s}^2) + \partial_y(\Phi_s U_s\hat{v}_s)\Big] \\ &-i\alpha(\Phi_s\hat{\tau}_{s11}) - \partial_y(\Phi_s\hat{\tau}_{s12} + \hat{\phi}_s T_{s12}) + i\alpha\hat{p}_c + i\alpha\hat{p}_f\Phi_s + \partial_x P_f\hat{\phi}_s = \mathrm{Da}\Big[\frac{2\Phi_s\hat{\phi}_s}{\Phi_f}(U_f - U_s) \\ &\qquad + \frac{{\Phi_s}^2}{{\Phi_f}^2}\hat{\phi}_s(U_f - U_s) + \frac{{\Phi_s}^2}{\Phi_f}(\hat{u}_f - \hat{u}_s)\Big],\end{aligned} \tag{4.3.10b}$$

$$\begin{aligned}&\frac{\mathrm{Re}}{r}\Big[c(\Phi_s\hat{v}_s) + i\alpha(\Phi_s U_s\hat{v}_s)\Big] - i\alpha(\Phi_s\hat{\tau}_{s21} + \hat{\phi}_s T_{s21}) \\ &\qquad -\partial_y(\Phi_s\hat{\tau}_{s22}) + \hat{\partial}_y p_c + \partial_y\hat{p}_f\Phi_s = \mathrm{Da}\frac{{\Phi_s}^2}{\Phi_f}(\hat{v}_f - \hat{v}_s).\end{aligned} \tag{4.3.10c}$$

For the case when the solid phase reaches maximum packing fraction $\phi_s = \phi_{\mathrm{crit}}$, the solid momentum equations (4.3.10b) and (4.3.10c) lose their validity and condition $\dot{\boldsymbol{\gamma}}_s = \boldsymbol{0}$ tells us that the solid is confined to rigid motions. Hence, in this case we drop the two solid momentum equations and set

$$\hat{\phi}_s = 0, \qquad \Phi_s = \phi_{\mathrm{crit}}, \qquad \hat{u}_s = 0, \qquad \hat{v}_s = 0.$$

This in turn also eliminates (4.3.10a) and the equation for the unyielded region becomes

$$\mathrm{Re}[c\Phi_f\hat{v}_f + i\alpha\Phi_f U_f\hat{v}_f] - i\alpha\Phi_f\hat{\tau}_{f21} - \partial_y(\Phi_f\hat{\tau}_{f22}) + \Phi_f\partial_y\hat{p}_f = -\mathrm{Da}\frac{{\Phi_s}^2}{\Phi_f}\hat{v}_f. \tag{4.3.11}$$

This solid region equation will only be needed in the Poiseuille flow computation, as the Couette flow does not contain an unyielded region.

4.4 Plane Couette flow

Consider a planar flow of a fluid confined between two walls at $y = 0$ and $y = L$, where we usually choose $L = 1$. The boundary conditions at the lower wall are

$$\boldsymbol{u}_s = \boldsymbol{u}_f = \mathbf{0} \qquad \text{at } y = 0, \tag{4.4.1a}$$

and for the upper wall are

$$\boldsymbol{u}_s = \boldsymbol{u}_f = \begin{pmatrix} L \\ 0 \end{pmatrix} \qquad \text{at } y = L. \tag{4.4.1b}$$

As shown in Section 3.1, the plane Couette flow allows for the derivation of an explicit solution with base states

$$U_s(y) = U_f(y) = y, \qquad V_s = V_f = 0, \qquad P_f = C_1, \qquad \Phi_s = C_2,$$

where $C_1 \in \mathbb{R}$ and $C_2 \in]0, \phi_{\text{crit}}[$ are free parameters.

Using the no-slip boundary conditions (4.4.1) in our ansatz (4.3.3) and (4.3.5) yields

$$\hat{u}_s = \hat{v}_s = \hat{v}_f = 0 \qquad \text{at } y = 0 \text{ and } L. \tag{4.4.2a}$$

The incompressibility condition (4.3.8) together with $\hat{v}_s = \hat{v}_f = 0$ yields

$$\Phi_f \partial_y \hat{v}_f + \Phi_s \partial_y \hat{v}_s = 0 \qquad \text{at } y = 0 \text{ and } L. \tag{4.4.2b}$$

Numerical solution of the spectrum

We use a finite-difference method for the numerical solution of the system above and use a central scheme of second order for all variables. The pure convection equation of the volume fraction (4.3.10a) showed an odd-even decoupling, which has been solved using a staggered grid approach.

The system (4.3.10) with boundary conditions (4.4.2), yielding a generalized eigenvalue problem for c, can then be solved using standard solvers. Details of the numerical approximation are given in Section A.3. We tested our scheme for the Newtonian Couette flow leading to the corresponding well-studied Orr-Sommerfeld equation [98] as well as for the non-Newtonian case leading to the Orr-Sommerfeld-Bingham equation [43], see also Section 4.2.

Compared to these classical problems the study of the spectrum for our system (4.3.10), (4.4.2) is more complicated as it depends on many additional parameters, which are Da, I_0, μ_1, μ_2, C_1, C_2, ϕ_{crit} and α. However, guided by physically relevant values for the parameters, our numerical parameter studies revealed two characteristic classes of instabilities.

Figure 4.3 shows two spectra for two exemplary choices of parameters, where the parameter values differ in the values of μ_1. One observes that nearly all eigenvalues have negative real parts and, consequently, are stable. On the other hand, we could identify multiple unstable modes in the system, which fall into two classes.

Figures 4.4 and 4.5 show exemplary modes from the two classes. The unstable mode shown in Figure 4.4 is observable for $\mu_1 < 1/2$ and its modes are symmetric, highly oscillatory and show zero values in $\hat{\phi}_s$. Most interestingly, as we will show in the following section, the eigenvalues of

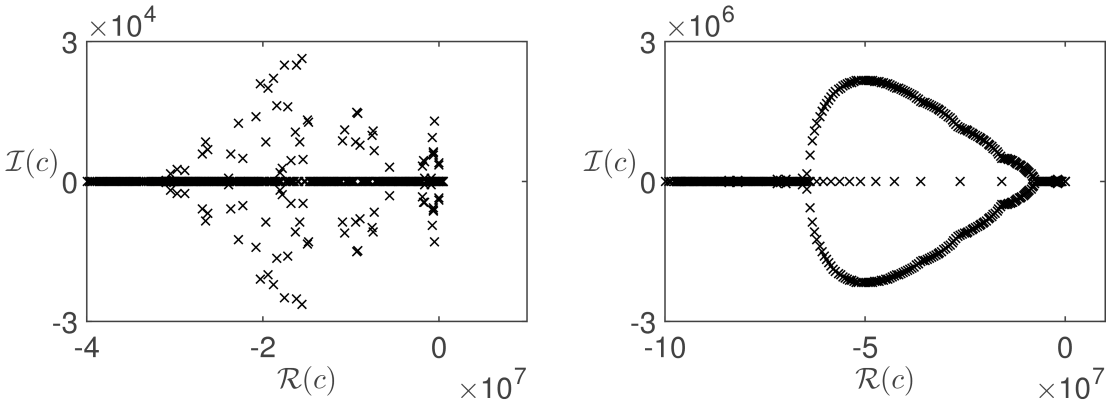

Figure 4.3: Shown are the two-phase plane Couette flow spectra with parameters chosen as $\mathrm{Re} = 1$, $\mathrm{Da} = 100$, $I_0 = 0.005$, $\mu_2 = \mu_1$, $\phi_{\mathrm{crit}} = 0.63$, $\Phi_s = 0.99\phi_{\mathrm{crit}}$, where $\mu_1 = 0.32$ (left) and $\mu_1 = 1$ (right). Both spectra contain unstable eigenvalues near the origin.

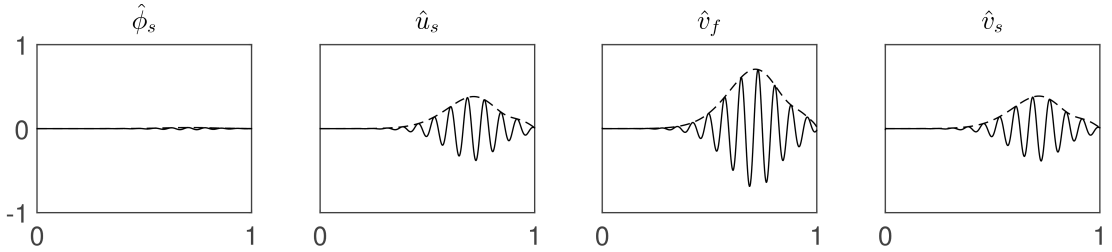

Figure 4.4: Shown is an unstable mode of first class for $\mu_1 = 0.32$ with the rest of the parameters as in Figure 4.3. The mode is symmetric, highly oscillatory and possess only a negligible dependence on ϕ_s.

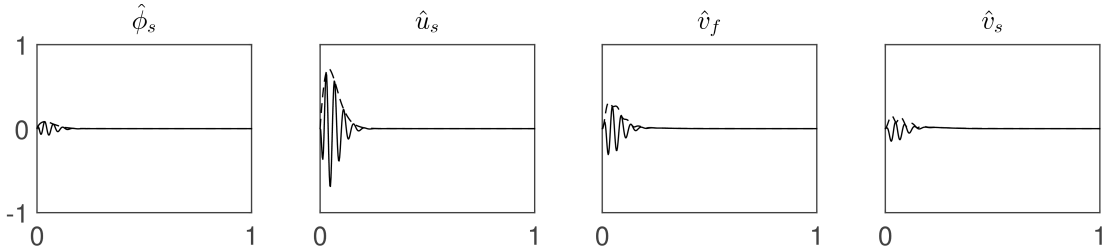

Figure 4.5: Shown is an unstable mode of second class for $\mu_1 = 1$ with the rest of the parameters as in Figure 4.3. The mode is non-symmetric and shows amplifications in all quantities.

these modes can grow with α without bounds, which hints at an ill-posedness in the model. The unstable mode shown in Figure 4.5 occurs as C_2 approaches ϕ_{crit}. Its modes have a non-symmetric

shape and the eigenvalues have positive real parts, which suggests an instability of the base state. These two cases are analyzed in detail in the following sections.

Collision pressure induced ill-posedness

The numerical computations above show that the system loses its well-posedness as soon as

$$\mu_1 < \frac{1}{2}.$$

In this case our numerical studies show that the positive real part $\mathcal{R}(c)$ of the eigenvalues grow to infinity as $\Phi_s \to \phi_{\text{crit}}$ and increasing α. As can be seen in Figure 4.4 from the corresponding eigenvector, the ill-posedness occurs even for $\hat{\phi}_s = 0$. Further, our numerical results showed that the quadratic velocity terms $\Phi_f U_f \hat{u}_f$, $\Phi_f U_f \hat{v}_f$, $\Phi_s U_s \hat{u}_s$ and $\Phi_s U_s \hat{v}_s$ in (4.3.9) and (4.3.10) have a negligible influence on the mode.

These properties can be used to reduce the system (4.3.4) further, so that we can study and understand the origin of the ill-posedness analytically. Hence, in (4.3.4) we set $\hat{\phi}_s = 0$ and neglected the quadratic velocity terms yielding

$$\begin{aligned}
\partial_x(\Phi_s\tilde{u}_s + \Phi_f\tilde{u}_f) + \partial_y(\Phi_s\tilde{v}_s + \Phi_f\tilde{v}_f) &= 0,\\
\mathrm{Re}\,\partial_t(\Phi_f\tilde{u}_f) - \partial_x(\Phi_f\tilde{\tau}_{f11}) - \partial_y(\Phi_f\tilde{\tau}_{f12}) + \Phi_f\partial_x\tilde{p}_f + \mathrm{Da}\left[\frac{{\Phi_s}^2}{\Phi_f}(\tilde{u}_f - \tilde{u}_s)\right] &= 0,\\
\mathrm{Re}\,\partial_t(\Phi_f\tilde{v}_f) - \partial_x(\Phi_f\tilde{\tau}_{f12}) - \partial_y(\Phi_f\tilde{\tau}_{f22}) + \Phi_f\partial_y\tilde{p}_f + \mathrm{Da}\left[\frac{{\Phi_s}^2}{\Phi_f}(\tilde{v}_f - \tilde{v}_s)\right] &= 0,\\
\frac{\mathrm{Re}}{r}\partial_t(\Phi_s\tilde{u}_s) - \partial_x(\Phi_s\tilde{\tau}_{s11}) - \partial_y(\Phi_s\tilde{\tau}_{s12}) + \partial_x\tilde{p}_c + \Phi_s\partial_x\tilde{p}_f - \mathrm{Da}\left[\frac{{\Phi_s}^2}{\Phi_f}(\tilde{u}_f - \tilde{u}_s)\right] &= 0,\\
\frac{\mathrm{Re}}{r}\partial_t(\Phi_s\tilde{v}_s) - \partial_x(\Phi_s\tilde{\tau}_{s12}) - \partial_y(\Phi_s\tilde{\tau}_{s22}) + \partial_y\tilde{p}_c + \Phi_s\partial_y\tilde{p}_f - \mathrm{Da}\left[\frac{{\Phi_s}^2}{\Phi_f}(\tilde{v}_f - \tilde{v}_s)\right] &= 0.
\end{aligned}$$

Eliminating the pressure and one of the velocities through the incompressibility conditions, this set of equation allows the standard Fourier ansatz

$$\{\tilde{u}_s, \tilde{v}_s, \tilde{v}_f\} = \{\hat{u}_s, \hat{v}_s, \hat{v}_f\}e^{i\alpha x + i\beta y + ct},$$

yielding the 3×3 matrix system of the form

$$(\boldsymbol{A} - c\boldsymbol{I})\boldsymbol{u} = \boldsymbol{0},$$

which is equivalent to

$$\det(\boldsymbol{A} - c\boldsymbol{I}) = 0 \qquad \text{for } \boldsymbol{u} \neq \boldsymbol{0}, \tag{4.4.4}$$

where an instability fulfills $\mathcal{R}(c) > 0$. Equation (4.4.4) is a polynomial of third order in c that can be solved using computer algebra [84].

We first study the simpler case $\alpha = \beta$, choose $\mathrm{Da} = 0, \mathrm{Re} = 1, \mu_2 = \mu_1$, $r = 1$ and drop the 5/2-term in the viscosity. Then, we are able to compute closed form solutions for the eigenvalues

and get the following amplification factors

$$
\begin{aligned}
c_1 &= -2\alpha^2, \\
c_2 &= -2\alpha^2 \frac{(\phi_{\text{crit}} - \Phi_s)^2 + \mu_1 \Phi_s}{(\phi_{\text{crit}} - \Phi_s)^2}, \\
c_3 &= 2\alpha^2 \frac{(1-2\mu_1)\Phi_s(1-\Phi_s) - 2(\phi_{\text{crit}} - \Phi_s)^2}{(\phi_{\text{crit}} - \Phi_s)^2}.
\end{aligned}
$$

The amplification factors c_1 and c_2 are always negative, i.e. are stable and correspond to the liquid and particle viscosity damping, respectively. The third amplification c_3 is always negative for $\mu_1 \geq 1/2$, but will always become positive for $\mu_1 < 1/2$ and grows without bound when $\Phi_s \to \phi_{\text{crit}}$. Hence, the ill-posedness is rooted in a competition between the collision pressure term and the particle viscosity and grows like

$$
c_3 \sim \frac{2\alpha^2}{(\phi_{\text{crit}} - \Phi_s)^2}.
$$

This eigenvalue grows without bound for increasing α and $\Phi_s \to \phi_{\text{crit}}$. Thus, it is necessary to set $\mu_1 \geq 1/2$ in order for the problem to be well-posed.

Next, we consider the case with $\alpha \neq \beta$, then the amplification factors are

$$
\begin{aligned}
c_1 &= -\frac{\alpha^2 + \beta^2}{\text{Re}}, \\
c_2 &= -r\eta_s \frac{\alpha^2 + \beta^2}{\text{Re}}, \\
c_3 &= 2r \frac{(1-\Phi_s)(\alpha\beta\eta_n - \Phi_s\eta_s(\alpha^2+\beta^2)) - {\Phi_s}^2(\alpha^2+\beta^2)}{\Phi_s \text{Re}(-\Phi_s + \Phi_s r + 1)}.
\end{aligned} \tag{4.4.6a}
$$

It is now easy to see, that a necessary condition for well-posedness is

$$
\alpha\beta\eta_n - \Phi_s\eta_s(\alpha^2+\beta^2) \leq 0 \text{ for all } \Phi_s,
$$

which can be rewritten as

$$
-\frac{1}{2}\eta_n (\alpha - \beta)^2 + (\alpha^2 + \beta^2)\left(\eta_n - \frac{1}{2}\Phi_s\eta_s\right) \leq 0 \text{ for all } \Phi_s. \tag{4.4.7}
$$

This asserts our notion, that the worst case scenario is obtained for $\alpha = \beta$ and gives the necessary criterion, that the particle viscosity must be at least half in size of the collision pressure for all possible choices of parameters. In case of the equivalence $\eta_n = \frac{1}{2}\Phi_s\eta_s$ the mode is stable, since the $-\Phi_s(\alpha^2+\beta^2)$ term has a stabilizing influence, which originates from the liquid viscosity. Note, Chapter 5 also yields this stability criterion, but with for general flows and a greater ratio.

Figure 4.6 shows the singular behavior of the ill-posedness' dispersion relation. Comparison between the analytic expression (4.4.6a) and numerical result for different Da values show good agreement although the numerical results do not use simplifications, e.g. boundary conditions are non-periodic and nonlinear terms are not eliminated in the computations.

For the case $\mathrm{Da} > 0$, the eigenmodes of the ill-posedness are

$$
\begin{aligned}
c_1 &= \frac{1}{2(\Phi_s-1)^2\mathrm{Re}}\Big(f_1 - (\alpha^2+\beta^2)(\Phi_s-1)^2(1+\eta_s r) \\
&\quad + \sqrt{(\alpha^2+\beta^2)^2(\Phi_s-1)^4(1-\eta_s r)^2 - \Phi_s f_1 - 2(\alpha^2+\beta^2)(\Phi_s-1)^2(r\eta_s-1)f_2}\Big), \\
c_2 &= \frac{1}{2(\Phi_s-1)^2\mathrm{Re}}\Big(f_1 - (\alpha^2+\beta^2)(\Phi_s-1)^2(1+\eta_s r) \\
&\quad - \sqrt{(\alpha^2+\beta^2)^2(\Phi_s-1)^4(1-\eta_s r)^2 - \Phi_s f_1 - 2(\alpha^2+\beta^2)(\Phi_s-1)^2(r\eta_s-1)f_2}\Big), \\
c_3 &= 2r\frac{(1-\Phi_s)(\alpha\beta\eta_n - \Phi_s\eta_s(\alpha^2+\beta^2)) - {\Phi_s}^2(\alpha^2+\beta^2)}{\Phi_s\mathrm{Re}(1-\Phi_s+\Phi_s r)} - r\frac{\mathrm{Da}\,\Phi_s}{(\Phi_s-1)^2\mathrm{Re}(1-\Phi_s+\Phi_s r)},
\end{aligned}
$$

where

$$
\begin{aligned}
f_1 &= \mathrm{Da}\Phi_s(\Phi_s(r-1)-r), \\
f_2 &= \mathrm{Da}\Phi_s(\Phi_s(r+1)-r).
\end{aligned}
$$

Notice, since physical relevant values for the density ratio are between zero and one, f_1 is always negative, thus it does not destabilize the model. Positive Darcy's numbers create terms that have a slight stabilizing effect. Nevertheless, the effect is only of order $O(\mathrm{Da})$ and is not able to compete with the singular terms in η_n and η_s. Thus, they do not change the result in an asymptotic sense for $\Phi_s \to \phi_{\mathrm{crit}}$ unless Da is chosen, more or less artificially, as a singular function as the maximum packing fraction is approached. In fact, in recent numerical work on related model equations the authors did just that, see for example [58]. Figure 4.6 shows that for different Da values the dispersion curve of the instability does hardly change.

Finally, we note that the quadratic velocity terms did not show a significant effect on the behavior described above, and we expect them to enter as an order one perturbation, which can be neglected as $\Phi_s \to \phi_{\mathrm{crit}}$.

Convection induced instability

As $\mu_1 \geq 1/2$ the modes of the collision pressure induced ill-posedness become stable, however, other unstable modes become apparent. An example of such a mode is shown in Figure 4.5. In contrast to the ill-posedness they have only small positive real parts that do not grow with α and their modes are non-symmetric and show significant amplifications in $\hat{\phi}_s$. Additionally, if we force $\hat{\phi}_s = 0$ then they vanish, which is contrary to the ill-posedness behavior. Nevertheless, our parameter studies showed that the instability arises also for vanishing inertial terms. So we set

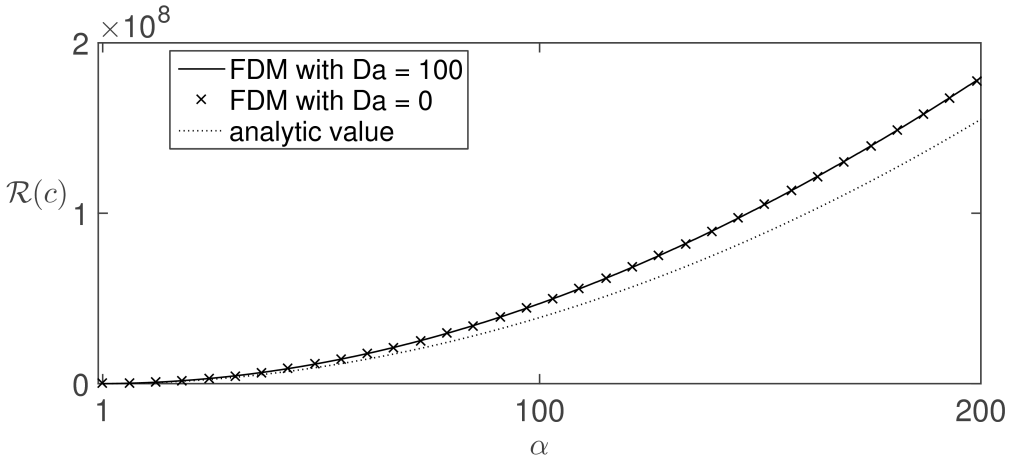

Figure 4.6: Shown is the dispersion relation of the collision pressure induced ill-posedness for the plane Couette flow with parameters as in Figure 4.4. The analytic curve is computed by equation (4.4.6a). Comparison of the numerical and the analytical result shows good matching although the numerical simulation uses non-periodic boundary conditions. The curves for different values of Da are nearly identical, showing the minor influence of the momentum coupling term on the ill-posedness.

$\mathrm{Re} = 0$ and the linearized system gives

$$
\begin{aligned}
\partial_t\tilde{\phi}_s + U_s\partial_x\tilde{\phi}_s + \Phi_s\partial_x\tilde{u}_s + \Phi_s\partial_y\tilde{v}_s &= 0,\\
\partial_x(\Phi_f\tilde{u}_f) + \partial_y(\Phi_f\tilde{v}_f) + \partial_x(\Phi_s\tilde{u}_s) + \partial_y(\Phi_s\tilde{v}_s) &= 0,\\
-\partial_x(\Phi_f\tilde{\tau}_{f11}) - \partial_y(\Phi_f\tilde{\tau}_{f12} + \tilde{\phi}_f T_{f12}) + \Phi_f\partial_x\tilde{p}_f &= \\
-\mathrm{Da}\left[\frac{2\Phi_s\tilde{\phi}_s}{\Phi_f}(U_f - U_s) - \frac{{\Phi_s}^2}{{\Phi_f}^2}\tilde{\phi}_f(U_f - U_s) + \frac{{\Phi_s}^2}{\Phi_f}(\tilde{u}_f - \tilde{u}_s)\right],&\\
-\partial_x(\Phi_f\tilde{\tau}_{f12} + \tilde{\phi}_f T_{f12}) - \partial_y(\Phi_f\tilde{\tau}_{f22}) + \Phi_f\partial_y\tilde{p}_f = -\mathrm{Da}\left[\frac{{\Phi_s}^2}{\Phi_f}(\tilde{v}_f - \tilde{v}_s)\right],&\\
-\partial_x(\Phi_s\tilde{\tau}_{s11}) - \partial_y(\Phi_s\tilde{\tau}_{s12} + \tilde{\phi}_s T_{s12}) + \partial_x\tilde{p}_c + \Phi_s\partial_x\tilde{p}_f &= \\
\mathrm{Da}\left[\frac{2\Phi_s\tilde{\phi}_s}{\Phi_f}(U_f - U_s) - \frac{{\Phi_s}^2}{{\Phi_f}^2}\tilde{\phi}_f(U_f - U_s) + \frac{{\Phi_s}^2}{\Phi_f}(\tilde{u}_f - \tilde{u}_s)\right],&\\
-\partial_x(\Phi_s\tilde{\tau}_{s12} + \tilde{\phi}_s T_{s12}) - \partial_y(\Phi_s\tilde{\tau}_{s22}) + \partial_y\tilde{p}_c + \Phi_s\partial_y\tilde{p}_f = \mathrm{Da}\left[\frac{{\Phi_s}^2}{\Phi_f}(\tilde{v}_f - \tilde{v}_s)\right].&
\end{aligned}
$$

A direct use of the Fourier ansatz is not helpful for this system, as the convective term $U_s\partial_x\tilde{\phi}_s$ would introduce derivatives in the wave-number α. However, the base state $U_s = U_f = y$ makes it suitable for a Kelvin-mode ansatz [123], which consists of two steps - firstly, using the method of characteristics and, secondly, using a Fourier transformation. The method of characteristics eliminates the convective part, but introduces time dependencies in previously stationary parts of the equation. Eventually, the spatial coordinates of the system are transformed into Fourier modes,

yielding an ordinary differential equation in time, that can be studied in order to understand the stability properties of the original system.

Therefore, we first use the transformation

$$\xi = x - yt \quad \text{and} \quad \mathsf{y} = y,$$

followed by a Fourier ansatz in space only, that is

$$\{\tilde{\phi}_s, \tilde{u}_s, \tilde{v}_s, \tilde{v}_f\} = \{\hat{\phi}_s(t), \hat{u}_s(t), \hat{v}_s(t), \hat{v}_f(t)\} e^{i\alpha\xi + i\beta\mathsf{y}}, \tag{4.4.10}$$

which gives the system

$$\begin{aligned}
0 &= \partial_t \hat{\phi}_s + \Phi_s((i\beta - ti\alpha)\hat{v}_s + i\alpha\hat{u}_s),\\
\hat{u}_f &= \frac{-1}{i\alpha\Phi_f}(i\alpha\Phi_s\hat{u}_s + (i\beta - ti\alpha)(\Phi_f\hat{v}_f + \Phi_s\hat{v}_s)),\\
\hat{p}_f &= \frac{-1}{i\alpha\Phi_f}(2\alpha^2\Phi_f\hat{u}_f - (i\beta - ti\alpha)(\Phi_f((i\beta - ti\alpha)\hat{u}_f + i\alpha\hat{v}_f) - \hat{\phi}_s) + \mathrm{Da}\frac{{\Phi_s}^2}{\Phi_f}(\hat{u}_f - \hat{u}_s)),\\
&\quad -i\alpha(\Phi_f((i\beta - ti\alpha)\hat{u}_f + i\alpha\hat{v}_f) - \hat{\phi}_s) - 2\Phi_f(i\beta - ti\alpha)^2\hat{v}_f\\
&\qquad + \Phi_f(i\beta - ti\alpha)\hat{p}_f + \mathrm{Da}\frac{{\Phi_s}^2}{\Phi_f}(\hat{v}_f - \hat{v}_s) = 0,\\
&\quad -i\alpha\Phi_s\eta_s 2i\alpha\hat{u}_s - (i\beta - ti\alpha)(\Phi_s\eta_s((i\beta - ti\alpha)\hat{u}_s + i\alpha\hat{v}_s) + \Phi_s\eta_s'\hat{\phi}_s + \hat{\phi}_s\eta_s) + i\alpha p_c\\
&\qquad + i\alpha\Phi_s\hat{p}_f - \mathrm{Da}\frac{{\Phi_s}^2}{\Phi_f}(\hat{u}_f - \hat{u}_s) = 0,\\
&\quad -i\alpha(\Phi_s\eta_s((i\beta - ti\alpha)\hat{u}_s + i\alpha\hat{v}_s) + \Phi_s\eta_s'\hat{\phi}_s + \hat{\phi}_s\eta_s) - 2\Phi_s\eta_s(i\beta - ti\alpha)^2\hat{v}_s\\
&\qquad + \Phi_s(i\beta - ti\alpha)\hat{p}_f - \mathrm{Da}\frac{{\Phi_s}^2}{\Phi_f}(\hat{v}_f - \hat{v}_s) + (i\beta - ti\alpha)p_c = 0.
\end{aligned}$$

This is of the form

$$\begin{pmatrix} A_{11} & A_{12} \\ A_{21} & A_{22} \end{pmatrix} \begin{pmatrix} \hat{\phi}_s \\ \boldsymbol{u} \end{pmatrix} = \begin{pmatrix} -\partial_t\hat{\phi}_s \\ \mathbf{0} \end{pmatrix}.$$

Thus, using the negative Schur complement $S = -(A_{11} - A_{12}A_{22}^{-1}A_{21})$ of A_{22} we get the ordinary differential equation

$$\partial_t\hat{\phi}_s(t) = S(t)\hat{\phi}_s(t), \tag{4.4.12}$$

with solution to (4.4.12)

$$\hat{\phi}_s(t) = \hat{\phi}_s(0) \cdot e^{\int_0^t S(T)\mathrm{d}T}, \tag{4.4.13}$$

so we expect a perturbation to grow for times t with $\mathcal{R}(S(t)) > 0$ and to shrink for $\mathcal{R}(S(t)) < 0$.

Using a computer algebra [84], S can be given explicitly as

$$S = \frac{f_1\left[\eta_n(\eta_s + \eta_s'\Phi_s)(\alpha^2 - f_3^2)^2 + \eta_s\Phi_s f_2[2\alpha f_3(\eta_s + \eta_s'\Phi_s) - \eta_n' f_2]\right] - 2\eta_s{\Phi_s}^2 f_2\alpha f_3}{2\eta_s f_2\left[f_1\left(\Phi_s\eta_s f_2 - \eta_n\alpha f_3\right) - f_2{\Phi_s}^2\right]},$$

where we denote $f_1 = \Phi_s - 1$, $f_2 = \alpha^2 + f_3^2$ and $f_3 = \beta - t\alpha$ and also set $\mathrm{Da} = 0$. From a theoretical point of view, the Kelvin-mode ansatz first transforms a non-Hermitian differential operator into a Hermitian operator, which allows for a spectral analysis. By the spectral theorem a Hermitian operator has only real eigenvalues, the eigenfunctions are orthogonal and form a complete set. Hence, the Schur complement S is always real and combinations of modes α and β only occur in even orders. Contrary to the analytic approach, the numerical eigenvalues computed by the full problem possess nonzero imaginary parts.

As one is interested in the growth of an initial perturbation $\hat{\phi}_s(0)$, it is conventional to discuss the growth factor defined as [116, 117]

$$G(t) = \sup_{\hat{\phi}_s(0)\neq 0} \left| \frac{\hat{\phi}_s(t)}{\hat{\phi}_s(0)} \right| = \left| e^{\int_0^t S(T)\mathrm{d}T} \right|.$$

Figure 4.7 shows the typical behavior of the growth factor for a range of parameter choices.

With the help of computer algebra [84], the long time limit of S with the constitutive laws (4.3.2) and $\mu_1 = \mu_2$ can be computed as

$$\lim_{t\to\infty} S = \frac{(1-\Phi_s)\Phi_s(7{\phi_{\mathrm{crit}}}^2 - 2{\Phi_s}^2)}{d_1 \cdot d_2},$$

where

$$\begin{aligned} d_1 &:= 2\Phi_s(\mu_1 + \Phi_s) - 9\Phi_s\phi_{\mathrm{crit}} + 7{\phi_{\mathrm{crit}}}^2, \\ d_2 &:= 2\mu_1(\Phi_s - 1)\Phi_s - (\Phi_s - \phi_{\mathrm{crit}})(-7\phi_{\mathrm{crit}} + 2\Phi_s + 5\phi_{\mathrm{crit}}\Phi_s). \end{aligned}$$

This expression is negative as long as $0 < \Phi_s < \phi_{\mathrm{crit}}$ and zero for $\Phi_s \in \{0, \phi_{\mathrm{crit}}\}$, which shows the growth factor G always becomes zero for $t \to \infty$. The expression for $\mu_1 \neq \mu_2$ is much harder to interpret, but contains the same behavior. Thus, for all other parameters fixed and $t \to \infty$ the value of S becomes always negative for our constitutive laws (4.3.2).

Yet, this convergence is not uniform in α and β, because using the transformation $\beta = C_1\alpha$ with $C_1 \in \mathbb{R}$, the Schur complement becomes

$$S = \frac{f_1[\eta_n(\eta_s + \eta_s'\Phi_s)(1-\tilde{f}_3^2)^2 + \eta_s\Phi_s\tilde{f}_2(2\tilde{f}_3(\eta_s + \eta_s'\Phi_s) - \eta_n'\tilde{f}_2)] - 2\eta_s{\Phi_s}^2\tilde{f}_2\tilde{f}_3}{2\eta_s\tilde{f}_2(f_1(\Phi_s\eta_s\tilde{f}_2 - \eta_n\tilde{f}_3) - \tilde{f}_2{\Phi_s}^2)},$$

where $\tilde{f}_2 = 1 + \tilde{f}_3^2$ and $\tilde{f}_3 = C_1 - t$, which is independent of β and α. Thus, only the mode ratio C_1 is of significance for the damping of a perturbation, which might be a way to transform the transient into infinite growth.

Remark

It is well-known that nonlinearities transport perturbations from one mode to another, see e.g. [104]. This process is generally referred to as energy cascade [104] and is also known to occur in multiphase models [14]. Thus, a perturbation being transported to bigger ratios, such that $\tilde{f}_3$ stays constant over time, can grow infinitely large in magnitude. In order for $\tilde{f}_3$ to stay constant the ratio C_1 must grow linear in time, which requires a change of frequency of the

perturbation. This means an observable instability might shift its Fourier modes from low to high frequencies over time, which is a mechanism able to produce shocks as is known from the inviscid Burgers equation [91]. Alternatively to a creation of a shock, the highest frequencies might be damped by another nonlinear effect, which in turn might result in a turbulent behavior, that transports perturbations into smaller structures, which are being damped when they approach a critical length scale [104]. This would correspond to the well-known Kolmogorov's hypothesis for single-phase media [104].

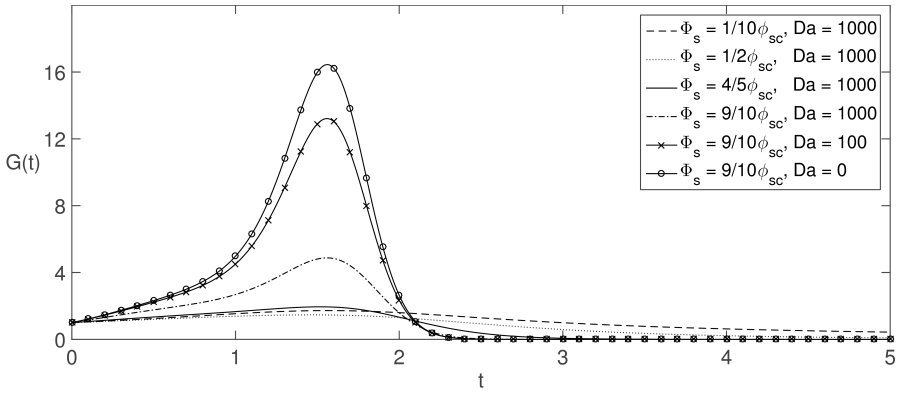

Figure 4.7: Growth factor for a typical parameter choice of $\alpha = 5, \beta = 8, \phi_{\text{crit}} = 0.63, \mu_1 = \mu_2 = 1, \text{Re} = 0$ and different solid volume fractions and Darcy's numbers. The transient growth behavior can obtain huge values, depending on how close Φ_s is to the maximum packing value. For the stated constitutive laws of η_n and η_s and for long times t the growth is always damped, i.e. $G \to 0$ for $t \to \infty$. Nonzero Darcy's numbers have a stabilizing effect, but do not eliminate the instability completely.

In order to understand the stability behavior of the full system, we have to understand the connection between the growth factor $S(t)$ and the unstable modes seen in the finite-difference approximation of the full system, consider in their appropriate spaces.

S depends on the Fourier modes α, β and on time t, whereas the finite-difference numerical approximation depends on the Fourier modes α, c and the spatial variable y. Considering the frozen system at $t = 0$, we would have a constant growth $c = S(0)$. This in turn together with equation (4.4.13) implies our growth is of the form

$$\hat{\phi}_s = \hat{\phi}_s(0)\mathrm{e}^{ct},$$

but this and equation (4.4.10) implies

$$\tilde{\phi}_s = \hat{\phi}_s(0)\mathrm{e}^{ct+i\alpha x+i\beta y}. \tag{4.4.14}$$

Now, the ansatz for the numeric normal mode analysis is

$$\tilde{\phi}_s = \hat{\phi}_s(y)\mathrm{e}^{ct+i\alpha x}.$$

Suppose $\hat{\phi}_s(y)$ is a periodic function, then rewriting $\hat{\phi}_s(y)$ as a Fourier series on a domain $[0, L]$ yields

$$\tilde{\phi}_s = \sum_{k=-\infty}^{\infty} \widehat{\phi_s}(k) \mathrm{e}^{ct+i\alpha x+iy2\pi k/L}, \tag{4.4.15}$$

where $\widehat{\phi_s}(k)$ represents the k-th Fourier coefficient. Comparison of (4.4.14) and (4.4.15) shows, that our numerics computes the frequencies

$$\beta = \frac{2\pi k}{L},$$

with $k \in \mathbb{Z}$ and L the domain size. In order for a direct comparison to work, we therefore need to change the boundary conditions (4.4.2) to periodic boundary conditions and have to consider small domain sizes L. For large L the non-periodic base state $U_s = y$ has a dominant influence on the solution, which makes a direct comparison of the non-periodic numeric and periodic analytic results impossible. If the non-periodicity becomes dominant we do not see single frequencies, but rather a sum of several modes next to the boundaries. which always occur in pairs - one on each wall - see Figure 4.5. In this case the real part of the maximum amplification is always smaller than $S(0)$, hinting at a damping effect of the boundary.

If we set the collision pressure to zero and use Newtonian viscosity, i.e. $\eta_n = \eta_n' = \eta_s' = 0$ and $\eta_s = 1$, then we still get $S > 0$ for some time. Hence, this instability is not driven by a collision pressure or a viscosity driven effect, but rather caused by the convection of the flow.

Analytic results for nonzero Darcy's number could not be computed. Nevertheless, numeric tests with positive Darcy's number showed the momentum coupling term has a stabilizing effect, but is not capable to completely eliminate this instability. Even for very large Darcy's numbers, i.e. Da > 1000, a transient growth is observable, cf. Figure 4.7.

Remark

A possible physical explanation of the instability is a resistance to high volume fractions in the model. For fluid region with near maximum packing a small perturbation is enough to disperse the densely packed particles. However, this instability is of a highly nonlinear nature for $\Phi_s \approx \phi_{\mathrm{crit}}$, as a small change in Φ_s induces a large change in viscosity and particle pressure.

4.5 Plane Poiseuille flow

Two-dimensional Poiseuille flow is another seemingly simple example for a fluid flow. However, in contrast to Couette flow, it contains four major complications. Firstly, the base state is not given in closed form anymore, so a stability analysis is much harder. Secondly, it does contain a plug-flow region, where the linearized set of equations change. Thirdly, the conditions at the yield surface are non-trivial and need to be derived explicitly. Lastly, as discussed in Section 2.2, the well-known loss-of-hyperbolicity problem [65, 77] that is connected to an ill-posedness, enters as soon as the velocities of the solid and liquid phases are different, which is the case for plane Poiseuille, but not for plane Couette flow.

Section 4.2 shows the single-phase Bingham problem to be unconditionally linearly stable to perturbations of the plane Poiseuille flow. This is in contrast to the Newtonian case, where a critical Reynolds number of $\mathrm{Re} \approx 5772.22$ exists, that creates unstable behavior. The different stability stems from different boundary conditions near the channel center. Whereas Newtonian flow uses a symmetric boundary condition at the channel enter, that allows for the growth of the perturbations there, Bingham flows, on the other side, possess a yield-surface near the channel center. The yield-surface boundary condition absorbs perturbations, thus rendering the single-phase Bingham flow stable in this case. This shows the importance of a yield-surface for the stability of the plane Poiseuille flow, which we like to understand in the two-phase case.

Two-phase flow model

Base state

The plane Poiseuille flow ansatz is to consider a stationary problem with no-slip boundary conditions

$$\boldsymbol{u}_s = \boldsymbol{u}_f = \boldsymbol{0} \qquad \text{at } y = \pm 1/2,$$

where all quantities, except for the pressure dependent only on y, i.e.

$$\phi_f = \phi_f(y), \qquad \phi_s = \phi_s(y), \qquad \boldsymbol{u}_f = \boldsymbol{u}_f(y), \qquad \boldsymbol{u}_s = \boldsymbol{u}_s(y), \qquad p_f = p_f(x, y),$$

and demand the solution to have exactly one plug-flow for $0 \leq |y| \leq y_B$. At the yield-surface, we demand continuity of the phasic velocities and the phasic normal shear rates similar to the Bingham flow case, i.e.

$$[\![\boldsymbol{u}_s]\!] = [\![\boldsymbol{u}_f]\!] = [\![\dot{\boldsymbol{\gamma}}_s \cdot \boldsymbol{n}]\!] = [\![\dot{\boldsymbol{\gamma}}_f \cdot \boldsymbol{n}]\!] = 0 \qquad \text{at } y = \pm y_B. \tag{4.5.1}$$

Note, we did not assume continuity of the tangential shear rates or solid volume fraction, since this would overdetermine the system. The conditions (4.5.1) imply these continuities for parallel shear flows. This shows that our assumption $[\![\Phi_s]\!] = 0$ in the derivation of the base states in Section 3.2 and the drift-flux derivation of Section 3.3 is indeed valid and consistent with the boundary conditions, here.

The base state for the two-phase model has been derived in Section 3.2 and it yields a linear liquid pressure $P_f(x) = p_1 x$ and a constant collision pressure with free parameters $p_1 < 0$ and $p_c > 0$. We denote by Y_B the base state solution of the yield-surface y_B.

In order to solve for the solid volume fraction and velocities, we use the transformation

$$y = \left(Y_B - \frac{1}{2}\right)\zeta + \frac{1}{2},$$

define the shorthand notation for the so-called friction coefficient, cf. [15, 75],

$$N(\Phi_s) \equiv \frac{\Phi_s\, \eta_s(\Phi_s)}{\eta_n(\Phi_s)},$$

and get the boundary value problem

$$\frac{1}{Y_B-\frac{1}{2}}\partial_\zeta\left(\frac{\left(\frac{1}{Y_B-\frac{1}{2}}\partial_\zeta N+\Phi_s\,p_1\right)(1-\Phi_s)}{\mathrm{Da}\,{\Phi_s}^2}\right)=\frac{p_1\left((Y_B-\frac{1}{2})\zeta+\frac{1}{2}\right)+N}{1-\Phi_s}+\frac{1}{\eta_n},$$

$$\partial_\zeta Y_B=0,$$

for the volume fraction base state Φ_s and Y_B with boundary conditions

$$\begin{aligned}
0&=\partial_\zeta N+\left(Y_B-\frac{1}{2}\right)\Phi_s\,p_1 && \text{at } \zeta=0,\\
\Phi_s&=\phi_{\mathrm{crit}} && \text{at } \zeta=1,\\
\partial_\zeta\Phi_s&=-\frac{2(Y_B-\frac{1}{2})}{5(1-\phi_{\mathrm{crit}})}\frac{\mathrm{Da}^{\frac{1}{2}}\phi_{\mathrm{crit}}(p_1Y_B+\mu_1)}{\tanh\left(\frac{\mathrm{Da}^{\frac{1}{2}}\phi_{\mathrm{crit}}}{1-\phi_{\mathrm{crit}}}Y_B\right)}+\frac{2}{5}\left(Y_B-\frac{1}{2}\right)p_1 && \text{at } \zeta=1.
\end{aligned}$$

These results can be used in

$$\begin{aligned}
p_c&=-\eta_n(\Phi_s)\partial_y U_s,\\
U_f&=\frac{(\partial_y N+\Phi_s p_1)(1-\Phi_s)}{\mathrm{Da}\,{\Phi_s}^2}+U_s,
\end{aligned}$$

for the fluid region $y>Y_B$ with no-slip boundary condition and

$$\begin{aligned}
\Phi_s&=\phi_{\mathrm{crit}},\\
\partial_y U_s&=0,\\
\partial_y U_f&=\frac{p_1 y}{1-\phi_{\mathrm{crit}}},
\end{aligned}$$

in the plug-flow region with boundary conditions

$$[\![U_s]\!]=[\![U_f]\!]=0 \qquad \text{at } y=Y_B,$$

which yields the solution for the base states of the Poiseuille flow. Figure 4.8 shows an exemplary base state with a plug-flow region at the center of the channel.

Boundary conditions for the stability problem

The linearized reduced two-phase system solves for the unknowns $\hat{\phi}_s, \hat{v}_f, \hat{u}_s$ and $\hat{v}_f$, where the last denotes the linearized y-component of liquid velocity for both - in the plug-flow and the liquid region. The corresponding equations have maximum orders of 0, 2, 2, and $4+4$. Adding the free-boundary conditions at y_B, we get a minimum number of 13 conditions.

The boundary condition for the plane Poiseuille flow are the no-slip boundary condition at the wall

$$\boldsymbol{u}_f=\boldsymbol{u}_s=\boldsymbol{0} \qquad \text{at } y=1/2, \tag{4.5.3}$$

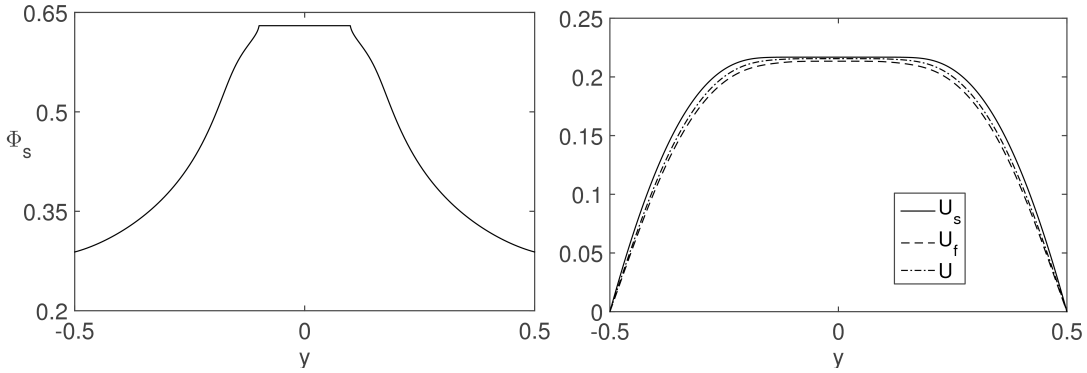

Figure 4.8: Shown is the multiphase base state with parameters chosen as $p_1 = -10$, $Da = 1000$, $I_0 = 0.005$, $\mu_1 = 1$,$\mu_2 = 1.5$, $\phi_{\text{crit}} = 0.63$ and $p_c = 1$.

symmetry around the center of the channel

$$\partial_y \boldsymbol{u}_f = \boldsymbol{0} \qquad \text{at } y = 0, \tag{4.5.4}$$

and continuity of the velocities and shear rates at the yield-surface

$$[\![\boldsymbol{u}_f]\!] = [\![\boldsymbol{u}_s]\!] = [\![\dot{\boldsymbol{\gamma}}_s \cdot \boldsymbol{n}]\!] = [\![\dot{\boldsymbol{\gamma}}_f \cdot \boldsymbol{n}]\!] = \boldsymbol{0} \qquad \text{at } y = y_B. \tag{4.5.5}$$

Just as in the plane Couette flow case, cf. (4.4.2), the no-slip conditions (4.5.3) yield

$$\hat{v}_f = \hat{u}_s = \hat{v}_s = 0 \qquad \text{and} \qquad \Phi_f \partial_y \hat{v}_f + \Phi_s \partial_y \hat{v}_s = 0 \qquad \text{at } y = 1/2.$$

The symmetry condition (4.5.4) at the channel center yields

$$\partial_y \hat{v}_f = 0 \quad \text{at } y = 0.$$

Differentiation of equation (4.3.6a) by y, the symmetry condition $\partial_y \hat{u}_f = 0$ implies

$$\partial_{yy} \hat{v}_f = 0 \quad \text{at } y = 0.$$

For the conditions at the yield-surface $y = y_B$ we note that for any quantity s with base state S and Fourier-transformed perturbation $\delta\hat{s}$, linearizing a condition

$$[\![s]\!] = 0$$

at the yield surface leads to the expression

$$[\![\partial_y S]\!]\tilde{h} = -[\![\hat{s}]\!],$$

where $y_b = Y_b + \delta\tilde{h}$. Therefore, the continuity condition (4.5.5) gives

$$[\![\tilde{u}_j]\!] = [\![\partial_y U_j]\!]\tilde{h}, \qquad [\![\tilde{v}_j]\!] = [\![\partial_y V_j]\!]\tilde{h}, \qquad [\![\tilde{\dot{\gamma}}_s]\!] = [\![\partial_y \Gamma_s]\!]\tilde{h}, \qquad [\![\tilde{\dot{\gamma}}_f]\!] = [\![\partial_y \Gamma_f]\!]\tilde{h}$$

and using the knowledge of the base states (e.g. continuity of $\partial_y U_f$), we obtain

$$[\![\tilde{u}_j]\!] = 0, \qquad [\![\tilde{v}_j]\!] = 0,$$

at the yield surface $y = y_B$ for $j \in \{f, s\}$.

This implies the boundary conditions

$$\hat{u}_s = 0, \qquad \hat{v}_s = 0, \qquad [\![\hat{v}_f]\!] = 0,$$

at the yield-surface $y = y_B$. We have, due to the continuum hypothesis (4.5.5) of the normal shear rates the representation

$$\left[\!\!\left[\begin{pmatrix} \partial_y \hat{u}_s + i\alpha \hat{v}_s \\ \partial_y \hat{v}_s \end{pmatrix}\right]\!\!\right] = -\left[\!\!\left[\begin{pmatrix} \partial_{yy} U_s \\ 0 \end{pmatrix}\right]\!\!\right] \tilde{h}, \qquad \left[\!\!\left[\begin{pmatrix} \partial_y \hat{u}_f + i\alpha \hat{v}_f \\ \partial_y \hat{v}_f \end{pmatrix}\right]\!\!\right] = -\left[\!\!\left[\begin{pmatrix} \partial_{yy} U_f \\ 0 \end{pmatrix}\right]\!\!\right] \tilde{h}.$$

Due to $\dot{\boldsymbol{\gamma}}_s = 0$ in Ω_s, we have

$$\partial_y \hat{v}_s = 0, \qquad [\![\partial_y \hat{v}_f]\!] = 0 \quad \text{at } y = y_B$$

as well as the free-boundary conditions

$$[\![\partial_y \hat{u}_s]\!] = -[\![\partial_{yy} U_s]\!] \tilde{h} \qquad \text{at } y = y_B.$$

Using $\hat{v}_s = \hat{u}_s = \partial_y \hat{v}_s = 0$ the solid transport equations yields

$$\hat{\phi}_s = 0 \quad \text{at } y = y_B.$$

In summary, we have derived the required 13 conditions, i.e. the wall boundary conditions

$$\hat{v}_f = \hat{u}_s = \hat{v}_s = 0, \qquad \text{and} \qquad \Phi_f \partial_y \hat{v}_f + \Phi_s \partial_y \hat{v}_s = 0, \quad \text{at } y = 1/2,$$

the symmetry conditions

$$\partial_y \hat{v}_f = \partial_{yy} \hat{v}_f = 0 \quad \text{at } y = 0,$$

the yield-surface conditions

$$\begin{aligned} \hat{u}_s = \hat{v}_s &= 0, \\ [\![\hat{v}_f]\!] &= 0, \\ \partial_y \hat{v}_s = [\![\partial_y \hat{v}_f]\!] &= 0, \\ \hat{\phi}_s &= 0, \end{aligned}$$

at the plug-flow region boundary $y = y_B$ and the free-boundary condition

$$[\![\partial_y \hat{u}_s]\!] = -[\![\partial_{yy} U_s]\!] \tilde{h}, \qquad \text{at } y = y_B.$$

For the numerical investigations of the above model we combine our experience with the solution of the stability problem for the Couette flow problem as well as for the classic Bingham problem, and expand our finite-difference code to also deal with the singularity at the yield-surface in the two-phase Poiseuille flow. The employed scheme details are described in Section A.3. We note first, that the two-phase Poiseuille flow also shows a collision pressure induced ill-posedness as well as a convection induced instability.

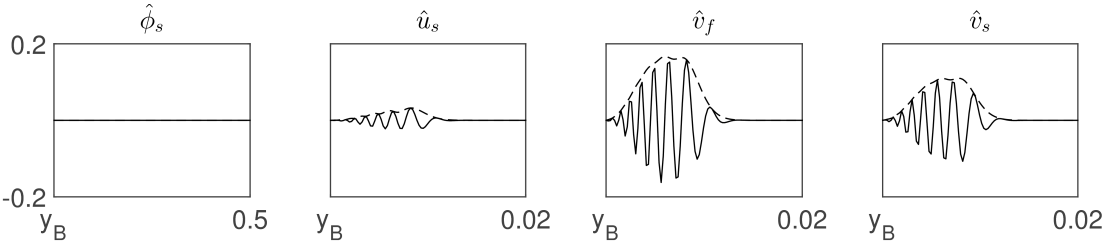

Figure 4.9: A collision pressure induced growth of a mode in the Poiseuille flow case with parameter values $\mathrm{Da} = 100, \mathrm{Re} = 1, \phi_{\mathrm{crit}} = 0.63, p_c = 1, p_1 = -10, \alpha = 1000, \mu_1 = \mu_2 = 0.1$. Shown are the real value (solid line) and the absolute value (dashed line) of the mode. Notice the lack of ϕ_s contributions, which shows a behavior similar to the Couette flow case. The spike next to the plug-flow region shows that the instability originates in the region of the highest particle concentration, as suggested by the analytic criterion (4.4.7).

Collision pressure induced ill-posedness

The collision pressure induced ill-posedness from Section 4.4 can be seen in numerical solutions starting at a ratio of $\phi_s\eta_s/\eta_n$ smaller $1/4$. This is in contrast to the Couette flow, where the ill-posedness is already seen for a ratio of $1/2$ in the simulations. This can be explained by looking at the analytic criterion (4.4.7), which shows that the ill-posedness occurs more likely in regions, where ϕ_s is close to maximum packing fraction. An unstable mode originates at the boundary of the plug-flow region, where the volume fraction is highest, but it is damped at the outer region, where the volume fraction is far from the maximum packing fraction. Figure 4.9 shows such a mode. Note the spike next to the plug-flow region, which shows that the growth is strongest there.

This suggest that the sufficient ratio between the viscosity of the solid phase and the collision pressure to suppress this ill-posedness depends on the base state. The employed normal mode approach yields stability criteria for the particular flow under consideration. A general stability criterion can only be derived by different techniques. The derivation of Chapter 5 shows this instability is linked with energy conservation and yields a ratio of greater 1 in order to guarantee stability, which is independent of a particular base state. In conclusion, a ratio greater 1 suppresses this instability for all flow cases, but for specific flows a smaller ratio can be sufficient.

Convection induced instability

Unless μ_1 is set too small, such that the collision pressure induced ill-posedness can be observed, unstable modes have real parts, which are of order one and have a similar signature as the convection induced unstable modes from Section 4.4. Figure 4.10 shows an exemplary unstable mode of that kind. Just as in the Couette flow case they appear in pairs and are strongest for the region between wall and plug-flow, where the velocities still change considerably, but ϕ_s is already near the maximum packing fraction. This is to be expected, since a high volume fraction and strong shearing are driving this instability.

We further note that large Reynolds and small Darcy numbers increase the convection induced instabilities, but seem not to introduce new instable modes for the Poiseuille flow case.

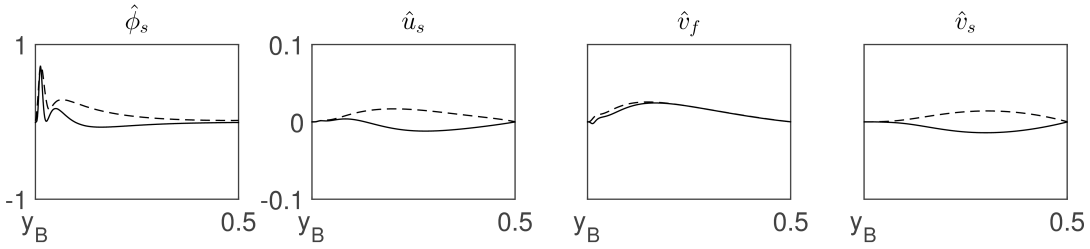

Figure 4.10: A convection induced growth mode or Poiseuille with parameter values as in Figure 4.9, except for $\mu_1 = \mu_2 = 1, \alpha = 10$. Shown are the real value (solid line) and the absolute value (dashed line) of the mode. In contrast to the collision pressure induced instability, $\tilde{\phi}_s$ exhibits the highest amplifications extending from the channel wall to the yield surface. To observe the small amplifications of the velocity modes we show only the region between [-0.1,0.1].

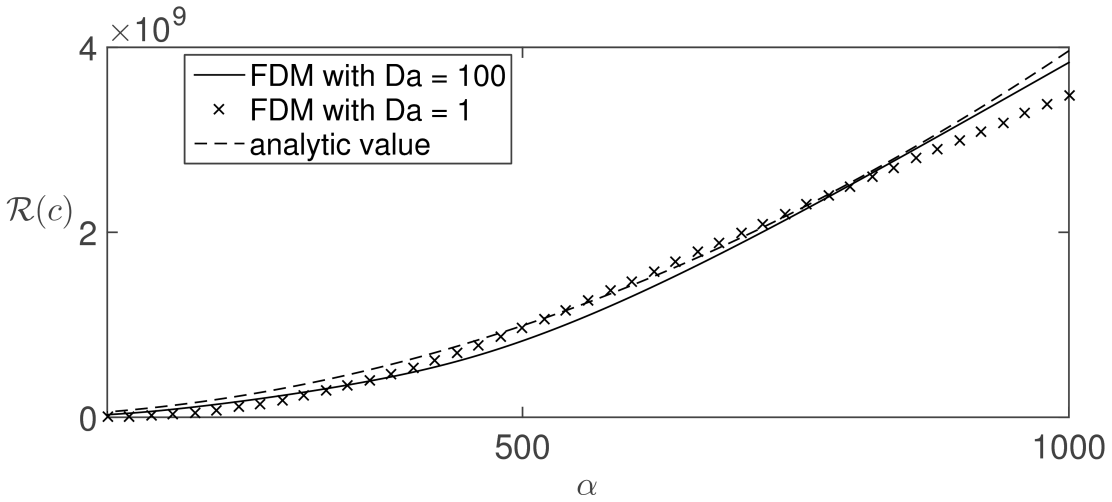

Figure 4.11: Shown is the dispersion relation of the collision pressure induced ill-posedness for the Poiseuille flow with parameters as in Figure 4.9. The analytic curve is computed by equation (4.4.6a) with $\Phi_s = 0.62$, which has been only derived for the plane Couette flow. Since numeric and analytic results match well, we believe this instability has the same origin as explained in the plane Couette flow case.

Comparison of single and multiphase stability

The single-phase Bingham flow and the multiphase model showed different stability behavior. As discussed in Section 4.2, the Bingham flow is unconditional linearly stable when used with the correct boundary conditions. For the multiphase model of Section 4.5 we found two instabilities: the collision pressure induced ill-posedness and the convection induced instability.

Nevertheless, the Bingham flow depends on only two parameters, i.e. the Reynolds number Re and the Bingham number B. The Reynolds number arises in both models, but the Bingham number is just contained in the single-phase model. As the Bingham number B has a direct influence on the size of the plug-region and the stress it plays a similar role as the solid viscosity η_s and maximum packing parameter ϕ_{crit} in the multiphase mode. Yet, it seems to miss the ability to model the competition relative to the collision pressure η_n.

Both multiphase model instabilities originate in mechanisms not contained in the single-phase model - the ill-posedness originates in the competition of the solid stress and solid pressure and the convection driven instability stems from the transport of particles due to convection. The Reynolds number does not play a significant role in either of the instabilities, which is similar to the single-phase model.

Chapter 5

Energy formulation

A derivation of the multiphase model using an average process has been shown in Chapter 2. The averaging process shows a connection between the interface resolving models and the Eulerian-Eulerian models. Thus, simulation results of an Eulerian-Eulerian model, can be physically interpreted and matched with experimental results. However, it does not guarantee a stable formulation nor are the necessary boundary conditions always apparent.

A different modeling ansatz is to formulate the problem based on energetic principles - specifically the second law of thermodynamics. There are two well-known energetic principles in the literature. Firstly, for dissipative systems one can use the gradient flow structure [101]; secondly, for inertia dominated systems one can use a Hamiltonian description [89]. Combinations of both are also possible, a popular example is the GENERIC framework [99].

The rest of this chapter is concerned with dissipative systems, i.e. gradient flow structures, as suspensions are generally highly viscous and typical velocities are small in our cases. This implies very small Reynolds numbers and dissipative effects are dominant.

5.1 Overview of dissipative formulations

Notation

First, let us introduce some notation that is needed in the course of this chapter. We refer to the space of all linear maps from a space X to Y as $L(X, Y)$.

The Fréchet derivative $F'(x) \in L(X, Y)$ of an operator $F : X \to Y$ is defined as

$$F(x + h) - F(x) = F'(x)[h] + o(\|h\|) \text{ for } h \to 0,$$

whenever this relation holds for at least one $x \in X$ for all h from a neighborhood of zero [136]. If a functional depends on multiple variables, we define the partial Fréchet derivative by

$$F(x_1, \ldots, x_{i-1}, x_i + h, x_{i+1}, \ldots, x_n) - F(x_1, \ldots, x_n) = F'(\boldsymbol{x})[h] + o(\|h\|)$$

for $h \to 0$ and denote it by $D_i F(x_1, x_2, \ldots, x_n)$.

The Gâteaux derivative $G'(x) \in L(X, Y)$ of an operator $G : X \to Y$ is defined as

$$G(x + tk) - G(x) = tG'(x)[k] + o(t) \text{ for } t \to 0,$$

for all k with $\|k\| = 1$ and all real numbers t in some neighborhood of zero [136].

The dual space X^* of a vector space X is defined as the set of all continuous linear functionals $f : X \to \mathbb{R}$ together with the norm

$$\|f\| := \sup_{\|x\| \leq 1} |f(x)|.$$

For $y \in X^*$ and $x \in X$, we define the pairing

$$(y, x)_{X^*,X} = y(x),$$

and in case the spaces are clear, we drop the index. For more details on the dual pairing see Section 6.4 and [136]. Occasionally, we refer to the subdifferential $D_s f$ at $x \in X$ of a functional $f : X \to \mathbb{R}$ that is defined as, cf. [109, 135, 138],

$$D_s f(x) := \{c \in X^* : f(y) - f(x) \geq (c, y - x) \quad \forall y \in X\}.$$

We denote the tangent space of X at $x \in X$ by $T_x X$, for a definition see e.g. [136].

Short introduction to gradient flow structures

A gradient flow is a triple $(H, \mathcal{D}, E)$, where H is the state space, $E : H \to \mathbb{R}$ an energetic functional and $\mathcal{D}$ is a dissipation mechanism that is any one of the four operators

$$\mathcal{D} \in \{G, K, \Psi, \Psi^*\}.$$

The operators differ in their respective domain and codomain, i.e.

$$\begin{aligned} G(h) &: T_h H \to T_h^* H, \\ K(h) &: T_h^* H \to T_h H, \\ \Psi(h, \cdot) &: T_h H \to \mathbb{R}, \\ \Psi^*(h, \cdot) &: T_h^* H \to \mathbb{R}. \end{aligned}$$

Thus, for a given energetic functional E, and depending on the dissipation mechanism in use, a gradient system has one of the respective forms

$$\partial_t h = -K(h)E'(h), \tag{5.1.1a}$$

$$G(h)\partial_t h = -E'(h), \tag{5.1.1b}$$

$$D_2\Psi(h, \partial_t h) = -E'(h), \tag{5.1.1c}$$

$$\partial_t h = D_2\Psi^*(h, -E'(h)),$$

where E' is the Frechet derivative of E and D_2 the Fréchet derivative with respect to the second variable. The operators G and K are believed to be non-negative and symmetric [87] and are

called the metric tensor and Onsager operator, respectively. Formulation (5.1.1a) and (5.1.1b) are equivalent, if G and K are invertible and we have $G = K^{-1}$. The connection between Ψ and G is given by the definition

$$\Psi(h, \partial_t h) = \frac{1}{2} (\partial_t h, G(h)\partial_t h)$$

and its dual to K through

$$\Psi^*(h, \tilde{h}) = \frac{1}{2} \left(\tilde{h}, K(h)\tilde{h}\right),$$

where $\tilde{h}$ is from the dual space H^* of H. Further, Ψ is the Legendre transformation of Ψ^* and vice versa, i.e.

$$\Psi^*(h, \tilde{h}) = \sup_{\partial_t h}[\tilde{h} \cdot \partial_t h - \Psi(h, \partial_t h)] \qquad \text{and} \qquad \Psi(h, \partial_t h) = \sup_{\tilde{h}}[\partial_t h \cdot \tilde{h} - \Psi^*(h, \tilde{h})].$$

The operators Ψ and Ψ^* are called dissipation potential and dual dissipation potential, respectively. As the names imply and the computation

$$\frac{\mathrm{d}}{\mathrm{d}t} E(h(t)) = E'(h)\partial_t h = -(\partial_t h, G(h)\partial_t h) = -2\Psi(h, \partial_t h)$$

shows, Ψ is half the dissipation of energy in time. Formulation (5.1.1c) can also be formulated as an optimization problem

$$\inf_{\boldsymbol{u}, \partial_t h} \{\Psi(h, \boldsymbol{u}) + E'(h)\partial_t h\}, \tag{5.1.2}$$

where we use a defined relation between the velocities u and $\partial_t h$

$$\partial_t h = P_h \boldsymbol{u}, \tag{5.1.3}$$

with P_h an operator mapping velocities to the tangents of the state space and (see [101])

$$\Psi(h, \boldsymbol{u}) := \inf_{\partial_t h}(\Psi(h, \partial_t h), \partial_t h = P_h \boldsymbol{u}).$$

A typical example is $P_h \boldsymbol{u} = -\nabla \cdot (\boldsymbol{u} h)$, such that (5.1.3) becomes the standard transport equation

$$\partial_t h + \nabla \cdot (\boldsymbol{u} h) = 0.$$

Using the operator P_h equation (5.1.2) can be reformulated as

$$\inf_{\boldsymbol{u}} \{\Psi(h, \boldsymbol{u}) + E'(h) P_h \boldsymbol{u}\}. \tag{5.1.4}$$

Another tool we use is the inclusion of constraints in the minimization of equation (5.1.4). Suppose $c : \mathbb{R}^2 \to \mathbb{R}$ and we like to enforce an algebraic constrain of the form $c(a, b) = 0$, then we define a functional

$$C(a, b, \lambda) = \int_{\Omega(T)} \lambda(\boldsymbol{x}) c(a(\boldsymbol{x}), b(\boldsymbol{x}))\, \mathrm{d}\boldsymbol{x},$$

where $\lambda : \mathbb{R}^n \to \mathbb{R}$ and solve instead of the minimization (5.1.4) the saddle point problem

$$\sup_{\lambda} \inf_{\boldsymbol{u}} \Psi(h, \boldsymbol{u}) + \langle E'(h), P_z \boldsymbol{u} \rangle + C(h, \boldsymbol{u}, \lambda),$$

which is the method of Lagrange multipliers for a constraint optimization problem, see e.g. [135].

From minimization to variational inequalities

It is well-known that for a real function the following is true:

Theorem 5.1. *Suppose f is convex, differentiable, and $\boldsymbol{x} \in \Omega \subset \mathbb{R}^n$ satisfies*

$$(\nabla f(\boldsymbol{x}), \boldsymbol{y} - \boldsymbol{x}) \geq 0 \qquad \forall \boldsymbol{y} \in \Omega$$

then we have

$$f(\boldsymbol{x}) = \min_{\boldsymbol{y} \in \Omega} f(\boldsymbol{y}).$$

Proof. See [69]. □

Additionally, the converse also holds true.

Theorem 5.2. *Suppose f is differentiable and there exists an $\boldsymbol{x} \in \Omega \subset \mathbb{R}^n$ such that*

$$f(\boldsymbol{x}) = \min_{\boldsymbol{y} \in \Omega} f(\boldsymbol{y}).$$

Then $\boldsymbol{x}$ is a solution of the variational inequality

$$(\nabla f(\boldsymbol{x}), \boldsymbol{y} - \boldsymbol{x}) \geq 0 \qquad \forall \boldsymbol{y} \in \Omega.$$

Proof. See [69]. □

The advantage of the inequality formulation is, that it naturally includes extrema at the domain's boundary. Interestingly, these principles for inequalities can be generalized to infinite dimensional spaces, where f becomes an operator on a Banach space, cf. [69, 112, 135] and Theorem 6.5.

Therefore, for differentiable Ψ the optimization problem (5.1.4) can be solved by differentiation as follows

$$D_2\Psi(h, \boldsymbol{u})(\boldsymbol{v} - \boldsymbol{u}) + E'(h)P_h(\boldsymbol{v} - \boldsymbol{u}) \geq 0 \qquad \forall \boldsymbol{v} \in T_h H.$$

and for the case that the extrema are not at a boundary of the domain, we have

$$D_2\Psi(h, \boldsymbol{u})\boldsymbol{v} + E'(h)P_h\boldsymbol{v} = 0 \qquad \forall \boldsymbol{v} \in T_h H. \tag{5.1.5}$$

However, often the dissipation potential Ψ consists of differentiable part J_1 and a non-differentiable part J_2, such that

$$\Psi = J_1 + J_2,$$

then it is not possible to define the differential of Ψ. Yet, for convex J_2, we can use the subdifferential $D_s J_2$, so that the optimization problem (5.1.4) becomes an inclusion, cf. [109, 135],

$$D_2 J_1(h, \boldsymbol{u}) + D_{s2} J_2(h, \boldsymbol{u}) \ni -E'(h)P_h.$$

or equivalent by testing with $\boldsymbol{v} - \boldsymbol{u}$ and using the definition of the subdifferential, it yields the variational inequality

$$D_2 J_1(h, \boldsymbol{u})[\boldsymbol{v} - \boldsymbol{u}] + J_2(h, \boldsymbol{v}) - J_2(h, \boldsymbol{u}) + E'(h) P_h[\boldsymbol{v} - \boldsymbol{u}] \geq 0 \qquad \forall \boldsymbol{v} \in T_h H. \tag{5.1.6}$$

This yields for a given state $h \in H$ a velocity $\boldsymbol{u} \in T_h H$, which can then be used via the process definition (5.1.3) to update the states. We come back to formulation (5.1.6) in case of single phase Bingham formulations, see Chapter 6. For multiphase models we stick with formulation (5.1.5) as our potentials are always assumed differentiable.

5.2 The normal velocity condition

Suppose we simulate a multiphase model in a domain with a free-boundary. Immediately, the question for correct boundary conditions on the free-boundary arises. The conditions must conserve momentum and mass of each phase. To solve this problem, we first derive a mass conserving condition, which is later used in the energetic framework and yields a suitable condition for momentum conservation.

In order to make the derivation of the mass conservation condition, we need the so-called general Reynolds transport theorem

$$\frac{\mathrm{d}}{\mathrm{d}t} \int_{\Omega(t)} f \, \mathrm{d}\boldsymbol{x} = \int_{\Omega(t)} \partial_t f \, \mathrm{d}\boldsymbol{x} + \oint_{\partial\Omega(t)} f \, \boldsymbol{u}_B \cdot \boldsymbol{n} \, \mathrm{d}\boldsymbol{s}, \tag{5.2.1}$$

where f is a time dependent scalar function defined on a domain $\Omega(t)$ with piecewise smooth boundary $\partial\Omega(t)$ and $\boldsymbol{u}_B$ is the velocity of the fluid at the control surface with respect to the coordinate reference frame [61].

Theorem 5.3. *Consider a domain $\Omega(t)$ with piece-wise smooth boundary $\partial\Omega(t)$. Let us assume convective transport of the solid and liquid volume fraction in domain $\Omega(t)$ as*

$$\begin{aligned} \partial_t \phi_s + \nabla \cdot (\phi_s \boldsymbol{u}_s) &= 0, \\ \partial_t \phi_f + \nabla \cdot (\phi_f \boldsymbol{u}_f) &= 0. \end{aligned}$$

Then, mass conservation demands

$$\boldsymbol{u}_f \cdot \boldsymbol{n} = \boldsymbol{u}_B \cdot \boldsymbol{n} = \boldsymbol{u}_s \cdot \boldsymbol{n} \qquad \text{on } \partial\Omega(t),$$

where $\boldsymbol{u}_B$ is the interface velocity.

Proof. A physically meaningful multiphase model should conserve mass unless chemical reaction take place between the phases. Consider the mass of liquid at time t in an arbitrary volume $\Omega(t)$ with smooth boundary $\partial\Omega(t)$. Conservation of liquid mass implies

$$\frac{\mathrm{d}}{\mathrm{d}t} \int_{\Omega(t)} \phi_f \, \mathrm{d}\boldsymbol{x}\mathrm{d}t = 0.$$

Using, the Reynolds transport theorem (5.2.1) and the divergence theorem, it yields

$$\begin{aligned} 0 = \frac{\mathrm{d}}{\mathrm{d}t}\int_{\Omega(t)} \phi_f \,\mathrm{d}\boldsymbol{x}\,\mathrm{d}t &= \int_{\Omega(t)} \frac{\partial \phi_f}{\partial t}\,\mathrm{d}\boldsymbol{x}\,\mathrm{d}t + \oint_{\partial\Omega(t)} \boldsymbol{u}_B \cdot \boldsymbol{n}\phi_f \,\mathrm{d}\boldsymbol{x}\,\mathrm{d}t \\ &= \int_{\Omega(t)} -\nabla\cdot(\phi_f \boldsymbol{u}_f)\,\mathrm{d}\boldsymbol{x}\,\mathrm{d}t + \oint_{\partial\Omega(t)} \phi_f \boldsymbol{u}_B\cdot\boldsymbol{n}\,\mathrm{d}\boldsymbol{x}\,\mathrm{d}t \\ &= \oint_{\partial\Omega(t)} \phi_f(-\boldsymbol{u}_f + \boldsymbol{u}_B)\cdot\boldsymbol{n}\,\mathrm{d}\boldsymbol{x}\,\mathrm{d}t. \end{aligned} \tag{5.2.2}$$

Since this should hold for arbitrary volumes and $\phi_f > 0$, equation (5.2.2) demands

$$(\boldsymbol{u}_f - \boldsymbol{u}_B)\cdot\boldsymbol{n} = 0 \qquad \text{on } \partial\Omega(t). \tag{5.2.3}$$

The same computation for the solid phase yields

$$0 = \frac{\mathrm{d}}{\mathrm{d}t}\int_{\Omega(t)} \phi_s \,\mathrm{d}\boldsymbol{x}\,\mathrm{d}t = \oint_{\partial\Omega(t)} \phi_s(-\boldsymbol{u}_s + \boldsymbol{u}_B)\cdot\boldsymbol{n}\,\mathrm{d}\boldsymbol{x}\,\mathrm{d}t,$$

such that

$$(\boldsymbol{u}_s - \boldsymbol{u}_B)\cdot\boldsymbol{n} = 0 \qquad \text{on } \partial\Omega(t) \tag{5.2.4}$$

holds. As this must be true for all control volume, the combination of (5.2.3) and (5.2.4) gives

$$\boldsymbol{u}_f\cdot\boldsymbol{n} = \boldsymbol{u}_B\cdot\boldsymbol{n} = \boldsymbol{u}_s\cdot\boldsymbol{n} \qquad \text{on } \partial\Omega(t).$$

□

Hence, in order to have volume preservation one needs to demand

$$\boldsymbol{n}\cdot(\boldsymbol{u}_s - \boldsymbol{u}_f) = 0,$$

which is an additional boundary condition, that needs to be enforced by our formulation. This boundary condition has been independently shown to hold in [22] using a different derivation.

5.3 Deriving a multiphase model using a gradient flow structure

Suppose we have a drop with a liquid-air interface $\Gamma_1(t)$ being on a substrate with solid-liquid boundary $\Gamma_2(t)$. In order to have mass conservation, we demand the condition $(\boldsymbol{u}_s - \boldsymbol{u}_f)\cdot\boldsymbol{n} = 0$ on the boundary strongly, that is we have the tangential space

$$U = \{(\boldsymbol{u}_s, \boldsymbol{u}_f, \partial_t\phi_s, \partial_t\phi_f) \;:\; (\boldsymbol{u}_s - \boldsymbol{u}_f)\cdot\boldsymbol{n} = 0 \text{ on } \Gamma_1, \quad \boldsymbol{u}_s = \boldsymbol{u}_f = \boldsymbol{0} \text{ on } \Gamma_2\}$$

with $\partial\Omega = \Gamma_1 \cup \Gamma_2$. The $\boldsymbol{u}_s, \boldsymbol{u}_f$ are velocities of the particles and liquid phase and $\partial_t\phi_s, \partial_t\phi_f$ are the partial time derivative of the respective phasic volume fractions. Further, we have the space for the Lagrangians

$$L = \{(p_s, p_f, p_v)\}$$

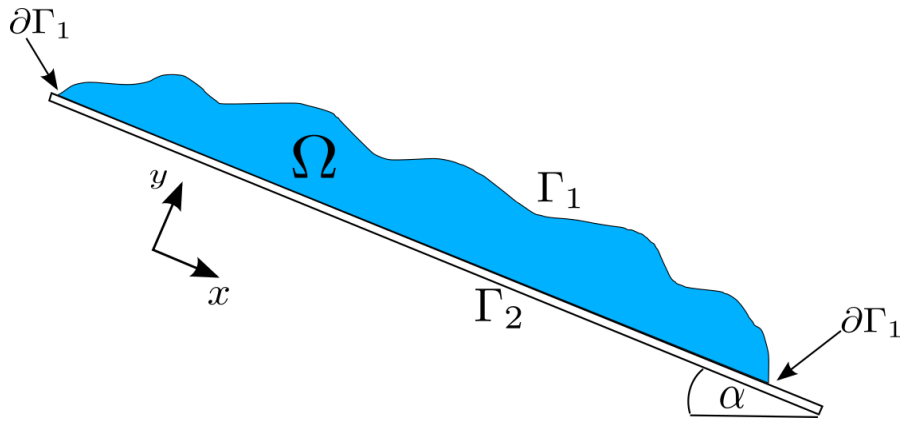

Figure 5.1: Domain for the energy derivation of the multiphase model.

with p_s, p_f the solid and liquid pressure, respectively. As we like the volume fraction to be transported using our velocities, we demand the process

$$\partial_t \boldsymbol{\phi} = P_z \boldsymbol{u} = \begin{pmatrix} -\nabla \cdot (\boldsymbol{u}_s \phi_s) \\ -\nabla \cdot (\boldsymbol{u}_f \phi_f) \end{pmatrix} \tag{5.3.1}$$

to hold.

In order to proceed we have to choose from one of the introduced gradient structures. We model the system in the form of equation (5.1.5). First, let us introduce the vectors

$$\boldsymbol{u} = \begin{pmatrix} \boldsymbol{u}_s \\ \boldsymbol{u}_f \end{pmatrix}, \quad \boldsymbol{\phi} = \begin{pmatrix} \phi_s \\ \phi_f \end{pmatrix}, \quad \boldsymbol{v} = \begin{pmatrix} \boldsymbol{u}_s \\ \boldsymbol{u}_f \end{pmatrix}, \quad \boldsymbol{\psi} = \begin{pmatrix} \psi_s \\ \psi_f \end{pmatrix}, \quad \boldsymbol{p} = \begin{pmatrix} p_f \\ p_s \\ p_v \end{pmatrix}, \quad \boldsymbol{q} = \begin{pmatrix} q_s \\ q_f \\ q_v \end{pmatrix}.$$

Then, the dissipation potential is chosen as

$$\begin{aligned} \Psi(\boldsymbol{\phi}, \boldsymbol{u}) = \frac{1}{2} \int_\Omega & \phi_s \mu_s (\nabla \boldsymbol{u}_s + \nabla \boldsymbol{u}_s{}^T) : (\nabla \boldsymbol{u}_s + \nabla \boldsymbol{u}_s{}^T) + \phi_f \mu_f (\nabla \boldsymbol{u}_f + \nabla \boldsymbol{u}_f{}^T) : (\nabla \boldsymbol{u}_f + \nabla \boldsymbol{u}_f{}^T) \\ & + \beta \phi_s \phi_f (\boldsymbol{u}_s - \boldsymbol{u}_f)^2 \, \mathrm{d}\boldsymbol{x}. \end{aligned}$$

The derivative of the dissipation is

$$\begin{aligned} D_2 \Psi(\boldsymbol{\phi}, \boldsymbol{u})[\boldsymbol{v}] = & \int_{\Omega(t)} -\nabla \cdot (\phi_s 2\mu_s (\nabla \boldsymbol{u}_s + \nabla \boldsymbol{u}_s{}^T)) \cdot \boldsymbol{v}_s + \beta \phi_s \phi_f (\boldsymbol{u}_s - \boldsymbol{u}_f) \boldsymbol{v}_s \, \mathrm{d}\boldsymbol{x} \\ & + \int_{\Omega(t)} -\nabla \cdot (\phi_f 2\mu_f (\nabla \boldsymbol{u}_f + \nabla \boldsymbol{u}_f{}^T)) \cdot \boldsymbol{v}_f - \beta \phi_s \phi_f (\boldsymbol{u}_s - \boldsymbol{u}_f) \boldsymbol{v}_f \, \mathrm{d}\boldsymbol{x} \\ & + \int_{\Gamma_1(t)} \boldsymbol{n} \cdot (\phi_s 2\mu_s (\nabla \boldsymbol{u}_s + \nabla \boldsymbol{u}_s{}^T)) \cdot \boldsymbol{v}_s \, \mathrm{d}\boldsymbol{s} \\ & + \int_{\Gamma_1(t)} \boldsymbol{n} \cdot (\phi_f 2\mu_f (\nabla \boldsymbol{u}_f + \nabla \boldsymbol{u}_f{}^T)) \cdot \boldsymbol{v}_f \, \mathrm{d}\boldsymbol{s} \\ & = \langle D_2 \Psi(\boldsymbol{\phi}, \boldsymbol{u}), \boldsymbol{v} \rangle \end{aligned}$$

Let us define $\boldsymbol{\tau}_s = 2\mu_s(\nabla \boldsymbol{u}_s + \nabla \boldsymbol{u}_s{}^T)$ and $\boldsymbol{\tau}_f = 2\mu_f(\nabla \boldsymbol{u}_f + \nabla \boldsymbol{u}_f{}^T)$. Now, we have to mind the fact, that we cannot independently vary the test functions $\boldsymbol{v}_s$ and $\boldsymbol{v}_f$ on the boundary anymore, so we rewrite the boundary integrals into normal (dependent) and tangential (independent) components. For easy of notation we concentrate on the two-dimensional case, where any vector $\boldsymbol{a}$ can be decomposed into normal and tangential components as

$$\boldsymbol{a} = (\boldsymbol{a} \cdot \boldsymbol{n})\boldsymbol{n} + (\boldsymbol{a} \cdot \boldsymbol{t})\boldsymbol{t}.$$

In higher dimensions, we have to use a tensorial ansatz of the form

$$\boldsymbol{a} = (\boldsymbol{n} \otimes \boldsymbol{n})\boldsymbol{a} + (\boldsymbol{I} - \boldsymbol{n} \otimes \boldsymbol{n})\boldsymbol{a}$$

instead. Thus, we write

$$\begin{aligned}\int_{\Gamma_1(t)} \boldsymbol{n}\phi_s\boldsymbol{\tau}_s \cdot \boldsymbol{v}_s + \boldsymbol{n}\phi_f\boldsymbol{\tau}_f \cdot \boldsymbol{v}_f \,\mathrm{d}\boldsymbol{s} &= \int_{\Gamma_1(t)} \boldsymbol{n}\phi_s\boldsymbol{\tau}_s \cdot ((\boldsymbol{v}_s \cdot \boldsymbol{n})\boldsymbol{n} + (\boldsymbol{v}_s \cdot \boldsymbol{t})\boldsymbol{t}) \\ &\quad + \boldsymbol{n}\phi_f\boldsymbol{\tau}_f \cdot ((\boldsymbol{v}_f \cdot \boldsymbol{n})\boldsymbol{n} + (\boldsymbol{v}_f \cdot \boldsymbol{t})\boldsymbol{t}) \,\mathrm{d}\boldsymbol{s} \\ &= \int_{\Gamma_1(t)} \boldsymbol{n}(\phi_s\boldsymbol{\tau}_s + \phi_f\boldsymbol{\tau}_f)\boldsymbol{n}\boldsymbol{v}_n \\ &\quad + \boldsymbol{n}\phi_s\boldsymbol{\tau}_s\boldsymbol{t}\boldsymbol{v}_{st} + \boldsymbol{n}\phi_f\boldsymbol{\tau}_f\boldsymbol{t}\boldsymbol{v}_{ft} \,\mathrm{d}\boldsymbol{s},\end{aligned}$$

with $\boldsymbol{v}_n = \boldsymbol{v}_s \cdot \boldsymbol{n} = \boldsymbol{v}_f \cdot \boldsymbol{n}$, $\boldsymbol{v}_{ft} = \boldsymbol{v}_f \cdot \boldsymbol{t}$ and $\boldsymbol{v}_{st} = \boldsymbol{v}_s \cdot \boldsymbol{t}$, which can be independently varied. The constraints are

$$C(\boldsymbol{\phi}, \boldsymbol{u}, \partial_t\boldsymbol{\phi}, \boldsymbol{p}) = \int_{\Omega(t)} p_v(\partial_t\phi_s + \partial_t\phi_f) + p_s(\partial_t\phi_s + \nabla \cdot (\phi_s\boldsymbol{u}_s)) + p_f(\partial_t\phi_f + \nabla \cdot (\phi_f\boldsymbol{u}_f)) \,\mathrm{d}\boldsymbol{x},$$

with derivative

$$\begin{aligned}D_{2\,3\,4}C(\boldsymbol{\phi}, \boldsymbol{u}, \partial_t\boldsymbol{\phi}, \boldsymbol{p})[\boldsymbol{v}, \partial_t\boldsymbol{\psi}, \boldsymbol{q}] &= \int_{\Omega(t)} q_v(\partial_t\phi_s + \partial_t\phi_f) + p_v(\partial_t\psi_s + \partial_t\psi_f) + p_s\partial_t\psi_s + p_f\partial_t\psi_f \\ &\quad + q_s(\partial_t\phi_s + \nabla \cdot (\phi_s\boldsymbol{u}_s)) + q_f(\partial_t\phi_s + \nabla \cdot (\phi_s\boldsymbol{u}_s)) \\ &\quad - \nabla p_s \cdot (\phi_s\boldsymbol{v}_s) - \nabla p_f \cdot (\phi_s\boldsymbol{v}_f) \,\mathrm{d}\boldsymbol{x} \\ &\quad + \int_{\Gamma_1(t)} \boldsymbol{v}_n(p_s\phi_s + p_f\phi_s) \,\mathrm{d}\boldsymbol{s} \\ &= \langle D_{2\,3\,4}C(\boldsymbol{\phi}, \boldsymbol{u}, \partial_t\boldsymbol{\phi}, \boldsymbol{p}), (\boldsymbol{v}, \partial_t\boldsymbol{\psi}, \boldsymbol{q})\rangle.\end{aligned}$$

We consider an energy functional E that includes gravitational, surface and collision forces and is defined as

$$E(\boldsymbol{\phi}) = \int_{\Omega(t)} g(y\cos\alpha - x\sin\alpha)(\rho_s\phi_s + \rho_f\phi_f) \,\mathrm{d}\boldsymbol{x} + \int_{\Gamma_1(t)} \sigma \,\mathrm{d}\boldsymbol{s} + \int_{\Omega(t)} \phi_s^2 \,\mathrm{d}\boldsymbol{x}. \tag{5.3.2}$$

In order to compute a suitable energy functional derivative, we use

$$\frac{\mathrm{d}E(\boldsymbol{\phi})}{\mathrm{d}t} = E'(\boldsymbol{\phi})\partial_t\boldsymbol{\phi} = E'(\boldsymbol{\phi})P_z\boldsymbol{u} \tag{5.3.3}$$

and then using our process definition (5.3.1) to yield the right hand side of (5.1.5).

The so-called first variation of area formula is, cf. [57, 79],

$$\frac{\mathrm{d}}{\mathrm{d}t}\int_{\Gamma(t)} 1\,\mathrm{d}\boldsymbol{s} = -(d-1)\int_{\Gamma(t)} \kappa \boldsymbol{v}_B\cdot\boldsymbol{n}_{\Gamma(t)}\,\mathrm{d}\boldsymbol{s} + \int_{\partial\Gamma(t)} \boldsymbol{v}_B\cdot\boldsymbol{n}_{\partial\Gamma(t)}\,\mathrm{d}l, \tag{5.3.4}$$

where $\boldsymbol{v}_B$ is the boundary velocity of the surface $\Gamma(t)\subset\mathbb{R}^{d-1}$ with boundary $\partial\Gamma(t)\subset\mathbb{R}^{d-2}$, κ is the mean curvature such that the unit hypersphere has $\kappa=1$ and $\boldsymbol{n}_D$ is a normal on D.

Thus, the time derivative of E, i.e. (5.3.3) of (5.3.2), can be computed via the Reynolds transport theorem (5.2.1) and the first variation of area (5.3.4) as

$$\begin{aligned}
\frac{\mathrm{d}E(\boldsymbol{\phi})}{\mathrm{d}t} &= \int_{\Omega(t)} g(y\cos\alpha - x\sin\alpha)(\rho_s\partial_t\phi_s + \rho_f\partial_t\phi_f)\,\mathrm{d}\boldsymbol{x}\\
&\quad + \int_{\Gamma_1(t)} (\boldsymbol{n}\cdot\boldsymbol{u}_B)[g(y\cos\alpha - x\sin\alpha)(\rho_s\phi_s+\rho_f\phi_f)]\,\mathrm{d}\boldsymbol{s}\\
&\quad - (d-1)\int_{\Gamma_1(t)} \sigma\kappa\boldsymbol{u}_B\cdot\boldsymbol{n}\,\mathrm{d}\boldsymbol{s} + \int_{\partial\Gamma_1(t)} \sigma\boldsymbol{u}_B\cdot\boldsymbol{n}\,\mathrm{d}l\\
&\quad + \int_{\Omega(t)} \phi_s\partial_t\phi_s\,\mathrm{d}\boldsymbol{x} + \int_{\Gamma_1(t)} (\boldsymbol{n}\cdot\boldsymbol{u}_B)\phi_s^2\,\mathrm{d}\boldsymbol{s}\\
&= \int_{\Omega(t)} -g(y\cos\alpha - x\sin\alpha)(\rho_s\nabla\cdot(\boldsymbol{u}_s\phi_s) + \rho_f\nabla\cdot(\boldsymbol{u}_f\phi_f))\,\mathrm{d}\boldsymbol{x}\\
&\quad + \int_{\Gamma_1(t)} (\boldsymbol{n}\cdot\boldsymbol{u}_B)[g(y\cos\alpha - x\sin\alpha)(\rho_s\phi_s+\rho_f\phi_f)]\,\mathrm{d}\boldsymbol{s}\\
&\quad - (d-1)\int_{\Gamma_1(t)} \sigma\kappa\boldsymbol{u}_B\cdot\boldsymbol{n}\,\mathrm{d}\boldsymbol{s} + \int_{\partial\Gamma_1(t)} \sigma\boldsymbol{u}_B\cdot\boldsymbol{n}\,\mathrm{d}l\\
&\quad + \int_{\Omega(t)} -\phi_s\nabla\cdot(\phi_s\boldsymbol{u}_s)\,\mathrm{d}\boldsymbol{x} + \int_{\Gamma_1(t)} (\boldsymbol{n}\cdot\boldsymbol{u}_B)\phi_s^2\,\mathrm{d}\boldsymbol{s}\\
&= \int_{\Omega(t)} \nabla(g(y\cos\alpha - x\sin\alpha)\rho_s)\cdot(\boldsymbol{u}_s\phi_s) + \nabla(g(y\cos\alpha - x\sin\alpha)\rho_f)\cdot(\boldsymbol{u}_f\phi_f)\,\mathrm{d}\boldsymbol{x}\\
&\quad + \int_{\Gamma_1(t)} \boldsymbol{n}\cdot(\boldsymbol{u}_B-\boldsymbol{u}_s)[g(y\cos\alpha - x\sin\alpha)\rho_s\phi_s]\\
&\qquad\quad + \boldsymbol{n}\cdot(\boldsymbol{u}_B-\boldsymbol{u}_f)[g(y\cos\alpha - x\sin\alpha)\rho_f\phi_f]\,\mathrm{d}\boldsymbol{s}\\
&\quad - (d-1)\int_{\Gamma_1(t)} \sigma\kappa\boldsymbol{u}_B\cdot\boldsymbol{n}\,\mathrm{d}\boldsymbol{s} + \int_{\Gamma_1(t)} \sigma\boldsymbol{u}_B\cdot\boldsymbol{n}\,\mathrm{d}l\\
&\quad + \int_{\Omega(t)} (\nabla\phi_s)\cdot(\phi_s\boldsymbol{u}_s)\,\mathrm{d}\boldsymbol{x} + \int_{\Gamma_1(t)} \boldsymbol{n}\cdot(\boldsymbol{u}_B-\boldsymbol{u}_s)\phi_s^2\,\mathrm{d}\boldsymbol{s}\\
&= \langle E'(\boldsymbol{\phi}), P_z\boldsymbol{u}\rangle,
\end{aligned}$$

where d is the dimension of Ω and κ is the curvature of the interface. Theorem 5.3 shows an

acceptable choice for the boundary velocity is $\boldsymbol{n} \cdot \boldsymbol{u}_B = \boldsymbol{n} \cdot \boldsymbol{u}_s = \boldsymbol{n} \cdot \boldsymbol{u}_f$, so we get

$$\begin{aligned}\langle E'(\boldsymbol{\phi}), P_z \boldsymbol{v} \rangle = &\int_\Omega \nabla(g(y\cos\alpha - x\sin\alpha)\rho_s) \cdot (\phi_s \boldsymbol{v}_s) + \nabla(g(y\cos\alpha - x\sin\alpha)\rho_f) \cdot (\phi_f \boldsymbol{v}_f)\,\mathrm{d}\boldsymbol{x} \\ &- (d-1)\int_{\Gamma_1(t)} \sigma\kappa v_n \,\mathrm{d}\boldsymbol{s} + \int_{\partial\Gamma_1(t)} \sigma v_n \,\mathrm{d}l + \int_{\Omega(t)} (\nabla\phi_s) \cdot (\phi_s \boldsymbol{v}_s)\,\mathrm{d}\boldsymbol{x}.\end{aligned}$$

Variational formulation

We like to find a solution of the saddle-point problem

$$\sup_{\boldsymbol{p}\in L} \inf_{(\boldsymbol{u},\partial_t\boldsymbol{\phi})\in U} \Psi(\boldsymbol{\phi}, \boldsymbol{u}) + \langle E'(\boldsymbol{\phi}), P_z \boldsymbol{u}\rangle + C(\boldsymbol{\phi}, \boldsymbol{u}, \partial_t\boldsymbol{\phi}, \boldsymbol{p}).$$

We assume the potentials and functions to be smooth enough. Therefore, this is equivalent to find $(\boldsymbol{u}, \partial_t\boldsymbol{\phi}, \boldsymbol{p}) \in U \times L$, so that

$$\langle D_2\Psi(\boldsymbol{\phi}, \boldsymbol{u}), \boldsymbol{v}\rangle + \langle E'(\boldsymbol{\phi}), P_z\boldsymbol{v}\rangle + \langle D_{2\,3\,4} C(\boldsymbol{\phi}, \boldsymbol{u}, \partial_t\boldsymbol{\phi}, \boldsymbol{p}), (\boldsymbol{v}, \partial_t\boldsymbol{\psi}, \boldsymbol{q})\rangle = 0, \tag{5.3.5}$$

for all $(\boldsymbol{v}, \partial_t\boldsymbol{\psi}, \boldsymbol{q}) \in U \times L$.

Resulting system

Identification of the strong form via variation of the test functions in (5.3.5) yields the partial differential equations

$$\begin{aligned}-\nabla\cdot(\phi_s 2\mu_s(\nabla\boldsymbol{u}_s + \nabla\boldsymbol{u}_s{}^T)) + \beta\phi_s\phi_f(\boldsymbol{u}_s - \boldsymbol{u}_f) - \phi_s\nabla p_s + \phi_s\nabla\phi_s \qquad &\text{(5.3.6a)}\\ = -\nabla(g(y\cos\alpha - x\sin\alpha)\rho_s)\phi_s,\\ -\nabla\cdot(\phi_f 2\mu_f(\nabla\boldsymbol{u}_f + \nabla\boldsymbol{u}_f{}^T)) - \beta\phi_s\phi_f(\boldsymbol{u}_s - \boldsymbol{u}_f) - \phi_f\nabla p_f \qquad &\text{(5.3.6b)}\\ = -\nabla(g(y\cos\alpha - x\sin\alpha)\rho_f)\phi_f,\\ \partial_t\phi_s + \partial_t\phi_f = 0, \qquad &\text{(5.3.6c)}\\ \partial_t\phi_s + \nabla\cdot(\boldsymbol{u}_s\phi_s) = 0, \qquad &\text{(5.3.6d)}\\ \partial_t\phi_f + \nabla\cdot(\boldsymbol{u}_f\phi_f) = 0, \qquad &\text{(5.3.6e)}\\ p_v + p_s = 0, \qquad &\text{(5.3.6f)}\\ p_v + p_f = 0, \qquad &\text{(5.3.6g)}\end{aligned}$$

in $\Omega(t)$ and on the free-boundary $\Gamma_1(t)$ the boundary conditions

$$\begin{aligned}\boldsymbol{n}(\phi_s\boldsymbol{\tau}_s + \phi_f\boldsymbol{\tau}_f)\boldsymbol{n} + (\phi_s p_s + \phi_f p_f) = (d-1)\sigma\kappa, \qquad &\text{(5.3.6h)}\\ \boldsymbol{n}\phi_s\boldsymbol{\tau}_s\boldsymbol{t} = 0, \qquad &\text{(5.3.6i)}\\ \boldsymbol{n}\phi_f\boldsymbol{\tau}_f\boldsymbol{t} = 0, \qquad &\text{(5.3.6j)}\\ \boldsymbol{n}\cdot(\boldsymbol{u}_s - \boldsymbol{u}_f) = 0, \qquad &\text{(5.3.6k)}\end{aligned}$$

at the triple points $\partial\Gamma_1(t)$, we have

$$\sigma = 0, \tag{5.3.6l}$$

and on the substrate boundary $\Gamma_2(t)$ the no-slip condition

$$\boldsymbol{u}_s = \boldsymbol{u}_f = \boldsymbol{0}. \tag{5.3.6m}$$

Removal of excess pressures

System (5.3.6) can be further reduced by usage of equations (5.3.6f) and (5.3.6g) to remove the solid pressure p_s and the mass conservation pressure p_v yielding the final system

$$\begin{aligned} -\nabla\cdot(\phi_s 2\mu_s(\nabla \boldsymbol{u}_s + \nabla \boldsymbol{u}_s{}^T)) + \beta\phi_s\phi_f(\boldsymbol{u}_s - \boldsymbol{u}_f) - \phi_s\nabla p_f + \phi_s\nabla\phi_s \qquad &(5.3.7a)\\ = -\nabla(g(y\cos\alpha - x\sin\alpha)\rho_s)\phi_s, \\ -\nabla\cdot(\phi_f 2\mu_f(\nabla \boldsymbol{u}_f + \nabla \boldsymbol{u}_f{}^T)) - \beta\phi_s\phi_f(\boldsymbol{u}_s - \boldsymbol{u}_f) - \phi_f\nabla p_f \qquad &(5.3.7b)\\ = -\nabla(g(y\cos\alpha - x\sin\alpha)\rho_f)\phi_f, \\ \partial_t\phi_s + \partial_t\phi_f = 0, \qquad &(5.3.7c)\\ \partial_t\phi_s + \nabla\cdot(\phi_s\boldsymbol{u}_s) = 0, \qquad &(5.3.7d)\\ \partial_t\phi_f + \nabla\cdot(\phi_f\boldsymbol{u}_f) = 0, \qquad &(5.3.7e) \end{aligned}$$

in $\Omega(t)$ together with the boundary conditions from (5.3.6).

5.4 Derivation of p_c term in energy formulation

The energy functional definition (5.3.2) contains the term

$$\int_{\Omega(t)} \phi_s^2 \,\mathrm{d}\boldsymbol{x}, \tag{5.4.1}$$

which is referred to as granular stress term, modulus of elasticity or collision pressure in the literature [49, 118] and yields the final term

$$\phi_s\nabla\phi_s$$

in the solid momentum equation (5.3.7a). Without such a term uniqueness of solutions is lost, which is easiest seen for flow cases like the shear-flow, where the two phases decouple and one has an additional grade of freedom left in the distribution of the volume fraction, cf. [32]. The collision pressure is also directly connected to the well-posedness of the system as has been discussed in Section 2.2.

This choice of the collision pressure is not unique and (5.4.1) is only the simplest choice. In Section 2.3 we propose the collision pressure term

$$\nabla p_c = \nabla(\eta_n|\dot{\boldsymbol{\gamma}}_s|) \tag{5.4.2}$$

in the solid momentum equation, where the solid shear rate and its norm is defined as

$$\begin{aligned} \dot{\boldsymbol{\gamma}}_s &= \nabla \boldsymbol{u}_s + \nabla \boldsymbol{u}_s{}^T, &(5.4.3a)\\ |\dot{\boldsymbol{\gamma}}_s| &= \sqrt{2(\partial_x u_s)^2 + (\partial_y u_s + \partial_x v_s)^2 + 2(\partial_y v_s)^2}. &(5.4.3b) \end{aligned}$$

As the collision pressure definition (5.4.2) is motivated by physical experiments, it would be nice to find an energetic generator term for this kind of collision pressure.

We have three locations, where we can add a term - the energy functional E, the Lagrangian C and the dissipation potential Ψ. We do not discuss combinations of those, as we hope to identify a single energetic cause.

As the energy must not depend on the velocity it is immediately clear that it cannot model a term of the form (5.4.2). A velocity can only enter through the change of the process definition P_z, which by (5.3.3) contributes only a linear term, hence is unable to create this nonlinear velocity structure. Another way is to model this term through an additional condition that is enforced in the Lagrangian C. It is unclear what this additional condition should be, therefore we decide to model the collision pressure using the dissipation potential Ψ instead. Nevertheless, note that the two-pressure models demand an additional condition in order to introduce a second pressure in the model [77], which would naturally lead to a modification of our Lagrangian C, here.

The previous discussion shows that we expect the collision pressure to be part of the dissipation potential. In essence this leads us to the question for the existence of a potential that generates a term of the form $\nabla\eta_n|\dot{\boldsymbol{\gamma}}_s|$ in the solid momentum equation. To answer this question, we state some facts from functional analysis.

Let X be a Banach space. We call an operator $A : X \to X^*$ a *potential operator*, iff there exists a Gâteaux differentiable functional $f : X \to \mathbb{R}$, such that $A = f'$ [135].

An operator $A : X \to X^*$ is called hemicontinuous, iff the map $\tilde{A} : \mathbb{R} \to \mathbb{R}$ defined as

$$\tilde{A}(t) = (A(u + tv), w)_{X^*,X}$$

is continuous for all $u, v, w \in X$, cf. [109].

A functional $F_A : X \to \mathbb{R}$ is called pseudopotential of A, iff [135]

$$F_A(u) = \int_0^1 (A(\xi u), u)_{X^*,X} \, \mathrm{d}\xi.$$

Proposition 5.4. *Suppose $A : X \to X^*$ is a hemicontinuous operator on the Banach space X. A is a potential operator if and only if*

$$F_A(u) - F_A(v) = \int_0^1 (A(v + \xi(u - v)), u - v)_{X^*,X} \, \mathrm{d}\xi \qquad \forall u, v \in X$$

holds. Then, the pseudopotential F_A is a potential, and an arbitrary potential for A differs from F_A only by a constant.

Proof. This proposition is part of Proposition 41.5 in Zeidler's third volume [135]. □

Proposition 5.4 is just an integral formula for the determination of the potential. In essence, we like to know, whether the operator $A_{\phi_s} : X \to X^*$ defined as

$$(A_{\phi_s}(\boldsymbol{u}_s), \boldsymbol{v}_s)_{X^*,X} = -\int_{\Omega(t)} (\eta_n(\phi_s)|\dot{\boldsymbol{\gamma}}_s|)\nabla \cdot \boldsymbol{v}_s \, \mathrm{d}\boldsymbol{x} \qquad \forall\, \boldsymbol{u}_s, \boldsymbol{v}_s \in X, \tag{5.4.4}$$

is a potential operator. Unfortunately, the correct space X is not known for our problem. However, we assume X to be a Banach space of the velocities such that all terms exist, are measurable and the operator A_{ϕ_s} is hemicontinuous. For example a valid choice for stationary problems is $X = (H^1(\Omega))^n$.

Theorem 5.5. *Let us assume there are $\boldsymbol{u}_s, \boldsymbol{v}_s \in X$, such that*

$$\nabla \cdot \boldsymbol{u}_s = 0, \qquad |\dot{\boldsymbol{\gamma}}_s| > 0, \qquad \nabla \cdot \boldsymbol{v}_s \neq 0.$$

Further assume $\eta_n(\phi_s) > 0$. Then, A_{ϕ_s} is not a potential operator.

Proof. First, let us derive the pseudopotential of A_{ϕ_s} by usage of Fubini's theorem, i.e.

$$\begin{aligned}
F_{A_{\phi_s}}(\boldsymbol{u}_s) &= -\int_0^1 \int_{\Omega(t)} (\eta_n(\phi_s)\sqrt{2(\xi\partial_x u_s)^2 + (\xi\partial_y u_s + \xi\partial_x v_s)^2 + 2(\xi\partial_y v_s)^2})\nabla \cdot \boldsymbol{u}_s \,\mathrm{d}\boldsymbol{x}\,\mathrm{d}\xi \\
&= -\int_0^1 \int_{\Omega(t)} (\eta_n(\phi_s)|\xi|\sqrt{2(\partial_x u_s)^2 + (\partial_y u_s + \partial_x v_s)^2 + 2(\partial_y v_s)^2})\nabla \cdot \boldsymbol{u}_s \,\mathrm{d}\boldsymbol{x}\,\mathrm{d}\xi \\
&= -\int_{\Omega(t)} \int_0^1 |\xi| \,\mathrm{d}\xi(\eta_n(\phi_s)|\dot{\boldsymbol{\gamma}}_s|)\nabla \cdot \boldsymbol{u}_s \,\mathrm{d}\boldsymbol{x} \\
&= -\frac{1}{2}\int_{\Omega(t)} (\eta_n(\phi_s)|\dot{\boldsymbol{\gamma}}_s|)\nabla \cdot \boldsymbol{u}_s \,\mathrm{d}\boldsymbol{x}.
\end{aligned}$$

However, a formal computation shows

$$(F'_{A_{\phi_s}}(\boldsymbol{u}_s), \boldsymbol{v}_s) = -\frac{1}{2}\int_\Omega \eta_n(\phi_s)|\dot{\boldsymbol{\gamma}}_s|(\nabla \cdot \boldsymbol{v}_s) + \eta_n(\phi_s)\frac{\dot{\boldsymbol{\gamma}}_s : \nabla \boldsymbol{v}_s}{|\dot{\boldsymbol{\gamma}}_s|}(\nabla \cdot \boldsymbol{u}_s)\,\mathrm{d}\boldsymbol{x}$$

and choosing $\boldsymbol{u}_s$ such that $\nabla \cdot \boldsymbol{u}_s = 0$, but $|\dot{\boldsymbol{\gamma}}_s| > 0$ yields

$$(F'_{A_{\phi_s}}(\boldsymbol{u}_s), \boldsymbol{v}_s) = -\frac{1}{2}\int_{\Omega(t)} (\eta_n(\phi_s)|\dot{\boldsymbol{\gamma}}_s|)\nabla \cdot \boldsymbol{v}_s \,\mathrm{d}\boldsymbol{x}.$$

Comparison with (5.4.4) shows that both forms differ by a factor of one half. Thus, this can only be identical if both sides are zero, which they are clearly not for the valid choices $\nabla \cdot \boldsymbol{v}_s \neq 0$ and $\eta_n > 0$. Therefore, by Proposition 5.4 the operator A_{ϕ_s} defined by (5.4.4) is not a potential operator. □

Theorem 5.5 tells us, we should rather look for a potential, so that

$$D_2\Phi(\boldsymbol{\phi}, \boldsymbol{u})[\boldsymbol{v}] = (A_{\phi_s}(\boldsymbol{u}_s), \boldsymbol{v}_s)_{X^*,X} + (r_{\phi_s}(\boldsymbol{u}_s), \boldsymbol{v}_s)_{X^*,X},$$

with r_{ϕ_s} some rest. Unfortunately, this would imply every potential Φ can be chosen, because we can always choose

$$r_{\phi_s} = D_2\Phi(\boldsymbol{\phi}, \boldsymbol{u})[\boldsymbol{v}] + \int_{\Omega(t)} (\eta_n|\dot{\boldsymbol{\gamma}}_s|)\nabla \cdot \boldsymbol{v}_s \,\mathrm{d}\boldsymbol{x}.$$

However, we would like to regain $r_{\phi_s} = 0$ for the particular cases of the plane Couette and plane Poiseuille flow, because this would show that our original formulation adheres to the second law of thermodynamics and an energetic principle in those cases.

A particular choice for the potential

The pseudopotential $F_{A_{\phi_s}}$ suggests considering a potential term of the form

$$\Phi(\boldsymbol{\phi}, \boldsymbol{u}) = -\int_\Omega \eta_n(\phi_s)|\dot{\boldsymbol{\gamma}}_s|(\nabla \cdot \boldsymbol{u}_s)\,\mathrm{d}\boldsymbol{x}, \tag{5.4.5}$$

with the first variation

$$\begin{aligned} D_2\Phi(\boldsymbol{\phi}, \boldsymbol{u})[\boldsymbol{v}] &= -\int_\Omega \eta_n(\phi_s)|\dot{\boldsymbol{\gamma}}_s|(\nabla \cdot \boldsymbol{v}_s) + \eta_n(\phi_s)\frac{\dot{\boldsymbol{\gamma}}_s : \nabla \boldsymbol{v}_s}{|\dot{\boldsymbol{\gamma}}_s|}(\nabla \cdot \boldsymbol{u}_s)\,\mathrm{d}\boldsymbol{x} \\ &= \int_\Omega \left(\nabla(\eta_n(\phi_s)|\dot{\boldsymbol{\gamma}}_s|) + \nabla \cdot \left(\eta_n(\phi_s)\frac{\dot{\boldsymbol{\gamma}}_s}{|\dot{\boldsymbol{\gamma}}_s|}(\nabla \cdot \boldsymbol{u}_s)\right)\right) \cdot \boldsymbol{v}_s\,\mathrm{d}\boldsymbol{x} \\ &\quad - \oint_\Gamma \eta_n(\phi_s)|\dot{\boldsymbol{\gamma}}_s|\boldsymbol{v}_s \cdot \boldsymbol{n} + \boldsymbol{n} \cdot \eta_n(\phi_s)\frac{\dot{\boldsymbol{\gamma}}_s}{|\dot{\boldsymbol{\gamma}}_s|}(\nabla \cdot \boldsymbol{u}_s) \cdot \boldsymbol{v}_s\,\mathrm{d}\boldsymbol{s} \end{aligned}$$

Thus, we have a term of the form (5.4.2) and the additional term

$$\boldsymbol{r} = \nabla \cdot \left(\eta_n(\phi_s)\frac{\dot{\boldsymbol{\gamma}}_s}{|\dot{\boldsymbol{\gamma}}_s|}(\nabla \cdot \boldsymbol{u}_s)\right),$$

which becomes zero for $\nabla \cdot \boldsymbol{u}_s = 0$. Thus, this is a good choice, since we showed the plane Couette and plane Poiseuille flow demand a phase-wise incompressibility in Chapter 3.

Positivity of the dissipation including a p_c term

In Section 5.1 we defined G to be a positive and symmetric operator, which implies that Ψ is positive. Yet, the dissipation potential (5.4.5) might become negative, so we have to show that

$$\Psi(\boldsymbol{\phi}, \boldsymbol{u}) = \int_{\Omega(t)} \frac{1}{2}\phi_s\mu_s\dot{\gamma}_s^2 + \frac{1}{2}\phi_f\mu_f\dot{\gamma}_f^2 + \beta\phi_s\phi_f(\boldsymbol{u}_s - \boldsymbol{u}_f)^2 - \eta_n(\phi_s)|\dot{\boldsymbol{\gamma}}_s|(\nabla \cdot \boldsymbol{u}_s)\,\mathrm{d}\boldsymbol{x} \tag{5.4.6}$$

is always non-negative. Let us define the so-called friction coefficient, cf. [15, 75],

$$\mu_{fr} = \frac{\phi_s\mu_s}{\eta_n}.$$

Theorem 5.6. *Let β, μ_f, μ_s and η_n be non-negative functions and $\phi_s, \phi_f \in [0, 1]$. Then, the dissipation (5.4.6) is non-negative for $\mu_{fr} \geq 1$.*

Proof. Without limit of generality consider the case $\mu_f = \beta = 0$, since these terms are always positive. Otherwise, an even smaller value of μ_{fr} is sufficient. Thus, we need to find a $\mu_{fr} > 0$, so that

$$\frac{\mu_{fr}}{2}\dot{\gamma}_s^2 - |\dot{\boldsymbol{\gamma}}_s|(\nabla \cdot \boldsymbol{u}_s) \geq 0$$

holds. Definition (5.4.3) shows this can be rearranged as

$$|\dot{\boldsymbol{\gamma}}_s|\left(\mu_{fr}|\dot{\boldsymbol{\gamma}}_s| - \nabla \cdot \boldsymbol{u}_s\right) \geq 0.$$

The worst case is for $\partial_y u_s + \partial_x v_s = 0$, so we need to check

$$\mu_{fr}\sqrt{2(\partial_x u_s)^2 + 2(\partial_y v_s)^2} - \partial_x u_s - \partial_y v_s \geq 0,$$

with its worst case being

$$\mu_{fr}\sqrt{2(\partial_x u_s)^2 + 2(\partial_y v_s)^2} - |\partial_x u_s| - |\partial_y v_s| \geq 0.$$

Defining

$$\boldsymbol{a} := \begin{pmatrix} \partial_x u_s \\ \partial_y v_s \end{pmatrix},$$

this is equivalent to

$$\mu_{fr}\sqrt{2}\|\boldsymbol{a}\|_2 - \|\boldsymbol{a}\|_1 \geq 0.$$

Basic linear algebra tells us this is fulfilled for $\mu_{fr} \geq 1$. □

The stability analysis in Chapter 4 yielded the criterion $\mu_1 > 1/2$ for the plane Couette flow and about $\mu_1 > 1/4$ for the plane Poiseuille flow. The constitutive laws of Chapter 4 give

$$\mu_{fr} \approx \mu_1.$$

This implies a necessary friction coefficient of $\mu_{fr} > 1/2$ and $\mu_{fr} > 1/4$ for plane Poiseuille and plane Couette flow, respectively. The non-negativity criterion of Theorem 5.6 is independent of a particular flow. Hence, the criterion $\mu_{fr} \geq 1$ is a generalization of the stability analysis from Chapter 4 to general flows and a value of $\mu_{fr} \geq 1$ - equivalently $\mu_1 \geq 1$ for the constitutive laws of Chapter 4 - is a necessary criterion for the stability in general flow situations. Nevertheless, particular flow situations - like the plane Poiseuille flow - might be stable for friction coefficients smaller one as shown in Chapter 4.

Chapter 6

Viscoplastic thin-film equation

As the multiphase model consists of two Navier-Stokes equations that are coupled in a highly nonlinear fashion twofold - directly through the momentum coupling term and indirectly through the volume fraction - we do not try to analyze the full system for existence and uniqueness of solutions.

A possible different approach is to look for simpler models that show similar behavior and analyze them instead. Section 7.2 shows that the assumption of a constant collision pressure

$$p_c = \eta_n(\phi_s)|\dot{\gamma}_s| = \text{const.}$$

leads to a reduction of the multiphase model into a thin-film model with yield-stress property, which has been first proposed by Balmforth et al. [9]. Therefore, we gain some insight into our multiphase model with yield-stress property by analyzing this much simpler model. A particular difficulty in the analysis of these simpler models is that their equations are of the form

$$\partial_t h + \partial_x(F(h, \dots, \partial_x^n h)) = 0$$

with $n \in \{2, 4\}$ and F is nonlinear in the highest order term $\partial_x^n h$. This renders existence proofs that depend heavily on compact embeddings or maximum principles futile, cf. [13, 39, 62]. Thus, we used a theorem based on the monotonicity of the differential operator due to Roubicek [109]. A short introduction into the background of monotonicity methods is also provided.

Our plan is the following: First, we give an alternative derivation of the Balmforth equation using a variational inequality ansatz, then we prove existence of solutions for a regularized second order equation. The occurring equation is quasilinear and, due to the yield-stress property, contains non-differential terms. This directly hints to problems hidden in the multiphase model with viscoplastic properties, which we expect to contain similar difficulties.

6.1 Governing equations

Usually, thin-film equations are derived starting from the partial differential Navier-Stokes equations with appropriate free-boundary conditions and reducing them using asymptotic techniques. This approach is viable whenever the partial differential equations are well-posed. Yet, it is known that for viscoplastic fluids with Bingham stress a non-uniqueness of the stress in unyielded domains exists [34, 47] and it is not clear whether the Navier-Stokes equation make any sense for these fluids [34]. Since we are interested in thin-film equations we neglect the inertial terms and concentrate on the appropriate Stokes equations, here. Nevertheless, we like to point out that inclusion of inertial terms in the variational inequality formulation is not a problem, see e.g. [34] for a possible approach.

For completeness sake, we first give the Stokes equations with appropriate boundary conditions and, afterwards, state a variational inequality that for smooth enough regions reduces to the same equations, but is also directly applicable in the unyielded regions, where the Stokes equations lose their well-posedness.

Assume a domain $\Omega(t) = \{(x, y) \in [0, L] \times \mathbb{R} : 0 \leq y \leq h(t, x)\}$, where h describes the free-boundary $\Gamma(t) = \{(x, y) \in [0, L] \times \mathbb{R} : y = h(t, x)\}$ with periodicity $L > 0$. The periodicity condition can also be substituted by a finite domain, where $h(t, 0) = h(t, L) = 0$. We use the shear-rate tensor

$$D(\boldsymbol{a}) := \nabla \boldsymbol{a} + (\nabla \boldsymbol{a})^T.$$

The Stokes equations with Bingham stress are defined as

$$\nabla \cdot \boldsymbol{u} = 0 \qquad \text{in } \Omega(t), \tag{6.1.1a}$$

$$\nabla \cdot \boldsymbol{\tau} - \nabla p = 0 \qquad \text{in } \Omega(t), \tag{6.1.1b}$$

with shear-rate norm

$$|D(\boldsymbol{u})| = \sqrt{\frac{1}{2} D(\boldsymbol{u}) : D(\boldsymbol{u})}, \tag{6.1.1c}$$

the stress relation

$$\boldsymbol{\tau} = \left(\frac{b}{|D(\boldsymbol{u})|} + \mu \right) D(\boldsymbol{u}) \qquad \text{for } |\boldsymbol{\tau}| \geq b, \tag{6.1.1d}$$

$$|D(\boldsymbol{u})| = 0 \qquad \text{for } |\boldsymbol{\tau}| < b, \tag{6.1.1e}$$

and no-slip and stress boundary conditions

$$\boldsymbol{u} = \boldsymbol{0} \qquad \text{at } y = 0, \tag{6.1.1f}$$

$$(\boldsymbol{\tau} - p\boldsymbol{I}) \cdot \boldsymbol{n} = \sigma \kappa \cdot \boldsymbol{n} \qquad \text{at } y = h(t, x). \tag{6.1.1g}$$

as well as the kinematic condition

$$\partial_t h + u_1 \partial_x h = u_2 \qquad \text{for } x \in [0, L],\ t \geq 0,$$

and initial condition

$$h(0, x) = h_0(x) \qquad \text{for } x \in [0, L].$$

Pseudo-plugs and inconsistencies

A straight-forward thin-film approximation of the Bingham equations (6.1.1) lead to the leading order system (7.2.8), which is solved by equation (6.3.7). The solution consists of two regions, i.e. $0 \leq y \leq Y_s$ and $Y_s < y \leq h$, which are called plastic region and pseudo-plug region, respectively. On the one side the plastic region shows a vertically sheared flow profile with the horizontal velocity u fulfilling $\partial_y u \neq 0$, whereas the pseudo-plug region moves seemingly stiff with $\partial_y u = 0$. On the other side in the horizontal direction both regions show a horizontal yielding $\partial_x u \neq 0$. The problem with this behavior can be found in the leading order approximation of the stress, which exceeds the yield-stress in the plastic region, but equals the yield-stress in the pseudo-plug. Since condition (6.1.1e) assumed vanishing shearing whenever the yield-stress is not exceeded this contradicts the horizontal yielding and renders the thin-film approximation seemingly inconsistent.

Balmforth and Craster [9] propose a solution to this problem by using two distinct expansions for the velocity in the plastic and pseudo-plug region followed by a matching procedure. Later, they show the stress is actually exceeding the yield-stress in the pseudo-plug region at next order. Thus, the original thin-film solution is consistent if derived using the correct asymptotic ansatz.

Nevertheless, their solution still suffers from at least two inconsistencies. Firstly, they propose a Bingham model using the standard equations (6.1.1) without stating any conditions at the yield-surface $|\boldsymbol{\tau}| = b$. Yet, they implicitly assume the stress and the velocity to be continuous at the yield-surface in order to derive their equations. Secondly, they assume the momentum equation to hold everywhere, without specifying the stress in possible plug-regions. This approach is common, but as Dean et al. [27] note, in case of a pure plug-flow the equation (6.1.1b) make no sense. Both inconsistencies can be solved by reformulating (6.1.1) as a variational inequality, cf. [27, 34, 47]. This is the approach we pursue.

Equivalent variational inequality

Let us define the sets

$$\begin{aligned} V &= \{\boldsymbol{v}(t,x,y) : \boldsymbol{v}(t,x,0) = \boldsymbol{0}, (x,y) \in \Omega(t)\}, \\ Q &= \{q(t,x,y) : (x,y) \in \Omega(t)\}, \end{aligned}$$

where we assume the functions to be "smooth enough" for the derivation. We use the shorthand notation

$$(\boldsymbol{a},\boldsymbol{b}) = \int_{\Omega(t)} \boldsymbol{a}\cdot\boldsymbol{b}\,\mathrm{d}\boldsymbol{x}, \qquad (\boldsymbol{A},\boldsymbol{B}) = \int_{\Omega(t)} \boldsymbol{A}:\boldsymbol{B}\,\mathrm{d}\boldsymbol{x}, \qquad \langle \boldsymbol{a},\boldsymbol{b}\rangle_x = \int_{\Gamma(t)} \boldsymbol{a}\cdot\boldsymbol{b}\,\mathrm{d}s$$

in the derivation and $\boldsymbol{n}$ denotes an outward pointing normal.

Using a combination of ideas by Duvaut et al. [34] and Acary-Robert [1], the variational inequality of the form (5.1.6) describing the behavior of system (6.1.1) is

$$\begin{aligned} \frac{\mu}{2}(D(\boldsymbol{u}), D(\boldsymbol{v}-\boldsymbol{u})) - (p, \nabla\cdot(\boldsymbol{v}-\boldsymbol{u})) & \\ +b(j(\boldsymbol{v}) - j(\boldsymbol{u})) \geq \langle \sigma\kappa, (\boldsymbol{v}-\boldsymbol{u})\cdot\boldsymbol{n}\rangle_x + (\boldsymbol{f}, \boldsymbol{v}-\boldsymbol{u}) & \qquad \forall \boldsymbol{v} \in V, \\ (q, \nabla\cdot\boldsymbol{u}) = 0 & \qquad \forall q \in Q, \end{aligned}$$

with

$$j(\boldsymbol{u}) = 2\int_{\Omega(t)} |D(\boldsymbol{u})| \,\mathrm{d}\boldsymbol{x},$$
$$\boldsymbol{f} = g\rho\nabla(x\sin\alpha - y\cos\alpha),$$

the kinematic equation

$$\partial_t h + u_1\partial_x h = u_2 \qquad \text{for } x \in [0, L],\ t \geq 0,$$

and the initial condition

$$h(0, x) = h_0(x) \qquad \text{for } x \in [0, L].$$

It is beneficial to use Gauss' theorem for the pressure terms, i.e.

$$\begin{aligned} &\frac{\mu}{2}(D(\boldsymbol{u}), D(\boldsymbol{v}-\boldsymbol{u})) + (\nabla p, \boldsymbol{v}-\boldsymbol{u}) && (6.1.2)\\ &\qquad +b(j(\boldsymbol{v}) - j(\boldsymbol{u})) \geq \langle \sigma\kappa + p, (\boldsymbol{v}-\boldsymbol{u})\cdot\boldsymbol{n}\rangle_x + (\boldsymbol{f}, \boldsymbol{v}-\boldsymbol{u}) && \forall \boldsymbol{v} \in V,\\ &\qquad (q, \nabla\cdot\boldsymbol{u}) = 0 && \forall q \in Q. \end{aligned}$$

6.2 Derivation of thin-film inequality

Nondimensionalization

Let us introduce the scales

$$\begin{aligned} h &= H\tilde{h}, & x &= L\tilde{x}, & p &= P\tilde{p}, & q &= P\tilde{q},\\ u_1 &= U\tilde{u}_1, & v_1 &= U\tilde{v}_1, & u_2 &= V\tilde{u}_2, & v_2 &= V\tilde{v}_2, \end{aligned}$$

and assume the height-length ratio is a very small number, i.e.

$$\frac{H}{L} = \varepsilon = o(1).$$

Using these scales in the variational inequality (6.1.2) and dropping the tildes, it gives

$$\begin{aligned} &\frac{U^2}{L^2}2\mu(\partial_x u_1, \partial_x v_1 - \partial_x u_1)\\ &+\frac{\mu}{2}\left(\frac{U}{H}\partial_y u_1 + \frac{V}{L}\partial_x u_2, \frac{U}{H}\partial_y v_1 - \frac{U}{H}\partial_y u_1 + \frac{V}{L}\partial_x v_2 - \frac{V}{L}\partial_x u_2\right)\\ &+\frac{V^2}{H^2}2\mu(\partial_y u_2, \partial_y v_2 - \partial_y u_2) + \frac{PU}{L}(\partial_x p, v_1 - u_1) + \frac{PV}{H}(\partial_y p, v_2 - u_2)\\ &\qquad +b\frac{U}{H}(\tilde{j}(\boldsymbol{v}) - \tilde{j}(\boldsymbol{u})) \geq U\langle\sigma\kappa + Pp, (v_1-u_1)n_1\rangle_x + V\langle\sigma\kappa + Pp, (v_2-u_2)n_2\rangle_x\\ &\qquad\qquad + g\rho U(\sin\alpha, v_1 - u_1) - g\rho V(\cos\alpha, v_2 - u_2), \end{aligned}$$

as well as

$$\frac{PU}{L}(q,\partial_x u_1)+\frac{PV}{H}(q,\partial_y u_2)=0,$$

with

$$\tilde{j}(\boldsymbol{u})=2\int_{\Omega(t)}\Big(2\varepsilon^2(\partial_x u_1)^2+(\partial_y u_1+\varepsilon^2\partial_x u_2)^2+2\varepsilon^2(\partial_y u_2)^2\Big)^{1/2}\mathrm{d}\boldsymbol{x}.$$

As we like to balance the continuum equation, we demand $U=\varepsilon V$, thus we get (after using the normal and surface integral scalings, i.e. $n_1\approx\varepsilon\partial_x h$ and $n_2=1$.)

$$\begin{aligned}&\frac{U^2}{L^2}2\mu(\partial_x u_1,\partial_x v_1-\partial_x u_1)+\frac{U^2}{H^2}\mu(\partial_y u_1-\varepsilon^2\partial_x u_2,\partial_y v_1-\partial_y u_1+\varepsilon^2\partial_x v_2-\varepsilon^2\partial_x u_2)\\ +&\frac{U^2}{L^2}2\mu(\partial_y u_2,\partial_y v_2-\partial_y u_2)+\frac{PU}{L}(\partial_x p,v_1-u_1)+\frac{PU}{L}(\partial_y p,v_2-u_2)\\ &+b\frac{U}{H}\big(\tilde{j}(\boldsymbol{v})-\tilde{j}(\boldsymbol{u})\big)\geq\varepsilon U\langle\sigma\kappa+Pp,(v_1-u_1)\partial_x h\rangle_x+\varepsilon U\langle\sigma\kappa+Pp,v_2-u_2\rangle_x\\ &\qquad+g\rho U(\sin\alpha,v_1-u_1)-\varepsilon g\rho U(\cos\alpha,v_2-u_2)\end{aligned}$$

as well as

$$(q,\partial_x u_1+\partial_y u_2)=0.$$

After division by $\mu\frac{U^2}{L^2}$ the momentum equation becomes

$$\begin{aligned}&2(\partial_x u_1,\partial_x v_1-\partial_x u_1)+\frac{1}{\varepsilon^2}(\partial_y u_1-\varepsilon^2\partial_x u_2,\partial_y v_1-\partial_y u_1+\varepsilon^2\partial_x v_2-\varepsilon^2\partial_x u_2)\\ +&2(\partial_y u_2,\partial_y v_2-\partial_y u_2)+\frac{PL}{\mu U}(\partial_x p,v_1-u_1)+\frac{PL}{\mu U}(\partial_y p,v_2-u_2)\\ &+\frac{bL^2}{\mu UH}\big(\tilde{j}(\boldsymbol{v})-\tilde{j}(\boldsymbol{u})\big)\geq\frac{HL}{\mu U}\langle\sigma\kappa+Pp,(v_1-u_1)\partial_x h\rangle_x+\frac{HL}{\mu U}\langle\sigma\kappa+Pp,v_2-u_2\rangle_x\\ &\qquad+\frac{g\rho L^2}{\mu U}\Big((\sin\alpha,v_1-u_1)-\varepsilon(\cos\alpha,v_2-u_2)\Big).\end{aligned}$$

We choose the non-dimensional pressure, Bingham number and velocity as

$$P=\mu\frac{U}{\varepsilon^2 L},\qquad B=b\frac{H}{\mu U},\qquad U=\frac{\rho g H^2\sin\alpha}{S\mu},$$

so the inequality becomes

$$\begin{aligned}&2(\partial_x u_1,\partial_x v_1-\partial_x u_1)+\frac{1}{\varepsilon^2}(\partial_y u_1-\varepsilon^2\partial_x u_2,\partial_y v_1-\partial_y u_1+\varepsilon^2\partial_x v_2-\varepsilon^2\partial_x u_2)\\ +&2(\partial_y u_2,\partial_y v_2-\partial_y u_2)+\frac{1}{\varepsilon^2}(\partial_x p,v_1-u_1)+\frac{1}{\varepsilon^2}(\partial_y p,v_2-u_2)\\ &+\frac{B}{\varepsilon^2}\big(\tilde{j}(\boldsymbol{v})-\tilde{j}(\boldsymbol{u})\big)\geq\frac{HL}{\mu U}\langle\sigma\kappa+\mu\frac{U}{\varepsilon^2 L}p,(v_1-u_1)\partial_x h\rangle_x+\frac{HL}{\mu U}\langle\sigma\kappa+\mu\frac{U}{\varepsilon^2 L}p,v_2-u_2\rangle_x\\ &\qquad+\frac{1}{\varepsilon^2}(S,v_1-u_1)-\frac{1}{\varepsilon^2}(1,v_2-u_2),\end{aligned}$$

where we chose $S = \varepsilon^{-1}\tan\alpha$, which is of order one for small α.
The integral terms also contain length and height scales, so we non-dimensionalize them as

$$(\cdot,\cdot) = HL\tilde{(}\cdot,\cdot\tilde{)}, \qquad \langle\cdot,\cdot\rangle_x = L\tilde{\langle}\cdot,\cdot\tilde{\rangle}_{\tilde{x}}.$$

Thus dropping the tildes again, one gets

$$\begin{aligned}
2(\partial_x u_1, \partial_x v_1 - \partial_x u_1) + \frac{1}{\varepsilon^2}(\partial_y u_1 - \varepsilon^2\partial_x u_2, \partial_y v_1 - \partial_y u_1 + \varepsilon^2\partial_x v_2 - \varepsilon^2\partial_x u_2) \\
+2(\partial_y u_2, \partial_y v_2 - \partial_y u_2) + \frac{1}{\varepsilon^2}(\partial_x p, v_1 - u_1) + \frac{1}{\varepsilon^2}(\partial_y p, v_2 - u_2) \\
+\frac{B}{\varepsilon^2}\left(\tilde{j}(\boldsymbol{v}) - \tilde{j}(\boldsymbol{u})\right) \geq \frac{L}{\mu U}\langle\sigma\kappa + \mu\frac{U}{\varepsilon^2 L}p, (v_1 - u_1)\partial_x h\rangle_x + \frac{L}{\mu U}\langle\sigma\kappa + \mu\frac{U}{\varepsilon^2 L}p, v_2 - u_2\rangle_x \\
+ \frac{1}{\varepsilon^2}(S, v_1 - u_1) - \frac{1}{\varepsilon^2}(1, v_2 - u_2).
\end{aligned}$$

Next, using the definition for the curvature and the capillary number, i.e.

$$\kappa = \frac{\partial_{xx} h}{(1 + (\partial_x h)^2)^{3/2}}, \qquad C = \frac{\sigma\varepsilon^3}{\mu U},$$

yields

$$\begin{aligned}
2(\partial_x u_1, \partial_x v_1 - \partial_x u_1) + \frac{1}{\varepsilon^2}(\partial_y u_1 - \varepsilon^2\partial_x u_2, \partial_y v_1 - \partial_y u_1 + \varepsilon^2\partial_x v_2 - \varepsilon^2\partial_x u_2) \\
+2(\partial_y u_2, \partial_y v_2 - \partial_y u_2) + \frac{1}{\varepsilon^2}(\partial_x p, v_1 - u_1) + \frac{1}{\varepsilon^2}(\partial_y p, v_2 - u_2) \\
+\frac{B}{\varepsilon^2}\left(\tilde{j}(\boldsymbol{v}) - \tilde{j}(\boldsymbol{u})\right) \geq \frac{1}{\varepsilon^2}\langle C\partial_{xx} h/(1 + \varepsilon^2(\partial_x h)^2)^{3/2} + p, (v_1 - u_1)\partial_x h\rangle_x \\
+ \frac{1}{\varepsilon^2}\langle C\partial_{xx} h/(1 + \varepsilon^2(\partial_x h)^2)^{3/2} + p, v_2 - u_2\rangle_x \\
+ \frac{1}{\varepsilon^2}(S, v_1 - u_1) - \frac{1}{\varepsilon^2}(1, v_2 - u_2).
\end{aligned}$$

Balancing

The leading order inequality is

$$\begin{aligned}
(\partial_y u_1, \partial_y v_1 - \partial_y u_1) + (\partial_x p, v_1 - u_1) + (\partial_y p, v_2 - u_2) + B\left(\hat{j}(\partial_y v_1) - \hat{j}(\partial_y u_1)\right) \geq \\
\langle C\partial_{xx} h + p, (v_1 - u_1)\partial_x h\rangle_x + \langle C\partial_{xx} h + p, v_2 - u_2\rangle_x + (S, v_1 - u_1) - (1, v_2 - u_2)
\end{aligned}$$

and the mass conservation becomes to leading order

$$(q, \partial_x u_1 + \partial_y u_2) = 0,$$

where we used

$$\hat{j}(a) = 2\int_{\Omega(t)} |a| \, \mathrm{d}\boldsymbol{x}.$$

Writing it in components of $\boldsymbol{v}$, we get

$$(\partial_y u_1, \partial_y v_1 - \partial_y u_1) + (\partial_x p, v_1 - u_1) \tag{6.2.1a}$$
$$+B\left(\hat{j}(\partial_y v_1) - \hat{j}(\partial_y u_1)\right) \geq \langle C\partial_{xx} h + p, (v_1 - u_1)\partial_x h\rangle_x + (S, v_1 - u_1),$$
$$(\partial_y p, v_2 - u_2) \geq \langle C\partial_{xx} h + p, v_2 - u_2\rangle_x - (1, v_2 - u_2), \tag{6.2.1b}$$

for all $\boldsymbol{v} = (v_1, v_2) \in V = V_1 \times V_2$, where we created the two inequalities by component-wise testing with either $v_1 = u_1$ or $v_2 = u_2$.

As the pressure is not restricted, the second inequality is in fact an equality, which can be seen by testing with positive and negative $v_2 - u_2$. Hence, we choose p to fulfill

$$p(x, h, t) = -C\partial_{xx} h \qquad \text{and} \qquad \partial_y p(x, y, t) = -1,$$

and, therefore,

$$p(x, y, t) = h - y - C\partial_{xx} h, \tag{6.2.2}$$

which is a particular solution of inequality (6.2.1b). Using (6.2.2) in (6.2.1a) yields an inequality for u_1, namely

$$(\partial_y u_1, \partial_y v_1 - \partial_y u_1) + (\partial_x h - C\partial_{xxx} h, v_1 - u_1) \tag{6.2.3a}$$
$$+B\left(\hat{j}(\partial_y v_1) - \hat{j}(\partial_y u_1)\right) \geq (S, v_1 - u_1) \qquad \forall v_1 \in V_1.$$

The continuum together with the kinematic equation gives

$$\partial_t h(x, t) + \partial_x \int_0^{h(x,t)} u_1(x, y, t)\mathrm{d}y = 0 \qquad \text{for } x \in [0, L], t \geq 0. \tag{6.2.3b}$$

6.3 Solution of thin-film inequality

Firstly, we derive a particular solution and, secondly, we show the solution to always hold, i.e. it is a general solution to the inequality system (6.2.3). Firstly, let us rename the velocities as $u := u_1$, $v := v_1$ and $V := V_1$ for convenience. Then, for given $h > 0$ the inequality (6.2.3a) only depends on y, so we have

$$\int_0^1 \frac{1}{h}\partial_z u(\partial_z v - \partial_z u) + h(\partial_x h - C\partial_{xxx} h)(v - u) \tag{6.3.1}$$
$$+2B(|\partial_z v| - |\partial_z u|)\mathrm{d}z \geq \int_0^1 hS(v - u)\mathrm{d}z \qquad \forall v \in V,$$

for arbitrary x, where we used the transformation $y = h \cdot z$.

The identification of a strong solution of (6.3.1) is impeded by the appearance of the absolute values. Therefore, we assume positivity of the involved terms, i.e.

$$\partial_z u \geq 0 \text{ and } \partial_z v \geq 0 \qquad \text{for } z \in [0, 1]. \tag{6.3.2}$$

Then, using the no-slip boundary conditions, inequality (6.3.1) becomes

$$\int_0^1 \frac{1}{h}\partial_z u(\partial_z v - \partial_z u) + h(\partial_x h - C\partial_{xxx}h)(v-u) + 2B(\partial_z v - \partial_z u)\mathrm{d}z \geq \int_0^1 hS(v-u)\mathrm{d}z \Leftrightarrow$$
$$\int_0^1 -\frac{1}{h}\partial_{zz}u(v-u) + h(\partial_x h - C\partial_{xxx}h)(v-u)\mathrm{d}z + \frac{1}{h}[\partial_z u(1)(v(1)-u(1))$$
$$-\partial_z u(0)(v(0)-u(0))] + 2B(v(1)-u(1)-v(0)+u(0)) \geq \int_0^1 hS(v-u)\mathrm{d}z \Leftrightarrow$$
$$\int_0^1 -\frac{1}{h}\partial_{zz}uw + h(\partial_x h - C\partial_{xxx}h)w\mathrm{d}z + \frac{1}{h}\partial_z u(1)w(1) + 2Bw(1) \geq \int_0^1 hSw\mathrm{d}z,$$

where we used $w = v - u$. Let us define

$$W = \{w : |\partial_z w| \leq \min(\partial_z u, \partial_z v)\}.$$

This set has the property, that for every $w \in W$, we have $-w \in W$. For this reduced set of test functions the inequality is actually an equality, since testing with the positive and negative of a function show the inequality to hold in both directions. So our problem becomes

$$\int_0^1 -\frac{1}{h}\partial_{zz}uw + h(\partial_x h - C\partial_{xxx}h)w\,\mathrm{d}z + \frac{1}{h}\partial_z u(1)w(1) + 2Bw(1) = \int_0^1 hSw\,\mathrm{d}z \quad \forall w \in W.$$

This motivates to look for a function u fulfilling

$$-\frac{1}{h}\partial_{zz}u + h(\partial_x h - C\partial_{xxx}h) = hS, \tag{6.3.3a}$$
$$\partial_z u(1) = -2Bh, \tag{6.3.3b}$$
$$u(0) = 0. \tag{6.3.3c}$$

Note $B, h > 0$, therefore, (6.3.3b) is not compatible with assumption (6.3.2). One solution is to assume an unyielded region for $z > Y_s \in [0,1]$, so our new assumptions are

$$\begin{aligned} \partial_z u \geq 0 \text{ and } \partial_z v \geq 0 \qquad & \text{for } z \in [0, Y_s], \\ \partial_z u = 0 \text{ and } u = v \qquad & \text{for } z \in [Y_s, 1]. \end{aligned}$$

The same steps as above with the new assumptions yield

$$\begin{aligned} -\frac{1}{h}\partial_{zz}u + h(\partial_x h - C\partial_{xxx}h) = hS \qquad & \text{for } z \in [0, Y_s], \\ \partial_z u = 0 \qquad & \text{for } z \in [Y_s, 1], \\ u = 0 \qquad & \text{at } z = 0. \end{aligned}$$

In the liquid region $z \in [0, Y_s]$ this gives

$$\partial_z u(z) = (Y_s - z)h^2(S - \partial_x h + C\partial_{xxx}h),$$
$$u(z) = \left(Y_s z - \frac{z^2}{2}\right)h^2(S - \partial_x h + C\partial_{xxx}h),$$

so that we have the particular solution

$$u(z) = \begin{cases} \left(Y_s z - \frac{z^2}{2}\right) h^2(S - \partial_x h + C\partial_{xxx} h) & \text{for } z \in [0, Y_s[\\ \frac{Y_s^2}{2} h^2(S - \partial_x h + C\partial_{xxx} h) & \text{for } z \in [Y_s, 1]. \end{cases} \tag{6.3.4}$$

Validity of particular solution and identification of yield surface Y_s

Using our particular solution for the plug-flow (6.3.4) in (6.3.1) yields

$$\int_0^{Y_s} \frac{1}{h}\partial_z u(\partial_z v - \partial_z u) + h(\partial_x h - C\partial_{xxx} h - S)(v - u) + 2B(|\partial_z v| - |\partial_z u|)\mathrm{d}z \\ + \int_{Y_s}^1 h(\partial_x h - C\partial_{xxx} h - S)(v - u) + 2B|\partial_z v|\mathrm{d}z \geq 0 \qquad \forall v \in V.$$

Using partial integration, the no-slip boundary condition and $\partial_z u(Y_s) = 0$, it gives

$$\int_0^{Y_s} -\frac{1}{h}\partial_{zz} u(v - u) + h(\partial_x h - C\partial_{xxx} h - S)(v - u) + 2B(|\partial_z v| - |\partial_z u|)\mathrm{d}z \\ + \int_{Y_s}^1 h(\partial_x h - C\partial_{xxx} h - S)(v - u) + 2B|\partial_z v|\mathrm{d}z \geq 0 \qquad \forall v \in V.$$

The first terms vanish due to (6.3.3a), so it becomes

$$\int_0^{Y_s} 2B(|\partial_z v| - |\partial_z u|)\mathrm{d}z + \int_{Y_s}^1 h(\partial_x h - C\partial_{xxx} h - S)(v - u) + 2B|\partial_z v|\mathrm{d}z \geq 0 \qquad \forall v \in V.$$

Using solution (6.3.4), we get

$$\frac{Y_s^2}{2} h^2 |S - \partial_x h + C\partial_{xxx} h| \left[-2B + h(1 - Y_s)|S - \partial_x h + C\partial_{xxx} h|\right] \tag{6.3.5}$$
$$+2B \int_0^1 |\partial_z v|\mathrm{d}z + h(\partial_x h - C\partial_{xxx} h - S) \int_{Y_s}^1 v\mathrm{d}z \geq 0 \qquad \forall v \in V.$$

We like the first term to vanish in (6.3.5), so we define the yield surface Y_s as

$$Y_s = \max\left(1 - \frac{2B}{h|S - \partial_x h + C\partial_{xxx} h|}, 0\right). \tag{6.3.6}$$

The final inequality is

$$2B \int_0^1 |\partial_z v|\mathrm{d}z + h(\partial_x h - C\partial_{xxx} h - S) \int_{Y_s}^1 v\mathrm{d}z \geq 0 \qquad \forall v \in V,$$

which can be rewritten using (6.3.6) as

$$h|\partial_x h - C\partial_{xxx} h - S| \left((1 - Y_s) \int_0^1 |\partial_z v|\mathrm{d}z - \mathrm{sign}(\partial_x h - C\partial_{xxx} h - S) \int_{Y_s}^1 v\mathrm{d}z\right) \geq 0 \qquad \forall v \in V.$$

This inequality holds for all $v \in V$ as long as $h > 0$. To see this, define $\xi = \operatorname{argmax}_{z\in[0,1]}(|v|)$ and consider the inequalities

$$\begin{aligned}(1-Y_s)\int_0^1 |\partial_z v|\mathrm{d}z &\geq (1-Y_s)\int_0^\xi |\partial_z v|\,\mathrm{d}z \\ &\geq (1-Y_s)\int_0^\xi \partial_z v\,\mathrm{d}z\,\operatorname{sign}(v(\xi)) \\ &= (1-Y_s)\max(|v|) \\ &= \int_{Y_s}^1 \max(|v|)\,\mathrm{d}z \\ &\geq \operatorname{sign}(\partial_x h - C\partial_{xxx}h - S)\int_{Y_s}^1 v\mathrm{d}z.\end{aligned}$$

Note, we have not supposed $\partial_z u \geq 0$ anymore, so for negative $\partial_{xxx}h$ we also have the opposite case. Nor did we make any assumptions about v besides some implicit smoothness requirements. Note also, for $Y_s = 0$ the fluid region size becomes zero and we are only left with a single unyielded region.

Final solutions

Usage of the velocity solution (6.3.4) in the kinematic boundary condition (6.2.3b) yields the general solution

$$0 = \partial_t h + \partial_x\left(\frac{1}{3}h^3(S - \partial_x h + C\partial_{xxx}h)Y_s^3 + (1-Y_s)u(Y_s)\right), \tag{6.3.7a}$$

with the initial condition

$$h(0,x) = h_0(x) \qquad \text{for } x \in [0,L], \tag{6.3.7b}$$

where the yield surface $Y_s \in [0,1]$ is of the form

$$Y_s = \max\left(1 - \frac{2B}{h|S - \partial_x h + C\partial_{xxx}h|}, 0\right). \tag{6.3.7c}$$

We can identify three special cases. Firstly, mind for $B \to 0$ we have $Y_s \to 1$ and the equation becomes the standard thin-film model for Newtonian fluids driven by surface tension and gravity, as already Balmforth et al. [9] recognized. Secondly, for $C = 0$, that is vanishing surface tension, we get

$$0 = \partial_t h + \partial_x\left(\frac{1}{3}h^3 Y_s^2 \frac{3-Y_s}{2}(S - \partial_x h)\right), \tag{6.3.8}$$

with

$$Y_s = \max\left(1 - \frac{2B}{h|S - \partial_x h|}, 0\right).$$

Thirdly, for vanishing gravitational forces, one derives

$$0 = \partial_t h + \partial_x \left(\frac{1}{3} h^3 Y_s^2 \frac{3 - Y_s}{2} C \partial_{xxx} h \right),$$

with

$$Y_s = \max \left(1 - \frac{2B}{Ch|\partial_{xxx} h|}, 0 \right).$$

6.4 Introduction into the theory of monotone operators

In Section 6.3 we have derived partial differential equations for the viscoplastic thin-film model. These equations share the common difficulty that they are nonlinear in the highest derivative in their flux. In order to cope with this difficulty we use the theory of monotone operators.

Tools from functional analysis

A real Banach space V is a complete vector space over the field $\mathbb{R}$ equipped with a norm $\|\cdot\|_V$. A real Hilbert space H is a complete vector space over the field $\mathbb{R}$ equipped with an inner product $(\cdot,\cdot)_H$.

We define the dual space X^* of a vector space X as the set of all continuous linear functionals $f : X \to \mathbb{R}$ on X together with the norm

$$\|f\|_{X^*} := \sup_{\|x\| \leq 1} |f(x)|.$$

For $f \in X^*$ and $x \in X$, we define the pairing

$$(f, x)_{X^*,X} := f(x).$$

We drop the index whenever it is clear from the context, what spaces we are referring to.

There is a surprising simple connection between a Hilbert space H and its dual space H^*.

Theorem 6.1 (Riesz representation theorem)**.** *Let H be a Hilbert space. For every continuous linear functional $f \in H^*$ there is exactly one element $y \in H$ such that*

$$(f, x)_{H,H^*} = (y, x)_H \qquad \forall\, x \in H$$

and

$$\|f\|_{H^*} = \|y\|_H.$$

Proof. For a proof, see e.g. [17]. □

Since the finite dimensional space $\mathbb{R}^n$ is a Hilbert space equipped with the inner product of vector spaces, the Riesz theorem can be used to identify $\tilde{y} \in \mathbb{R}^{n*}$ with $y \in \mathbb{R}^n$ and we define

$$(\tilde{y}, x)_{\mathbb{R}^{n*},\mathbb{R}^n} = (y, x)_{\mathbb{R}^n,\mathbb{R}^n} = y \cdot x.$$

Let $(x_n) \in X$ be a sequence, $x \in X$, $(f_n) \in X^*$ a sequence in the dual space and $f \in X^*$. We have the following definitions

$$x_n \to x \qquad :\Leftrightarrow \qquad \lim_{n\to\infty} \|x - x_n\|_X = 0, \tag{6.4.1}$$

$$f_n \to f \qquad :\Leftrightarrow \qquad \lim_{n\to\infty} \|f - f_n\|_{X^*} = 0, \tag{6.4.2}$$

$$x_n \rightharpoonup x \qquad :\Leftrightarrow \qquad \lim_{n\to\infty} (f, x - x_n)_{X^*,X} = 0 \qquad \forall\, f \in X^*, \tag{6.4.3}$$

$$f_n \overset{*}{\rightharpoonup} f \qquad :\Leftrightarrow \qquad \lim_{n\to\infty} (f_n - f, x)_{X^*,X} = 0 \qquad \forall\, x \in X, \tag{6.4.4}$$

and we call (6.4.1) and (6.4.2) strong convergence, (6.4.3) weak convergence and (6.4.4) weak* convergence.

We call a map $f : Y \subset X \to Z$ between two Banach spaces X and Z continuous at $x \in Y$, iff

$$x_n \to x \text{ implies } f(x_n) \to f(x).$$

An operator $A : X \to X^*$ is called hemicontinuous, iff the map $\tilde{A} : \mathbb{R} \to \mathbb{R}$ defined as

$$\tilde{A}(t) = (A(u + tv), w)_{X^*,X}$$

is continuous for all $u, v, w \in X$.

We denote the bidual space by $X^{**} = (X^*)^*$. In a Banach space we can identify an element $x \in X$ with $x^{**} \in X^{**}$ by

$$(x^{**}, f)_{X^{**},X^*} = (f, x)_{X^*,X} \qquad \forall\, f \in X^*,$$

which creates a map $J : X \to X^{**}$, with $x \mapsto x^{**}$. If J is surjective, then X is called reflexive and one can identify X with its bidual X^{**}, which is denoted by $X = X^{**}$. Reflexive Banach spaces have a very important convergence property similar to the well-known Bolzano–Weierstrass theorem for finite dimensional sequences.

Theorem 6.2 (Eberlein-Šmuljan theorem)**.** *The Banach space X is reflexive, if and only if every bounded sequence $(x_n) \in X$ has a weakly convergent subsequence.*

Proof. See for example [17, 136]. □

We call a Banach space X separable, iff it contains a dense subset $Y \subset X$ that is countable, i.e. $\bar{Y} = X$, where the bar denotes the closure of Y.

Let X and Y be vector spaces. Then, we call a map $A : X \to Y$ an operator. The operator is usually equipped with the norm

$$\|A\|_{op} = \sup_{x\in X, x\neq 0} \frac{\|Ax\|_Y}{\|x\|_X}.$$

We call A a linear operator, iff it is a linear map.

Let us call a map $\boldsymbol{f} : X \to X^*$ coercive, iff

$$\frac{(\boldsymbol{f}(x), x)_{X^*,X}}{\|x\|_X} \to \infty \qquad \text{as } \|x\| \to \infty.$$

Let us call a map $\boldsymbol{f} : X \to X'$ monotone, iff

$$(\boldsymbol{f}(\boldsymbol{a}) - \boldsymbol{f}(\boldsymbol{b}), \boldsymbol{a} - \boldsymbol{b})_{X^*,X} \geq 0 \qquad \forall\, \boldsymbol{a}, \boldsymbol{b} \in X$$

holds. If $\boldsymbol{f} : X \to X^*$ is monotone and $\boldsymbol{a} \neq \boldsymbol{b}$ implies

$$(\boldsymbol{f}(\boldsymbol{a}) - \boldsymbol{f}(\boldsymbol{b}), \boldsymbol{a} - \boldsymbol{b})_{X^*,X} > 0,$$

then we call $\boldsymbol{f}$ strictly monotone.

An operator $A : X \to X^*$ on a real Banach space X is strongly continuous, iff

$$u_n \rightharpoonup u \qquad \text{implies} \qquad Au_n \to Au.$$

Let X, Y be real Banach spaces. An operator $A : X \to Y$ is compact, iff A is continuous and A maps bounded set of X into relative compact sets in Y.

Note, if $Y = X^*$ and X is reflexive, then strongly continuous and compactness are equivalent.

Consider a domain $\Omega \subset \mathbb{R}^n$ having a Lipschitz boundary. Then, we denote by $L^p(\Omega)$ the space defined as

$$L^p(\Omega) = \{u : \|u\|_{L^p(\Omega)} < \infty, u : \mathbb{R}^n \to \mathbb{R}, u \text{ is Lebesgue measurable } \},$$

The employed norm $\|\cdot\|_{L^p(\Omega)}$ is

$$\|u\|^p_{L^p(\Omega)} := \int_\Omega |u(\boldsymbol{x})|^p \, \mathrm{d}\boldsymbol{x}$$

and the integral is meant in the Lebesgue sense. Thus, redefining $L^p(\Omega)$ as the quotient space with respect to the null set

$$N = \{u : \|u\|_{L^p(\Omega)} = 0\}$$

creates a Banach space.

We define the generalized derivative $\partial_{x_i} u$ of a function u in the distribution sense as

$$\int_\Omega \partial_{x_i} u(\boldsymbol{x}) \varphi(\boldsymbol{x}) \mathrm{d}\boldsymbol{x} = -\int_\Omega u(\boldsymbol{x}) \partial_{x_i} \varphi(\boldsymbol{x}) \mathrm{d}\boldsymbol{x} \qquad \forall \varphi \in C_0^\infty(\Omega),$$

where $C_0^\infty(\Omega)$ denotes the space of all infinite differentiable functions with compact support in Ω. Then, we define the so-called Sobolev spaces $W^{q,p}(\Omega)$ as

$$W^{q,p}(\Omega) = \{u \in L^p(\Omega) : \partial_{\boldsymbol{\alpha}} u \in L^p(\Omega) \quad \forall \|\boldsymbol{\alpha}\|_1 \leq q, \boldsymbol{\alpha} \in \mathbb{N}_0^n\},$$

and equip these spaces with the norm

$$\|u\|^p_{W^{q,p}(\Omega)} := \sum_{\|\boldsymbol{\alpha}\|_1 \leq q} \|\partial_{\boldsymbol{\alpha}} u\|_{L^p(\Omega)}.$$

For time dependent partial differential equations, we use functions

$$u : I \to X,$$

where $I \subset \mathbb{R}$ and X is a Banach space. We denote by $L^p(I;X)$ the space of all functions that are Bochner integrable and fulfill

$$\|u\|_{L^p(I;X)} < \infty,$$

where the norm is defined as the Bochner integral

$$\|u\|_{L^p(I;X)} = \int_I \|u(t)\|^p_X \, \mathrm{d}t.$$

Further, we define a generalized time derivative $\frac{\mathrm{d}u}{\mathrm{d}t}$ in the sense

$$\int_I \frac{\mathrm{d}u(t)}{\mathrm{d}t}\varphi(t)\mathrm{d}t = -\int_I u(t)\varphi'(t)\mathrm{d}t \qquad \forall \varphi \in C_0^\infty(I).$$

This allows us to define the space of generalized time derivatives $W^{1,p,p'}(I;X;X^*)$ as

$$W^{1,p,p'}(I;X;X^*) = \{u : u \in L^p(I;X), \frac{\mathrm{d}u}{\mathrm{d}t} \in L^{p'}(I;X^*)\},$$

where $1/p' + 1/p = 1$. The fact that the derivative $\frac{\mathrm{d}u}{\mathrm{d}t}$ lies in the dual space of the original function u comes from the fact, that we like to have the relation

$$\frac{\mathrm{d}}{\mathrm{d}t}(u(t), v)_H = (\frac{\mathrm{d}u}{\mathrm{d}t}(t), v)_{X,X^*} \qquad \forall v \in X$$

for any Gelfand triple $X \subset H = H^* \subset X^*$, where X is a Banach space that is a embedded continuously and densely into a Hilbert space H.

We call $f : \Omega \times \mathbb{R}^m \to \mathbb{R}$ a Carathéodory function, iff $f(\cdot, r) : \Omega \to \mathbb{R}$ is measurable for all $r \in \mathbb{R}^m$ and $f(\boldsymbol{x}, \cdot) : \mathbb{R} \to \mathbb{R}$ is continuous for almost all $\boldsymbol{x} \in \Omega$.

We call F a Nemyckii operator defined as

$$F(\boldsymbol{u})(\boldsymbol{x}) := f(\boldsymbol{x}, \boldsymbol{u}(\boldsymbol{x})),$$

iff f is a Carathéodory function that adheres to the growth condition

$$|f(\boldsymbol{x}, r)| \leq |a(\boldsymbol{x})| + b\sum_{i=1}^m |\eta^i|^{p_i/q},$$

where b is a positive constant, $a \in L^q(\Omega)$, $1 \leq p_i, q < \infty$, $i \in \{1, \ldots, m\}$.

The following theorem is central for the continuity of operators used in the Browder/Minty theorem.

Theorem 6.3. *Let $f : \Omega \times \mathbb{R}^m \to \mathbb{R}$ be a Carathéodory function, then the Nemyckii operator*

$$F : \prod_{i=1}^{m} L^{p_i}(\Omega) \to L^q(\Omega)$$

is measurable, bounded and continuous. Further, for all $\boldsymbol{u} \in \prod_{i=1}^m L^{p_i}(\Omega)$ it is bounded by

$$\|F(\boldsymbol{u})\|_{L^q(\Omega)} \leq C \left(\|a\|_{L^q(\Omega)} + \sum_{i=1}^{m} \|u_i\|_{L^{p_i}(\Omega)}^{p_i/q} \right).$$

Proof. Proofs can be found in [109, 112, 138]. □

The definition of Nemyckii operators for time dependent problems in Bochner spaces also exists, cf. [109].

Finite dimensional case

In order to understand monotonicity methods for infinite dimensional spaces, we first look at a finite dimensional example. Suppose for given $\boldsymbol{f} : \mathbb{R}^n \to \mathbb{R}^n$ and $\boldsymbol{b} \in \mathbb{R}^n$ we like to solve

$$\boldsymbol{f}(\boldsymbol{u}) = \boldsymbol{b} \tag{6.4.5}$$

for $\boldsymbol{u} \in \mathbb{R}^n$. An interesting question is what are sufficient assumptions on $\boldsymbol{f}$ for the existence of a solution to (6.4.5). Further, what are additional assumptions on $\boldsymbol{f}$ for uniqueness of the solution.

In the one-dimensional case, i.e. $n = 1$, sufficient assumptions are that $\boldsymbol{f}$ should be continuous and coercive. This follows directly from the intermediate value theorem for continuous functions. However, this generalizes to $n > 1$.

Theorem 6.4. *Assume $\boldsymbol{f}$ is a continuous, coercive function and let $n \in \mathbb{N}$. Then, there exists a solution $\boldsymbol{u} \in \mathbb{R}^n$ for equation (6.4.5).*

Proof. The proof is based on Brouwers' fixed point theorem, see e.g. [112]. □

If we demand $\boldsymbol{f}$ to be strictly monotone and assume $\boldsymbol{u}_1$ and $\boldsymbol{u}_2$ to be two solutions of (6.4.5) with $\boldsymbol{u}_1 \neq \boldsymbol{u}_2$, then

$$0 = (\boldsymbol{b} - \boldsymbol{b}) \cdot (\boldsymbol{u}_1 - \boldsymbol{u}_2) = (\boldsymbol{f}(\boldsymbol{u}_1) - \boldsymbol{f}(\boldsymbol{u}_2)) \cdot (\boldsymbol{u}_1 - \boldsymbol{u}_2) > 0,$$

which is a contradiction. Hence, strict monotonicity implies uniqueness.

Another interesting choice is to demand $\boldsymbol{f}$ to be continuous and monotone only, because this implies the equivalence of the variational inequality

$$(\boldsymbol{f}(\boldsymbol{v}) - \boldsymbol{b}) \cdot (\boldsymbol{v} - \boldsymbol{u}) \geq 0 \qquad \forall\, \boldsymbol{v} \in \mathbb{R}^n$$

with equation (6.4.5), see e.g. [112].

Therefore, sufficient assumptions for the existence and uniqueness of solutions to (6.4.5) are that $\boldsymbol{f}$ should be continuous, strictly monotone and coercive. Note, we did not demand $\boldsymbol{f}$ to be linear. Thus, these properties hold for nonlinear functions, too! Additionally, these assumptions allow for direct generalizations of the solution properties of finite dimensional functions to operators on infinite dimensional spaces.

Infinite dimensional case

Let X be a Banach space. Suppose we like to solve the operator equation

$$Fu = b,$$

where $u \in X$, F is an operator from X to X^* and $b \in X^*$. This contains the finite dimensional case (6.4.5) using the choice $X = \mathbb{R}^n$. However, we are now interested in infinite dimensional cases. A typical example is the Poisson equation with the choices

$$\Omega \subset \mathbb{R}^n, \qquad b(v) = \int_\Omega a(\boldsymbol{x})v(\boldsymbol{x})\mathrm{d}\boldsymbol{x},$$

$$X = \{u \in W^{1,2}(\Omega) : u = 0 \text{ on } \partial\Omega\}, \qquad (F(u))(v) = \int_\Omega \sum_{i=1}^{n} \partial_{x_i} u(\boldsymbol{x})\partial_{x_i} v(\boldsymbol{x})\mathrm{d}\boldsymbol{x},$$

where n is a positive integer, $a \in W^{1,2}(\Omega)$ and Ω is a Lipschitz domain.

We have seen the sufficient assumptions for finite dimensional F are strict monotonicity, continuity and coercivity in order to guarantee existence and even uniqueness of solutions. It is a surprising result, that the same holds for infinite dimensional spaces if we additionally demand the space to be reflexive and separable.

Theorem 6.5 (Minty, 1962)**.** *Let X be a reflexive, real Banach space and let $A : X \to X^*$ a hemicontinuous, monotone operator. Then, the following holds:*

1. *The operator A is maximal monotone, that is let $u \in X$ and $b \in X^*$, such that*

   $$(b - Av, u - v)_{X^*,X} \geq 0 \qquad \forall v \in X$$

   then it follows $Au = b$.

2. *Operator A fulfills property (M), i.e.*

   $$\begin{aligned} u_n &\rightharpoonup u, \\ Au_n &\rightharpoonup b, \\ (Au_n, u_n)_{X^*,X} &\to (b, u)_{X^*,X} \end{aligned}$$

   implies $Au = b$.

3. *Either*

   $$u_n \rightharpoonup u \text{ in } X, \qquad Au_n \to b \text{ in } X^*$$

   or

   $$u_n \to u \text{ in } X, \qquad Au_n \rightharpoonup b \text{ in } X^*$$

   implies $Au = b$.

Proof. See e.g. [112]. □

Theorem 6.6 (Browder and Minty, 1963)**.** *Let X be a separable, reflexive, real Banach space with base $(w_n) \in X$. Further, let $A : X \to X^*$ be a monotone, hemicontinuous, coercive operator. Then, there exists a solution $u \in X$ of*

$$Au = b, \tag{6.4.6}$$

for all $b \in X^*$. The set of solutions is closed, bounded and convex. Additionally, if A is strictly monotone, then the solution $u \in X$ of (6.4.6) is unique.

Proof. For a complete proof see e.g. [112, 138]. □

The main steps of the proof are:

1. Approximation of the solution through a Galerkin ansatz

$$u_k = \sum_{n=1}^{k} c_n w_n,$$

   where $c_n \in \mathbb{R}$ and w_n are base functions of X.

2. The Galerkin ansatz yields a (possible nonlinear) algebraic system of equations for c_n. Since A is coercive and hemi-continuous, we can use Theorem 6.4 in order to show existence of a solution for the c_n, which imply the existence of a sequence $u_k \in X$ of solutions.

3. The proof of Theorem 6.4 yields the sequence of solutions is a-priori bounded. Using the Eberlein-Šmuljan theorem this implies $u_k \rightharpoonup u$.

4. Due to the monotonicity of A we can proof the boundness of (Au_k, w_n) and (Au_k, u_k). This gives weak convergence and implies

$$\begin{aligned}(Au_k, w_n) &\to (Au, w_n),\\ (Au_k, u_k) &\to (b, u).\end{aligned}$$

5. Additionally, monotonicity yields

$$0 \leq (Au_n - Av, u_n - v) \to (Au - Av, u - v) = (b - Av, u - v) \qquad \forall v \in X. \tag{6.4.7}$$

6. The monotonicity trick (6.4.7) implies

$$(b - Av, u - v) \geq 0 \qquad \forall v \in X,$$

   which itself implies the solution (6.4.6) via Minty's trick, i.e. Theorem 6.5.

We call $A : X \to X^*$ a pseudo-monotone operator for the reflexive Banach space X, iff

$$\begin{aligned} u_n &\rightharpoonup u,\\ \limsup_{n\to\infty} (Au_n, u_n - u)_{X^*,X} &\leq 0\end{aligned}$$

implies

$$(Au, u - w)_{X^*,X} \leq \liminf_{n\to\infty} (Au_n, u_n - w)_{X^*,X} \qquad \forall\, w \in X.$$

Theorem 6.5 shows the weaker property (M) is also sufficient for the proof and pseudo-monotone operators fulfill property (M) and generalize the notion of monotone and compact operators.

Theorem 6.7. *Let $A, B : X \to X^*$ operators, where X is a real, reflexive Banach space. Then, the following statements are true:*

1. *If A is monotone and hemi-continuous, then A is pseudo-monotone.*
2. *If A is strongly continuous, then A is pseudo-monotone.*
3. *If A and B are pseudo-monotone, then so is $A + B$.*
4. *If A is pseudo-monotone, then it fulfills property (M).*

Proof. The proof and theorem can be found in [112]. □

This theorem shows that pseudo-monotone operators can also consist of two parts, where one is monotone and the other one strongly continuous. Many problems in partial differential equations create operators, where the highest order derivative fulfills a monotonicity property, but lower order parts do not. On the other side lower order derivatives often fulfill compactness results. Thus, a generalized theorem by Brezis yields:

Theorem 6.8 (Brezis, 1968)**.** *Let $A : X \to X^*$ be a pseudo-monotone, bounded and coercive operator, where X is a separable and reflexive Banach space. Then, there exists a solution $u \in X$ of*

$$Au = b,$$

for all $b \in X^*$.

Proof. The proof can be found in any of [109, 112, 138]. □

In order to proof pseudo-monotonicity for elliptic operators, it is often easier to proof the so-called Leray-Lions theorem, which just demands us to show that the operator is coercive and bounded as well as monotone and continuous in the highest order terms, cf. Problem 27.6 in [138] and Theorem 6.1.22 in [29]. This allows a rather general existence theory for elliptic problems of arbitrary order.

Time dependence

The discussion for elliptic problems needs to be generalized to problems involving time, before we can apply the theory to parabolic equations of the form

$$\frac{\mathrm{d}u}{\mathrm{d}t} + A(t, u(t)) = f(u) \text{ for almost all } t \in I, \qquad u(0) = u_0, \tag{6.4.8}$$

where $u \in X$, $A : I \times X \to X^*$, $I := [0, T]$ and $f : I \to X^*$. We demand X to be a separable, reflexive Banach space that is embedded continuously and densly into a Hilbert space H, such that the following Gelfand triple relation

$$V \subset H = H^* \subset V^*$$

is fulfilled. The equality sign stems from the Riesz representation theorem.

Application of the Galerkin approximation in the proof of Theorem 6.6 yielded a nonlinear algebraic system, that could be shown to have a solution using a fixed point argument. Using a Galerkin method in (6.4.8), however, yields a system of ordinary differential equations of the form

$$\frac{\mathrm{d}u}{\mathrm{d}t} = f(t, u(t)), \tag{6.4.9}$$

where $u : [T_0 - c, T_0 + c] \to X$ and X is some Banach space. The simplest case is $X = \mathbb{R}$. In order to show the existence of solutions for every approximation, we need a well-known theorem due to Peano.

Theorem 6.9 (Peano)**.** *Let $T_0 \in \mathbb{R}$, $u_0 \in X$, and*

$$Q_b = \{(t, u) \in \mathbb{R} \times X : |t - T_0| \leq a, \|u - u_0\|_X \leq b\},$$

for fixed numbers, $0 \leq a, b \leq \infty$. Suppose that $f : Q_b \to X$ is compact and that $\|f(t, y)\| \leq K$ for all $(t, u) \in Q_b$ with fixed $K > 0$. We set $c = \min(a, b/K)$. Then, (6.4.9) has a continuously differentiable solution on $[T_0 - c, T_0 + c]$.

Proof. See [136]. □

In order to apply Peano's theorem, we need a-priori bounds of the solution to (6.4.9), which can be gained by usage of the following lemma.

Lemma 6.1 (Gronwall's inequality)**.** *Let $u, g : [T_0, T] \to \mathbb{R}$ be continuous functions, with g nondecreasing. If they satisfy the inequality*

$$u(t) \leq g(t) + C \int_{T_0}^{T} u(s)\,\mathrm{d}s,$$

where $C > 0$, then

$$u(t) \leq g(t)\mathrm{e}^{c(t - T_0)}$$

for all $t \in [T_0, T]$.

Proof. See [136]. □

This yields bounds on the time derivative $\frac{\mathrm{d}u}{\mathrm{d}t}$. Since the operator A is assumed to be bounded anyway, the sequence of Galerkin solutions u_k, $k \in \mathbb{N}$ is weakly converging, i.e.

$$u_k \rightharpoonup u \text{ in } L^p(I;V).$$

Converting the weak limit to the strong limit in A goes along the same lines as in Theorem 6.6. However, we also need to show that it is a strong limit for the generalized time derivative $\frac{\mathrm{d}u}{\mathrm{d}t}$. This can be done by usage of the integration by parts formula

$$\int_I (\frac{\mathrm{d}u_k}{\mathrm{d}t}(t), w_k)_{V^*,V} \varphi(t)\, \mathrm{d}t = -\int_I (u_k(t), w_k)_H \varphi'(t)\, \mathrm{d}t - (u_k(0), w_k)_{V^*,V}$$

where $w_k \in V_k$ is base function of the Galerkin ansatz and $\varphi \in C^1(I)$ with $\varphi(T) = 0$. Then, showing the right hand side contains two bounded linear functionals, which are, therefore, continuous, we can take the limit $k \to \infty$. Using the fact, that the convex hull of all w_k is dense in V, we show this limit to actually having the form

$$-\int_I u(t)\varphi'(t)\, \mathrm{d}t,$$

where we now use $\varphi \in C_0^\infty(I)$, which eliminates the $t = 0$ term. Then, the definition of the generalized time derivative shows that $\frac{\mathrm{d}u}{\mathrm{d}t}$ exists and, therefore, that $u \in W^{1,p,p'}(I;V;V^*)$. For detailed proofs see e.g. [109, 137, 138].

The generalization of Theorem 6.6 to linear first order time dependent problems is the following.

Theorem 6.10 (Roubicek, 2005)**.** *Let the collection* $\{V_k\}_{k\in\mathbb{N}}$ *satisfy*

$$\forall k \in \mathbb{N} : V_k \subset V_{k+1} \subset V \text{ and } \cup_{k\in\mathbb{N}} V_k \text{ is dense in } V.$$

Let $A : I \times V \to V^*$ *be a Carathédory function that satisfies the growth condition*

$$\exists \gamma \in L^{p'}(I), c : \mathbb{R} \to \mathbb{R} \text{ increasing } : \|A(t,v)\|_{V^*} \le c(\|v\|_H)(\gamma(t) + \|v\|_V^{p-1})$$

and the semi-coercivity

$$\exists C_0 > 0, c_1 \in L^{p'}(I), c_2 \in L^1(I) \forall v \in V : (A(t,v), v)_{V^*,V} \ge C_0 |v|_V^p - c_1(t)|v|_V - c_2(t)\|v\|_H^2,$$

where $|\cdot|_V$ *is a seminorm on* V *such that the Poincaré inequality*

$$\|u\|_V \le C(|u|_V + \|u\|_H) \qquad \forall u \in V$$

is fulfilled. Let $A(t,\cdot)$ *be pseudo-monotone for almost all* $t \in I$ *and let* $u_{0k} \to u_0$ *in* H *with* $u_{0k} \in V_k$.

Then, $u_k \rightharpoonup u$ *in* $L^p(I;V)$ *(possibly in terms of subsequences) and* u *is a strong solution to the Cauchy problem* (6.4.8).

Proof. See [109]. □

Thus, defining a particular differential operator A and proving the necessary assumptions of Theorem 6.10 yields the existence of solutions to a parabolic equation of the form (6.4.8).

6.5 Existence proof for regularized second order equation

Let $\Omega = [0, L]$ with boundary $\Gamma = \{0, L\}$, denote by $I = [0, T]$, $Q = I \times \Omega$, $\Sigma = I \times \Gamma$. We study the existence of solutions for the regularized equation

$$0 = \partial_t h + \partial_x \left(\frac{1}{3} |h|^3 Y_s^2 \frac{3 - Y_s}{2} (S - \partial_x h) - \varepsilon (\partial_x h)^3 \right) \quad \text{in } (t, x) \in Q \tag{6.5.1a}$$

with $T, L, S, \varepsilon > 0$,

$$Y_s(h, \partial_x h) = \max \left(1 - \frac{2B}{|h|\,|S - \partial_x h|}, 0 \right) \tag{6.5.1b}$$

and Neumann boundary conditions

$$n \cdot \left(\frac{1}{3} |h|^3 Y_s^2 \frac{3 - Y_s}{2} (S - \partial_x h) - \varepsilon (\partial_x h)^3 \right) = 0 \qquad \text{on } (t, x) \in \Sigma, \tag{6.5.1c}$$

with initial condition $h(0, x) = h_0(x)$ for $x \in \Omega$, using the existence theory of pseudomonotone mappings for quasilinear parabolic equations by Roubicek [109]. This equation is similar to solution (6.3.8) for a gravity driven thin-film with Bingham stress. The regularizations are necessary since for non-positive h this equation degenerates. This degeneration introduces problems, because the highest derivative vanishes or changes sign. In the existence proof at hand, this would translate into missing coercivity or monotonicity of the differential operator, which is reestablished by the introduction of the regularization.

It is essential for the following proof that equation (6.5.1) is mass conserving. This can be shown by integrating (6.5.1) over x, using the Gauß' theorem and the Neumann boundary conditions (6.5.1c) in order to yield

$$\frac{\mathrm{d}}{\mathrm{d}t} \int_0^L h(t, x)\, \mathrm{d}x = 0.$$

This shows that the average value of h is a constant, i.e.

$$h_\Omega = \frac{1}{L} \int_0^L h(t, x)\, \mathrm{d}x = \frac{1}{L} \int_0^L h(0, x)\, \mathrm{d}x = \text{const.} \tag{6.5.2}$$

Using property (6.5.2), we transform the solution via

$$u = h - h_\Omega, \tag{6.5.3}$$

where u has zero mean, i.e. $u_\Omega = 0$. Thus, equation (6.5.1) is modified as

$$0 = \partial_t u + \partial_x \left(\frac{1}{3} |u + h_\Omega|^3 \tilde{Y}_s^2 \frac{3 - \tilde{Y}_s}{2} (S - \partial_x u) - \varepsilon (\partial_x u)^3 \right) \quad \text{in } (t, x) \in Q, \tag{6.5.4a}$$

$$\tilde{Y}_s(u, \partial_x u) = \max \left(1 - \frac{2B}{|u + h_\Omega|\,|S - \partial_x u|}, 0 \right), \tag{6.5.4b}$$

$$0 = n \cdot \left(\frac{1}{3} |u + h_\Omega|^3 \tilde{Y}_s^2 \frac{3 - \tilde{Y}_s}{2} (S - \partial_x u) - \varepsilon (\partial_x u)^3 \right) \qquad \text{on } (t, x) \in \Sigma. \tag{6.5.4c}$$

Existence theorem

Consider the quasilinear parabolic equation

$$\partial_t u - \partial_x a(t,x,u,\nabla u) = 0 \qquad \text{for } (t,x) \in Q, \tag{6.5.5a}$$
$$n(x) \cdot a(t,x,u,\nabla u) = 0 \qquad \text{for } (t,x) \in \Sigma, \tag{6.5.5b}$$
$$u(0,x) = u_0(x) \qquad \text{for } x \in \Omega, \tag{6.5.5c}$$

where n denotes the unit outward normal to Γ.

Let us denote the zero-mean subspace of $W^{q,p}(\Omega)$ by

$$W^{q,p}_\diamondsuit(\Omega) := \{u \in W^{q,p}(\Omega) : u_\Omega = 0\},$$

that is a reflexive, separable Banach space iff $W^{q,p}(\Omega)$ is one. It is equipped with the usual Sobolev norm

$$\|\cdot\|_{W^{q,p}_\diamondsuit(\Omega)} = \|\cdot\|_{W^{q,p}(\Omega)}.$$

We call $u \in W^{1,p,p'}(I; W^{1,p}_\diamondsuit(\Omega), W^{1,p}_\diamondsuit(\Omega)^*)$ a weak solution of (6.5.5) if it fulfills the weak formulation

$$\int_\Omega \partial_t u \cdot v \,\mathrm{d}x + \int_\Omega a(t,x,u,\partial_x u) \cdot \partial_x v(x) \,\mathrm{d}x = 0 \tag{6.5.6}$$

for all $v \in W^{1,p}_\diamondsuit(\Omega)$, for almost all $t \in I$ and $u(0,x) = u_0(x)$.

The condition on the embedding and integrability coefficients are

$$p^{\hat{*}} = 3p, \qquad p^{\hat{\#}} = 3p-2, \qquad p' = \frac{p}{p-1},$$
$$p^* = \infty, \qquad p^\# = \infty,$$

for one-dimensional domains and $p > \frac{4}{3}$.

We use a proposition for the existence of second order quasilinear equations due to Roubicek [109], which is based on the ideas presented in Section 6.4. However, we have to allow an additional constant in the coercivity assumption. Additionally, we reformulate the semi-coercivity in integral form, so we can use the Poincaré inequality when we apply it to equation (6.5.4).

Proposition 6.11 (Existence of a weak solution)**.** *Let*

$$a : Q \times (\mathbb{R} \times \mathbb{R}^n) \to \mathbb{R}^n,$$

be a Carathéodory mapping. Let $a : Q \times \mathbb{R} \times \mathbb{R}^n \to \mathbb{R}$ satisfy the Leray-Lions condition

$$(a(t,x,r,s) - a(t,x,r,\tilde{s})) \cdot (s - \tilde{s}) \geq 0,$$
$$(a(t,x,r,s) - a(t,x,r,\tilde{s})) \cdot (s - \tilde{s}) = 0 \Rightarrow s = \tilde{s}.$$

Let the coercivity assumption

$$\int_0^L a(t,x,v,\partial_x v)\partial_x v \,\mathrm{d}x \geq c_0 \|\partial_x v\|^p_{L^p(\Omega)} - c_1(t)\|\partial_x v\|_{L^p(\Omega)} - c_2(t)\|v\|^2_{L^2(\Omega)} - c_3,$$

hold for all $v \in W^{1,p}_{\Diamond}(\Omega)$ *with* $c_0 > 0$, $c_1 \in L^{p'}(I)$, $c_2 \in L^1(I)$ *and* $c_3 > 0$. *Let for some* $\varepsilon_1 > 0$, $c_4 < \infty$ *the growth condition*

$$\exists \gamma \in L^{p'}(Q): \qquad |a(t,x,r,s)| \le \gamma(t,x) + c_4 |r|^{(p^\ast - \varepsilon_1)/p'} + c_4 |s|^{p-1},$$

hold and let $u_0 \in L^2(\Omega)$ *with zero-mean. Then, the initial-boundary-value problem* (6.5.5) *has a weak solution* (6.5.6).

Proof. This is just a special case of Proposition 8.40 in [109] stated with the semi-coercivity condition as used in the proof of Proposition 8.40, but with an additional positive constant c_3. The semi-coercivity condition is only used in the proof of Lemma 8.8 in [109]. There, we only need to add the constant c_3 to ζ_k and the rest of the proof stays exactly the same, cf. page 222 and 223 in [109]. □

Next, we show existence of solutions for equation (6.5.1) using Proposition 6.11.

Theorem 6.12. *There exists a solution* $u \in W^{1,4,4/3}(I, W^{1,4}_{\Diamond}(\Omega), W^{1,4}_{\Diamond}(\Omega)^*)$ *of*

$$\int_\Omega \partial_t u \cdot v \,\mathrm{d}x + \int_\Omega \left(\frac{1}{3} |u + h_\Omega|^3 \tilde{Y}_s^2 \frac{3 - \tilde{Y}_s}{2} (\partial_x u - S) + \varepsilon (\partial_x u)^3 \right) \partial_x v \,\mathrm{d}x = 0$$

for all $v \in W^{1,4}_{\Diamond}(\Omega)$, *for almost all* $t \in I$, *with initial condition* $u(0,x) = u_0(x) \in L^2(\Omega)$ *with zero-mean and no-flux boundary conditions*

$$\boldsymbol{n} \cdot \left(\frac{1}{3} |u + h_\Omega|^3 \tilde{Y}_s^2 \frac{3 - \tilde{Y}_s}{2} (S - \partial_x u) - \varepsilon (\partial_x u)^3 \right) = 0, \qquad \text{on } \Gamma.$$

Proof. In order to use Proposition 6.11, we choose $p = 4$ and

$$a(t,x,r,s) = \frac{1}{3} |r + h_\Omega|^3 f(\tilde{Y}_s)(s - S) + \varepsilon s^3, \qquad f(w) = w^2 \frac{3 - w}{2},$$

where

$$\tilde{Y}_s(r,s) = \begin{cases} \max\left(1 - \frac{2B}{|r + h_\Omega||s - S|}, 0\right) & \text{for } (r + h_\Omega)(s - S) \neq 0 \\ 0 & \text{otherwise,} \end{cases}$$

Thus, we have to show the properties for $a : Q \times \mathbb{R} \times \mathbb{R} \to \mathbb{R}$.

The function Y_s is continuous, since the concatenation of continuous functions is continuous. Thus, we just have to show that

$$g(r,s) = \frac{2B}{|r + h_\Omega||s - S|}$$

is continuous for $|r+h_\Omega||s-S| \geq 2B$. This is true, since for $\alpha_n \to \alpha \in \mathbb{R}$, $\beta_n \to \beta \in \mathbb{R}$, we have

$$\begin{aligned}
\left|\frac{1}{|\alpha||\beta|} - \frac{1}{|\alpha_n||\beta_n|}\right| &= \left|\frac{1}{|\alpha||\beta|} - \frac{1}{|\alpha||\beta_n|} + \frac{1}{|\alpha||\beta_n|} - \frac{1}{|\alpha_n||\beta_n|}\right| \\
&= \frac{1}{|\alpha|}\left|\frac{1}{|\beta|} - \frac{1}{|\beta_n|}\right| + \frac{1}{|\beta_n|}\left|\frac{1}{|\alpha|} - \frac{1}{|\alpha_n|}\right| \\
&= \frac{1}{|\alpha||\beta_n||\beta|}\Big||\beta_n| - |\beta|\Big| + \frac{1}{|\beta_n||\alpha_n||\alpha|}\Big||\alpha_n| - |\alpha|\Big| \\
&\leq C_1\Big||\beta| - |\beta_n|\Big| + C_2\Big||\alpha| - |\alpha_n|\Big| \\
&\to 0,
\end{aligned}$$

since the convergent sequences are bounded and $|\alpha_n||\beta_n| \geq 1$ implies $C \geq |\alpha_n| \geq \frac{1}{|\beta_n|}$, where C is a positive constant.

The function a is easily seen to be Carathéodory, since Y_s is continuous, so is a. Further, a does not directly depend on t and x, and for fixed r and s the function a is a finite constant. Since our domain is of finite size, every finite constant is measurable.

In order to show the Leray-Lions conditions, we first use the transformation $\xi_1 = s_1 - S$, so it becomes

$$\begin{aligned}
&\Big(\frac{1}{3}|r+h_\Omega|^3 f(\tilde{Y}_{\xi_1})\xi_1 - \frac{1}{3}|r+h_\Omega|^3 f(\tilde{Y}_{\xi_2})\xi_2\Big)(\xi_1-\xi_2) + \varepsilon(s_1^3 - s_2^3)(s_1 - s_2) \geq 0, \\
&\Big(\frac{1}{3}|r+h_\Omega|^3 f(\tilde{Y}_{\xi_1})\xi_1 - \frac{1}{3}|r+h_\Omega|^3 f(\tilde{Y}_{\xi_2})\xi_2\Big)(\xi_1-\xi_2) + \varepsilon(s_1^3 - s_2^3)(s_1 - s_2) = 0 \Rightarrow s_1 = s_2
\end{aligned}$$

where

$$\tilde{Y}_\xi(r,\xi) = \begin{cases} \max\left(1 - \frac{2B}{|r+h_\Omega||\xi|}, 0\right) & \text{for } (r+h_\Omega)\xi \neq 0, \\ 0 & \text{otherwise.} \end{cases}$$

In fact, due to $\varepsilon > 0$, the regularizing term is strictly monotone increasing. So we just have to show

$$\Big(f(\tilde{Y}_{\xi_1})\xi_1 - f(\tilde{Y}_{\xi_2})\xi_2\Big)(\xi_1 - \xi_2) \geq 0,$$

which is equivalent to $f(\tilde{Y}_\xi)\xi$ being (not necessarily strictly) monotone increasing. First, note $\tilde{Y}_\xi \in [0,1]$ and the polynomial $f(u)$ is positive and monotone increasing for $u \in [0,2]$. We consider two cases, i.e. $\xi \geq 0$ and $\xi \leq 0$. For non-negative ξ the function $\tilde{Y}_\xi$ is monotone increasing and for non-positive ξ it is monotone decreasing. Therefore, $f(\tilde{Y}_\xi)$ is also monotone increasing for $\xi > 0$ and monotone decreasing for $\xi < 0$. Then for $\xi_1 > \xi_2$ we have the three cases

$$\begin{aligned}
\xi_1, \xi_2 \geq 0 &: f(\tilde{Y}_{\xi_1})\xi_1 - f(\tilde{Y}_{\xi_2})\xi_2 \geq f(\tilde{Y}_{\xi_2})(\xi_1 - \xi_2) \geq 0 \\
\xi_1, \xi_2 \leq 0 &: f(\tilde{Y}_{\xi_1})\xi_1 - f(\tilde{Y}_{\xi_2})\xi_2 \geq f(\tilde{Y}_{\xi_1})(\xi_1 - \xi_2) \geq 0 \\
\xi_1 \geq 0, \xi_2 \leq 0 &: f(\tilde{Y}_{\xi_1})\xi_1 - f(\tilde{Y}_{\xi_2})\xi_2 \geq 0.
\end{aligned}$$

Therefore, $f(\tilde{Y}_\xi)\xi$ is monotone increasing and we have shown the Leray-Lions conditions.

Next, let us consider the coercivity condition. We denote by C_i a positive constant. Then, we have

$$a(t,x,r,s)\cdot s = \frac{1}{3}|r+h_\Omega|^3 f(\tilde{Y}_s)(s-S)s + \varepsilon s^4.$$

Clearly, only $(s-S)s$ can be negative with minimum $s = S/2$. Therefore, since $f(\tilde{Y}_s) \in [0,1]$, we have the estimate

$$\begin{aligned} a(t,x,r,s)\cdot s &\geq \varepsilon s^4 - \frac{S^2}{12}|r+h_\Omega|^3 \\ &\geq \varepsilon s^4 - C_1|r|^3 - C_2 h_\Omega^3. \end{aligned}$$

Young's inequality gives

$$a(t,x,r,s)\cdot s \geq \varepsilon s^4 - \frac{C_3}{\delta^2}r^2 - \delta^2 C_4 r^4 - C_2 h_\Omega^3,$$

where $\delta > 0$ can be chosen arbitrary. Integration yields

$$\begin{aligned} \int_0^L a(t,x,v,\partial_x v)\partial_x v \,\mathrm{d}x &\geq \int_0^L \varepsilon|\partial_x v|^4 - \frac{C_3}{\delta^2}|v|^2 - \delta^2 C_4|v|^4 - C_2 h_\Omega^3 \,\mathrm{d}x \\ &= \varepsilon\|\partial_x v\|_{L^4(\Omega)}^4 - \frac{C_3}{\delta^2}\|v\|_{L^2(\Omega)}^2 - \delta^2 C_4\|v\|_{L^4(\Omega)}^4 - C_2 h_\Omega^3. \end{aligned}$$

Since v is from a space with zero mean, the Poincaré inequality is

$$\|v\|_{L^4(\Omega)} \leq C\|\partial_x v\|_{L^4(\Omega)},$$

which yields

$$\int_0^L a(t,x,v,\partial_x v)\partial_x v \,\mathrm{d}x \geq \varepsilon\|\partial_x v\|_{L^4(\Omega)}^4 - \frac{C_3}{\delta^2}\|v\|_{L^2(\Omega)}^2 - \delta^2 C_5\|\partial_x v\|_{L^4(\Omega)}^4 - C_2 h_\Omega^3.$$

Now, choosing δ small enough such that

$$C_6 = \varepsilon - \delta^2 C_5 > 0$$

gives

$$\int_0^L a(t,x,v,\partial_x v)\partial_x v \,\mathrm{d}x \geq C_6\|\partial_x v\|_{L^4(\Omega)}^4 - C_7\|v\|_{L^2(\Omega)}^2 - C_2 h_\Omega^3,$$

which shows the coercivity condition to hold with $c_0 = C_6$, $c_1 = 0$, $c_2 = C_7$ and $c_3 = C_2 h_\Omega^3$. Concerning the growth condition, we note

$$|s|^1 \leq |s|^3 + 1 \quad \text{and} \quad |s|^2 \leq |s|^3 + 1$$

holds, so using Young's inequality and $|f(Y_s)| \leq 1$, we can estimate

$$\begin{aligned} |a(t,x,r,s)| &\leq \varepsilon|s|^3 + \frac{1}{3}|r+h_\Omega|^3|s-S| \\ &\leq \varepsilon|s|^3 + \frac{1}{6}|r+h_\Omega|^6 + \frac{1}{2}|s-S|^2 \\ &\leq \varepsilon|s|^3 + C_1|r|^6 + C_2|s|^3 + C_3 \end{aligned}$$

that is $\gamma = C_3$, $c_4 = \max(\varepsilon + C_2, C_1)$ and $\varepsilon_1 = 4$.

In conclusion we showed all assumptions for Proposition 6.11, which yields the existence and regularity of our solution. □

The existence of a solution u for (6.5.4) directly implies the existence of a solution h for (6.5.1) via the relation (6.5.3).

Remarks

In Theorem 6.12 we use two regularizations. In order to guarantee non-negativity of a, we use $|h|$ instead of h. Further, we introduced a regularization $\varepsilon > 0$, which is needed for growth condition and the coercivity of the operator.

The same regularizations are needed in proofs for the Newtonian case $Y_s \equiv 1$ for degenerate fourth order equations, cf. [13]. There, one can go to the limit $\varepsilon \to 0$ as the essential step is to bound the mobility $|h|^3$ uniformly, which is possible since the regularity of h does not depend on ε. Usually, non-negativity of h is shown using an entropy estimate for the equations, which for $\varepsilon \to 0$ yields a contradiction in case $h < 0$. However, our mobility depends on the second highest derivative $\partial_x h$, which is directly controlled by estimates based on the ε-regularization. Thus, for $\varepsilon \to 0$ we lose control of the derivatives and our estimates are not valid anymore.

Chapter 7

(Further) Reduced models

The full set of non-dimensional equations (2.4.1) models momentum and mass conservation of two fully miscible fluids. Nevertheless, a simple gedankenexperiment shows that the system can also model single-phase behavior. Suppose we use the multiphase model and set the solid volume fraction ϕ_s to zero. Then, system (2.4.1) becomes

$$\begin{aligned} \phi_f &\equiv 1, \\ \phi_s &\equiv 0, \\ \nabla \cdot \boldsymbol{u}_f &= 0, \\ \mathrm{Re}[\partial_t \boldsymbol{u}_f + \nabla \cdot (\boldsymbol{u}_f \otimes \boldsymbol{u}_f)] &= \Delta \boldsymbol{u}_f - \nabla p_f, \end{aligned}$$

which are the well-known single-phase incompressible Navier-Stokes equations. This motivates a systematic study of reduced models contained in the Eulerian-Eulerian multiphase model. These reduced models turn out to be models well-known from the literature. And it allows us to understand the connection between modeling choices of multiphase models and single-phase models. We also derive a drift-flux model similar to Section 3.3 for more general geometries and flows, which explicitly shows how the constitutive laws enter the drift-flux term. Additionally, the effect of gravitation is now being considered.

Having such a connection between multiphase and single-phase models, it would allow us to know which constitutive laws lead to unphysical behavior and how experimental results can lead to new modeling choices for multiphase models. On the other side, it also enhances the understanding of single-phase models, since additional mass transport of particles - a process that is naturally solved for in multiphase models - has often been hypothesized in single-phase models in form of an additional transport equation, but the terms involved have to be guessed by physical intuition, cf. Section 1.2. Therefore, finding connections between models, it helps in doing these choices.

7.1 Limit models

Firstly, we give a more general version of the derived system (2.4.1), where we do not specify the constitutive laws, but rather state the dependence of the laws on the free variables. Secondly, some reduced models are more familiar when one considers gravitation as a driving force, which we include in our general system. The derivation of the gravity term is given in Chapter 5 by an energetic principle for the Stokes equations and gives the body force term

$$\boldsymbol{f} = -g\nabla(y\cos\alpha - x\sin\alpha).$$

Using the same average process as in Section 2.2 for a domain Ω, it yields the system

$$\partial_t(\rho_f\phi_f) + \nabla\cdot(\rho_f\phi_f\boldsymbol{u}_f) = 0, \tag{7.1.1a}$$

$$\partial_t(\rho_f\phi_f\boldsymbol{u}_f) + \nabla\cdot(\rho_f\phi_f\boldsymbol{u}_f\otimes\boldsymbol{u}_f) - \nabla\cdot(\mu_f\phi_f(\nabla\boldsymbol{u}_f + \nabla\boldsymbol{u}_f{}^T))+ \tag{7.1.1b}$$
$$\phi_f\nabla p = -M(\boldsymbol{u}_f - \boldsymbol{u}_s) - g\rho_f\phi_f\nabla(y\cos\alpha - x\sin\alpha),$$

$$\partial_t(\rho_s\phi_s) + \nabla\cdot(\rho_s\phi_s\boldsymbol{u}_s) = 0, \tag{7.1.1c}$$

$$\partial_t(\rho_s\phi_s\boldsymbol{u}_s) + \nabla\cdot(\rho_s\phi_s\boldsymbol{u}_s\otimes\boldsymbol{u}_s) - \nabla\cdot(\mu_s\phi_s(\nabla\boldsymbol{u}_s + \nabla\boldsymbol{u}_s{}^T))+ \tag{7.1.1d}$$
$$\phi_s\nabla p + \nabla p_c = M(\boldsymbol{u}_f - \boldsymbol{u}_s) - g\rho_s\phi_s\nabla(y\cos\alpha - x\sin\alpha),$$

where we assume

$$\rho_s = \text{const.}, \qquad \rho_f = \text{const.}, \qquad g = \text{const.}, \qquad \alpha = \text{const.}, \qquad \phi_s + \phi_f = 1,$$

as well as μ_s, μ_f, p_c and M are functions of the solid volume fraction ϕ_s and p_c depends additionally on the solid velocity $\boldsymbol{u}_s$. The functions μ_s and μ_f represent the constitutive laws for the solid and fluid viscosity, respectively. The function M is called momentum-coupling term as a large value in M represents a strong exchange of momentum between the two phases and we chose $\boldsymbol{M}_s^d = M\boldsymbol{w}$, cf. Section 2.3. The function p_c is the collision pressure discussed in Section 2.2 and represents the difference between fluid and solid pressure. It might depend on the solid velocity, which in turn might create a Bingham like character as we have seen in Chapter 3. Typical choices for p_c are listed in Section 2.3.

We assume no-slip boundary condition

$$\boldsymbol{u}_s = \boldsymbol{u}_f = \boldsymbol{0} \qquad \text{on } \partial\Omega,$$

but are mostly interested in the bulk equations in our derivations.

For reductions with a strong coupling between the solid and fluid velocity, such that their difference is small, it has been shown to be beneficial, cf. Section 3.3, to rewrite system (7.1.1) in the volumetric mixture velocity $\boldsymbol{v}$ and the difference velocity $\boldsymbol{w}$ defined as

$$\boldsymbol{v} = \phi_f\boldsymbol{u}_f + \phi_s\boldsymbol{u}_s,$$
$$\boldsymbol{w} = \boldsymbol{u}_f - \boldsymbol{u}_s.$$

Let us further define the mixture viscosity and density as

$$\rho = \phi_f\rho_f + \phi_s\rho_s,$$
$$\mu = \phi_f\mu_f + \phi_s\mu_s.$$

Next, we can deduce equations in $\boldsymbol{v}$ and $\boldsymbol{w}$, i.e.

$$\nabla \cdot \boldsymbol{v} = 0, \tag{7.1.2a}$$

$$\frac{\partial \phi_f}{\partial t} + \boldsymbol{v} \cdot \nabla \phi_f + \nabla \cdot (\phi_f \phi_s \boldsymbol{w}) = 0, \tag{7.1.2b}$$

$$\begin{aligned} &\frac{\partial}{\partial t}(\rho \boldsymbol{v} + \phi_f \phi_s (\rho_f - \rho_s)\boldsymbol{w}) + \nabla \cdot (\rho \boldsymbol{v} \otimes \boldsymbol{v} + (\rho_f - \rho_s)\phi_f \phi_s (\boldsymbol{v} \otimes \boldsymbol{w} + \boldsymbol{w} \otimes \boldsymbol{v})) \\ &+\nabla \cdot (\phi_f \phi_s (\rho_s \phi_f + \rho_f \phi_s)\boldsymbol{w} \otimes \boldsymbol{w}) - \nabla \cdot (\mu[(\nabla \boldsymbol{v} + \nabla \boldsymbol{v}^T) - (\nabla \phi_f \otimes \boldsymbol{w} + \boldsymbol{w} \otimes \nabla \phi_f)] \\ &\quad +\phi_f \phi_s (\mu_f - \mu_s)(\nabla \boldsymbol{w} + \nabla \boldsymbol{w}^T)) + \nabla p + \nabla p_c(\phi_s, \boldsymbol{v} - \phi_f \boldsymbol{w}) = -g\rho \nabla (y \cos\alpha - x \sin\alpha), \end{aligned} \tag{7.1.2c}$$

$$\begin{aligned} &\rho_f \rho_s \phi_f \phi_s \frac{\partial \boldsymbol{w}}{\partial t} + \rho_f \rho_s \phi_f \phi_s [(1 - 2\phi_f)\boldsymbol{w} \cdot \nabla \boldsymbol{w} - (\nabla \phi_f \cdot \boldsymbol{w})\boldsymbol{w} + \boldsymbol{v} \cdot \nabla \boldsymbol{w} + \boldsymbol{w} \cdot \nabla \boldsymbol{v}] \\ &\quad -\rho_s \phi_s \nabla \cdot (\mu_f \phi_f [\nabla \boldsymbol{v} + \nabla \boldsymbol{v}^T + \nabla \phi_s \otimes \boldsymbol{w} + \boldsymbol{w} \otimes \nabla \phi_s + (\nabla \boldsymbol{w} + \nabla \boldsymbol{w}^T)\phi_s]) \\ &\quad +\rho_f \phi_f \nabla \cdot (\mu_s \phi_s [\nabla \boldsymbol{v} + \nabla \boldsymbol{v}^T - \nabla \phi_f \otimes \boldsymbol{w} - \boldsymbol{w} \otimes \nabla \phi_f - (\nabla \boldsymbol{w} + \nabla \boldsymbol{w}^T)\phi_f]) \\ &\quad +(\rho_s - \rho_f)\phi_f \phi_s \nabla p - \phi_f \rho_f \nabla p_c(\phi_s, \boldsymbol{v} - \phi_f \boldsymbol{w}) = -\rho M \boldsymbol{w}, \end{aligned} \tag{7.1.2d}$$

where we used

$$\begin{aligned} (7.1.2c) &= (7.1.1b) + (7.1.1d), \\ (7.1.2d) &= \phi_s \rho_s (7.1.1b) - \phi_f \rho_f (7.1.1d). \end{aligned}$$

The no-slip boundary condition becomes

$$\boldsymbol{v} = \boldsymbol{w} = \boldsymbol{0} \qquad \text{on } \partial\Omega.$$

As can be seen from system (7.1.2) the volumetric mixture velocity is exactly divergence free, which is the reason we call this an incompressible multiphase system. Further, the difference velocity $\boldsymbol{w}$ is directly related to the drift flux velocity via

$$\boldsymbol{u}_d = \boldsymbol{u}_s - \boldsymbol{v} = -\phi_f \boldsymbol{w},$$

see Section 1.2 and [61]. Models that are traditionally associated with a drift flux, allow an easier derivation in these new velocities. Since drift flux models are suited for fluids with a strong momentum coupling between phases, one expects $\boldsymbol{w}$ to be much smaller than $\boldsymbol{v}$, whereas $\boldsymbol{u}_s$ and $\boldsymbol{u}_f$ are of similar order. This permits an asymptotic ansatz in the $\boldsymbol{v}/\boldsymbol{w}$ variables, whereas the same ansatz does not work in the original phasic velocities.

Non-dimensionalization and asymptotic ansatz

As in Section 2.4 we introducing the non-dimensional Reynolds, Darcy, density ratio and Froude numbers defined as

$$\mathrm{Re} = \frac{UL\rho_f}{\mu_n}, \qquad \mathrm{Da} = \frac{L^2}{K}, \qquad \mathrm{R} = \frac{\rho_s}{\rho_f}, \qquad \mathrm{Fr} = \frac{U^2}{gL}$$

and using the scales

$$\begin{aligned} x &= Lx', & y &= Ly', & z &= Lz', \\ t &= \frac{L}{U}t', & \boldsymbol{u}_k &= U\boldsymbol{u}_k', & p &= \frac{U\mu_n}{L}p', \end{aligned}$$

for the variables and

$$M = \frac{\mu_n}{K} M', \qquad p_c = \frac{U\mu_n}{L} {p_c}', \qquad \mu_f = \mu_n \mu_f', \qquad \mu_s = \mu_n \mu_s',$$

for the functions and we transform (7.1.1) into

$$\partial_t \phi_f + \nabla \cdot (\phi_f \boldsymbol{u}_f) = 0, \tag{7.1.3a}$$

$$\mathrm{Re}[\partial_t(\phi_f \boldsymbol{u}_f) + \nabla \cdot (\phi_f \boldsymbol{u}_f \otimes \boldsymbol{u}_f)] - \nabla \cdot (\mu_f \phi_f (\nabla \boldsymbol{u}_f + \nabla {\boldsymbol{u}_f}^T)) + \tag{7.1.3b}$$
$$\phi_f \nabla p = -\mathrm{Da}\, M(\boldsymbol{u}_f - \boldsymbol{u}_s) - \frac{\mathrm{Re}}{\mathrm{Fr}} \phi_f \nabla (y \cos\alpha - x \sin\alpha),$$

$$\partial_t \phi_s + \nabla \cdot (\phi_s \boldsymbol{u}_s) = 0, \tag{7.1.3c}$$

$$\mathrm{Re}\,\mathrm{R}[\partial_t(\phi_s \boldsymbol{u}_s) + \nabla \cdot (\phi_s \boldsymbol{u}_s \otimes \boldsymbol{u}_s)] - \nabla \cdot (\mu_s \phi_s (\nabla \boldsymbol{u}_s + \nabla {\boldsymbol{u}_s}^T)) + \tag{7.1.3d}$$
$$\phi_s \nabla p + \nabla p_c = \mathrm{Da}\, M(\boldsymbol{u}_f - \boldsymbol{u}_s) - \frac{\mathrm{Re}\,\mathrm{R}}{\mathrm{Fr}} \phi_s \nabla (y \cos\alpha - x \sin\alpha),$$

where we dropped the primes of the non-dimensional variables. The non-dimensional boundary conditions are the same as the dimensional one. Doing the same procedure for equation (7.1.2) with the additional scales

$$w = U w', \qquad v = U v', \qquad \mu = \mu_n \mu', \qquad \rho = \rho_f \rho',$$

yields

$$\nabla \cdot \boldsymbol{v} = 0, \tag{7.1.4a}$$

$$\frac{\partial \phi_f}{\partial t} + \boldsymbol{v} \cdot \nabla \phi_f + \nabla \cdot (\phi_f \phi_s \boldsymbol{w}) = 0, \tag{7.1.4b}$$

$$\mathrm{Re}\Big[\frac{\partial}{\partial t}(\rho \boldsymbol{v} + \phi_f \phi_s (1 - \mathrm{R}) \boldsymbol{w}) + \nabla \cdot (\rho \boldsymbol{v} \otimes \boldsymbol{v} + (1 - \mathrm{R}) \phi_f \phi_s (\boldsymbol{v} \otimes \boldsymbol{w} + \boldsymbol{w} \otimes \boldsymbol{v})) \tag{7.1.4c}$$
$$+ \nabla \cdot (\phi_f \phi_s (\mathrm{R}\,\phi_f + \phi_s) \boldsymbol{w} \otimes \boldsymbol{w})\Big] - \nabla \cdot (\mu [(\nabla \boldsymbol{v} + \nabla \boldsymbol{v}^T) - (\nabla \phi_f \otimes \boldsymbol{w} + \boldsymbol{w} \otimes \nabla \phi_f)]$$
$$+ \phi_f \phi_s (\mu_f - \mu_s)(\nabla \boldsymbol{w} + \nabla \boldsymbol{w}^T)) + \nabla p + \nabla p_c(\phi_s, \boldsymbol{v} - \phi_f \boldsymbol{w}) = -\frac{\mathrm{Re}}{\mathrm{Fr}} \rho \nabla (y \cos\alpha - x \sin\alpha),$$

$$\mathrm{Re}\,\mathrm{R}\Big[\phi_f \phi_s \frac{\partial \boldsymbol{w}}{\partial t} + \phi_f \phi_s [(1 - 2\phi_f) \boldsymbol{w} \cdot \nabla \boldsymbol{w} - (\nabla \phi_f \cdot \boldsymbol{w}) \boldsymbol{w} + \boldsymbol{v} \cdot \nabla \boldsymbol{w} + \boldsymbol{w} \cdot \nabla \boldsymbol{v}]\Big] \tag{7.1.4d}$$
$$- \mathrm{R}\,\phi_s \nabla \cdot (\mu_f \phi_f [\nabla \boldsymbol{v} + \nabla \boldsymbol{v}^T + \nabla \phi_s \otimes \boldsymbol{w} + \boldsymbol{w} \otimes \nabla \phi_s + (\nabla \boldsymbol{w} + \nabla \boldsymbol{w}^T) \phi_s])$$
$$+ \phi_f \nabla \cdot (\mu_s \phi_s [\nabla \boldsymbol{v} + \nabla \boldsymbol{v}^T - \nabla \phi_f \otimes \boldsymbol{w} - \boldsymbol{w} \otimes \nabla \phi_f - (\nabla \boldsymbol{w} + \nabla \boldsymbol{w}^T) \phi_f])$$
$$+ (\mathrm{R} - 1) \phi_f \phi_s \nabla p - \phi_f \nabla p_c(\phi_s, \boldsymbol{v} - \phi_f \boldsymbol{w}) = -\rho \mathrm{Da}\, M \boldsymbol{w}.$$

Just as in the previous non-dimensionalization, the boundary conditions do not change compared to the dimensional one.

The two systems (7.1.3) and (7.1.4) contain the non-dimensional parameters Re, Da, r and Fr as well as the freedom in the unspecified functions μ_s, μ_f, p_c, M. All of these parameters can be large or small relative to each other, depending purely on the fluid and problem under consideration. Even more freedom can be gained by considering certain domain and flow properties, e.g. very thin flows or time dependent changes. Hence, we do not try to give an exhaustive list of all possible

u_f/u_s variables / v/w variables	$\phi_s \sim \varepsilon$	$\phi_s \sim 1$ $\phi_s \neq \phi_{crit} - o(1)$	$\phi_s = \phi_{crit} - o(1)$
$\mathrm{Da} = \varepsilon^{\beta}$	dilute suspension (Stokes settling)	weak coupling	concentrated suspension (two-pressure system)
$\mathrm{Da} = 1$	dilute suspension (Stokes settling)	Full model	concentrated suspension
$\mathrm{Da} = \varepsilon^{-\beta}$	dilute suspension (Stokes settling)	Drift flux model	Darcy's law

Table 7.1: Overview of asymptotic regimes depending on momentum coupling and volume fraction in the multiphase model, where β denotes a positive constant and ε an asymptotic small, positive value.

reductions, but concentrate on the size of the solid volume fraction ϕ_s, the momentum coupling term M and the typical domain size ratio L/H. Figure 7.1 shows a graphical representation of the different regimes, we like to discuss first.

We use asymptotic expansions of the scalar variables ϕ_s, ϕ_f, p, the velocities $\boldsymbol{u}_s, \boldsymbol{u}_f$ or $\boldsymbol{w}, \boldsymbol{v}$ and of the functions μ_s, μ_f, p_c and M in the following sections. For a function $f(t,x) \sim \varepsilon^{\beta}$ with $\beta \in \mathbb{R}$, we use the asymptotic series expansion, cf. [36],

$$f(t,x) = \sum_{k=0}^{N} \varepsilon^{k+\beta} f_k(t,x) + o(\varepsilon^{N+\beta}), \tag{7.1.5}$$

where $f_k = O(1)$. For the sake of clarity, we assume the functions μ_s and p_c have the same asymptotic behavior for $\phi_s \to \phi_{\mathrm{crit}}$. In some cases we look at the boundary layer problem

$$\phi_s = \phi_{\mathrm{crit}} - o(1),$$

in which case we use the expansion

$$\phi_s = \phi_{\mathrm{crit}} - \sum_{k=0}^{N} \varepsilon^{k+1} \phi_{sk}(t,x) + o\left(\varepsilon^{N+1}\right).$$

General drift flux model

Consider the scales

$$\phi_s \sim 1, \qquad \phi_s \neq \phi_{\text{crit}} - o(1), \qquad \text{Da} = \varepsilon^{-1}$$

and take $p_c, \mu_s \sim 1$. Further, assume negligible inertial and order one gravity contributions, i.e. $\text{Re} = O(\varepsilon^2)$, $\text{Re}/\text{Fr} \sim 1$. Then, using an expansion ansatz in equation (7.1.4) yields to leading order

$$\boldsymbol{w}_0 = 0, \tag{7.1.6a}$$
$$\nabla \cdot \boldsymbol{v}_0 = 0, \tag{7.1.6b}$$
$$-\nabla \cdot (\mu_0(\nabla \boldsymbol{v}_0 + \nabla \boldsymbol{v}_0^T)) + \nabla p_0 + \nabla p_{c0} = -\frac{\text{Re}}{\text{Fr}} \rho_0 \nabla(y \cos\alpha - x \sin\alpha), \tag{7.1.6c}$$
$$\partial_t \phi_{s0} + \boldsymbol{v}_0 \nabla \phi_{s0} = \frac{D\phi_s}{Dt} = 0. \tag{7.1.6d}$$

These are the single-phase Stokes equations, where the solid volume fraction ϕ_s acts as a domain indicator function. System (7.1.6) misses the ability to simulate an accumulation of solids or fluids in parts of the domain. For example, consider a constant solid volume fraction $\phi_s \equiv 1/2$ for $\boldsymbol{x} \in \Omega(0)$ with $\phi_{\text{crit}} > 0.5$. Then, the solid volume fraction stays $\phi_s \equiv 1/2$ for all $\boldsymbol{x} \in \Omega(t)$. In order to add the ability to vary the volume fraction in the domain, we consider the next order approximation, which is

$$\begin{aligned} -\text{R}\,\phi_{s0} \nabla \cdot (\mu_{f0}(1-\phi_{s0})[\nabla \boldsymbol{v}_0 + \nabla \boldsymbol{v}_0^T]) + (1-\phi_{s0}) \nabla \cdot (\mu_{s0}\phi_{s0}[\nabla \boldsymbol{v}_0 + \nabla \boldsymbol{v}_0^T]) \\ +(\text{R}-1)(1-\phi_{s0})\phi_{s0}\nabla p_0 - (1-\phi_{s0})\nabla p_{c0} = -\rho_0 M_0 \boldsymbol{w}_1, \end{aligned} \tag{7.1.7a}$$

$$\begin{aligned} -\nabla \cdot (\mu_0(\nabla \boldsymbol{v}_1 + \nabla \boldsymbol{v}_1^T)) + \nabla p_1 + \nabla p_{c1} = -\frac{\text{Re}}{\text{Fr}} \rho_1 \nabla(y \cos\alpha - x \sin\alpha) \\ +\nabla \cdot (\nabla \phi_{s0} \otimes \boldsymbol{w}_1 + \boldsymbol{w}_1 \otimes \nabla \phi_{s0}) + \nabla \cdot (\mu_1(\nabla \boldsymbol{v}_0 + \nabla \boldsymbol{v}_0^T)) \\ +\nabla \cdot (\phi_{s0}(1-\phi_{s0})(\mu_f - \mu_s)(\nabla \boldsymbol{w}_1 + \nabla \boldsymbol{w}_1^T)), \end{aligned} \tag{7.1.7b}$$

$$\nabla \cdot \boldsymbol{v}_1 = 0, \tag{7.1.7c}$$
$$\partial_t \phi_{s1} + \boldsymbol{v}_1 \cdot \nabla \phi_{s0} + \boldsymbol{v}_0 \cdot \nabla \phi_{s1} = \nabla \cdot (\phi_{s0}(1-\phi_{s0})\boldsymbol{w}_1). \tag{7.1.7d}$$

In order to compute the next time step, we first solve for $\boldsymbol{v}_0$ via an incompressible Stokes system (7.1.6c), and then for $\boldsymbol{w}_1$ via the algebraic relation (7.1.7a). Next, we get $\boldsymbol{v}_1$ via another incompressible system (7.1.7b) and finally we use the transport equations (7.1.6d) and (7.1.7d) to update ϕ_{s0} and ϕ_{s1}.

Equation (7.1.7d) allows for the transport of solids just like the leading order equation (7.1.6d), but additionally contains the left hand side term, which produces accumulations of solid or fluid in the domain. In order to see this, we substitute $\boldsymbol{w}_1$ in transport equation (7.1.7d) with equation

(7.1.7a), which gives

$$\begin{aligned}\partial_t\phi_{s1} + \boldsymbol{v}_1\cdot\nabla\phi_{s0} + \boldsymbol{v}_0\cdot\nabla\phi_{s1} = -\nabla\cdot\Bigg(\frac{\phi_{s0}(1-\phi_{s0})}{\rho_0 M_0}\Bigg[&-\rho_s\phi_{s0}\nabla\cdot(\mu_f(1-\phi_{s0})(\nabla\boldsymbol{v}_0+\nabla\boldsymbol{v}_0^T))\\&+\rho_f(1-\phi_{s0})\nabla\cdot(\mu_s\phi_{s0}(\nabla\boldsymbol{v}_0+\nabla\boldsymbol{v}_0^T))\\&+(\mathrm{R}-1)(1-\phi_{s0})\phi_{s0}\nabla p_0\\&-(1-\phi_{s0})\nabla p_{c0}\Bigg]\Bigg)\end{aligned}$$

The effect of gravity can be seen by a further substitution of the pressure p_0 from (7.1.6c), which yields

$$\begin{aligned}\partial_t\phi_{s1} + \boldsymbol{v}_1\cdot\nabla\phi_{s0} + \boldsymbol{v}_0\cdot\nabla\phi_{s1} = -\nabla\cdot\Bigg(\frac{\phi_{s0}(1-\phi_{s0})}{\rho_0 M_0}\Bigg[&-\mathrm{R}\,\phi_{s0}\nabla\cdot(\mu_f(1-\phi_{s0})(\nabla\boldsymbol{v}_0+\nabla\boldsymbol{v}_0^T))\\&+(1-\phi_{s0})\nabla\cdot(\mu_s\phi_{s0}(\nabla\boldsymbol{v}_0+\nabla\boldsymbol{v}_0^T))\\&+(\mathrm{R}-1)\phi_{s0}(1-\phi_{s0})\nabla\cdot(\mu(\nabla\boldsymbol{v}_0+\nabla\boldsymbol{v}_0^T))\\&-(1-\phi_{s0})\rho_0\nabla p_{c0}\\&-(\mathrm{R}-1)\phi_{s0}(1-\phi_{s0})\frac{\mathrm{Re}}{\mathrm{Fr}}\rho_0\nabla(y\cos\alpha - x\sin\alpha)\Bigg]\Bigg).\end{aligned}$$

For the special case $\mu_f = \mu_s$ we have

$$\begin{aligned}\partial_t\phi_{s1} + \boldsymbol{v}_1\cdot\nabla\phi_{s0} + \boldsymbol{v}_0\cdot\nabla\phi_{s1} = \nabla\cdot\Bigg(\frac{\phi_{s0}(1-\phi_{s0})}{M_0}\Bigg[&-\mu_f(\nabla\boldsymbol{v}_0+\nabla\boldsymbol{v}_0^T)\cdot\nabla\phi_{s0}\\&+(1-\phi_{s0})\nabla p_{c0}\\&+(R-1)\phi_{s0}(1-\phi_{s0})\frac{\mathrm{Re}}{\mathrm{Fr}}\nabla(y\cos\alpha - x\sin\alpha)\Bigg]\Bigg),\end{aligned}$$

which is easily seen to contain second derivatives of the leading order solid volume fraction ϕ_{s0}. The essential step in this derivation is to get a closed form for $\boldsymbol{w}$, which contains the drift-velocity

$$\boldsymbol{u}_d = -\phi_f\boldsymbol{w}$$

and can be used to close the transport equation for ϕ_s. See the discussion in Section 1.2 for the definition of the drift velocity and some typical usage.

The derivation of a drift flux model from the Eulerian-Eulerian model is already known from the literature, see e.g. [16, 60, 95]. Nevertheless, a formal asymptotic approach is missing. Nott et al. [95] derive their model for a unidirectional shear-flow without variations in x direction. Ishii et al. [60] derived the drift-flux model from an average process of the total mass, momentum and energy conservation, which gives different equations than we have derived above. Boyer [16] derived a drift-flux model for spinodal decomposition driven fluids by considering a particular set of parameters and neglected terms with small constants. There, Boyer proposes a different scaling, such that the inertial terms can be retained in the formulation. In essence the scales

$$\phi_s \sim 1, \qquad \phi_s \neq \phi_{\mathrm{crit}} - o(1), \qquad \mathrm{Da} = \varepsilon^{-1}, \qquad \boldsymbol{w} \sim \varepsilon^{\gamma}, \qquad \rho_s - \rho_f \sim \varepsilon^{\gamma}$$

are considered, with $\gamma \in]0,1[$, which yields the leading order system

$$\begin{aligned}
\nabla \cdot \boldsymbol{v}_0 &= 0, \\
\partial_t \phi_{f0} + \boldsymbol{v}_0 \cdot \nabla \phi_{f0} + \frac{1}{\mathrm{Pe}} \nabla \cdot (\phi_f \phi_s \boldsymbol{w}_0) &= 0, \\
\partial_t(\rho_0 \boldsymbol{v}_0) + \nabla \cdot (\rho_0 \boldsymbol{v}_0 \otimes \boldsymbol{v}_0) - \nabla \cdot (\mu_0(\nabla \boldsymbol{v}_0 + \nabla \boldsymbol{v}_0^T)) + \nabla p_0 + \nabla p_{c0} &= -g\rho_0 \nabla(y \cos\alpha - x \sin\alpha), \\
-\phi_{f0}\rho_f \nabla p_{c0} &= -\rho_0 M_0 \boldsymbol{w}_0.
\end{aligned}$$

But this system is not a leading order system in the transport equation, since an additional ε order is hidden in the Peclet number definition

$$\frac{1}{\mathrm{Pe}} = \varepsilon^\gamma.$$

Further, Boyer chooses the collision pressure p_c in form of a chemical potential, which yields the convective Cahn-Hilliard equation as the transport mechanism for ϕ_f [16].

Other limits

Besides the drift-flux model, the multiphase model contains a number of other interesting limits depending on the asymptotic scales of ϕ_s and Da. Well-known limits like Darcy's law, Stokes settling, single-phase Navier-Stokes equations and two-pressure models can be retrieved in this fashion as the following part shows.

Dilute suspension

Consider the scales

$$\phi_s \sim \varepsilon, \qquad \mathrm{Da} = \varepsilon^\gamma,$$

where $\gamma \in]-1,1[$. A $\gamma > 0$ represents weak and a $\gamma < 0$ strong coupling effects. As a suspension becomes more dilute its rheology approaches that of the liquid phase, i.e.

$$\lim_{\phi_s \to 0} \mu_s = \mu_f, \qquad \lim_{\phi_s \to 0} p_c = 0.$$

Thus, for a dilute suspension $\phi_s \sim \varepsilon$, we assume

$$\mu_{s0} = \mu_{f0}, \qquad p_{c0} \sim \varepsilon^\beta,$$

with $\beta \geq 1$ in the following derivation, which is consistent with our choices for the constitutive laws from Section 2.3. Not assuming these scales, would imply a nontrivial $\boldsymbol{w}_0$ term, which in turn couples with the $\boldsymbol{v}_0$ and it becomes much harder to see the basic physics of this regime.

Considering all these scales and substituting the appropriate asymptotic expansions into the $\boldsymbol{v}/\boldsymbol{w}$-system (7.1.4), the leading order approximation becomes

$$\boldsymbol{w}_0 = 0, \tag{7.1.8a}$$

$$\mathrm{Re}[\partial_t \boldsymbol{v}_0 + \nabla \cdot (\boldsymbol{v}_0 \otimes \boldsymbol{v}_0)] - \nabla \cdot (\mu_f(\nabla \boldsymbol{v}_0 + \nabla \boldsymbol{v}_0^T)) + \nabla p_0 = -\frac{\mathrm{Re}}{\mathrm{Fr}} \nabla(y \cos\alpha - x \sin\alpha), \tag{7.1.8b}$$

$$\nabla \cdot \boldsymbol{v}_0 = 0, \tag{7.1.8c}$$

$$\partial_t \phi_0 + \boldsymbol{v}_0 \cdot \nabla \phi_0 = 0, \tag{7.1.8d}$$

which shows a dilute suspension is described by the single-phase Navier-Stokes equations.

Suppose the flow takes place in a confined box with no-slip boundary conditions. Then, system (7.1.8) yields $\boldsymbol{v}_0 = 0$. Using the fact that $\boldsymbol{w}_0 = 0$ and $p_{c0} \sim \varepsilon^\beta$, the next order approximation of $\boldsymbol{w}$ is

$$-\mathrm{R}\phi_0 \nabla \cdot (\mu_f[\nabla \boldsymbol{v}_0 + \nabla \boldsymbol{v}_0^T]) + \nabla \cdot (\mu_f \phi_0 [\nabla \boldsymbol{v}_0 + \nabla \boldsymbol{v}_0^T]) + (\mathrm{R}-1)\phi_0 \nabla p_0 = -\varepsilon^\gamma M_0 \boldsymbol{w}_1. \quad (7.1.9)$$

Then, using equation (7.1.8b) the pressure becomes

$$\nabla p_0 = -\frac{\mathrm{Re}}{\mathrm{Fr}} \nabla (y \cos\alpha - x \sin\alpha).$$

Substitution of this term in equation (7.1.9) together with the fact that $\boldsymbol{v}_0 = 0$ yields

$$\boldsymbol{w}_1 = \frac{\mathrm{R}-1}{\varepsilon^\gamma M_0} \phi_0 \frac{\mathrm{Re}}{\mathrm{Fr}} \nabla (y \cos\alpha - x \sin\alpha).$$

Now suppose the solid and liquid phases have different densities, i.e. $\mathrm{R} \neq 1$. This implies a drift flux that segregates the solid and liquid phase, which is known as Stokes' settling velocity. Since, we have the relation

$$\boldsymbol{w}_1 \sim \frac{1}{M_0} \quad (7.1.10)$$

the momentum coupling term is sometimes chosen as the hindered settling term [95]. Mind, that depending on γ the settling is either fast or slow - corresponding to $\gamma > 0$ and $\gamma < 0$, respectively.

The case $\gamma \leq -1$ shifts this argument to higher order approximations with the leading orders all being zero. The case $\gamma \geq 1$ is more complicate, since $\boldsymbol{w}$ is not zero to leading order. Nevertheless, Darcy's number is usually a large value, rather than a very small one, since small Darcy's number correspond to huge particles, see below. If particles become too big, then scaling assumptions of the average operator needed for the derivation of the model might be infringed.

Equation (7.1.10) shows the direct connection between the momentum coupling M and settling of particles. Thus, some relations for M are based on the hindered settling function f, cf. [107], defined as

$$f(\phi_s) = (1 - \phi_s)^\alpha,$$

with common choices of $\alpha \in \{5, 5.1\}$. Recall from (1.1.6) that the volume fraction is defined as

$$\phi = \frac{nV_p}{V}$$

where n is the number of particles, V the cell volume and V_p is the volume of a single particle. Then, for spherical particles, we have

$$N := \frac{n}{V} = \frac{\phi_s}{V_p} = \frac{\phi_s}{4/3\pi a^3}, \quad (7.1.11)$$

where a is the radius of the particle and N is called the number density of particles. A common form of the momentum coupling term in use is

$$M = -6\pi\eta a N f^{-1}(\phi_s), \quad (7.1.12)$$

which is - using the appropriate form for f and (7.1.11) - equivalent to the constitutive law proposed by Morris et al. [88] as shown in Table 2.1. Further, equation (7.1.12) physically justifies our assumption of asymptotic large Da terms, since $aN \sim \frac{1}{a^2}$ and a is a very small number.

A note on the scaling assumptions contained in M. Let us assume a domain to particle ratio of

$$\frac{H^2}{a^2} = \varepsilon^{-\beta},$$

with H the characteristic height of the domain and a the radius of the particles. Further, we know from (7.1.11)

$$\phi_s = \frac{4}{3}\pi a^3 N = \frac{4}{3}\pi H^3 \varepsilon^{\frac{3}{2}\beta} N = \frac{4}{3}\pi \varepsilon^{\frac{3}{2}\beta}\varepsilon^{x},$$

where we assumed $N = \frac{\varepsilon^{\gamma}}{H^3}$. For a dilute suspension, i.e. $\phi_s = \varepsilon\phi_0$, we get $\gamma = -\frac{3}{2}\beta + 1$. Assuming the particles are much smaller than the domain, e.g. $\beta \approx 1$, this corresponds to $N \approx \varepsilon^{-1/2}$, which seems plausible as the number of particles is large even in the case of a dilute suspension. On the other side, if the considered particles are large relative to the domain, then we have very few particles. This could violate the continuum hypothesis of the macroscopic model or the scaling assumptions needed for the derivation of multiphase models using an average process.

Weak momentum coupling

Suppose the variables are of the orders

$$\phi_s \sim 1, \qquad \phi_s \neq \phi_{\text{crit}} - o(1), \qquad \text{Da} = \varepsilon^{\beta},$$

with $\beta > 0$ and the other variables are of order one. A small order in the momentum coupling term can be interpreted as a weak momentum transfer between the liquid and the solid phase. Thus, we expect the phase velocities to act independent and use formulation (7.1.1) for the asymptotic ansatz. Using the expansion ansatz (7.1.5) in system (7.1.3) yields to leading order

$$\begin{aligned}
\partial_t \phi_f + \nabla \cdot (\phi_f \boldsymbol{u}_f) &= 0, \\
\text{Re}[\partial_t(\phi_f \boldsymbol{u}_f) + \nabla \cdot (\phi_f \boldsymbol{u}_f \otimes \boldsymbol{u}_f)] - \nabla \cdot (\mu_f \phi_f (\nabla \boldsymbol{u}_f + \nabla \boldsymbol{u}_f{}^T)) + & \\
\phi_f \nabla p &= -\frac{\text{Re}}{\text{Fr}} \phi_f \nabla (y \cos\alpha - x \sin\alpha), \\
\partial_t \phi_s + \nabla \cdot (\phi_s \boldsymbol{u}_s) &= 0, \\
\text{Re}\,\text{R}[\partial_t(\phi_s \boldsymbol{u}_s) + \nabla \cdot (\rho_s \phi_s \boldsymbol{u}_s \otimes \boldsymbol{u}_s)] - \nabla \cdot (\mu_s \phi_s (\nabla \boldsymbol{u}_s + \nabla \boldsymbol{u}_s{}^T)) + & \\
\phi_s \nabla p + \nabla p_c &= -\frac{\text{Re}\,\text{R}}{\text{Fr}} \phi_s \nabla (y \cos\alpha - x \sin\alpha), \\
\phi_s + \phi_f &= 1
\end{aligned}$$

where we dropped the zeros at the indices. Although it looks like the two phases are not exchanging momentum to leading order anymore, there is still a highly nonlinear coupling in form of the incompressibility and the volume fraction condition, i.e.

$$\begin{aligned}
\nabla \cdot (\phi_s \boldsymbol{u}_s + \phi_f \boldsymbol{u}_f) &= 0, \\
\phi_s + \phi_f &= 1.
\end{aligned}$$

If we use the relation (compare with Section 2.3)

$$\mathrm{Da} \sim \frac{1}{a^2},$$

where a is the particle radius, then a very small momentum coupling term implies huge particles, which in turn could lead to a breakdown of the scale assumptions needed for the averaging ansatz in the derivation of our multiphase model. Thus, this regime might have no physical justification.

Concentrated suspension with weak momentum coupling

Since for $\phi_s \to \phi_{\mathrm{crit}}$ the functions μ_s, M and p_c might all contain singularities of different orders, it is not practical to list all possible leading order systems, here. We concentrate on the simplest example, where all the functions are of order one or μ_s contains the highest order singularity.

Suppose the variables are of the orders

$$\phi_s = \phi_{\mathrm{crit}} - o(1), \qquad \mathrm{Da} = \varepsilon^\beta,$$

with $\beta > 0$ and we choose the other variables and functions all of order one. Then, in the case $p_{c0}, \mu_s \sim 1$, we get the system

$$\nabla \cdot \boldsymbol{u}_f = 0, \tag{7.1.13a}$$

$$\mathrm{Re}[\partial_t \boldsymbol{u}_f + \nabla \cdot (\boldsymbol{u}_f \otimes \boldsymbol{u}_f)] - \mu_f \Delta \boldsymbol{u}_f + \nabla p = -\frac{\mathrm{Re}}{\mathrm{Fr}} \nabla (y \cos\alpha - x \sin\alpha), \tag{7.1.13b}$$

$$\nabla \cdot \boldsymbol{u}_s = 0, \tag{7.1.13c}$$

$$\mathrm{Re}\,\mathrm{R}[\partial_t \boldsymbol{u}_s + \nabla \cdot (\boldsymbol{u}_s \otimes \boldsymbol{u}_s)] - \mu_s \Delta \boldsymbol{u}_s + \nabla p + \frac{\nabla p_c}{\phi_{\mathrm{crit}}} = -\frac{\mathrm{Re}\,\mathrm{R}}{\mathrm{Fr}} \nabla (y \cos\alpha - x \sin\alpha), \tag{7.1.13d}$$

$$\phi_s = \phi_{\mathrm{crit}}, \tag{7.1.13e}$$

$$\phi_s + \phi_f = 1. \tag{7.1.13f}$$

Note, we have assumed $\mu_{s0}(\phi_{s0}), \mu_{f0}(\phi_{s0}) \sim 1$, here. Essentially, this excludes solid and liquid viscosities that contain singularities for $\phi_s \to \phi_{\mathrm{crit}}$.

Note, system (7.1.13) has no coupling of the two phases anymore. In contrast to Section 7.1 even the nonlinear coupling through the volume fraction and incompressibility vanishes to leading order. Through the vanishing of coupling between liquid and solid phase, the problem becomes overdetermined. As the volume fractions are set to a constant value, the free variables are $\boldsymbol{u}_s$, $\boldsymbol{u}_f$ and p. Yet, those three variables have to fulfill two incompressibility constraints (7.1.13a),(7.1.13c) and two momentum equations (7.1.13b),(7.1.13d). In general this system does not have a solution unless we take the collision pressure as $p_c = \phi_s(p_s - p)$, see definition (2.2.18), so the solid momentum equation becomes

$$\mathrm{Re}\,\mathrm{R}[\partial_t \boldsymbol{u}_s + \nabla \cdot (\boldsymbol{u}_s \otimes \boldsymbol{u}_s)] - \mu_s \Delta \boldsymbol{u}_s + \nabla p_s = -\frac{\mathrm{Re}\,\mathrm{R}}{\mathrm{Fr}} \nabla (y \cos\alpha - x \sin\alpha).$$

This highlights the problem of explicitly modeling the collision pressure p_c by a simple equation rather than using a second pressure explicitly as done in the two-pressure models, see e.g. [77].

For the case $p_c \sim 1$ and $\mu_s(\phi_{s0}) \sim \varepsilon^{-\gamma}$, $\mu_f \sim 1$ with $\gamma > 0$, we get

$$\begin{aligned}
\nabla \cdot \boldsymbol{u}_f &= 0, \\
\mathrm{Re}[\partial_t \boldsymbol{u}_f + \nabla \cdot (\boldsymbol{u}_f \otimes \boldsymbol{u}_f)] - \mu_f \Delta \boldsymbol{u}_f + \nabla p &= -\frac{\mathrm{Re}}{\mathrm{Fr}} \nabla (y \cos\alpha - x \sin\alpha), \\
\nabla \cdot \boldsymbol{u}_s &= 0, \\
\nabla \cdot (\mu_s (\nabla \boldsymbol{u}_s + \nabla \boldsymbol{u}_s{}^T)) &= 0, \\
\phi_s &= \phi_{\mathrm{crit}}, \\
\phi_s + \phi_f &= 1.
\end{aligned}$$

In contrast to (7.1.13) this system is not overdetermined, since the solid momentum and mass conservation equations constraint $\boldsymbol{u}_s$ to have purely rotational and translational motion. This system describes the transport of a pure solid and a liquid, that do not interact to leading order. Note, just as in Section 7.1 the physical justification for very small momentum coupling terms Da is controversial as this implies huge particles, which might imply a breakdown of the scaling assumptions for the used average.

Choosing Darcy's number to be of order one, $\mathrm{Da} = 1$, yields in essence the same behavior as described above, but with an additional momentum coupling term to leading order.

Darcy's law

Assume

$$\phi_s \sim \phi_{\mathrm{crit}}, \qquad p_c(\phi_s) \sim \varepsilon^{-\gamma}, \qquad \mu_s(\phi_s) \sim \varepsilon^{-\gamma}, \qquad p \sim \varepsilon^{-\beta}, \qquad \mathrm{Da} = \varepsilon^{-\beta}, \qquad \frac{\mathrm{Re}}{\mathrm{Fr}} = \varepsilon^{-\beta} C,$$

where $\gamma > \beta > 0$ and C is a positive constants.

Then, using the phasic velocity formulation (7.1.3), it yields to leading order

$$\begin{aligned}
\nabla \cdot \boldsymbol{u}_f &= 0, \\
\phi_f \nabla p_f &= -M_0 \boldsymbol{w} - \phi_f C \nabla (y \cos\alpha - x \sin\alpha), \qquad (7.1.14) \\
\nabla \cdot \boldsymbol{u}_s &= 0, \\
-\nabla \cdot (\mu_{s0} \phi_s (\nabla \boldsymbol{u}_s + \nabla \boldsymbol{u}_s{}^T)) + \nabla p_{c0} &= 0. \qquad (7.1.15)
\end{aligned}$$

Equation (7.1.15) is fulfilled for $\dot{\boldsymbol{\gamma}}_s = 0$. Thus, the solids perform stiff rotation and translations only. Rewriting (7.1.14) for $\boldsymbol{w}$ gives

$$\boldsymbol{w} = -\frac{\phi_f}{M_0} C \nabla (y \cos\alpha - x \sin\alpha) - \frac{\phi_f}{M_0} \nabla p_f. \qquad (7.1.16)$$

Assume $\boldsymbol{u}_s = \boldsymbol{0}$ and take the definition of the momentum coupling term from Chapter 2, i.e. $M = m\,{\phi_s}^2/\phi_f$ with m a positive constant. Then, rewriting equation (7.1.16) as the seepage velocity (1.2.5) it becomes

$$\bar{\boldsymbol{u}} = -\frac{{\phi_f}^3}{m\,{\phi_s}^2} (\nabla p_f + C \nabla (y \cos\alpha - x \sin\alpha)),$$

which for appropriate C and m is the non-dimensionalized Darcy's law with gravity, compare with equation (1.2.4) and (1.2.6).

7.2 Reduction to thin-film models

For the present discussion we confine ourself to the two-dimensional case in Cartesian coordinates. Let us denote by

$$\boldsymbol{v} = (v_x, v_y)^T, \qquad \boldsymbol{w} = (w_x, w_y)^T$$

the Cartesian velocity components and by

$$\boldsymbol{v}_i = (v_{xi}, v_{yi})^T, \qquad \boldsymbol{w}_i = (w_{xi}, w_{yi})^T$$

the components of the velocity expansions. Then, we use the scales

$$x = Lx', \qquad y = Hy',$$
$$t = \frac{L}{U}t', \qquad p = \frac{U\mu_n L}{H^2}p',$$

for the variables and

$$M = \frac{\mu_n}{K}M', \qquad p_c = \frac{U\mu_n}{H}{p_c}', \qquad \mu_f = \mu_n\mu_f', \qquad \mu_s = \mu_n\mu_s',$$

for the functions. The reason to scale p_c by $\frac{U\mu_n}{H}$ instead of $\frac{U\mu_n}{L}$ is that the standard form of the collision pressure is

$$p_c = g(\phi_s)|\dot{\boldsymbol{\gamma}}_s|,$$

where g is an arbitrary function of ϕ_s, often containing a singularity for $\phi_s \to \phi_{\text{crit}}$. Then, non-dimensionalization of $|\dot{\boldsymbol{\gamma}}_s|$ yields $\frac{U}{H}$ as largest scaling term. In the following we use a small parameter defined as

$$\varepsilon = \frac{H}{L}$$

and change the definition of Darcy's number as

$$\mathrm{Da} = \frac{H^2}{K} = \varepsilon^{-\beta},$$

where $\beta > 0$. The velocity must be scaled differently in x and y directions, due to the incompressibility condition. Hence, we use

$$v_x = Uv_x', \qquad v_y = \varepsilon U v_y',$$

and similar scales for the components of $\boldsymbol{w}$, $\boldsymbol{v}_i$ and $\boldsymbol{w}_i$. In fact we choose the velocity scale as quotient of gravity and viscous force, i.e.

$$U = \frac{g\rho_f \sin\alpha H^2}{\mu_f S},$$

where S is a positive constant expressing the influence of gravitation and is specified later on.

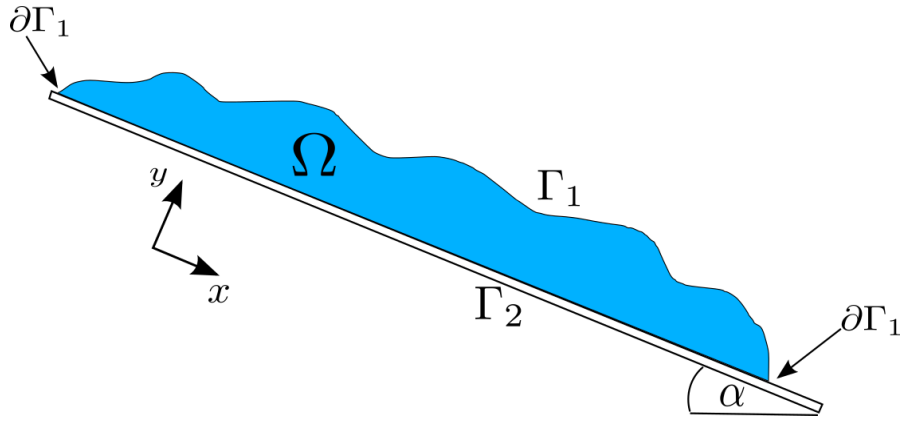

Figure 7.1: Shown is a visualization of the domain under consideration for the thin-film model discussion. The fluid is in domain Ω with Γ_1 and Γ_2 being the free-boundary and substrate, respectively. $\partial\Gamma_1$ is the set of all triple points, where fluid, substrate and air meet.

For the sake of readability, we denote the components of a quantity by an index before a comma and a derivative by an index after a comma in this section, i.e. we define

$$a_{b,c} := \partial_c a_b.$$

Dropping the primes, the momentum equations for the difference in velocity $\boldsymbol{w}$ become

$$\begin{aligned}
\varepsilon^2 \mathrm{Re}\,\mathrm{R}\phi_f\phi_s[\partial_t w_x + (1-2\phi_f)(w_x w_{x,x} + w_y w_{x,y}) - (\phi_{f,x} w_x + \phi_{f,y} w_y) w_x \\
+ v_x w_{x,x} + v_y w_{x,y} + w_x v_{x,x} + w_y v_{x,y}] \\
-\mathrm{R}\,\phi_s\varepsilon^2(2\mu_f\phi_f[v_{x,x} + \phi_{s,x} w_x + w_{x,x}\phi_s])_{,x} \\
-\mathrm{R}\,\phi_s(\mu_f\phi_f[v_{x,y} + \varepsilon^2 v_{y,x} + \varepsilon^2\phi_{s,x} w_y + w_x\phi_{s,y} + \phi_s(w_{x,y} + \varepsilon^2 w_{y,x})])_{,y} \\
+\phi_f\varepsilon^2(2\mu_s\phi_s[v_{x,x} - w_x\phi_{f,x} - w_{x,x}\phi_f])_{,x} \\
+\phi_f(\mu_s\phi_s[v_{x,y} + \varepsilon^2 v_{y,x} - \varepsilon^2\phi_{f,x} w_y - w_x\phi_{f,y} - \phi_f(w_{x,y} + \varepsilon^2 w_{y,x})])_{,y} \\
+(\mathrm{R}-1)\phi_f\phi_s p_{,x} - \phi_f\varepsilon p_c(\phi_s, \boldsymbol{v} - \phi_f\boldsymbol{w})_{,x} = -\frac{\rho}{\varepsilon^\beta} M w_x,
\end{aligned} \tag{7.2.1a}$$

and

$$\begin{aligned}
\varepsilon^3 \mathrm{Re}\,\mathrm{R}\phi_s\phi_f[\partial_t w_y + (1-2\phi_f)(w_x w_{y,x} + w_y w_{y,y}) - (\phi_{f,x} w_x + \phi_{f,y} w_y) w_y \\
v_x w_{y,x} + v_y w_{y,y} + w_x v_{y,x} + w_y v_{y,y}] \\
-\mathrm{R}\,\phi_s(\mu_f\phi_f[\varepsilon v_{x,y} + \varepsilon^3 v_{y,x} + \varepsilon\phi_{s,y} w_x + \varepsilon^3 w_y\phi_{s,x} + \phi_s(\varepsilon w_{x,y} + \varepsilon^3 w_{y,x})])_{,x} \\
-\mathrm{R}\,\phi_s\varepsilon(\mu_f\phi_f[2v_{y,y} + 2\phi_{s,y} w_y + 2w_{y,y}\phi_s])_{,y} \\
+\phi_f(\mu_s\phi_s[\varepsilon v_{x,y} + \varepsilon^3 v_{y,x} - \varepsilon\phi_{f,y} w_x - \varepsilon^3 w_y\phi_{f,x} - (\varepsilon w_{x,y} + \varepsilon^3 w_{y,x})\phi_f])_{,x} \\
+\phi_f\varepsilon(\mu_s\phi_s[2v_{y,y} - 2\phi_{f,y} w_y - 2w_{y,y}\phi_f])_{,y} \\
+\frac{\mathrm{R}-1}{\varepsilon}\phi_f\phi_s p_{,y} - \phi_f p_c(\phi_s, \boldsymbol{v} - \phi_f\boldsymbol{w})_{,y} = -\frac{\rho}{\varepsilon^{\beta-1}} M w_y,
\end{aligned} \tag{7.2.1b}$$

for the x and y component, respectively. Doing the same for the component-wise momentum equations of $\boldsymbol{v}$, it yields

$$\begin{aligned}
\varepsilon^2\mathrm{Re}[\partial_t(\rho v_x + \phi_f\phi_s(1-\mathrm{R})w_x) + (\rho v_x^2 + 2(1-\mathrm{R})\phi_f\phi_s v_x w_x)_{,x} \\
+(\rho v_x v_y + (1-\mathrm{R})\phi_f\phi_s(v_x w_y + v_y w_x))_{,y} \\
+(\phi_f\phi_s(\mathrm{R}\phi_f + \phi_s)w_x^2)_{,x} + (\phi_f\phi_s(\mathrm{R}\phi_f + \phi_s)w_x w_y)_{,y}] \\
-\varepsilon^2(\mu[2v_{x,x} - 2\phi_{f,x}w_x])_{,x} - (\mu[(v_{x,y} + \varepsilon^2 v_{y,x}) - (\varepsilon^2\phi_{f,x}w_y + w_x\phi_{f,y})])_{,y} \\
-\varepsilon^2(2\phi_f\phi_s(\mu_f - \mu_s)w_{x,x})_{,x} - (\phi_f\phi_s(\mu_f - \mu_s)(w_{x,y} + \varepsilon^2 w_{y,x}))_{,y} \\
+p_{,x} + \varepsilon p_c(\phi_s, \boldsymbol{v} - \phi_f\boldsymbol{w})_{,x} = \rho S,
\end{aligned} \tag{7.2.1c}$$

and

$$\begin{aligned}
\varepsilon^3\mathrm{Re}[\partial_t(\rho v_y + \phi_f\phi_s(1-\mathrm{R})w_y) + (\rho v_x v_y + (1-\mathrm{R})\phi_f\phi_s[v_x w_y + w_x v_y])_{,x} \\
+(\rho v_y^2 + 2(1-\mathrm{R})\phi_f\phi_s v_y w_y)_{,y} \\
+(\phi_f\phi_s(\mathrm{R}\,\phi_f + \phi_s)w_x w_y)_{,x} + (\phi_f\phi_s(\mathrm{R}\,\phi_f + \phi_s)w_y^2)_{,y}] \\
-(\mu[(\varepsilon v_{x,y} + \varepsilon^3 v_{y,x}) - (\varepsilon\phi_{f,y}w_x + \varepsilon^3 w_y\phi_{f,x})])_{,x} - \varepsilon(\mu[2v_{y,y} - 2\phi_{f,y}w_y])_{,y} \\
-(\phi_f\phi_s(\mu_f - \mu_s)(\varepsilon^3 w_{y,x} + \varepsilon w_{x,y}))_{,x} - \varepsilon(\phi_f\phi_s(\mu_f - \mu_s)2w_{y,y})_{,y} \\
+\frac{1}{\varepsilon}p_{,y} + p_c(\phi_s, \boldsymbol{v} - \phi_f\boldsymbol{w})_{,y} = -\rho S\cot\alpha.
\end{aligned} \tag{7.2.1d}$$

The incompressible condition (7.1.2a) becomes

$$\nabla\cdot\boldsymbol{v} = 0, \tag{7.2.1e}$$

and the transport equation (7.1.2b) gives

$$\partial_t\phi_s + \boldsymbol{v}\nabla\phi_s - \nabla\cdot(\phi_f\phi_s\boldsymbol{w}) = 0. \tag{7.2.1f}$$

We use the boundary conditions derived in Chapter 5, since we have a free-boundary at Γ_1. Thus, transformation of boundary conditions (5.3.6) into $\boldsymbol{v}/\boldsymbol{w}$ variables yields

$$\begin{aligned}
\boldsymbol{n}\cdot\Big(\mu[\nabla\boldsymbol{v} + \nabla\boldsymbol{v}^T] - \mu[\nabla\phi_f\otimes\boldsymbol{w} + \boldsymbol{w}\otimes\nabla\phi_f] \\
+\phi_f\phi_s(\mu_f - \mu_s)[\nabla\boldsymbol{w} + \nabla\boldsymbol{w}^T]\Big)\cdot\boldsymbol{n} - p = (d-1)\sigma\kappa, \\
\boldsymbol{n}\cdot\left(\phi_f\mu_f[\nabla\boldsymbol{v} + \nabla\boldsymbol{v}^T] + \phi_f\mu_f[\nabla(\phi_s\boldsymbol{w}) + \nabla(\phi_s\boldsymbol{w})^T]\right)\cdot\boldsymbol{t} = 0, \\
\boldsymbol{n}\cdot\left(\phi_s\mu_s[\nabla\boldsymbol{v} + \nabla\boldsymbol{v}^T] - \phi_s\mu_s[\nabla(\phi_f\boldsymbol{w}) + \nabla(\phi_f\boldsymbol{w})^T]\right)\cdot\boldsymbol{t} = 0, \\
\boldsymbol{n}\cdot\boldsymbol{w} = 0,
\end{aligned}$$

on the free-boundary Γ_1, the condition on the triple points $\partial\Gamma_1$ is $\sigma = 0$ and the no-slip condition becomes

$$\boldsymbol{v} = \boldsymbol{w} = \boldsymbol{0}$$

on the surface Γ_2. At the free-boundary we additionally assume the kinematic equation (1.2.8), i.e.

$$J = \rho(\boldsymbol{v} - \boldsymbol{u}_i)\cdot\boldsymbol{n},$$

which together with $\boldsymbol{w} \cdot \boldsymbol{n} = 0$ becomes the mass conserving condition from Theorem 5.3 in the case $J = 0$. In two-dimensional thin-film scales the no-slip and triple-point conditions stay the same, but the stress-free condition becomes

$$-p = C\partial_{xx} h, \tag{7.2.1g}$$
$$\phi_f \mu_f \partial_y (v_x + \phi_s w_x) = 0, \tag{7.2.1h}$$
$$\phi_s \mu_s \partial_y (v_x - \phi_f w_x) = 0, \tag{7.2.1i}$$
$$w_y - w_x \partial_x h = 0, \tag{7.2.1j}$$

and the kinematic boundary condition gives

$$\partial_t h + u\partial_x h - v = -\frac{J}{\rho}, \tag{7.2.1k}$$

where we assumed Γ_2 can be represented as $y = h(t, x)$ and introduced the capillary number

$$C = \frac{\sigma \varepsilon^3}{U \mu_n}.$$

We are interested in regimes with strong momentum coupling, small height-length ratio for dilute or intermediate concentrated suspensions.

Drift flux thin-film model

Consider the scales

$$\phi_s \sim 1, \qquad \phi_s \neq \phi_{\text{crit}} - o(1), \qquad \beta > 0,$$

and take all the other functions to be of order one. Let us use

$$\tan \alpha \sim \varepsilon, \qquad S = \varepsilon^{-1} \tan \alpha,$$

where we assumed small angles, so that $S \sim 1$. Then, the leading order approximation for system (7.2.1) becomes

$$\begin{aligned}
-\frac{\rho_0}{\varepsilon^\beta} M_0 w_{x0} &= 0, \\
(\mathrm{R} - 1)(1 - \phi_{s0})\phi_{s0} \partial_y p_0 &= -\frac{\rho_0}{\varepsilon^{\beta-2}} M_0 w_y, \\
-\partial_y(\mu_0(\partial_y v_{x0} + w_{x0}\partial_y \phi_{s0})) - \partial_y((1 - \phi_{s0})\phi_{s0}(\mu_f - \mu_s)\partial_y w_{x0}) + \partial_x p_0 &= S\rho_0, \\
\partial_y p_0 &= -\rho_0, \\
\nabla \cdot \boldsymbol{v}_0 &= 0, \\
\partial_t \phi_{s0} + \boldsymbol{v}_0 \nabla \phi_{s0} - \nabla \cdot (\phi_{f0}\phi_{s0}\boldsymbol{w}_0) &= 0.
\end{aligned}$$

The case $\beta = 2$ yields

$$w_{x0} = 0, \tag{7.2.2a}$$
$$-\partial_y(\partial_y \mu_0 v_{x0}) + \partial_x p_0 = S\rho_0, \tag{7.2.2b}$$
$$\partial_y p_0 = -\rho_0, \tag{7.2.2c}$$
$$\nabla \cdot \boldsymbol{v}_0 = 0, \tag{7.2.2d}$$
$$\partial_t \phi_{s0} + \boldsymbol{v}_0 \nabla \phi_{s0} - \partial_y \left(\frac{(1-\phi_{s0})^2 \phi_{s0}}{M_0} \phi_{s0} (\mathrm{R} - 1) \right) = 0, \tag{7.2.2e}$$

that is a gravity driven thin-film equation with particle settling and the case $\beta > 2$ yields

$$\begin{aligned} w_{x0} &= 0, \\ w_{y0} &= 0, \\ -\partial_y(\partial_y \mu_0 v_{x0}) + \partial_x p_0 &= S\rho_0, \\ \partial_y p_0 &= -\rho_0, \\ \nabla \cdot \boldsymbol{v}_0 &= 0, \\ \partial_t \phi_{s0} + \boldsymbol{v}_0 \nabla \phi_{s0} &= 0, \end{aligned}$$

which corresponds to a gravity driven single-phase thin-film. For $\beta < 2$, there is an inconsistency between orders, as we have

$$-\rho_0 = \partial_y p_0 = 0.$$

Sometimes the collision pressure contains a very large term, for example in case of a chemical potential acting, cf. [16]. Then, choosing $\beta = 2$ and scaling the collision pressure as $p_c \sim 1/\varepsilon$, it yields

$$\begin{aligned} w_{x0} &= 0, \\ -\partial_y(\partial_y \mu_0 v_{x0}) + \partial_x p_0 + \partial_x p_{c0} &= S\rho_0, \\ \partial_y p_0 + \partial_y p_{c0} &= -\rho_0, \\ \nabla \cdot \boldsymbol{v}_0 &= 0, \\ \partial_t \phi_{s0} + \boldsymbol{v}_0 \nabla \phi_{s0} - \partial_y \left(\frac{(1-\phi_{s0})^2 \phi_{s0}}{M_0} [\partial_y p_{c0} + \phi_s (\mathrm{R} - 1)] \right) &= 0. \end{aligned}$$

Alternatively, let $\beta \in]0, 2[$, $p_c \sim 1$ and assume

$$S = 1, \qquad \cot \alpha \sim 1,$$

which gives to leading order

$$w_{x0} = 0,$$
$$-\partial_y(\mu_0 \partial_y v_{x0}) + \partial_x p_0 = \rho_0, \tag{7.2.5a}$$
$$\partial_y p_0 = 0, \tag{7.2.5b}$$
$$\nabla \cdot \boldsymbol{v}_0 = 0, \tag{7.2.5c}$$
$$\partial_t \phi_{s0} + \boldsymbol{v}_0 \nabla \phi_{s0} - \partial_y \left((1-\phi_{s0}) \phi_{s0} w_{y0} \right) = 0. \tag{7.2.5d}$$

We are still missing an expression for w_{y0}, so we take the next order approximation of the second components of the momentum equations, which give

$$\begin{aligned}(R-1)\phi_{f0}\phi_{s0}\partial_y p_1 - (1-\phi_{s0})\partial_y p_{c0} &= -\rho_0 M_0 w_{y0},\\ \partial_y p_1 + \partial_y p_{c0} &= -\rho_0 \cot\alpha.\end{aligned}$$

Substitution for p_1 yields

$$w_{y0} = \frac{(1-\phi_{s0})}{\varepsilon^{1-\beta}M_0}\Big[\partial_y p_{c0} + (\mathrm{R}-1)\phi_{s0}\cot\alpha\Big], \tag{7.2.6}$$

which can be used in the transport equation to give the drift-flux model

$$\partial_t\phi_{s0} + \boldsymbol{v}_0\nabla\phi_{s0} - \partial_y\left(\frac{(1-\phi_{s0})^2\phi_{s0}}{\varepsilon^{1-\beta}M_0}\Big[\partial_y p_{c0} + (\mathrm{R}-1)\phi_{s0}\cot\alpha\Big]\right) = 0.$$

The coefficient β, which tells us the strength of momentum coupling, decides whether the drift-flux is dominant, vanishing or balancing with the convective particle transport. Supplying the correct boundary conditions, system (7.2.5) is a thin-film approximation system with a transport equation containing a drift-flux term. Those systems are often encountered in the literature, see e.g. [93, 111], but the transport equation and its drift-flux form had to be hypothesized in all these works, see Section 1.2. In contrast to that, we derive this equation and their components from a basic form of the Eulerian-Eulerian multiphase model. The reduction of multiphase models to drift-flux models is known for some time, see e.g. [95] and [16], but all this works missed a formal asymptotic approach. Note, the formal derivation of the drift-flux term (3.3.4) from Chapter 3 has exactly the form (7.2.6) with $R = 1$, $\beta = 1$ and appropriately chosen M_0 and p_{c0} as

$$M_0 = \frac{\phi_{s0}^2}{1-\phi_{s0}}, \qquad\qquad p_{c0} = \dot{\boldsymbol{\gamma}}_s\eta_n.$$

Dilute suspension with strong coupling and thin-film scales

Consider the scale

$$\phi_s \sim \varepsilon, \qquad\qquad \beta \in]0,1[,$$

and assume

$$p_c(\varepsilon)\sim\varepsilon^2, \qquad \mu_f(\varepsilon)\sim 1, \qquad \mu_s(\varepsilon)\sim\mu_f, \qquad M(\varepsilon)\sim 1, \qquad \cot\alpha = \varepsilon^{-\gamma}, \qquad S\sim 1,$$

with $0 \le \gamma < 1$. Then, we get to leading order the system

$$\begin{aligned}-\varepsilon^{-\beta}M_0 w_{x0} &= 0,\\ (\mathrm{R}-1)\phi_{s0}\partial_y p_0 &= 0,\\ -\partial_y(\mu_f\partial_y v_{x0}) + \partial_x p_0 &= S,\\ \partial_y p_0 &= 0,\\ \nabla\cdot\boldsymbol{v}_0 &= 0,\\ \partial_t\phi_{s0} + \boldsymbol{v}_0\cdot\nabla\phi_{s0} - \nabla\cdot(\phi_{s0}\boldsymbol{w}_0) &= 0.\end{aligned}$$

This system can be simplified to

$$\begin{aligned} -\partial_y(\mu_{f0}\partial_y v_{x0}) + \partial_x p_0 &= S, \\ \partial_y p_0 &= 0, \\ \nabla \cdot \boldsymbol{v}_0 &= 0, \\ \partial_t \phi_{s0} + \boldsymbol{v}_0 \cdot \nabla \phi_{s0} - \partial_y(\phi_{s0} w_{y0}) &= 0. \end{aligned}$$

Note, for Newtonian liquids μ_{f0} does not depend on ϕ_{s0}. Therefore, the first three equations are a closed system and correspond to the usual thin-film system without particle transport.

In order to understand what is happening to the particle transport, one needs to find an expression for w_{y0}. At next order the second components of the momentum equations yields

$$\begin{aligned} (\mathrm{R}-1)\phi_{s0}\partial_y p_1 &= -\varepsilon^{-\beta} M_0 w_{y0}, \\ \partial_y p_1 &= -\varepsilon^{-\gamma} S, \end{aligned}$$

which demands $\beta = \gamma$, unless a higher order term in the $\boldsymbol{w}$-momentum equation balances the gravity term. Thus, in case of equality, we get

$$w_{y0} = \frac{\mathrm{R}-1}{M_0}\phi_{s0} S.$$

Summarizing, the leading order system is

$$\begin{aligned} -\partial_y(\mu_{f0}\partial_y v_{x0}) + \partial_x p_0 &= S, \\ \partial_y p_0 &= 0, \\ \nabla \cdot \boldsymbol{v}_0 &= 0, \end{aligned}$$

and, in case of order one momentum coupling, particles are transported to order ε by convection and gravitation as

$$\partial_t \phi_{s0} + \boldsymbol{v}_0 \cdot \nabla \phi_{s0} - \partial_y \left(\frac{\phi_{s0}^2}{M_0}(\mathrm{R}-1) S \right) = 0.$$

In case of strong momentum coupling, i.e. $\beta > \gamma$, the particles are transported as

$$\partial_t \phi_{s0} + \boldsymbol{v}_0 \cdot \nabla \phi_{s0} = 0.$$

Viscoplastic thin-film model

Using the scalings

$$\phi_s \sim 1, \qquad \phi_s \neq \phi_{\mathrm{crit}} - o(1), \qquad \beta > 0,$$

with $S = \frac{L}{H}\tan\alpha$ and $\tan\alpha \sim \varepsilon$. Further, we choose

$$\mu_f = 1, \qquad \mu_s = 1 + \frac{\eta_n(\phi_s)}{\phi_s}, \qquad p_c = \eta_n(\phi_s)|\dot{\boldsymbol{\gamma}}_s|, \qquad \beta > 1,$$

which yields the leading order system

$$\begin{aligned} -\partial_y \left((1 + \eta_n(\phi_s)) \, \partial_y v_{x0} \right) + \partial_x p_0 &= S\rho_0, \\ \partial_y p_0 &= -\rho_0, \\ \nabla \cdot \boldsymbol{v}_0 &= 0, \\ w_{x0} &= 0, \\ w_{y0} &= 0, \\ \partial_t \phi_{s0} + \boldsymbol{v}_0 \cdot \nabla \phi_{s0} &= 0. \end{aligned}$$

We have seen a Bingham-type rheology in multiphase models in the case of a plane Poiseuille or plane Couette flow. Their solution gives the condition

$$\eta_n(\phi_s)|\dot{\gamma}_s| = B, \tag{7.2.7}$$

where B is a positive constant, see Sections 3.1 and 3.2. This motivates the hypothesis that condition (7.2.7) holds for more general flows. Thus, we assume (7.2.7) to hold unconditionally, which allows us to substitute η_n and creates a Bingham stress in the momentum equation, that introduces a yield stress behavior. Substitution of the condition together with the fact that $\boldsymbol{w}_0 = \boldsymbol{0}$ gives the system

$$-\partial_y \left(\left[1 + \frac{B}{|\partial_y v_{x0}|} \right] \partial_y v_{x0} \right) + \partial_x p_0 = S\rho_0, \tag{7.2.8a}$$

$$\partial_y p_0 = -\rho_0, \tag{7.2.8b}$$

$$\nabla \cdot \boldsymbol{v}_0 = 0, \tag{7.2.8c}$$

$$\partial_t \phi_{s0} + \boldsymbol{v}_0 \cdot \nabla \phi_{s0} = 0. \tag{7.2.8d}$$

For density matched flows, that is $R = 1 \Rightarrow \rho_0 = 1$, system (7.2.8) is equivalent to the starting point in Balmforth et al. [9] and, using the appropriate boundary conditions, yields the same final free-boundary equation for the profile height h. This connection between viscoplastic multiphase models and Balmforth's thin-film model led us to further study the viscoplastic thin-film models in Chapter 6.

Comparison to thin-film models from the literature

The constitutive laws for the multiphase models are still a matter of discussion and no universal laws are accepted as of now. Once a reduced model has been derived from the multiphase model, we can identify the connection between constitutive laws used in multiphase models and constitutive laws used in these reduced models. The advantage is, that reduced models like the drift-flux model and single-phase models in general are much better mathematically and physically understood. Further, experimental results are more numerous for them - thus we try to get new insight into multiphase models by looking for the constitutive laws that would create well-known and well-tested reduced models.

Sections 7.2 and 7.2 show that for dominant momentum coupling we are able to get the trivial leading order mass transport equations

$$\partial_t \phi_s + \boldsymbol{v} \cdot \nabla \phi_s = 0.$$

Nevertheless, some regimes allow a nontrivial transport mechanism such as

$$\partial_t \phi_s + \boldsymbol{v} \cdot \nabla \phi_s - \partial_y \left(\frac{(1-\phi_s)^2 \phi_s}{\varepsilon^{1-\beta} M_0} \left[\partial_y p_{c0} + (\mathrm{R}-1)\phi_s \cot\alpha \right] \right) = 0,$$

in case of intermediate concentrated suspensions and

$$\partial_t \phi_s + \boldsymbol{v} \cdot \nabla \phi_s - \partial_y \left({\phi_s}^2 \frac{\mathrm{R}-1}{M_0} \cot\alpha \right) = 0,$$

in case of dilute suspensions.

In summary, choices for the functions p_c and M decide about the form of the transport equation. For a list of common choices see Section 2.3. Here, we give a short comparison to some well-known thin-film models with particle transport from the literature.

Thin-film equations have been used in combination with transport equations for particles for quite some time, for a recent review see e.g. [124]. Usually, those models consist of equation for the free-boundary and a transport equations for the particles of the form [124]

$$\begin{aligned} \partial_t h &= -\nabla J_c - J_e, \\ \partial_t (\phi_s h) &= -\nabla \cdot (\phi_s J_c + J_d), \end{aligned}$$

where J_c, J_e and J_d are convective, evaporative and diffusive fluxes, respectively. In Table 7.2 we list some examples from a rich literature.

Model proposed by	Transport equation
Routh and Russel [111]	$\partial_t \phi_s + \nabla \cdot (\phi_s \boldsymbol{v}) = \partial_y (K(\phi_s)(\phi_s Z(\phi_s))' \partial_y \phi_s)$, and $\partial_t (h\phi_s) + \partial_x (\phi_s h u) = 0$
Maki and Kumar [81]	$\partial_t \phi_s + \nabla \cdot (\phi_s \boldsymbol{v}) = \frac{1}{\mathrm{Pe}} \left[\partial_z \left(\frac{D}{D_0} \partial_z \phi_s \right) \right]$, with $D = D_0 (1-\phi_s)^{6.55} \left(\frac{1.85\phi_s}{0.64-\phi_s} \right)'$
Craster et al. [25]	$\partial_t \phi_s + u \partial_x \phi_s = h^{-1} \mathrm{Pe}^{-1} \partial_x (h \partial_x \phi_s) + 2(h\mathrm{Pe}(\phi_{\mathrm{crit}} - \phi_s))^{-1} (h \partial_x \phi_s) + \frac{(\phi_{\mathrm{crit}} - \phi_s)\phi_s}{\phi_{\mathrm{crit}} h} J$
Murisic et al. [93]	$\partial_t \int_0^h \phi_s \mathrm{d}y + \partial_x \int_0^h \phi_s u \, \mathrm{d}y = 0$, with the y-profile computed as $0 = \frac{K_c}{4} \phi_s (u' \phi_s)' + \frac{K_v}{2} \frac{{\phi_s}^2 u' {\phi_s}'}{\phi_{\mathrm{crit}} - \phi_s} + \frac{\rho_s \cot\alpha}{18} \phi_s (1-\phi_s) \left(\frac{\phi_{\mathrm{crit}} - \phi_s}{\phi_s} \right)^2$

Table 7.2: Transport equations used in thin-film approximations in the literature.

We define the flux J as

$$J = \frac{(1-\phi_{s0})^2 \phi_{s0}}{\varepsilon^{1-\beta} M_0} \left[\partial_y p_{c0}(\phi_{s0}, v_{x0}) + (\mathrm{R}-1)\phi_{s0} \cot\alpha \right].$$

Then, the standard collision pressure and coupling term choices [88, 95]

$$p_c = K_n \left(\frac{\phi_s}{\phi_{\text{crit}} - \phi_s} \right)^2 |\dot{\gamma}|,$$
$$M = 4.5 \frac{\phi_s}{{\phi_f}^3}$$

yield

$$J = \frac{(1-\phi_s)^5}{4.5} \left[K_N \left\{ \partial_y \dot{\gamma} \left(\frac{\phi_s}{\phi_{\text{crit}} - \phi_s} \right)^2 + 2\dot{\gamma} \frac{\phi_s \phi_{\text{crit}}}{(\phi_{\text{crit}} - \phi_s)^3} \partial_y \phi_s \right\} + (\mathrm{R} - 1)\phi_s \cot \alpha \right].$$

This is similar to the flux used in Murisic et al. [93], but an even better choice is

$$p_c = 4.5 K_c \frac{\phi_{\text{crit}}^2}{\phi_f} \left(\frac{\phi_s}{\phi_{\text{crit}} - \phi_s} \right)^2 |\dot{\gamma}|,$$
$$M = 18 \phi_s \phi_f \left(\frac{\phi_{\text{crit}}}{\phi_{\text{crit}} - \phi_s} \right)^2,$$

which yields

$$J = \frac{K_c}{4} {\phi_s}^2 \partial_y |\dot{\gamma}| + |\dot{\gamma}| \partial_y \phi_s \frac{K_c}{4} \left(\frac{2\phi_s \phi_{\text{crit}}}{(\phi_{\text{crit}} - \phi_s)} + \frac{{\phi_s}^2}{\phi_f} \right) + \frac{\mathrm{R} - 1}{18} \phi_f \phi_s \cot \alpha \left(\frac{\phi_{\text{crit}} - \phi_s}{\phi_{\text{crit}}} \right)^2$$

which is still not quite exact. The first and last term are exact, but the middle term is only exact if $\phi_f = \phi_s = 1/2$ and $\phi_{\text{crit}} = \frac{K_v}{K_c} \phi_s$. The quotient of the proportionality constants K_v and K_c is believed to be, cf. [95],

$$\frac{K_v}{K_c} = 0.66.$$

This shows, the model in [93] is consistent with the multiphase model structure for $\phi_s = 0.5$ and $\phi_{\text{crit}} = 0.66$.

Chapter 8

Discussion and outlook

In this thesis we studied concentrated suspensions using thin-film and multiphase models. A new multiphase model for viscoplastic fluids has been proposed, analyzed for stability and reduced to simpler models using asymptotic techniques. Further, we showed novel connections between multiphase models and thin-film equations, which led us to look deeper into the analytic behavior of viscoplastic thin-film equations.

Models for multiphase flow and in particular concentrated suspensions will pose new challenges for the foreseeable future. To emphasize this, we list some open questions that directly result from the present thesis.

Model consideration

Chapter 1 shows a new model for the horizontal drying front behavior, which has some shortcomings for concentrated suspensions. However, Chapter 7 shows how to derive such a thin-film model directly from the multiphase model, which in theory allows us to derive the hypothesized transport equation in a more formal way. Thus, it would be interesting to check whether it is possible to derive the boundary conditions of a drying front using the multiphase model ansatz in the future. Another interesting extension is to use the new drift-flux term of Chapter 3 in the model.

The particular solutions of Chapter 3 for plane Couette and plane Poiseuille flow should be compared to experiments. A first step in this direction has been done by Lecampion et al. [75], who use the constitutive laws of Boyer et al. [15] in order to derive a drift-flux model and compare it with experimental measurements. Our model seems to generalize their approach, so we expect similar results.

The new drift-flux model of Section 3.3 has also not been tested in a real-life experiment or against full simulations of the multiphase model as of now. It would be interesting to relate the evolution of the jammed region to experimental results on the transition length over which a steady state develops in space from homogeneous inlet conditions. In the future we plan on doing

simulations and like to compare them with known experimental results. This could lead to new proposals of constitutive laws for multiphase or thin-film models.

Stability

In case of parallel shear flows, the stability analysis of Chapter 4 revealed a transient growth of modes in the multiphase model that could lead to turbulence. This behavior should be further studied by a direct numerical simulation of the full three-dimensional model or a stability analysis based on pseudospectra as proposed by Trefethen et al. [128] in the future. Of interest is also the loss-of-hyperbolicity problem of multiphase models, which is still open to debate as discussed in Section 2.2. Our linear stability analysis of Chapter 4 could not identify the loss-of-hyperbolicity problem, however, it remains to be shown if this picture changes for higher resolution, smaller viscosity terms or perhaps different base states. A well-known solution to this instability is a two-pressure model, cf. [77], but as far as we know viscoplastic two-pressure models have not yet been proposed.

Further, it would be interesting to see if the ill-posedness of our two-phase flow model can also be connected to the existence of a singular shock, such as has been seen in applications detailed in Carpio et al. [19] or Bell et al. [11], but more recently also in connection with other operators studied by Zhou et al. [139] and Cook et al. [23]. The idea is that singular shocks and our instability are both connected to the entropy of the system. Additionally, we show in Chapter 7 that the collision pressure is contained in the thin-film equation and particle transport equation, which is part of systems known to produce these shocks, cf. [23].

The given multiphase continuity conditions at the yield-surface are based on our experience with the conditions of single-phase Bingham flow. However, even for Bingham flow the correctness of these conditions is not entirely clear in more than one dimension, see e.g. the comments in [56]. We think a derivation of the yield-surface boundary conditions based on the $\boldsymbol{v}/\boldsymbol{w}$-formulation (7.1.4) could lead to more insight, yet has not been pursued as of now.

Energetic formulation

Since Chapter 5 shows how to derive the free-boundary conditions for the multiphase model, it would be interesting to simulate a flow with a free-boundary such as a sessile drop on a substrate using the full model. This asks for a numeric method capable to handle moving meshes, free-boundary conditions and mass-conservation, preferable of higher order. Most methods like the standard finite element methods or finite volume methods possess only a subset of the required features. A possible candidate is the discontinuous Galerkin method, see e.g. [51], that has never been used for multiphase models with free-boundaries to the best of our knowledge.

The energetic derivation of the multiphase model based on a gradient flow structure is only applicable to purely dissipative cases like Stokes flow. Addition of inertial terms in the framework would allow deriving the complete model from Chapter 2 and could also lead to new insights into the structure of multiphase models. A possible candidate is the GENERIC framework [99]. Another interesting extension includes non-differentiable, but convex potentials as has been done for single-phase Bingham fluids, see e.g. [27, 34, 47].

Analysis of thin-film approximations

The analysis of multiphase models of Chapter 6 is just in its infancy. Since multiphase models naturally degenerate to the Newtonian incompressible Navier-Stokes equations, we expect its existence theory to be at least as hard as the well-known millennium problem. Possibly, a first step would be the analysis of numeric schemes for the most simple constant viscosity case of the multiphase model. Our particular choice of viscoplastic constitutive laws pose complete new questions for the analysis, since the question of well-posedness might only be answered in the framework of variational inequalities, as it is the case for the Bingham Navier-Stokes equations [34].

Reduced equations like Balmforth's viscoplastic thin-film equation also lack a sophisticated analysis. This is in particular true for the case of surface tension driven fluids, which yield fourth order quasilinear equations. Standard proofs for fourth order equations based on strong theories like in Bernis et al. [13] or Schauder fixpoint estimates like in Jin et al. [62] fail due to missing a-priori estimates and consequentially non-existent compactness results for the third derivative. Our analysis of the second order equation showed monotonicity methods are a good starting point, but degeneration of the thin-film equations for $h = 0$ and $Y_s = 0$ might pose major problems for the theory, since it destroys coercitivity of the operator. Therefore, it would be interesting to show existence of a non-regularized equation of second order in a future work. This would need a comprehensive study of pseudo-monotonicity of the differential operator including the degenerated cases. Another topic is the existence theory of the fourth order equation, which generally contains the same problem as the second order problem.

Finally, the analysis of uniqueness of the non-regularized thin-film equations will lead to questions of non-negativity like in the Newtonian case, see [13].

Asymptotic regimes

Our analysis of Chapter 3 suggests that the boundary layer acts as a source for the particle migration towards the unyielded region. The quantities w_1, w_2, which denote the difference between the velocities u_f, u_s and v_f, v_s, respectively, are by $O(\varepsilon)$ smaller than the actual flow variables. The fact that the particle transport acts on a different time scale than the phase-averaged flow field also indicates how to systematically develop an asymptotic theory leading to a complete coupled flow model that includes both transport and jamming of particles. Such an analysis could also rationalize some suspension flow models that are found in the literature.

It would be interesting to use a formal asymptotic approach on the energetic level of Chapter 5, rather than on the partial differential equation level in order to reduce the multiphase model to well-known models from the literature. This might allow a direct comparison to hypothesized energetic approaches, e.g. the framework by Thiele [124].

The asymptotic derivations in Chapter 7 should be extended to different parameters of large and small value. Parameters we have not yet fully considered are the Reynolds number, the density ratio or the viscosity terms. The nearly fully packed regime needs further analysis, which we started already with the derivation of the drift-flux term for viscoplastic fluids in Chapter 3. Another unexplored topic is the behavior of the boundary conditions in the considered regimes. Further, a more comprehensive comparison of the known single-phase models with the reduced multiphase models would enhance the understanding of both classes of models.

Bibliography

[1] C. Acary-Robert, E. D. Fernández-Nieto, G. Narbona-Reina, and P. Vigneaux. A well-balanced finite volume-augmented Lagrangian method for an integrated Herschel-Bulkley model. *Journal of Scientific Computing*, 53(3):608–641, Apr 2012. ISSN 1573-7691. doi:10.1007/s10915-012-9591-x.

[2] T. Ahnert, A. Münch, and B. Wagner. A two-phase flow model for concentrated suspensions. *Journal of Non-Newtonian Fluid Mechanics*, 2014. To appear in Non-Newtonian Fluid Mechanics.

[3] Vladimir S. Ajaev. Spreading of thin volatile liquid droplets on uniformly heated surfaces. *J. Fluid Mech.*, 528:279–296, 2005. ISSN 1469-7645. doi:10.1017/s0022112005003320.

[4] Vladimir S. Ajaev. *Interfacial Fluid Mechanics*. Springer US, 2012. ISBN 978-1-4614-1341-7. doi:10.1007/978-1-4614-1341-7.

[5] Vladimir S. Ajaev and G.M. Homsy. Steady vapor bubbles in rectangular microchannels. *Journal of Colloid and Interface Science*, 240(1):259–271, Aug 2001. ISSN 0021-9797. doi:10.1006/jcis.2001.7562.

[6] Christophe Ancey. Plasticity and geophysical flows: A review. *Journal of Non-Newtonian Fluid Mechanics*, 142(1-3):4–35, Mar 2007. ISSN 0377-0257. doi:10.1016/j.jnnfm.2006.05.005.

[7] D. M. Anderson, G. B. McFadden, and A. A. Wheeler. Diffuse-interface methods in fluid mechanics. *Annual Review of Fluid Mechanics*, 30(1):139–165, Jan 1998. ISSN 1545-4479. doi:10.1146/annurev.fluid.30.1.139.

[8] Woon-Hyuk Baek, Hyun Yang, Tae-Sik Yoon, C.J. Kang, Hyun Ho Lee, and Yong-Sang Kim. Effect of P3HT:PCBM concentration in solvent on performances of organic solar cells. *Solar Energy Materials and Solar Cells*, 93(8):1263–1267, Aug 2009. ISSN 0927-0248. doi:10.1016/j.solmat.2009.01.019.

[9] N.J. Balmforth and R.V. Craster. A consistent thin-layer theory for Bingham plastics. *Journal of Non-Newtonian Fluid Mechanics*, 84(1):65–81, Jul 1999. ISSN 0377-0257. doi:10.1016/s0377-0257(98)00133-5.

[10] G. K. Batchelor. *An Introduction to Fluid Dynamics*. Cambridge Mathematical Library. Cambridge University Press, 2000. ISBN 9780521663960. doi:10.1017/CBO9780511800955.

[11] John B. Bell, John A. Trangenstein, and Gregory R. Shubin. Conservation laws of mixed type describing three-phase flow in porous media. *SIAM Journal on Applied Mathematics*, 46(6):1000–1017, Dec 1986. ISSN 1095-712X. doi:10.1137/0146059.

[12] Carl M. Bender and Steven A. Orszag. *Advanced Mathematical Methods for Scientists and Engineers I*. Springer Science + Business Media, 1978. ISBN 978-1-4419-3187-0. doi:10.1007/978-1-4757-3069-2.

[13] Francisco Bernis and Avner Friedman. Higher order nonlinear degenerate parabolic equations. *Journal of Differential Equations*, 83(1):179–206, Jan 1990. ISSN 0022-0396. doi:10.1016/0022-0396(90)90074-y.

[14] Igor A. Bolotnov, Richard T. Lahey, Donald A. Drew, and Kenneth E. Jansen. Turbulent cascade modeling of single and bubbly two-phase turbulent flows. *International Journal of Multiphase Flow*, 34(12):1142–1151, Dec 2008. ISSN 0301-9322. doi:10.1016/j.ijmultiphaseflow.2008.06.006.

[15] François Boyer, Élisabeth Guazzelli, and Olivier Pouliquen. Unifying suspension and granular rheology. *Phys. Rev. Lett.*, 107(18):188301, October 2011. doi:10.1103/PhysRevLett.107.188301.

[16] Franck Boyer. A theoretical and numerical model for the study of incompressible mixture flows. *Computers & Fluids*, 31(1):41–68, Jan 2002. ISSN 0045-7930. doi:10.1016/s0045-7930(00)00031-1.

[17] Haim Brezis. *Functional Analysis, Sobolev Spaces and Partial Differential Equations*. Springer Science + Business Media, 2010. ISBN 978-0-387-70914-7. doi:10.1007/978-0-387-70914-7.

[18] H. C. Brinkman. A calculation of the viscous force exerted by a flowing fluid on a dense swarm of particles. *Appl. Sci. Res.*, 1(1):27–34, 1949. doi:10.1007/BF02120313.

[19] A. Carpio, S. J. Chapman, and J. J. L. Velázquez. Pile-up solutions for some systems of conservation laws modelling dislocation interaction in crystals. *SIAM Journal on Applied Mathematics*, 61(6):2168–2199, Jan 2001. ISSN 1095-712X. doi:10.1137/s0036139999364347.

[20] C. Carstensen, B.D. Reddy, and M. Schedensack. A natural nonconforming FEM for the Bingham flow problem is quasi-optimal. *Numerische Mathematik*, 2015. doi:10.1007/s00211-015-0738-1.

[21] Jonathan R. Clausen. Using the suspension balance model in a finite-element flow solver. *Computers & Fluids*, 87:67–78, Oct 2013. ISSN 0045-7930. doi:10.1016/j.compfluid.2012.12.004.

[22] Francisco J. Collado. Reynolds transport theorem for a two-phase flow. *Appl. Phys. Lett.*, 90(2):024101, 2007. ISSN 0003-6951. doi:10.1063/1.2430675.

[23] Benjamin P. Cook, Andrea L. Bertozzi, and A. E. Hosoi. Shock solutions for particle-laden thin films. *SIAM Journal on Applied Mathematics*, 68(3):760–783, Jan 2008. ISSN 1095-712X. doi:10.1137/060677811.

[24] R. Craster and O. Matar. Dynamics and stability of thin liquid films. *Rev. Mod. Phys.*, 81 (3):1131–1198, Aug 2009. ISSN 1539-0756. doi:10.1103/revmodphys.81.1131.

[25] R. V. Craster, O. K. Matar, and K. Sefiane. Pinning, retraction, and terracing of evaporating droplets containing nanoparticles. *Langmuir*, 25(6):3601–3609, Mar 2009. ISSN 1520-5827. doi:10.1021/la8037704.

[26] A Davey. On the numerical solution of difficult eigenvalue problems. *Journal of Computational Physics*, 24(3):331–338, Jul 1977. ISSN 0021-9991. doi:10.1016/0021-9991(77)90041-9.

[27] E. J. Dean, R. Glowinski, and G. Guidoboni. On the numerical simulation of Bingham visco-plastic flow: Old and new results. *J. Non-Newtonian Fluid Mech.*, 142(1):36–62, 2007. doi:10.1016/j.jnnfm.2006.09.002.

[28] Robert D. Deegan, Olgica Bakajin, Todd F. Dupont, Greb Huber, Sidney R. Nagel, and Thomas A. Witten. Capillary flow as the cause of ring stains from dried liquid drops. *Nature*, 389(6653):827–829, Oct 1997. ISSN 0028-0836. doi:10.1038/39827.

[29] Pavel Drábek and Jaroslav Milota. *Methods of Nonlinear Analysis*. Springer Science + Business Media, 2013. ISBN 978-3-0348-0387-8. doi:10.1007/978-3-0348-0387-8.

[30] P. G. Drazin and W. H. Reid. *Hydrodynamic Stability*. Cambridge University Press, 2004. ISBN 9780521525411. doi:10.1017/cbo9780511616938.

[31] Donald Allen Drew. Mathematical modeling of two-phase flow. *Annu. Rev. Fluid Mech.*, 15 (1):261–291, 1983. doi:10.1146/annurev.fl.15.010183.001401.

[32] Donald Allen Drew and Stephen L. Passman. *Theory of Multicomponent Fluids*, volume 135 of *Applied Mathematical Sciences*. Springer, 1999. doi:10.1007/b97678.

[33] Donald Allen Drew and Lee A. Segel. Averaged equations for two-phase flows. *Stud. Appl. Math.*, 50(2):205–231, 1971. ISSN 0022-2526.

[34] Georges Duvaut and Jacques Louis Lions. *Inequalities in Mechanics and Physics*. Springer Berlin Heidelberg, 1976. ISBN 978-3-642-66165-5. doi:10.1007/978-3-642-66165-5.

[35] Stephen Ebbens, Richard Hodgkinson, Andrew J. Parnell, Alan Dunbar, Simon J. Martin, Paul D. Topham, Nigel Clarke, and Jonathan R. Howse. In situ imaging and height reconstruction of phase separation processes in polymer blends during spin coating. *ACS Nano*, 5(6):5124–5131, Jun 2011. ISSN 1936-086X. doi:10.1021/nn201210e.

[36] Wiktor Eckhaus. *Asymptotic Analysis of Singular Perturbations*, volume 9 of *Studies in Mathematics and Its Applications*. North-Holland, 1979. ISBN 978-0-444-85306-6. URL `http://www.sciencedirect.com/science/bookseries/01682024/9`.

[37] Albert Einstein. Eine neue Bestimmung der Moleküldimensionen. *Ann. Phys. (Berlin)*, 324 (2):289–306, 1906. doi:10.1002/andp.19063240204.

[38] Albert Einstein. Berichtigung zu meiner Arbeit: "Eine neue Bestimmung der Moleküldimensionen". *Annalen der Physik*, 339(3):591–592, 1911. ISSN 1521-3889. doi:10.1002/andp.19113390313.

[39] Lawrence Evans. *Partial Differential Equations*. American Mathematical Society, Mar 2010. ISBN 9781470411442. doi:10.1090/gsm/019.

[40] Philipp Forchheimer. Wasserbewegung durch Boden. *Zeitschrift fur Acker und Pflanzenbau*, 45:1736–1749, 1901.

[41] Andrew Fowler. *Mathematical models in the applied sciences*. Cambridge Texts in Applied Mathematics. Cambridge University Press, New York, 1997. ISBN 9780521467032.

[42] I. A. Frigaard and C. Nouar. On the three-dimensional linear stability of Poiseuille flow of Bingham fluids. *Physics of Fluids*, 15:2843–2851, 2003. doi:10.1063/1.1602451.

[43] I. A. Frigaard, S. D. Howison, and I. J. Sobey. On the stability of Poiseuille flow of a Bingham fluid. *J. Fluid Mech.*, 263:133–150, 1994. doi:10.1017/S0022112094004052.

[44] F. A. Garifullin and K. Z. Galimov. Hydrodynamic stability of non-Newtonian media. *Soviet Applied Mechanics*, 10(8):807–824, Aug 1974. ISSN 1573-8582. doi:10.1007/bf00882508.

[45] D. V. Georgievskii. Stability of Bingham flows: from the earliest works of A. A. Il'yushin to the present. *J. Eng. Math.*, 78:9–17, 2013. doi:10.1007/s10665-011-9471-7.

[46] Dimitri Gidaspow, Rukmini Bezburuah, and J. Ding. Hydrodynamics of circulating fluidized beds: Kinetic theory approach. Technical report, Illinois Inst. of Tech., Chicago, IL (United States). Dept. of Chemical Engineering, 1991.

[47] R. Glowinski, Jacques Louis Lions, and Raymond Trémolières. *Numerical Analysis of Variational Inequalities*. Studies in Mathematics and its Applications. North-Holland, 1981. ISBN 978-0-444-86199-3. URL http://www.sciencedirect.com/science/bookseries/01682024/8.

[48] Lucas Goehring, William J. Clegg, and Alexander F. Routh. Solidification and ordering during directional drying of a colloidal dispersion. *Langmuir*, 26(12):9269–9275, June 2010. ISSN 0743-7463, 1520-5827. doi:10.1021/la100125v.

[49] P. S. Gough and F. J. Zwarts. Modeling heterogeneous 2-phase reacting flow. *AIAA J.*, 17 (1):17–25, 1979. ISSN 0001-1452. doi:10.2514/3.61057.

[50] R. E. Hampton. Migration of particles undergoing pressure-driven flow in a circular conduit. *J. Rheol.*, 41(3):621–640, May 1997. ISSN 01486055. doi:10.1122/1.550863.

[51] J.S. Hesthaven and T. Warburton. *Nodal Discontinuous Galerkin Methods: Algorithms, Analysis, and Applications*. Texts in Applied Mathematics Series. Springer-Verlag New York, 2008. ISBN 978-0-387-72065-4. doi:10.1007/978-0-387-72067-8.

[52] Kai Hiltunen, Ari Jäsberg, Sirpa Kallio, Hannu Karema, Markku Kataja, Antti Koponen, Mikko Manninen, and Veikko Taivassalo. *Multiphase Flow Dynamics*, volume 722. VTT Publications, 2009. ISBN 978-951-38-7365-3. URL http://www.vtt.fi/inf/pdf/publications/2009/P722.pdf.

[53] P. Hohenberg and B. Halperin. Theory of dynamic critical phenomena. *Rev. Mod. Phys.*, 49(3):435–479, Jul 1977. ISSN 0034-6861. doi:10.1103/revmodphys.49.435.

[54] Harald Hoppe and Niyazi Serdar Sariciftci. Organic solar cells: An overview. *J. Mater. Res.*, 19(07):1924–1945, Jul 2004. ISSN 2044-5326. doi:10.1557/jmr.2004.0252.

[55] Chun Huh and L.E Scriven. Hydrodynamic model of steady movement of a solid/liquid/fluid contact line. *Journal of Colloid and Interface Science*, 35(1):85–101, Jan 1971. ISSN 0021-9797. doi:10.1016/0021-9797(71)90188-3.

[56] Raja R. Huilgol. *Fluid Mechanics of Viscoplasticity*. Springer Berlin Heidelberg, 2015. ISBN 978-3-662-45616-3. doi:10.1007/978-3-662-45617-0.

[57] R. Huth, S. Jachalski, G. Kitavtsev, and D. Peschka. Gradient flow perspective on thin-film bilayer flows. *Journal of Engineering Mathematics*, Aug 2014. ISSN 1573-2703. doi:10.1007/s10665-014-9698-1.

[58] Nathanael J. Inkson, Jose Plasencia, and Simon Lo. Predicting emulsion pressure drop in pipes through CFD multiphase rheology models. In *CFD2014: The 10th International Conference on Computational Fluid Dynamics In the Oil & Gas, Metallurgical and Process Industries.*, pages 453–458, 2014. URL http://www.sintef.no/globalassets/project/cdf2014/docs/official_proceedings_cfd2014-redusert-filstr.pdf.

[59] Lucio Isa, Rut Besseling, and Wilson C. K. Poon. Shear zones and wall slip in the capillary flow of concentrated colloidal suspensions. *Phys. Rev. Lett.*, 98:198305, May 2007. doi:10.1103/PhysRevLett.98.198305.

[60] Mamoru Ishii and Takashi Hibiki. *Thermo-Fluid Dynamics of Two-Phase Flow*. Springer, 2011. doi:10.1007/978-1-4419-7985-8.

[61] Hugo A Jakobsen. *Chemical reactor modeling*. Springer, 2008. ISBN 978-3-540-25197-2. doi:10.1007/978-3-540-68622-4.

[62] Zhengmeng Jin and Xiaoping Yang. Strong solutions for the generalized Perona-Malik equation for image restoration. *Nonlinear Analysis: Theory, Methods & Applications*, 73 (4):1077–1084, Aug 2010. ISSN 0362-546X. doi:10.1016/j.na.2010.04.039.

[63] Pierre Jop, Yoël Forterre, and Olivier Pouliquen. A constitutive law for dense granular flows. *Nature*, 441(7094):727–730, 2006. doi:10.1038/nature04801.

[64] Boško S. Jovanović and Endre Süli. *Analysis of Finite Difference Schemes*, volume 46 of *Springer Series in Computational Mathematics*. Springer London, 2014. ISBN 978-1-4471-5459-4. doi:10.1007/978-1-4471-5460-0.

[65] Barbara Keyfitz, Michael Sever, and Richard Sanders. Lack of hyperbolicity in the two-fluid model for two-phase incompressible flow. *Discrete and Continuous Dynamical Systems - Series B*, 3(4):541–563, Aug 2003. ISSN 1531-3492. doi:10.3934/dcdsb.2003.3.541.

[66] Barbara Lee Keyfitz. Mathematical properties of nonhyperbolic models for incompressible two-phase flow. In *Proc. Fourth Int. Conf. Multiphase Flow*. ICMF, May 2001.

[67] Barbara Lee Keyfitz. Singular shocks: Retrospective and prospective. *Confluentes Mathematici*, 03(03):445–470, Sep 2011. ISSN 1793-7434. doi:10.1142/s1793744211000424.

[68] Barbara Lee Keyfitz and Herbert C. Kranzer. Spaces of weighted measures for conservation laws with singular shock solutions. *Journal of Differential Equations*, 118:420–451, 1995.

[69] David Kinderlehrer and Guido Stampacchia. *An Introduction to Variational Inequalities and Their Applications*. Society for Industrial & Applied Mathematics (SIAM), Jan 2000. ISBN http://id.crossref.org/isbn/978-0-89871-945-1. doi:10.1137/1.9780898719451.

[70] Nikolay Ivanov Kolev. *Multiphase Flow Dynamics 1: Fundamentals*. Multiphase Flow Dynamics. Springer-Verlag Berlin Heidelberg, 2005. ISBN 9783540268291. doi:10.1007/b138144.

[71] C.Y. Kwong, A.B. Djurišić, P.C. Chui, K.W. Cheng, and W.K. Chan. Influence of solvent on film morphology and device performance of poly(3-hexylthiophene):tio2 nanocomposite solar cells. *Chemical Physics Letters*, 384(4-6):372–375, Jan 2004. ISSN 0009-2614. doi:10.1016/j.cplett.2003.12.045.

[72] R. G. Larson. *The Structure and Rheology of Complex Fluids*. Topics in Chemical Engineering. Oxford University Press USA, 1999. ISBN 9780195121971.

[73] Peter D. Lax. The formation and decay of shock waves. *The American Mathematical Monthly*, 79(3):227–241, Mar 1972. ISSN 0002-9890. doi:10.2307/2316618.

[74] Peter D. Lax. *Hyperbolic Systems of Conservation Laws and the Mathematical Theory of Shock Waves*. Society for Industrial and Applied Mathematics, Jan 1973. ISBN 978-1-61197-056-2. doi:10.1137/1.9781611970562.

[75] Brice Lecampion and Dmitry I. Garagash. Confined flow of suspensions modelled by a frictional rheology. *Journal of Fluid Mechanics*, 759:197–235, Oct 2014. ISSN 1469-7645. doi:10.1017/jfm.2014.557.

[76] David Leighton and Andreas Acrivos. Shear-induced migration of particles in concentrated suspensions. *J. Fluid Mech.*, 181(1):415–439, 1987. doi:10.1017/S0022112087002155.

[77] Daniel Lhuillier, Chih-Hao Chang, and Theo G. Theofanous. On the quest for a hyperbolic effective-field model of disperse flows. *J. Fluid Mech.*, 731:184–194, Aug 2013. ISSN 1469-7645. doi:10.1017/jfm.2013.380.

[78] Joaquim Li, Bernard Cabane, Michael Sztucki, Jérémie Gummel, and Lucas Goehring. Drying dip-coated colloidal films. *Langmuir*, 28(1):200–208, January 2012. ISSN 0743-7463. doi:10.1021/la203549g.

[79] Martin Man-chun Li. A general existence theorem for embedded minimal surfaces with free boundary. *Commun. Pur. Appl. Math.*, 68(2):286–331, Mar 2014. ISSN 0010-3640. doi:10.1002/cpa.21513.

[80] Andrea J. Liu and Sidney R. Nagel. The jamming transition and the marginally jammed solid. *Annu. Rev. Condens. Matter Phys.*, 1(1):347–369, Aug 2010. ISSN 1947-5462. doi:10.1146/annurev-conmatphys-070909-104045.

[81] Kara L. Maki and Satish Kumar. Fast evaporation of spreading droplets of colloidal suspensions. *Langmuir*, 27(18):11347–11363, Sep 2011. ISSN 1520-5827. doi:10.1021/la202088s.

[82] Mikko Manninen, Veikko Taivassalo, and Sirpa Kallio. *On the mixture model for multiphase flow*, volume 288 of *VTT Publications*. Technical Research Centre of Finland Finland, 1996. ISBN 9513849465.

[83] M. Lisa Manning, B. Bamieh, and J. M. Carlson. Descriptor approach for eliminating spurious eigenvalues in hydrodynamic equations. *arxiv.org*, May 2007. URL `arxiv.org/abs/0705.1542v2`.

[84] Maple 16. Maplesoft, a division of Waterloo Maple Inc., Waterloo, Ontario.

[85] MATLAB 2014b. The MathWorks, Inc., Natick, Massachusetts, United States.

[86] C. Métivier, C. Nouar, and J.-P. Brancher. Linear stability involving the Bingham model when the yield stress approaches zero. *Physics of Fluids*, 17(10):104106, 2005. ISSN 1070-6631. doi:10.1063/1.2101007.

[87] Alexander Mielke. Thermomechanical modeling of energy-reaction-diffusion systems, including bulk-interface interactions. *DCDS-S*, 6(2):479–499, Nov 2012. ISSN 1937-1632. doi:10.3934/dcdss.2013.6.479.

[88] Jeffrey F. Morris and Fabienne Boulay. Curvilinear flows of noncolloidal suspensions: The role of normal stresses. *J. Rheol.*, 43:1213–1237, 1999. doi:10.1122/1.551021.

[89] P. J. Morrison. Hamiltonian description of the ideal fluid. *Rev. Mod. Phys.*, 70(2):467–521, Apr 1998. ISSN 1539-0756. doi:10.1103/revmodphys.70.467.

[90] Adam J. Moule, Dieter Neher, and Sarah T. Turner. P3HT-based solar cells: Structural properties and photovoltaic performance. *Advances in Polymer Science*, 2014. ISSN 1436-5030. doi:10.1007/12_2014_289.

[91] David J. Muraki. A simple illustration of a weak spectral cascade. *SIAM Journal on Applied Mathematics*, 67(5):1504–1521, Jan 2007. ISSN 1095-712X. doi:10.1137/040619090.

[92] N. Murisic and L. Kondic. On evaporation of sessile drops with moving contact lines. *J. Fluid Mech.*, 679:219–246, Apr 2011. ISSN 1469-7645. doi:10.1017/jfm.2011.133.

[93] N. Murisic, B. Pausader, D. Peschka, and A. L. Bertozzi. Dynamics of particle settling and resuspension in viscous liquid films. *J. Fluid Mech.*, 717:203–231, Feb 2013. ISSN 1469-7645. doi:10.1017/jfm.2012.567.

[94] Jenny Nelson. *The Physics of Solar Cells*. Imperial College Press, 2003. ISBN 978-1-86094-340-9. doi:10.1142/p276.

[95] Prabhu R. Nott and John F. Brady. Pressure-driven flow of suspensions: simulation and theory. *J. Fluid Mech.*, 275(1):157–199, 1994. doi:10.1017/S0022112094002326.

[96] Dirk Olbers, Jürgen Willebrand, and Carsten Eden. Conservation laws for moving fluids. *Ocean Dynamics*, pages 25–105, 2012. doi:10.1007/978-3-642-23450-7_2.

[97] Alexander Oron and S. George Bankoff. Long-scale evolution of thin liquid films. *Rev. Mod. Phys.*, 69(3):931–980, Jul 1997. ISSN 1539-0756. doi:10.1103/revmodphys.69.931.

[98] Steven A. Orszag. Accurate solution of the Orr-Sommerfeld stability equation. *J. Fluid Mech.*, 50(04):689, Dec 1971. ISSN 1469-7645. doi:10.1017/s0022112071002842.

[99] Hans Christian Öttinger. *Beyond Equilibrium Thermodynamics*. Wiley-Blackwell, Jan 2005. ISBN 9780471666585. doi:10.1002/0471727903.

[100] K. B. Pavlov, A. S. Romanov, and S. L. Simkhovich. Hydrodynamic stability of Poiseuille flow of a viscoplastic non-Newtonian fluid. *Fluid Dynamics*, 9(6):996–998, 1974. ISSN 1573-8507. doi:10.1007/bf01020033.

[101] Mark A. Peletier. Variational modelling: Energies, gradient flows, and large deviations. *arXiv:1402.1990*, February 2014. URL `arxiv.org/abs/1402.1990`.

[102] K. A. Pericleous and S. N. Drake. An algebraic slip model of PHOENICS for multi-phase applications. *Lecture Notes in Engineering*, pages 375–385, 1986. ISSN 0176-5035. doi:10.1007/978-3-642-82781-5_29.

[103] Ronald J. Phillips, Robert C. Armstrong, Robert A. Brown, Alan L. Graham, and James R. Abbott. A constitutive equation for concentrated suspensions that accounts for shear-induced particle migration. *Phys. Fluids A*, 4(1):30–40, January 1992. ISSN 0899-8213, 1089-7666. doi:10.1063/1.858498.

[104] Stephen B. Pope. *Turbulent Flows*. Cambridge University Press, 2000. ISBN 9780511840531. doi:10.1017/cbo9780511840531.

[105] A. Prosperetti and A.V. Jones. The linear stability of general two-phase flow models - ii. *International Journal of Multiphase Flow*, 13(2):161–171, Mar 1987. ISSN 0301-9322. doi:10.1016/0301-9322(87)90027-9.

[106] Maria-Eleni Ragoussi and Tomás Torres. New generation solar cells: concepts, trends and perspectives. *Chem. Commun.*, 51(19):3957–3972, 2015. ISSN 1364-548X. doi:10.1039/c4cc09888a.

[107] J.F. Richardson and W.N. Zaki. Sedimentation and fluidisation: Part i. *Chemical Engineering Research and Design*, 75:82–100, Dec 1954. ISSN 0263-8762. doi:10.1016/s0263-8762(97)80006-8.

[108] Jonathan Rivnay, Robert Steyrleuthner, Leslie H. Jimison, Alberto Casadei, Zhihua Chen, Michael F. Toney, Antonio Facchetti, Dieter Neher, and Alberto Salleo. Drastic control of texture in a high performance n-type polymeric semiconductor and implications for charge transport. *Macromolecules*, 44(13):5246–5255, Jul 2011. ISSN 1520-5835. doi:10.1021/ma200864s.

[109] Tomáš Roubíček. *Nonlinear Partial Differential Equations with Applications*. Springer Science + Business Media, 2013. ISBN 978-3-0348-0513-1. doi:10.1007/978-3-0348-0513-1.

[110] Alexander F Routh. Drying of thin colloidal films. *Reports on Progress in Physics*, 76(4): 046603, Mar 2013. ISSN 1361-6633. doi:10.1088/0034-4885/76/4/046603.

[111] Alexander F. Routh and William B. Russel. Horizontal drying fronts during solvent evaporation from latex films. *AIChE Journal*, 44(9):2088–2098, Sep 1998. ISSN 1547-5905. doi:10.1002/aic.690440916.

[112] Michael Růžička. *Nichtlineare Funktionalanalysis*. Springer Science + Business Media, 2004. ISBN 3-540-20066-5. doi:10.1007/3-540-35022-5.

[113] W. B. Russel, D. A. Saville, and W. R. Schowalter. *Colloidal Dispersions*. Cambridge University Press, 1989. ISBN 9780511608810. doi:10.1017/cbo9780511608810.

[114] H. Schade and E. Kunz. *Strömungslehre*. de Gruyter Lehrbuch. De Gruyter, 2007. ISBN 9783110189728.

[115] Herrmann Schlichting and Klaus Gersten. *Boundary-Layer Theory*. Springer-Verlag Berlin Heidelberg, 8 edition, 2000. ISBN 978-3-540-66270-9.

[116] P. J. Schmid and H. K. Kytömaa. Transient and asymptotic stability of granular shear flow. *J. Fluid Mech.*, 264:255–275, 1994. doi:10.1017/S0022112094000650.

[117] Peter J. Schmid. Nonmodal stability theory. *Annual Review of Fluid Mechanics*, 39(1): 129–162, Jan 2007. ISSN 1545-4479. doi:10.1146/annurev.fluid.38.050304.092139.

[118] Bjoern Sjoegreen, Katarina Gustavsson, and Reynir Levi Gudmundsson. A model for peak formation in the two-phase equations. *Mathematics of Computation*, 76(260):1925–1941, Oct 2007. ISSN 0025-5718. doi:10.1090/s0025-5718-07-01992-8.

[119] Jacco H. Snoeijer. Free-surface flows with large slopes: Beyond lubrication theory. *Physics of Fluids*, 18(2):021701, 2006. ISSN 1070-6631. doi:10.1063/1.2171190.

[120] H. B. Stewart and Burton Wendroff. Two-phase flow: Models and methods. *Journal of Computational Physics*, 56(3):363–409, Dec 1984. ISSN 0021-9991. doi:10.1016/0021-9991(84)90103-7.

[121] H.Bruce Stewart. Stability of two-phase flow calculation using two-fluid models. *Journal of Computational Physics*, 33(2):259–270, Nov 1979. ISSN 0021-9991. doi:10.1016/0021-9991(79)90020-2.

[122] Manuj Swaroop. *The bulk viscosity of suspensions*. Thesis, California Institute of Technology, 2010. URL `http://resolver.caltech.edu/CaltechTHESIS:05282010-012507201`.

[123] T. Tatsuno, F. Volponi, and Z. Yoshida. Transient phenomena and secularity of linear interchange instabilities with shear flows in homogeneous magnetic field plasmas. *Phys. Plasmas*, 8(2):399, 2001. ISSN 1070-664X. doi:10.1063/1.1336532.

[124] Uwe Thiele. Patterned deposition at moving contact lines. *Advances in Colloid and Interface Science*, 206:399–413, Apr 2014. ISSN 0001-8686. doi:10.1016/j.cis.2013.11.002.

[125] Uwe Thiele, Santiago Madruga, and Lubor Frastia. Decomposition driven interface evolution for layers of binary mixtures. I. Model derivation and stratified base states. *Physics of Fluids*, 19(12):122106, 2007. ISSN 1070-6631. doi:10.1063/1.2824404.

[126] J. W. Thomas. *Numerical Partial Differential Equations: Finite Difference Methods*, volume 22 of *Texts in Applied Mathematics*. Springer New York, 1995. ISBN 978-1-4419-3105-4. doi:10.1007/978-1-4899-7278-1.

[127] O. Thual and L. Lacaze. Fluid boundary of a viscoplastic Bingham flow for finite solid deformations. *Journal of Non-Newtonian Fluid Mechanics*, 165:84–87, 2010. doi:10.1016/j.jnnfm.2009.09.005.

[128] N. L. Trefethen, A. E. Trefethen, S. C. Teddy, and T. A Driscoll. Hydrodynamic stability without eigenvalues. *Science*, 261(5121):578–584, 1993. doi:10.1126/science.261.5121.578.

[129] Martin Trulsson, Bruno Andreotti, and Philippe Claudin. Transition from the viscous to inertial regime in dense suspensions. *Phys. Rev. Lett.*, 109(11):118305, 2012. doi:10.1103/PhysRevLett.109.118305.

[130] Grétar Tryggvason, Ruben Scardovelli, and Stéphane Zaleski. *Direct Numerical Simulations of Gas-Liquid Multiphase Flows*. Cambridge University Press, 2011. ISBN 9780511975264. doi:10.1017/cbo9780511975264.

[131] Stephen Whitaker. Flow in porous media I: A theoretical derivation of Darcy's law. *Trans. Porous Media*, 1(1):3–25, 1986. ISSN 0169-3913. doi:10.1007/BF01036523.

[132] Stephen Whitaker. *The Method of Volume Averaging*, volume 13. Springer, 1998. doi:10.1007/978-94-017-3389-2.

[133] Martin Wörner. Numerical modeling of multiphase flows in microfluidics and micro process engineering: a review of methods and applications. *Microfluid Nanofluid*, 12(6):841–886, Mar 2012. ISSN 1613-4990. doi:10.1007/s10404-012-0940-8.

[134] Jacob Yström. On two-fluid equations for dispersed incompressible two-phase flow. *Computing and Visualization in Science*, 4(2):125–135, Dec 2001. ISSN 1433-0369. doi:10.1007/s007910100064.

[135] Eberhard Zeidler. *Nonlinear Functional Analysis and its Applications*, volume 3. Springer New York, 1985. ISBN 978-1-4612-5020-3. doi:10.1007/978-1-4612-5020-3.

[136] Eberhard Zeidler. *Nonlinear Functional Analysis and its Applications*, volume 1. Springer New York, 1986. ISBN 978-0-387-90914-1.

[137] Eberhard Zeidler. *Nonlinear Functional Analysis and Its Applications*, volume 2a. Springer New York, 1990. ISBN 978-1-4612-0985-0. doi:10.1007/978-1-4612-0985-0.

[138] Eberhard Zeidler. *Nonlinear Functional Analysis and its Applications*, volume 2b. Springer New York, 1990. ISBN 978-1-4612-0981-2. doi:10.1007/978-1-4612-0981-2.

[139] Junjie Zhou, B. Dupuy, A. Bertozzi, and A. Hosoi. Theory for shock dynamics in particle-laden thin films. *Physical Review Letters*, 94(11):117803, Mar 2005. ISSN 1079-7114. doi:10.1103/physrevlett.94.117803.

Appendix A

Numerical Methods for Complex Fluid Simulation

In the course of this thesis, we had to solve boundary value problems and partial differential equations in form of systems or single equations. Most of the mentioned equations do not possess known analytic solutions. For some of them, like the incompressible Navier-Stokes equations (1.1.11), even the existence of solutions for three-dimensional problems is still unknown, let alone an analytic solution for general flows. Therefore, methods are needed in order to approximate (possible) solutions to sufficient accuracy. Since we were interested in one-dimensional solutions of nonlinear systems of equations with non-standard boundary conditions, we decided on using the finite difference method due to its easy implementation and simple generalizability to systems of equations. Nevertheless, this method limits us to regular meshes with smooth solutions.

We first introduce the finite difference method and state some known analytic results, which allow us to verify our methods in Section A.2. We also explain the Euler-Euler-2-steps method as a variable time step algorithm and explain the usage of Maple [84] for the derivation of the Jacobian in our solver.

A.1 Finite difference method

Notation and discretized derivatives

The finite difference method (FDM) can be dated back to Euler. For modern and comprehensive introductions see e.g. [64, 126]. The FDM computes the values of a solution at discrete points of the domain. Therefore, we first need to partition our domain into $n_x + 1$ discrete points x_k and call it the numeric grid Ω_h, which is sometimes also referred to as numeric mesh in the literature. Without loss of generality we concentrate on one-dimensional domains $\Omega = [0, L]$ and demand

the ordering

$$0 = x_0 < x_1 < x_2 < \ldots < x_{n_x-1} < x_{n_x} = L,$$

where we concentrate on the special situation of a regular grid, where the grid size is constant, i.e.

$$x_{k+1} - x_k = h = \frac{1}{n_x} \qquad \forall k \in \{0, 1, \ldots, n_x - 1\}.$$

Similar definitions are used for the time grid T_h, i.e.

$$0 = t_0 < t_1 < t_2 < \ldots < t_{n_t-1} < t_{n_t} = T,$$
$$t_{k+1} - t_k = \tau = \frac{1}{n_t} \qquad \forall k \in \{0, 1, \ldots, n_t - 1\}.$$

For convenience, we define

$$f_k^l := f(t_l, x_k) = f(l\tau, kh)$$

and we drop the l in expressions, where the time is chosen arbitrary, but fixed.

As the name finite difference method implies, it is based on the idea that derivatives of smooth enough functions f at a position $x_d \in [0, L]$ can be approximated by combinations of function values at the grid points x_k, e.g. of the form

$$f'_d \approx \frac{1}{h} \sum_{k=0}^{n} a_k f_k =: \nabla_h f_k,$$

where $a_k \in \mathbb{R}$ is chosen appropriately.

For smooth enough functions, its theoretical basis and concrete coefficients a_k can be derived by usage of Taylor's theorem.

Theorem A.1 (Taylor's theorem)**.** *If the first $n \in \mathbb{N}$ derivatives of a function $f : D \to W$ exist, then we can represent f in a neighborhood $U \subset D$ of x_0 as*

$$f(x_0 + h) = \sum_{k=0}^{n-1} \frac{h^k}{k!} f^{(k)}(x_0) + R_n(x_0 + h),$$

where $x_0 + h \in U$ and the rest R_n can be given in Lagrange form as

$$R_n(x_0 + h) = \frac{h^n}{n!} f^{(n)}(\xi),$$

for some $\xi \in]x_0, x_0 + h[$.

Proof. For a proof, see e.g. [136]. □

For smooth enough f being n times continuous differentiable, the rest can be estimated by

$$R_n(x_0 + h) = O(h^n).$$

In particular, Taylor's theorem yields for a twice continuous differentiable function f, that

$$f(x_k + h) = f_{k+1} = f_k + f'_k h + f''_k \frac{h^2}{2} + O(h^3) \tag{A.1.1}$$

holds. Rewriting this for f'_k gives

$$f'_k = \frac{1}{h}(f_{k+1} - f_k) + O(h).$$

This shows that for small h we can define

$$D^f_x f_k := (f_{k+1} - f_k)/h$$

and use D^f_x as ∇_h. This particular choice is called the forward difference formula. The choice for ∇_h is not unique, since considering

$$f(x_k - h) = f_{k-1} = f_k - f'_k h + f''_k \frac{h^2}{2} + O(h^3) \tag{A.1.2}$$

yields

$$D^b_x f_k := (f_k - f_{k-1})/h, \qquad f'_k = D^b_x f_k + O(h),$$

which is the backward difference formula. Further, combination of (A.1.1) with (A.1.2) yields

$$f'_k = \frac{1}{2h}(f_{k+1} - f_{k-1}) + O(h^2),$$

so an alternative definition for ∇_h is

$$D^c_x f_k := (f_{k+1} - f_{k-1})/(2h),$$

which is referred to as central difference formula.

Higher order derivatives can be either directly derived by Taylor expansions or by concatenating first order derivatives, e.g.

$$f''_k = D^f_x D^b_x f_k = D^b_x D^f_x f_k = \frac{1}{h^2}(f_{k+1} - 2f_k + f_{k-1}) + O(h^2),$$

and its discrete definition

$$\nabla^2_h f_k := D^c_{xx} f_k := \frac{1}{h^2}(f_{k+1} - 2f_k + f_{k-1}), \tag{A.1.3}$$

which is the central difference formula for the second order derivative.

Since the Taylor approximation can also be performed in time, we can similarly approximate the time derivative $\partial_t f_k|_{t=t_l}$ as

$$D^f_t f^l_k := (f^{l+1}_k - f^l_k)/\tau, \tag{A.1.4}$$
$$D^b_t f^l_k := (f^l_k - f^{l-1}_k)/\tau. \tag{A.1.5}$$

If only two consecutive time steps are involved in the computation at any time, we call it a two level difference scheme.

Periodic equations

For periodic boundary conditions, we simply demand

$$f_{n_x} = f_0$$

and apply the discretized spatial derivatives at every point x_k. For example, consider the one-dimensional heat equation

$$\begin{aligned} \partial_t f(t,x) &= \partial_{xx} f(t,x) && \text{for } (t,x) \in [0,T] \times \Omega, \\ f(0,x) &= g(x) && \text{for } x \in \Omega, \end{aligned}$$

with periodic boundary conditions, where g is a given smooth function. Then, using the discretized approximations of the time and spatial derivatives, (A.1.4) and (A.1.3), respectively, yields

$$\begin{aligned} f_k^{l+1} - f_k^l &= \frac{\tau}{h^2}(f_{k+1}^l - 2f_k^l + f_{k-1}^l), \\ f_k^0 &= g_k, \end{aligned} \tag{A.1.6}$$

for every point $x_k \in \Omega_h$ and $t_l \in T_h$. This is a so-called explicit scheme, because it can be rearranged for the value of the function at the new time step, i.e. f_k^{l+1}.

In order to solve this equation, we start at time $t = 0\tau$ and solve for f_k^{l+1} for all k. Then, we advance to the next time step $t = 1\tau$ and continue until we reach $t = n_t\tau = T$. Since, (A.1.6) is a linear equation, we can reformulate this in matrix/vector notation, as

$$\boldsymbol{f}^{l+1} = (\tau \boldsymbol{D}_{xx}^c + \boldsymbol{I})\boldsymbol{f}^l, \tag{A.1.7}$$

where

$$\boldsymbol{D}_{xx}^c = \frac{1}{h^2}\begin{pmatrix} -2 & 1 & 0 & 0 & \dots & 0 & 1 \\ 1 & -2 & 1 & 0 & \ddots & 0 & 0 \\ 0 & 1 & -2 & 1 & 0 & \ddots & \vdots \\ \vdots & \ddots & \ddots & \ddots & \ddots & \ddots & \vdots \\ \vdots & \dots & 0 & 1 & -2 & 1 & 0 \\ 0 & \dots & \dots & 0 & 1 & -2 & 1 \\ 1 & 0 & \dots & \dots & 0 & 1 & -2 \end{pmatrix}, \qquad \boldsymbol{f}^l = \begin{pmatrix} f_0^l \\ f_1^l \\ f_2^l \\ \vdots \\ f_{n_x-3}^l \\ f_{n_x-2}^l \\ f_{n_x-1}^l \end{pmatrix}.$$

Typically, the finite difference equations contain banded matrices, which allows a sparse representation for minimal memory usage and the application of fast matrix solvers.

If one uses (A.1.5) instead of (A.1.4) for the time discretization, it yields

$$\begin{aligned} f_k^l - f_k^{l-1} &= \frac{\tau}{h^2}(f_{k+1}^l - 2f_k^l + f_{k-1}^l), \\ f_k^0 &= g_k, \end{aligned}$$

which contains multiple spatial positions of the largest time step $t = t_l$. Thus, it cannot be explicitly rewritten for f_k^l anymore and is called an implicit scheme with an implicit Euler method. The corresponding matrix equation is

$$\boldsymbol{f}^{l+1} = (\tau \boldsymbol{D}_{xx}^c + \boldsymbol{I})^{-1} \boldsymbol{f}^l, \tag{A.1.8}$$

and demands the solution of a matrix equation at every time step.

Boundary conditions

For Dirichlet boundary conditions

$$f_0 = a, \qquad f_{n_x} = b,$$

with $a, b \in \mathbb{R}$, the values a and b of f_0 and f_{n_x}, respectively, are directly used, e.g.

$$D_x^b f_1 = (f_1 - a)/h.$$

Similarly, Neumann boundary conditions

$$f_0' = c, \qquad f_{n_x}' = d, \tag{A.1.9}$$

are enforced by demanding

$$D_x^f f_0 = (f_1 - f_0)/h = c, \qquad D_x^b f_{n_x} = (f_{n_x-1} - f_{n_x})/h = d. \tag{A.1.10}$$

The matrix equations (A.1.7) or (A.1.8) need to be modified accordingly. There are two strategies common. The first is to eliminate the rows corresponding to the boundary condition positions in the matrices and create a suitable right hand side.

We employ a different method and introduce additional points for the boundaries, where equations (A.1.9) or (A.1.10) are explicitly enforced. This is also commonly referred to as ghost-points. The matrix and vector definition for Dirichlet boundary condition is accordingly changed to

$$\boldsymbol{f}^l = \begin{pmatrix} f_0^l \\ f_1^l \\ \vdots \\ f_{n_x-1}^l \\ f_{n_x}^l \end{pmatrix}, \qquad \tilde{\boldsymbol{D}}_{xx}^c = \frac{1}{h^2} \begin{pmatrix} 0 & \dots & \dots & \dots & \dots & \dots & 0 \\ 1 & -2 & 1 & 0 & \ddots & 0 & 0 \\ 0 & 1 & -2 & 1 & 0 & \ddots & \vdots \\ \vdots & \ddots & \ddots & \ddots & \ddots & \ddots & \vdots \\ \vdots & \dots & 0 & 1 & -2 & 1 & 0 \\ 0 & \dots & \dots & 0 & 1 & -2 & 1 \\ 0 & \dots & \dots & \dots & \dots & \dots & 0 \end{pmatrix},$$

$$\boldsymbol{b} = \begin{pmatrix} a \\ 0 \\ \vdots \\ 0 \\ b \end{pmatrix}, \qquad \tilde{\boldsymbol{I}} = \begin{pmatrix} 0 & \dots & \dots & \dots & 0 \\ 0 & 1 & \dots & 0 & 0 \\ \vdots & \ddots & \ddots & \ddots & \vdots \\ 0 & \dots & \dots & 1 & 0 \\ 0 & \dots & \dots & \dots & 0 \end{pmatrix},$$

and the explicit form (A.1.7) becomes

$$\boldsymbol{f}^{l+1} = (\tau \tilde{\boldsymbol{D}}_{xx}^c + \tilde{\boldsymbol{I}})\boldsymbol{f}^l + \boldsymbol{b},$$

whereas the implicit form (A.1.8) becomes

$$\boldsymbol{f}^{l+1} = (\tau \tilde{\boldsymbol{D}}_{xx}^c + \boldsymbol{I})^{-1}(\tilde{\boldsymbol{I}}\boldsymbol{f}^l + \boldsymbol{b}).$$

The ghost-point method increases the size of the system by the number of boundary condition points, but is often easier to implement and less prone to human errors, since no explicit elimination process is necessary. Additionally, it allows for a straightforward implementation in combination with computer algebra, see below.

Convergence theory of the finite difference methods

Let us consider a differential problem of the form

$$Au = f, \qquad \text{for all } (t,x) \in [0,T] \times \Omega, \tag{A.1.11}$$

where $A : U \to V$ is a differential operator, $u \in U$ the solution and $f \in V$ a given function. Depending on the problem at hand, this can also be either an initial value problem or an elliptic problem. The corresponding discrete problem is

$$A_h u_h = f_h, \qquad \text{for all } (t,x) \in T_h \times \Omega_h, \tag{A.1.12}$$

where $A_h : U_h \to V_h$ is a finite difference approximation of A, $u_h \in U_h$ is the discretized solution and $f_h \in V_h$ the discretized form of f. Further, let us define a projection operator $r_h : U \to U_h$ defined as

$$(r_h u)(t_l, x_k) = u(t_l, x_k).$$

Let us call a discretization A_h of an operator A consistent, if

$$\|A_h(r_h u) - A_h u_h\| \to 0 \qquad \text{as } h \to 0.$$

We call A_h consistent of order p, if

$$\|A_h(r_h u) - A_h u_h\| = O(h^p) \qquad \text{as } h \to 0.$$

We call the discrete operator A_h stable, if for some constant $M > 0$

$$\|u - v\| \leq M \|A_h u - A_h v\| \qquad \forall u, v \in U_h \tag{A.1.13}$$

holds.

Let us call a numeric approximation convergent, if

$$\|(r_h u) - u_h\| \to 0 \qquad \text{as } h \to 0.$$

And it is convergent of order p, if

$$\|(r_h u) - u_h\| = O(h^p) \qquad \text{as } h \to 0.$$

For consistent linear systems, stability and convergence is equivalent as the following well-known theorem tells us.

Theorem A.2 (Lax Equivalence Theorem)**.** *A consistent, two level difference scheme for a well-posed linear initial-value problem is convergent if and only if it is stable.*

Proof. For a proof see for example [126] and the references therein. □

For consistent nonlinear systems we can still prove that stability implies convergence.

Theorem A.3. *Assume the problem (A.1.11) is well-posed and the discrete problem (A.1.12) has a unique solution, is consistent and stable with respect to the same norm $\|\cdot\|$. Then, the method is convergent in the norm $\|\cdot\|$ with at least the order of consistency.*

Proof. Stability together with consistency of order p yields convergence, since

$$\|(r_h u) - u_h\| \leq M \|A_h(r_h u) - A_h u_h\| \leq M\, O(h^p),$$

and for $h \to 0$ this term goes to zero. □

Thus, a stable scheme with higher order of consistency is preferable, since it converges faster to the exact solution. Generally, consistency is easy to prove from Taylor's theorem. On the other side, stability can be hard to show analytically. However, for a linear problem, A_h is just a matrix and stability (A.1.13) is equivalent to having a $M > 0$, such that

$$\|u_h\| \leq M \|A_h u_h\|.$$

If we choose $\|\cdot\|$ to be the standard 2-norm of vectors, and denote by $\rho(A_h)$ the spectral radius, i.e. largest eigenvalue magnitude, of A_h, then

$$\|A_h u_h\| \geq \rho(A_h) \|u_h\|,$$

such that

$$\|u_h\| \leq \frac{1}{\rho(A_h)} \|A_h u_h\|. \tag{A.1.14}$$

Thus, a sufficient stability criterion is that $\rho(A_h) > 0$, which implies A_h needs to be a nonsingular matrix. On the other side, time dependent problems with an implicit scheme have a structure of the form

$$A_h u_h^{l+1} = u_h^l,$$

so that (A.1.14) becomes

$$\|u_h^{l+1}\| \leq \frac{1}{\rho(A_h)} \|u_h^l\|,$$

which is only well posed if there exists a $M > 0$, so that

$$\frac{1}{\rho(A_h)} < 1 + \tau M, \tag{A.1.15}$$

which implies the growth of values is bounded by an exponential term in time [126]. Generally, this is only a necessary criterion, but for the case of a real symmetric matrix A_h the equality holds in (A.1.14) and it becomes a sufficient stability criterion [126].

Thus, even for very difficult schemes this criterion allows us to obtain insight in the convergence of a finite difference scheme by usage of a numeric eigenvalue decomposition of the resulting matrix system. Unfortunately, our schemes do not yield symmetric matrices due to the nonlinearities involved. Therefore, we can only rule out finite difference schemes that violate this criterion, but currently do not know whether our schemes converge to the solution unless we tested with a known analytic solution or a different numeric method.

Nonlinearities and the Maple mechanism

In order to cope with nonlinearities in our system, we use Newton's method. Suppose we have a nonlinear differential equation of the form

$$Nu = f,$$

where N is a nonlinear differential operator. Then, we first discretize the equation using a finite difference method for the differentials and obtain a new equation of the form

$$N_h u_h = f_h.$$

We construct a fixpoint iteration with sequence u_h^n, such that $\lim_{n\to\infty} u_h^n = u_h$. First, we linearized around the last known state u_h^n by usage of Taylors theorem as

$$N_h u_h^n + J_h \delta + O(\delta^2) = f_h, \tag{A.1.16}$$

where $\delta = u_h^{n+1} - u_h^n$ and

$$J_h \delta = \lim_{\varepsilon \to 0} \frac{1}{\varepsilon}(N_h(u_h + \varepsilon\delta) - N_h(u_h))$$

is the Jacobian of N_h. Rewriting (A.1.16) for δ gives

$$J_h \delta = (f_h - N_h u_h^n) + O(\delta^2).$$

Neglecting higher order perturbations, this is a linear equation of the form (A.1.12) with J_h a matrix, and the right hand side a vector of known values. Thus, we can solve for δ via

$$\delta = J_h^{-1}(f_h - N_h u_h^n), \tag{A.1.17}$$

and compute a newly refined solution as

$$u_h^{n+1} = u_h^n + \delta.$$

This algorithm has the disadvantage, that the Jacobian J_h needs to be computed, which can get complicated and error-prone for systems of equations. A workaround is to implement the scheme into Maple [84], let Maple derive the Jacobian and output $N_h u_h^n$, f_h and J_h as a MATLAB scripts [85]. Then, the MATLAB solver just needs to call these external scripts and solves equations of the form (A.1.17). This allows us to use the same code for very different equations and even systems. Additionally, the code looks exactly like the mathematical definition of a discretized equation, e.g. (A.1.6) and boundary conditions are defined as in (A.1.9) and (A.1.10) using the ghost-point method.

Euler-Euler-2-steps method

In case of time dependent problems, we use a variable time step based on the Richardson extrapolation. Suppose an algorithm $u_\tau^{n+1} = Q_\tau u_\tau^n$ is of convergence order p. Then

$$Q_\tau u(0) = u(T) + C\tau^p + O(\tau^{p+1}) \tag{A.1.18}$$

Let us choose $s > 0$ and define the method

$$R_\tau u = \frac{s^p Q_\tau u - Q_{s\tau} u}{s^p - 1}. \tag{A.1.19}$$

Using the error estimate (A.1.18) in the new method (A.1.19) gives

$$R_\tau u(0) = \frac{s^p[u(T) + C\tau^p + O(\tau^{p+1})] - [u(T) + Cs^p\tau^p + O(\tau^{p+1})]}{s^n - 1} = u(T) + O(\tau^{p+1}).$$

Thus, the new solution operator R_τ converges one order faster. This is called Richardson extrapolation.

In order to control the error as

$$\|Q_\tau u - Q_{s\tau} u\| \leq \text{tol}$$

define the relative error

$$e_{\text{rel}} = \frac{\|Q_\tau u - Q_{s\tau} u\|}{\text{tol}}$$

and demand

$$e_{\text{rel}} \leq 1.$$

However, we know from (A.1.18) that

$$e_{\text{rel}} = \frac{C}{\text{tol}} \tau^p (1 - s^p)$$

and

$$1 = \frac{C}{\text{tol}} \tau_{\text{opt}}^p (1 - s^p),$$

which we can substitute for C and get

$$\tau_{\text{opt}} = \frac{\tau}{e_{\text{rel}}^{1/p}}.$$

For numeric reasons the factor of τ is often multiplied by a value $f_{\text{num}} \in [0.8, 0.95]$ and is forbidden to increase or decrease by too big factors. A common choice is

$$\tau_{\text{opt}} = \tau \max(f_{\min}, \min(f_{\max}, f_{\text{num}} e_{\text{rel}}^{-1/p}))$$

and valid factors are for example

$$f_{\text{num}} = 0.8, \qquad f_{\min} = 0.1, \qquad f_{\max} = 2.0.$$

Our solver uses the maximum norm, $s = 2$ and the implicit Euler method, which is convergent to order $p = 1$. This is called an Euler-Euler-2-steps method.

A.2 Numerical scheme for thin-film and drift-flux models

Simulation of the thin-film model proposed in Section 1.3 and the drift-flux model in Section 3.3 is done using a finite difference method of second order with Euler-Euler-2-steps and ghost-point methods. The scheme uses neighboring half points for the approximation of the derivatives. Suppose we have mesh points $x_i \in \mathbb{R}$ with constant width $h = x_{i+1} - x_i$ and suppose we have a function $f(x)$ with $f_i := f(x_i)$. Let us further denote the half-points by $x_{i+1/2} := (x_i + x_{i+1})/2$ and $f_{i+1/2} := (f_{i+1} + f_i)/2$, and then we define the discrete derivatives as

$$\begin{aligned}
\nabla_h f_{i+1/2} &= (f_{i+1} - f_i)/h, \\
\nabla_h f_i &= (f_{i+1/2} - f_{i-1/2})/h && = (f_{i+1} - f_{i-1})/(2h), \\
\nabla_h^2 f_i &= (\nabla_h f_{i+1/2} - \nabla_h f_{i-1/2})/h && = (f_{i+1} - 2f_i + f_{i-1})/h^2, \\
\nabla_h^2 f_{i+1/2} &= (\nabla_h f_{i+1} - \nabla_h f_i)/h && = (f_{i+2} - f_{i+1} - f_i + f_{i-1})/(2h^2), \\
\nabla_h^3 f_i &= (\nabla_h^2 f_{i+1/2} - \nabla_h^2 f_{i-1/2})/h && = (1/2 f_{i+2} - f_{i+1} - f_{i-1} + 1/2 f_{i-2})/h^3, \\
\nabla_h^3 f_{i+1/2} &= (\nabla_h^2 f_{i+1} - \nabla_h^2 f_i)/h && = (f_{i+2} - 3f_{i+1} + 3f_i - f_{i-1})/h^3, \\
\nabla_h^4 f_i &= (\nabla_h^3 f_{i+1/2} - \nabla_h^3 f_{i-1/2})/h && = (f_{i+2} - 4f_{i+1} + 6f_i - 4f_{i-1} + f_{i-2})/h^4,
\end{aligned}$$

which is reduced to the standard central scheme of second order for entire points. This scheme is applied to any term behind a derivative, e.g. in (1.4.8) the flux term due to surface tension, gravity and disjoining pressure is

$$F = \partial_x \left(\frac{h^3}{3} \partial_x (\partial_{xx} h + \psi h^{-3} - h\, B) \right). \tag{A.2.2}$$

The finite difference discretization of flux (A.2.2) is

$$\begin{aligned}
p_i &:= (-\nabla_h^2 h_i - \psi h_i^{-3} + B h_i), \\
u_{i+1/2} &:= -\frac{1}{3} \nabla_h p_{i+1/2} h_{i+1/2}^2, \\
u_{i-1/2} &:= -\frac{1}{3} \nabla_h p_{i-1/2} h_{i-1/2}^2, \\
F_i &= (h_{i+1/2} u_{i+1/2} - h_{i-1/2} u_{i-1/2})/h.
\end{aligned}$$

In all our simulations, we computed the eigenvalues of the solution matrix and found the stability constant M to adhere

$$0 < M < 100$$

even for time steps $\tau < 10^{-6}$. Hence, the necessary criterion (A.1.15) is fulfilled for our finite difference methods and we believe to have a stable method.

A.3 Numerical scheme for the stability problem

The numerical scheme of stability problem (4.3.10) is the same as in Section A.2. Additionally, we use a staggered grid scheme for the multiphase model, where the velocities $\hat{u}_s, \hat{v}_f$ and $\hat{v}_s$ are placed

on entire points and the volume fraction on half points, i.e. $\hat{u}_{si} := \hat{u}_s(x_i)$ and $\hat{\phi}_{sj} := \hat{\phi}_s(x_{j+1/2})$. This approach evades a decoupling of odd and even points in the volume fraction, that has been observed when using the standard central scheme for the transport equation (4.3.10a) in the multiphase model.

After discretization of system (4.3.10) and possibly equation (4.3.11), we get two matrices. The first matrix contains the spatial derivatives and the second matrix the discretization for the time mode c. This gives a system of the form

$$\boldsymbol{A}\boldsymbol{v} = c\boldsymbol{B}\boldsymbol{v},$$

which has been solved using the generalized eigenvalue solvers of Matlab [85].

The boundary conditions are implemented using the ghost-point method and they are explicitly eliminated before solving the generalized eigenvalue problems. This circumvents the appearance of pseudo-eigenvalues stemming from the ghost-points, which can be of any value, even infinity and do not give new insight into the stability of the system.

As system (4.3.10) is complex and its implementation prone to errors, we looked for a possible validation method. If we drop the convective term $\partial_x(U_s\hat{\phi}_s)$ and set $\mathrm{Re} = 0$, then the Couette flow of Section 4.4 permits an analytic solution. Using the Fourier ansatz $e^{ikx+i\ell y-imt}$ in system (4.3.4), we are able to derive an algebraic system. The derived algebraic system and the appropriate numerical approximation produce exactly the same results, which shows that our numerical implementation produces trustworthy solutions.

A.4 Riccati method for the Orr-Sommerfeld-Bingham problem

The Orr-Sommerfeld-Bingham problem is solved using the finite difference method from Section A.3. Since the problem contains singularities at the yield-surface, the stability of the finite difference method is questionable. We therefore try to validate the FDM using a shooting method. However, a direct application of the shooting method for problem (4.2.13) is not even stable for the Newtonian case and a so-called Riccati method is employed, cf. [26]. Additionally, the singularity contained in problem (4.2.13) is circumvented using a Frobenius series ansatz.

The Riccati method has been first proposed by Davey [26] for the Orr-Sommerfeld problem. It is essentially a transformation of the unstable linear problem to a stable nonlinear problem. Davey [26] describes the Riccati methods' stabilization property as follows:

> The basic solutions of a linear differential system are usually exponential in character and if the real parts of the characteristic values of the operator are widely separated then, when using an explicit integration scheme, parasitic growth problems occur and a special method, such as orthonormalization, will be needed to resolve the problem. The importance of the Riccati method lies in the fact that it transforms the linear problem into a nonlinear problem whose characteristic values all have negative real parts thus ensuring that the integration will be stable. The exponential character is essentially transformed by the nonlinearity to a tanh type behavior.

Further, the well-known results from Frigaard et al. [43] have also been obtained using the Riccati method. Unfortunately, they do not describe the method in his original publication [43] and apparently use the wrong boundary conditions.

Suppose we like to solve a linear boundary value problem of fourth order in $x(t)$ for $t \in [t_0, t_1]$ with a linear affine boundary condition at $t = t_0$. Then, we can employ the Riccati method. Let us denote by

$$\boldsymbol{y}(t) = \begin{pmatrix} x(t) \\ x'(t) \end{pmatrix}, \qquad \boldsymbol{z}(t) = \begin{pmatrix} x''(t) \\ x'''(t) \end{pmatrix}$$

the solution vectors, which are split into two parts and suppose our equation is of the form

$$\boldsymbol{y}'(t) = \boldsymbol{A}(t)\boldsymbol{y}(t) + \boldsymbol{B}(t)\boldsymbol{z}(t) + \boldsymbol{f}(t), \tag{A.4.1a}$$
$$\boldsymbol{z}'(t) = \boldsymbol{C}(t)\boldsymbol{y}(t) + \boldsymbol{D}(t)\boldsymbol{z}(t) + \boldsymbol{g}(t), \tag{A.4.1b}$$

with boundary conditions

$$\boldsymbol{y}(t_0) = \Gamma(t_0)\boldsymbol{z}(t_0) + \boldsymbol{\alpha}, \qquad \boldsymbol{h}(\boldsymbol{y}(t_1), \boldsymbol{z}(t_1)) = \boldsymbol{0},$$

where $\boldsymbol{A}$, $\boldsymbol{B}$, $\boldsymbol{C}$, $\boldsymbol{D}$, and $\boldsymbol{\Gamma}$ are matrix valued functions, $\boldsymbol{f}$, $\boldsymbol{g}$, $\boldsymbol{h}$ are vector valued functions and $\boldsymbol{\alpha}$ is a constant vector.

Then, we insert the ansatz

$$\boldsymbol{y}(t) = \boldsymbol{R}(t)\boldsymbol{z}(t) + \boldsymbol{w}(t), \tag{A.4.2}$$

into (A.4.1) and get

$$\begin{aligned} \boldsymbol{R}'\boldsymbol{z} + \boldsymbol{R}\boldsymbol{z}' + \boldsymbol{w}' &= \boldsymbol{A}\boldsymbol{R}\boldsymbol{z} + \boldsymbol{A}\boldsymbol{w} + \boldsymbol{B}\boldsymbol{z} + \boldsymbol{f}, \\ \boldsymbol{z}' &= \boldsymbol{C}\boldsymbol{R}\boldsymbol{z} + \boldsymbol{C}\boldsymbol{w} + \boldsymbol{D}\boldsymbol{z} + \boldsymbol{g}, \end{aligned} \tag{A.4.3}$$

which can be combined to yield

$$\boldsymbol{R}'\boldsymbol{z} + \boldsymbol{R}\boldsymbol{C}\boldsymbol{R}\boldsymbol{z} + \boldsymbol{R}\boldsymbol{C}\boldsymbol{w} + \boldsymbol{R}\boldsymbol{D}\boldsymbol{z} + \boldsymbol{R}\boldsymbol{g} + \boldsymbol{w}' = \boldsymbol{A}\boldsymbol{R}\boldsymbol{z} + \boldsymbol{A}\boldsymbol{w} + \boldsymbol{B}\boldsymbol{z} + \boldsymbol{f}.$$

A variational argument than gives the new nonlinear differential equation for the transformation matrix

$$\boldsymbol{R}' = -\boldsymbol{R}\boldsymbol{C}\boldsymbol{R} - \boldsymbol{R}\boldsymbol{D} + \boldsymbol{A}\boldsymbol{R} + \boldsymbol{B} \tag{A.4.4}$$

and the rest

$$\boldsymbol{w}' = -\boldsymbol{R}\boldsymbol{C}\boldsymbol{w} + \boldsymbol{A}\boldsymbol{w} + \boldsymbol{f} - \boldsymbol{R}\boldsymbol{g}.$$

The boundary conditions become

$$\begin{aligned} \boldsymbol{R} &= \boldsymbol{\Gamma} && \text{at } t = t_0, \\ \boldsymbol{w} &= \boldsymbol{\alpha} && \text{at } t = t_0, \\ \boldsymbol{h}(\boldsymbol{R}\boldsymbol{z} + \boldsymbol{w}, \boldsymbol{z}) &= \boldsymbol{0} && \text{at } t = t_1. \end{aligned}$$

Then, for given $\boldsymbol{R}$ and $\boldsymbol{w}$, we can reconstruct the original result by first solving for $\boldsymbol{z}$ using the ODE (A.4.3), and then, using our ansatz (A.4.2) for $\boldsymbol{y}$.

For the Orr-Sommerfeld-Bingham problem (4.2.13), we have $t_0 = 1$ and $t_1 = y_B$ as well as

$$\begin{aligned}
\boldsymbol{A} &= \begin{pmatrix} 0 & 1 \\ 0 & 0 \end{pmatrix}, & \boldsymbol{C} &= \begin{pmatrix} 0 & 0 \\ i\alpha \mathrm{Re}(-(U_B - c)\alpha^2 - \partial_{yy} U_B) - \alpha^4 & -\frac{2\alpha^2 \mathrm{B}}{\xi^2} \end{pmatrix}, \\
\boldsymbol{B} &= \begin{pmatrix} 0 & 0 \\ 1 & 0 \end{pmatrix}, & \boldsymbol{D} &= \begin{pmatrix} 0 & 1 \\ i\alpha \mathrm{Re}(U_B - c) + 2\alpha^2 + \frac{2\alpha^2 \mathrm{B}}{\xi} & 0 \end{pmatrix}, \\
\boldsymbol{f} &= \boldsymbol{0}, & \boldsymbol{g} &= \boldsymbol{0}, \\
\boldsymbol{\Gamma} &= \boldsymbol{0}, & \boldsymbol{\alpha} &= \boldsymbol{0}, \\
\boldsymbol{h}(\boldsymbol{y}, \boldsymbol{z}) &= \boldsymbol{y}, &&
\end{aligned}$$

where we used $\xi = (y - y_B)/(1/2 - y_B)$. Our case yields $\boldsymbol{w} \equiv \boldsymbol{0}$ and the boundary condition $\boldsymbol{R}\boldsymbol{z} = \boldsymbol{0}$ at $t = t_1$ can also be expressed as

$$\det \boldsymbol{R} = 0 \qquad \text{at } t = t_1.$$

A direct application of the method might fail, since $t = t_1 = y_B$ yields $\xi = 0$ and system (A.4.4) runs into a singularity, which might introduce numeric problems. A workaround is to expand the solution of the fourth order equation into a Frobenius series around the singularity at y_B.

Let us derive a Frobenius series around the singularity at $t = y_B$, following the book of Bender and Orszag [12]. We consider a linear homogeneous ordinary differential equation of fourth order of the form

$$\frac{\mathrm{d}^4}{\mathrm{d}t^4} x(t) + b_3(t) \frac{\mathrm{d}^3}{\mathrm{d}t^3} x(t) + b_2(t) \frac{\mathrm{d}^2}{\mathrm{d}t^2} x(t) + b_1(t) \frac{\mathrm{d}}{\mathrm{d}t} x(t) + b_0(t) x(t) = 0. \tag{A.4.5}$$

We call a point $t_o \in \mathbb{R}$ an ordinary point of (A.4.5), iff all the functions $b_i(t)$ with $i \in \{0, 1, 2, 3\}$ are analytic in a neighborhood of t_o [12]. We call a point $t_s \in \mathbb{R}$ a regular singular point of (A.4.5), iff it is not an ordinary point and all the functions

$$(t - t_s)^{4-i} b_i(t)$$

with $i \in \{0, 1, 2, 3\}$ are analytic in a neighborhood of t_s [12].

From these definitions we see $t_0 = y_B$ is a regular singular point of problem (4.2.13), thus a theorem due to Fuchs guarantees we can expand the solution around $t = y_B$ into at least one so-called Frobenius series of the form

$$x(t) = \sum_{n=0}^{\infty} a_n (t - t_s)^{n+\beta}, \tag{A.4.6}$$

where $a_i, \beta \in \mathbb{R}$ for all $i \in \mathbb{N}$ [12].

Inserting ansatz (A.4.6) into (4.2.13) yields the equation

$$\beta(\beta - 1)(\beta - 2)(\beta - 3) = 0,$$

which fixes the exponent β. Since, the solutions are separated by integers, we can derive four Frobenius series with an increasing number of degrees of freedom, cf. [12]. However, only $\beta \in \{2, 3\}$

give particular solutions that are zero at the singularity and fulfill the boundary condition of our problem.

The case $\beta = 3$ yields

$$
\begin{aligned}
a_1 &= \frac{1}{4}\alpha^2 \mathrm{B} a_0, \\
a_2 &= \frac{1}{120}(a_0(i\alpha\mathrm{Re}(1-c)6 + 12\alpha^2) + a_1 16\alpha^2\mathrm{B}), \\
a_3 &= -\frac{i}{80}\alpha^3 a_0 c\,\mathrm{B}\,\mathrm{Re} + \frac{1}{40}\alpha^4 \mathrm{B} a_0 + \frac{i}{80}\alpha^3 \mathrm{B} a_0 \mathrm{Re} + \frac{1}{360}\alpha^6 B^3 a_0, \\
a_4 &= \frac{\alpha a_0}{12600}(\alpha^3(45 + 38\alpha^2\mathrm{B}^2 + 2\alpha^4\mathrm{B}^4) - i(60 + \alpha^2(45 + 19\alpha^2\mathrm{B}^2)(c-1))\mathrm{Re} - 15\alpha(c-1)^2\mathrm{Re}^2) \\
a_5 &= \frac{\alpha^3 a_0 \mathrm{B}}{604800}(-1020i\mathrm{Re} + \alpha(4\alpha^2(135 + 34\alpha^2\mathrm{B}^2 + \alpha^4\mathrm{B}^4) \\
&\qquad - 4i\alpha(135 + 17\alpha^2\mathrm{B}^2)(c-1)\mathrm{Re} - 165(c-1)^2\mathrm{Re}^2)) \\
a_6 &= \frac{\alpha^2 a_0}{19051200}(1926\alpha^6\mathrm{B}^2 + 220\alpha^8\mathrm{B}^4 + 4\alpha^10\mathrm{B}^6 - 30i\alpha^3(160\mathrm{B}^2 + 63(c-1))\mathrm{Re} \\
&\quad - 1926i\alpha^5\mathrm{B}^2(c-1)\mathrm{Re} - 110i\alpha^7\mathrm{B}^4(c-1)\mathrm{Re} - 6930(c-1)\mathrm{Re}^2 - 1260\alpha^2(c-1)^2\mathrm{Re}^2 \\
&\quad + 12\alpha^4(105 - 47\mathrm{B}^2(c-1)^2\mathrm{Re}^2) + 315i\alpha\mathrm{Re}(-24 + (c-1)^3\mathrm{Re}^2))
\end{aligned}
$$

with $a_0 \in \mathbb{R}$. A second ansatz for $\beta = 2$ yields

$$
\begin{aligned}
c_2 &= \frac{1}{24}(2\alpha c_0(i\mathrm{Re}(1-c) + 2\alpha) + c_1 6\alpha^2\mathrm{B}), \\
c_3 &= \frac{1}{120}(c_1(i\alpha\mathrm{Re}(1-c) + 12\alpha^2) + c_2\alpha^2 16\mathrm{B}), \\
c_4 &= \frac{\alpha^2}{2160}(2\alpha^2(3c_1\mathrm{B}(9 + \alpha^2\mathrm{B}^2) + c_0(9 + 2\alpha^2\mathrm{B}^2)) \\
&\qquad - \alpha(27c_1\mathrm{B} + 2c_0(9 + \alpha^2\mathrm{B}^2))(c-1)i\mathrm{Re} - 6c_0(c-1)^2\mathrm{Re}^2) \\
c_5 &= \frac{\alpha}{37800}(2\alpha^7\mathrm{B}^3(2c_0 + 3c_1\mathrm{B}) + 2\alpha^5\mathrm{B}(29c_0 + 57c_1\mathrm{B}) - 180c_1 i\mathrm{Re} - 135\alpha^2 c_1(c-1)i\mathrm{Re} \\
&\qquad - 2\alpha^6 c_0\mathrm{B}^3(c-1)i\mathrm{Re} - \alpha^4\mathrm{B}(58c_0 + 57c_1\mathrm{B})(c-1)i\mathrm{Re} - 45\alpha c_1(c-1)^2\mathrm{Re}^2 \\
&\qquad + \alpha^3(135c_1 - 16c_0\mathrm{B}(c-1)^2\mathrm{Re}^2)) \\
c_6 &= \frac{\alpha^2}{1814400}(4\alpha^8\mathrm{B}^4(2c_0 + 3c_1\mathrm{B}) + 4\alpha^6\mathrm{B}^2(59c_0 + 102c_1\mathrm{B}) - 4\alpha^7 c_0\mathrm{B}^4(c-1)i\mathrm{Re} \\
&\qquad - 540\alpha^3(c_0 + 3c_1\mathrm{B})(c-1)i\mathrm{Re} - 4\alpha^5\mathrm{B}^2(59c_0 + 51c_1\mathrm{B})(c-1)i\mathrm{Re} \\
&\qquad - 900c_0(c-1)\mathrm{Re}^2 - 45\alpha^2(8c_0 + 11c_1\mathrm{B})(c-1)^2\mathrm{Re}^2 + 2\alpha^4(810c_1\mathrm{B} \\
&\qquad + c_0(180 - 31\mathrm{B}^2(c-1)^2\mathrm{Re}^2)) + 90\alpha i\mathrm{Re}(-34c_1\mathrm{B} + c_0(-8 + (c-1)^3\mathrm{Re}^2)))
\end{aligned}
$$

where we have two free parameters $c_0, c_1 \in \mathbb{R}$. In both series we computed the coefficients using computer algebra [84] and checked the first and second nontrivial coefficients manually.

Let us denote by

$$f_1(t) = \sum_{n=0}^{6} a_n (t - y_B)^{n+3}, \qquad f_2(t) = \sum_{n=0}^{6} c_n (t - y_B)^{n+2}$$

the two truncated Frobenius series solutions and by

$$\boldsymbol{f}_i = \begin{pmatrix} f_i \\ f_i' \\ f_i'' \\ f_i''' \end{pmatrix} \quad \text{at } t = y_B + \varepsilon, \text{ for } i \in \{1, 2\}$$

the solution vectors next to the singularity and ε is a small positive number. The free parameters a_0, c_0 and c_1 can be chosen arbitrary, but such that f_1 and f_2 are non-identical. We choose

$$a_0 = 1, \qquad c_0 = 1, \qquad c_1 = 0.$$

We solve for $\boldsymbol{R}$ from $t = 1/2$ to $y_B + \varepsilon$. Then, we numerically reconstruct two solutions

$$\boldsymbol{x}_i(t) = \begin{pmatrix} \boldsymbol{y}_i(t) \\ \boldsymbol{z}_i(t) \end{pmatrix} \qquad \text{for } i \in \{1, 2\}$$

using the initial values from $\boldsymbol{f}_1$ and $\boldsymbol{f}_2$, respectively, and define

$$\boldsymbol{n}_i = \boldsymbol{x}_i(y_B + \varepsilon)$$

as the solution vector of the numerical result next to the singularity.

Method	Resolution	Most unstable eigenvalue
FDM	$N = 10$	$-0.03902008 - 0.30997035i$
FDM	$N = 30$	$-0.06835490 - 0.32025448i$
FDM	$N = 100$	$-0.06335157 - 0.32574404i$
FDM	$N = 300$	$-0.06297985 - 0.32628388i$
FDM	$N = 1000$	$-0.06293781 - 0.32634614i$
Riccati with Frobenius ansatz	n/a	$-0.06293351 - 0.32635226i$

Table A.1: Comparison of eigenvalues computed by the finite difference method (FDM) explained in Section A.3 with the Riccati method from Section A.4 with parameters Re = 5772.22, $\alpha = 1$ and B = 10. The Riccati method uses an initial guess for the eigenvalue from the FDM and refines the solution using a gradient descent method. The convergence of the FDM towards the result of the Riccati method is apparent and shows both methods to be accurate starting from very small resolutions despite the presence of a regular singularity.

For an admissible eigenmode the solution vectors $\boldsymbol{f}_1$, $\boldsymbol{f}_2$, $\boldsymbol{n}_1$ and $\boldsymbol{n}_2$ are linear dependent, so the solution criterion becomes

$$\det \boldsymbol{M} = \det \begin{pmatrix} \boldsymbol{f}_1 & \boldsymbol{f}_2 & \boldsymbol{n}_1 & \boldsymbol{n}_2 \end{pmatrix} = 0.$$

The degree of freedoms are the solutions $\boldsymbol{y}_1$ and $\boldsymbol{y}_2$, since the initial conditions set $\boldsymbol{z}_1$ and $\boldsymbol{z}_2$. Thus, we reconstruct four values, that is the same as one column in matrix $\boldsymbol{M}$.

In order to solve for an eigenmode or eigenvalue, we need a good initial guess and can refine the guess using a gradient descent method that minimizes $|\det \boldsymbol{M}|$. The solution of the initial value problems is done using the *ode15s* method [85]. Table A.1 shows a comparison of the results between the finite difference method and the Riccati method. Starting from relative low resolutions, both methods are accurate. The Riccati method is more accurate, but needs a good initial guess.

The results also suggest that the FDM is not sensitive to the particular singularity at the yield-surface. This fact deepens our trust in the FDM method employed for the similar multiphase stability problem of Chapter 4, because unfortunately a shooting method is extremely difficult to apply for this particular problem.

Appendix B

Vita

Personal details

Name	Tobias Ahnert
Date of Birth	1985 - 11 - 29
Place of Birth	Berlin
Nationality	German
Name of Parents	Claudia Ahnert, Gerald Ahnert
Email	ahnert@gmail.com

Education

06/2005	Abitur at Gerhart-Hauptmann-Oberschule Berlin (diploma from German secondary school)
07/2005 - 04/2006	Compulsory Community Service at Hochschule für Technik und Wirtschaft
09/2009	Bachelor of Science in Computational Life Science at Universität Lübeck
01/2012	Master of Science in Scientific Computing at Technische Universität Berlin

Awards and distinctions

2004	School price by physikalische Gesellschaft zu Berlin e.V. (PGzB)
2005	School price by physikalische Gesellschaft zu Berlin e.V. (PGzB)
2012	Award for master thesis at Dies Mathematicus 2012

Academic activities

2007 - 2009	Student job at the Mathematical Institute at Universität Lübeck
2010 - 2012	Student job at DFG project "Methods of modeling and large scale simulation of multi-destination pedestrian crowds"
2010	Internship at Technische Universität Berlin with subject "Cell Cluster Programming"
2012 - 2015	Research Assistant at Mathematical Institute at Technische Universität Berlin
2013	Visit of summer school "Mathematical approaches to complex fluids" at Newton Institute, UK
2013	Tutor at "Autumn School Hanoi for Applied Mathematics" at Hanoi, Vietnam
2015	Tutor at Mathematical Institute at Technische Universität Berlin

Talks

2013	"BMS Intensive Course on Evolution Equations and their Applications", Germany
2013	"Organic Photovoltaic Workshop Oxford", UK
2014	"European Consortium for Mathematics in Industry 2014", Italy

Ph.D. studies

Beginning	2012 - 3 - 1
Supervisors	Prof. Barbara Wagner and Prof. Andreas Münch

Publications in journals or proceedings

- A Multispecies Pedestrian Model based on a 3d multiphase incompressible fluid flow model; Ahnert, Bärwolff, Schwandt; International Association for Information and Management Science; 2012
- Modeling and Numerical Simulation of Multi-destination Pedestrian Crowds; Bärwolff, Ahnert, Chen, Huth, Plaue, Schwandt; Computational Science and Its Applications - ICCSA 2013; 2013
- Time-stepping methods for the simulation of the self-assembly of nano-crystals in Matlab on a GPU; Korzec, Ahnert; Journal of Computational Physics; 2013
- Numerical comparison of hybridized discontinuous Galerkin and finite volume methods for incompressible flow; Ahnert, Bärwolff; Journal for Numerical Methods in Fluids; 2014

Preprints

- A two-phase flow model for concentrated suspensions; Ahnert, Münch, Wagner; WIAS Preprint 1901; 2013

- Models for the two-phase flow of concentrated suspensions; Ahnert, Münch, Wagner; WIAS Preprint 2047; 2014
- Stability of concentrated suspensions under Couette and Poiseuille flow; Ahnert, Münch, Niethammer, Wagner; TU Berlin Preprint 15/2015; 2015